Doctoral Dissertation
Doctoral Program in Chemical Engineering (31th Cycle)

Novel microbe-based technologies for bioelectricity and biofuel production

By

Simona Pentassuglia

Supervisors
Prof. G. Saracco, Supervisor
Prof. C.F. Pirri, Co-Supervisor
Dr. T. Tommasi, Co-Supervisor

Doctoral Examination Committee: **Doctoral Prog. Coordinator:**
Prof. C. Barolo, University of Turin, Turin   Prof. D. Marchisio
Prof. C. Santoro, University of the West of England, Bristol

Politecnico di Torino
2019

Declaration

I hereby declare that, the contents and organisation of this dissertation constitute my own original work and does not compromise in any way the rights of third parties, including those relating to the security of personal data.

Simona Pentassuglia
Turin, 2019

Summary

The global concern about energy security, increases in GHG (Greenhouse gas) emissions as well as the effects of climate changes have encouraged the scientific community to provide bioenergy solutions as sustainable alternatives to conventional fossil-fuel sources. The endeavors pursued so far are witnessed by the ongoing development of novel green technologies. This thesis primarily emphasizes the successful employment of two emerging microbe-based biotechnologies: Microbial Fuel Cells (MFCs) and Gas fermentation. Whilst seemingly divergent, these approaches are both reliant on the potential implementation of bacteria as cell factories.

Microbial Fuel Cells (MFCs) are bioelectrochemical systems (BESs) able to harvest the chemical energy stored in organic matter and directly convert it into electrical energy, via the action of special microbes termed exoelectrogens, natively capable of transferring electrons to an insoluble electron acceptor. As demonstration of the practical value of MFC technology, multiple applications have been reported so far. Notably, the first part of this thesis deals with the application of floating MFCs (FMFC) in real marine environment, with the aim to investigate their potential exploitation as portable power sources for low energy-demanding devices. The research activity has been carried out in the framework of a cooperation between the Italian Ministry of Defence and the US Department of Defence. During the experimental activity, open air cathode single chamber MFCs were gathered within a polymeric floating set-up, resulting in a compact and cost-effective system compared to the large-scale systems reported so far. The novelty of this work also lies in developing an *in situ* enrichment procedure. This strategy was undertaken with the aim to enrich the carbon felt material used as anode electrode with the native marine biological community. The new enrichment approach was experimentally validated during both laboratory tests and *in situ* measurement campaigns in Mediterranean See (La Spezia, Italy). Additionally, to ensure a gradual nutrient release, the effectiveness of an agar-based sythetic solid-state electrolyte (SSE), containing both carbon and nitrogen sources, was validated for the first time in real marine environment. Electrochemical performances were investigated by voltage monitoring (VM) over time and electrochemical impedance spectroscopy (EIS). A stable output power of 6 mW/m^2 was achieved during the two distinct *in situ* measurement campaigns, with no appreciable seasonal effects. This observation demonstrated that FMFCs can successfully release electricity using seawater as fuel and electrolyte.

In line with the ongoing energy revolution, many efforts have also been made to produce low-carbon fuels and chemicals. Gas fermentation is a novel technology based on the use of bacteria able to grow using C1 gases as carbon and energy source, producing biofuels and chemicals. The biocatalyst used was the anaerobic acetogen *Clostridium autoethanogenum*, which is capable of growing autotrophically on C1 gases (CO and/or CO_2) producing acetate, ethanol, lactate and 2,3-Butanediol (BDO) by the means of the Wood-Ljungdahl pathway. The second part of this dissertation illustrates the research work carried out over 21 months at the Synthetic Biology Research Centre (SBRC) (Nottingham, UK). The focus of this research activity was the investigation of the redox-sensing transcriptional repressor Rex in *C. autotethanogenum*, found to modulate the expression of genes involved in fermentation metabolism. With this purpose, a *rex* knock-out (KO) mutant was constructed using the advanced genome editing tool CRISPR-Cas9. Fermentation experiments were performed in CO-batch bottle and in a stirred tank reactor (STR) operated in semi-batch mode with batch liquid and continuous CO supply. The phenotypic characterization of batch cultures showed that deletion of the *rex* gene enhanced 2,3-BDO and lactate production compared to the Wild Type whereas no substantial changes were observed in metabolite spectra when cultures were continuously fed with CO. These findings highlighted that the *rex* gene is not a valuable target for metabolic engineering studies seeking to increase ethanol production in *C. autoethanogenum*.

Acknowledgments

I would like to dedicate this thesis to who made this work possible

Contents

List of Figures

List of Tables

List of Abbreviations

2,3-BDO 2,3-Butanediol

ABE Acetone Butanol Ethanol

ACE Allele-Coupled Exchange

ATP Adenosine Triphosphate

BES Bioelectrochemical System

BLAST Basic Local Alignment Search Tool

BOD Biological Oxygen Demand

bp Base pair

Cas CRISPR associated proteins

CE Columbic Efficiency

cm centimeter

Cm Chloraphenicol

CoA CoenzymeA

COD Chemical Oxygen Demand

CRISPR Clustered Regularly Interspaced Short Palindromic Repeats

D-cyc D-cycloserine

DET Direct Electron Transfer

DIET Direct Interspecies Electron transfer

DMRB Dissimilatory Metal-Reducing Bacteria

DNA Deoxyribonucleic Acid

HR Homology Recombination

DSB Double Strand Break

EAB Electroactive Biofilm

EAM Electroactive Microorganism

EET Extracellular Electron Transfer

EIS Electrochemical Impedance Spectroscopy

EPS Extracellular Polymeric Substances

FMFC Floating Microbial Fuel Cell

FMN Flavin mononucleotide

FOA Fluorootic Acid

FT Fischer-Tropsch

GC Gas Chromatography

gDNA genomic DNA

GHA Great Homology Arm

GHG Greenhouse Gas

HPLC High Perfomance Liquid Chromotography

Hz Hertz

Kb Kilobase

K$_{La}$ Mass transfer coefficient

KO Knock Out

LHA Left Homology Arm

mA milliampere

MES 4-morpholineethanesulfonic acid

MET Mediated Electron Transfer

MFC Microbial Fuel Cell

mg milligram

ml millilitre

mm millimetres

mM millimolar

mRNA Messenger Ribonucleic Acid

MSW Municipal Solid Waste

mW milliwatt

NAD Nicotinamide Adenine Dinucleotide

nm nanometres

OCV Open Circuit Voltage

OD Optical Density

OMCs Outer-membrane c-type Cytochromes

ORF Open Reading Frame

ORP Oxidation Reduction Potential

PAM Protospacer Adjacent Motif

PBS Phosphate Buffer Saline

PCR Polymerase Chain Reaction

PEM Proton Exchange Membrane

PMS Power Management System

ppb Part per billion

ppm Part per million

RBS Ribosome Binding Site

Rex Redox sensing transcriptional repressor

R_{ext} External Resistance

RHA Right Homology Arm

RNA Ribonucleic Acid

rpm Rotations Per Minute

rRNA ribosomal Ribonucleic Acid

sgRNA Single guide RNA

SEM Scanning Electron Microscopy

SHA Short Homology Arm

SLP Substrate Level Phosphorylation

SMFC Sedimentary Microbial Fuel Cell

SNP Single Nucleotide Polymorphism

SOE Splicing by Overlapping Extension

SSE Solid State Electrolyte

STR Stirred Tank Reactor

Tm Thiamphenicol

UV Ultraviolet

V Volt

VM Voltage Monitoring

WGS Water Gas Shift

WLP Wood Ljungdahl Pathway

WT Wild Type

YE Yeast Extract

YTF Yeast-Tryptone-Fructose

μg microgram

μL microliter

μm micrometre

μW microwatt

Ω Ohm

Chapter 1

Overview

1.1   Global concern for energy crisis

According to the energy outlook, the already mounting demand of energy will increase by approximately 36% from 2011 to 2030, due to the worldwide economic growth observed in the last century (Raza et al. 2018). This scenario will initiate important repercussions in the near future, as already witnessed by increase in GHG (Greenhouse gas) emissions and by rising global temperature and sea levels (Kumar and Kumar, 2017).

Notably, as reported by the Intergovernmental Panel on Climate Change (IPCC), the employment of fossil fuels for electricity and heat generation, and for transportation accounts for 25% and 14% of the total GHG emissions, respectively (IPCC, 2014). The massive utilization of fossil fuel sources (i.e. coal, oil and natural gas) started with the advent of the industrial era, which took place in 1750 and brought about radical changes that largely contributed to the increases in GHGs emissions. According to the World Meteorological Organization (WMO), the changes in the atmosphere occurred over the last 70 years are without precedent (WMO, 2017). Atmospheric concentration of carbon dioxide (CO_2) increased with a record-breaking speed of 2 ppm/year in the last ten years (WMO, 2017). The latest analysis referred to 2017 reported that CO_2 reached new highs, with a global abundance of 405.5 ± 0.1 ppm, representing 146% of pre-industrial level (WMO 2018). The top three largest emitter countries include China (9839 $MtCO_2$), followed by USA (5270 $MtCO_2$) and India (2467 $MtCO_2$) (**Figure 1**). Beside CO_2, GHGs such as methane (CH_4) and nitrous oxide (N_2O) were found to be 1859 ± 2 ppb and 329.9 ± 0.1 ppb, representing 257% and 122% of pre-industrial levels, respectively (WMO, 2018).

Enhanced deposition of greenhouse gases in the atmosphere results in an abrupt and unprecedented global warming (WMO, 2017). In 2015, during the 21st Conference of the Parties to the United Nations Framework Convention on Climate Change, 195 countries negotiated the Paris agreement. This agreement aims to limit the increases in global temperature to "well below 2°C above pre-industrial levels" along with "foster climate resilience and low greenhouse gas emissions development, in a manner that does not threaten food production" (United Nations, 2015). To achieve the goal defined by the Paris agreement, it has been estimated that a third of oil reserves, half of gas reserves and over 80% of coal reserves should remain unused until 2050 (Liew et al. 2016).

A potential approach to tackle the global concern for energy crisis while simultaneously mitigate climate changes, relies on the utilization of low-carbon fuels and chemicals (Liew et al. 2016). In line with the on-going energy revolution, it has been predicted that in the second half of the 21st century, renewable energies will be the cornerstone of the energy system, leading GHG emissions approaching

zero (Zhang, 2016). Producing bioelectricity and biofuels by the action of microorganisms implemented as cell factories can certainly provide a valuable contribution (Kumar and Kumar, 2017).

Rank	Country	MtCO$_2$
1	China	9839
2	United States of America	5270
3	India	2467
4	Russian Federation	1693
5	Japan	1205
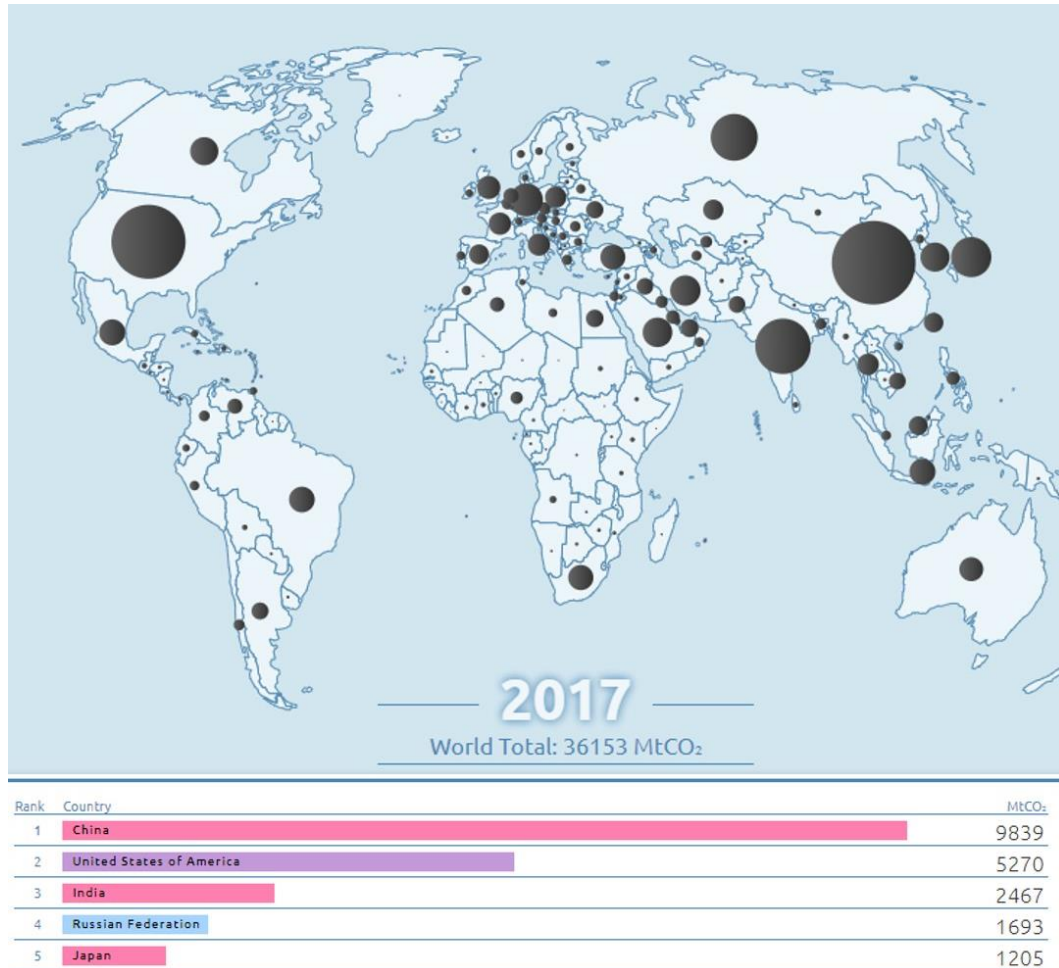
Figure 1 Territorial-based CO$_2$ emissions measured in metric tones (MtCO$_2$) deriving from fossil fuels combustion in 2017. The chart shows the territorial MtCO$_2$ values for the top five emitters of the 2017 rank. Adapted from http://www.globalcarbonatlas.org/en/CO.

1.2 Biomass for bioenergy solutions

In an effort to diminish dependence on depleting sources such as fossil fuels, biomass utilization as non-fossil derived energy resource has gained much attention (Metz et al. 2007). Whilst their extensive development, stable power production from wind or through photovoltaic technologies is hindered by their nature. Biomass from being the fourth biggest source of energy, following solar, geothermal and wind, is supposed to become the most prominent renewable energy

due to its versatility, which allows its implementation as either liquid, solid or gas state (Metz et al. 2007; Zhang et al. 2016).

The biomass resulting from photosynthetic activity is about 200 Gt. It has been estimated that by employing just 10% of this biomass, 4 Gt of ethanol biofuel or other bioenergy products could be released, which correspond to 4.13 Gt of petroleum consumed worldwide in 2014 (Zhang et al. 2016). Today, biofuel generation represents one of the most debated scientific topics. So far, the majority of efforts undertaken to encourage commercial biofuel production envisaged the utilization of simple sugars from sugar cane and starch (Gustavsson and Lee, 2016). These are referred to as first generation biofuels. The use of agricultural products as feedstock is advantageous due to the economically feasible production, high sugar content and low energy investment required for the cultivation (Renouf et al. 2008). However, the concept of employing products intended for human consuming and food processing, entails food security issues and price rise. Additionally, secondary environmental pollution may occur (Zhang et al. 2016). Indeed, the required deforestation of the local vegetation would result in a larger CO_2 net emissions than fossil fuels (Hu et al. 2012). Some of these limitations have been addressed by switching toward the utilization of lignocellulosic biomass for the so-called second-generation biofuels. This represents the most abundant biomass with an estimated production of 150-170 x 10^9 tons/year, out of which just 2 x 10^9 tons are used (Pauly and Keegstra, 2008). However, lignocellulose deconstruction into fermentable sugars needs extensive pre-treatments followed by enzymatic hydrolysis steps or consolidated bioprocessing (Kumar and Kumar, 2017). Hence, this feedstock is considered more difficult to work with compared to the raw materials employed for first generation biofuels. Lately, a concrete step toward reduction of GHG emissions is offered by a novel technology termed gas fermentation, which currently has been receiving considerable scientific interest. Through thermochemical conversion, biomass can be gasified to the so-called synthesis gas or syngas, a gaseous mixture mainly composed by carbon monoxide (CO), carbon dioxide (CO_2), hydrogen (H_2) and nitrogen (N_2) (Liew et al. 2016). This approach allows the conversion of almost all the carbon incorporated into the biomass, without neglecting the otherwise inaccessible lignin component and avoiding pre-treatment steps (Liew et al. 2016). As alternative to biomass gasification, carbon can be capture and utilized by directly using CO/CO_2 as feedstock and hence bypassing the fixation of CO_2 into plant biomass.

The energetic utilization of biomass results not only in biofuel generation but also in the production of electricity and heat (Freiberg et al. 2018). Biomass-based electricity can be generated using several approaches, which comprise direct combustion, gasification, pyrolysis and anaerobic digestion. An attractive route relies on particular microbes that can actually produce electricity by transferring electrons to conductive surfaces. This interesting future has been exploited in

bioelectrochemical systems (BESs) such as Microbial Fuel Cells (MFCs) and Microbial Electrolysis Cells (MECs), for bioelectricity and hydrogen production, respectively (Kumar and Kumar, 2017). Notably, in MFCs the so-called electroactive microorganisms (EAMs) directly convert the chemical energy incorporated in organic waste matter and renewable biomass into bioelectricity. Even though extremely attractive, to some extent MFCs are still considered a scientific curiosity rather than a solid technology. However, the practical value of MFCs has emerged with their on-field implementation in remote areas, where these devices can serve as power source for low energy-demanding environmental sensors (Santoro et al. 2017; Massaglia et al. 2018).

1.3 Microbes as sustainable factories

Many bioenergy solutions that have been realized so far foresee the use of microbes as real cell factories. Microbial cell factories represent an innovative, versatile, efficient and environmental-friendly alternative to traditional chemical-catalyst. Even though generally chemical processes are faster compared to biocatalyst-based processes, in the latter case a complete conversion of substrate into products occurs because of the irreversibility of biological reactions (Liew et al. 2016). Additionally, enzymatic activity ensures higher selectivity resulting in the formation of fewer undesired by-products (Liew et al. 2016). Since working with microbes typically requires mild conditions, this trait makes their industrial application particularly beneficial. Selection of the appropriate microbial cell factory is pivotal to ensure the successful production of the target product. Microbes can be employed as either mixed, pure or co-cultures. The selection of mixed rather than pure culture depends on the complexity of the bioprocess involved. Pure cultures are often a prerequisite when specific conversion from a pure substrate is required; indeed most of the bioproduction processes are based on the utilization of pure culture. However, "mixed cultures are the rule in nature" (Sabra and Zeng, 2014). Advantages related to the employment of mixed culture include their functional redundancy and their resilience from environmental challenges (Marshall et al. 2013). Additionally, industrial applications of mixed cultures might be more economically sustainable since sterility is not a stringent requirement. The versatility of microorganisms' application is also exhibited by their ability to grow as either biofilm or planktonic cells. The strategy to form biofilm displayed by many bacteria represents a biotechnological resource for energy and environmental applications (Pentassuglia et al. 2017). As above mentioned, electro-active microbes are capable of growing in biofilm onto an electrode surface, hence allowing electricity generation. Moreover, nowadays the tremendous advances of metabolic engineering and synthetic biology provide fruitful opportunities to retool industrial strains, by even incorporating heterologous pathways.

1.4 Aims of this thesis

The primary focus of this thesis was to give an insight of the attractive implementation of two recently established technologies, Microbial Fuel Cells (MFCs) and gas fermentation. Whilst, seemingly divergent, these approaches are both reliant on the potential use of microbes as sustainable route toward the development of a renewable energy system. With this purpose, two types of special microbial catalysts were employed: a marine mixed community and a pure culture of the gas-fermenting *Clostridium autoethanogenum*.

The **first** objective of this study was the investigation of the applicability of MFCs as portable power source for low-energy demanding devices in real marine environment. With this aim, the construction of a floating system comprising multiple small-scale MFCs was conducted and an alternative *in situ* enrichment approach for anodic biofilm formation was validated. Hence, the electrochemical performances were monitored in both laboratory and marine environments.

Despite numerous advantages have been reported so far in the use of gas fermentation, this technology still needs some efforts to be pursued. Optimization can be performed at different levels, ranging from modification of process parameters, reactor design or by the means of metabolic engineering tools. The redox-sensing transcriptional regulator Rex has been found to play a key role in redox homeostasis, and the deletion of its gene resulted in the increase of solvent production. Thus, the **second** purpose of my PhD project concerns to investigate for the first time the role of Rex repressor in the industrially-relevant acetogen *C. autoethanogenum*. With this aim, construction of *C. autoethanogenum rex* deficient strain was performed using CRISPR-Cas9 genome editing tool. In order to ascertain whether the *rex* gene was involved in modulation of fermentative pathways in *C. autoethanogenum*, phenotypical characterizations were conducted in both serum-flasks and in a stirred tank reactor (STR) using CO as sole carbon and energy source.

1.5 Thesis structure

In providing the reader a smooth understanding of the content, the current thesis is structured as follows. First, the body of the dissertation is divided into two main sections, **Section 1** and **Section 2**, with their focus on Microbial Fuel Cells (MFCs) and Gas fermentation technologies, respectively. Chapters describing the Material

and Methods adopted have been developed independently for each section and are assigned as **Chapter 3 and Chapter 7,** respectively.

Section 1 is the outcome of the research work conducted during my first year at the IIT-Italian Institute of Technology (Turin, Italy). Within this section, **Chapter 2** offers a theoretical background of MFCs, notably emphasizing the importance of anodic electroactive biofilm (EAB) (**Subchapter 2.3**). The latter is an amended version of a published Encyclopedia chapter (Pentassuglia et al. 2017). **Chapter 4** deals with the experimental activity performed using a floating MFCs set-up placed and monitored in the bay of La Spezia (north of Italy). This chapter shows the results, modified for the incorporation in this thesis, of a published paper (Massaglia et al. 2018).

Section 2 is focused on the 21 months research work carried out at the Synthetic Biology Research Centre of the University of Nottingham (Nottingham, UK), directed by Professor Nigel Minton. As for the first section, the second part of this thesis encompasses the **Chapter 6**, which gives an insight of gas fermentation technology, starting with its theoretical fundamentals and concluding with the improvements required for its industrial applications. **Subchapter 6.2** described the features of acetogenic microorganisms, with special attention to *Clostridium autoethanogenum*. Successively, **Chapter 8** begins with an overview of the status of literature on redox sensing transcriptional repressor-Rex, followed by the results achieved during *C. autoethanogenum* mutant strains construction. As follows, **Chapter 9** illustrates and discusses the results obtained during CO-fermentation experiments.

The thesis ends with a general discussion presented in **Chapter 10**, where the key findings are critically summaries, while simultaneously providing future perspective of the thesis work.

1.6   References

Freiberg, A., Scharfe, J., Murta, V.C. and Seidler, A. (2018). The Use of Biomass for Electricity Generation: A Scoping Review of Health Effects on Humans in Residential and Occupational Settings. *International Journal of Environmental Research and Public Health*, 15: 1-27.

Gustavsson, M. and Lee, S.Y (2016). Prospects of microbial cell factories developed through systems metabolic engineering. *Microbial Biotechnology*, 9: 610-617.

Hu, L.L., Li, L. and Li, J.S. (2012). The characteristics of biomass energy and its environmental effects. *Energy and Environment*, 1: 47-49 (in Chinese).

IPCC (2014). Climate Change 2014: Mitigation of Climate Change," in Contribution of Working Group III to the Fifth Assessment Report of the Intergovernmental Panel on Climate Change, eds Edenhofer, O., Pichs-Madruga, R., Sokona, Y., Farahani, E., Kadner, S., Seyboth, K., Adler, A., Baum, I., Brunner, S., Eickemeier, P., Kriemann, B., Savolainen, J., Schlömer, S., von Stechow, C., Zwickel, T. and Minx, J.C. (Cambridge; New York, NY: Cambridge University Press), 7–9.

Kumar, R. and Kumar, P. (2017). Future microbial applications for bioenergy production: a perspective. *Frontiers in Microbiology*, 8: 1–4.

Liew, F., Martin, M.E., Tappel, R.C., Heijstra, B.D., Mihalcea, C. and Köpke, M. (2016). Gas Fermentation—A Flexible Platform for Commercial Scale Production of Low-Carbon-Fuels and Chemicals from Waste and Renewable Feedstocks. *Frontiers in Microbiology*, 7: 1-28.

Marshall, C.W., LaBelle, E.V. and May, H.D. (2013). Production of fuels and chemicals from waste by microbiomes. *Current Opinion in Biotechnology*, 24: 391-397.

Massaglia, G., Margaria, V., Sacco, A., Tommasi, T., Pentassuglia, S., Ahmed, D., Mo, R., Pirri, C.F. and Quaglio, M. (2018). *In situ* continuous current production from marine floating microbial fuel cells. *Applied Energy*, 230: 78-85.

Metz, B., Davidson, O. R., Bosch, P. R., Dave, R. and Meyer, L. A. (eds.). (2007). Contribution of Working Group III to the Fourth Assessment Report of the Intergovernmental Panel on Climate Change, 2007. Cambridge: Cambridge University Press.

Pauly, M. and Keegstra, K. (2008). Cell-wall carbohydrates and their modification as a resource for biofuels. *The Plant Journal*, 54: 559-568.

Pentassuglia, S., Agostino, V. and Tommasi, T. (2017). EAB—Electroactive Biofilm: A Biotechnological Resource. In: *Reference Module in Encyclopedia of Interfacial Chemistry: Surface Science and Electrochemistry*, Elsevier (Chapter 131461).

Raza, A., Meiyu, G., Gholami, R., Rezaee, R., Rasouli, V., Sarmadivaleh, M. and Bhatti, A.A. (2018). Shale gas: A solution for energy crisis and lower CO_2 emission in Pakistan. *Energy Sources, Part A: Recovery, Utilization, and Environmental Effects*, 40: 1647-1656.

Renouf, M.A., Wegener, M.K. and Nielsen, L.K. (2008). An environmental life cycle assessment comparing Australian sugarcane with US corn and UK sugar beet as producers of sugars for fermentation. *Biomass and Bioenergy*, 32: 1144-1155.

Sabra, W. and Zeng, A.P (2014). Mixed Microbial Cultures for Industrial Biotechnology: Success, Chance, and Challenges. In: *Industrial Biocatalysis*, Pan Stanford (Chapter).

Santoro, C., Arbizzani, C., Erable, B., Ieropoulos, I. (2017). Microbial fuel cells: From fundamentals to applications. A review. *Journal of Power Sources*, 356: 225-244.

United Nations (2015). Adoption of the Paris Agreement. 21932, 32. Available online at: http://unfccc.int/resource/docs/2015/cop21/eng/l09r01.pdf.

WMO (2017). Greenhouse gas bulletin, the state of greenhouse gases in the atmosphere based on global observations through 2016. Geneva, Switzerland.

WMO (2018). Greenhouse gas bulletin, the state of greenhouse gases in the atmosphere based on global observations through 2017. Geneva, Switzerland.

Zhang, X.Y. (2016). Developing bioenergy to tackle climate change: Bioenergy path and practice of Tianguan group. *Advances in Climate Change Research*, 7: 17-25.

Section 1

Electroactive microbes: an alternative power source

Chapter 2

Introduction

2.1 Fundamentals of Microbial Fuel Cells (MFCs)

Over the past decades, Bioelectrochemical systems (BESs) have gained wide scientific attention as novel technologies able to combine electrochemical reactions and physics with biological redox activity via microbe-electrode interactions (Ivars-Barcelò et al. 2018). BESs are generally classified according to their applications, which range from bioelectricity generation to production of fuels and high value chemicals (Ivars-Barcelò et al. 2018; Bajracharya et al. 2016). BESs include Microbial Fuel Cells (MFCs), Microbial Electrolysis Cells (MECs), Microbial Desalination Cells (MDCs) and Microbial Electrosynthesis Cells (MESs). Notably, MFCs are bioelectrochemical devices purposefully designed to extract chemical energy stored in organic matter and directly deliver it as electrical energy (Santoro et al. 2017; Gajda et al. 2018). MFCs can exhibit a conversion efficiency up to 80%, far higher compared to other established technologies (Pandit and Das, 2018). With this concept in mind, MFCs constitute a viable and low-cost approach for wastewater treatment, with simultaneous sustainable production of electricity. Many configurations have been implemented so far; however, the wider employed MFC design consists of two chambers, an anode and a cathode, which are separated through a proton exchange membrane (PEM) (**Figure 2.1**). Anaerobic oxidation reaction of the organic substrate occurs in the anaerobic anodic compartment, with resulting release of protons and electrons (Pant et al. 2010). Once captured by the anode electrode, electrons are transferred to the cathodic chamber via an external circuit whereas protons pass through the PEM (Ivars-Barcelò et al. 2018). As opposed to common fuel cells, in MFCs the breakdown of the biodegradable organic matter is carried out via biochemical oxidation reactions by microbes referred to as exoelectrogens, which proliferate under anaerobic conditions arranging in biofilms onto the anode electrode (bioanode) (Margaria et al. 2017). At the cathode electrode, the circuit is closed through a reduction reaction, commonly the reduction of molecular oxygen to water, by exploiting protons and electrons coming from the anode (Massaglia et al. 2018). This cascade of reactions results in electricity generation.

The original idea of microbial electrocatalysis was conceived more than a century ago when Potter showed electricity production from an *E. coli* culture on platinum electrode using mediated electron transfer (Potter, 1911). Twenty years later, Branet Cohen demonstrated the generation of an overall voltage of 35 V and 0.2 mA of current by using multiple MFCs connected in series (Cohen, 1931). From this early example, research into MFC field has made substantial progresses but there are still efforts to be pursued. The first challenge is the low power released that is orders of magnitude lower than that of conventional fuel cells (Santoro et al. 2017). This intrinsic characteristic has strongly hindered MFC applicability in real environment (Gajda et al. 2018). However, employment of MFCs as power supply for low energy-demanding devices in remote area is still considered a valid alternative (Massaglia et al. 2018).
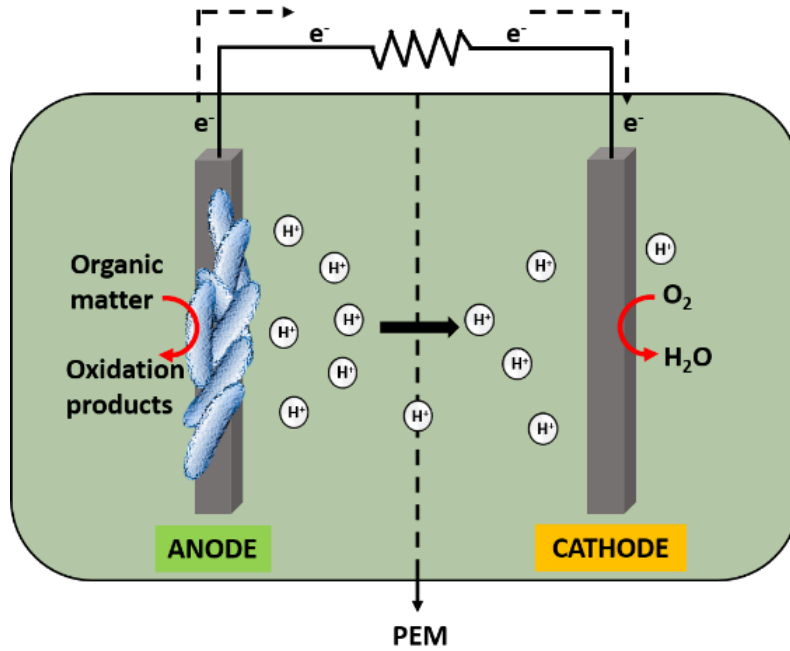
Figure 2.1 Schematic representation of a dual-chamber microbial fuel cell (MFC).

2.2 Thermodynamic principles of MFCs

Electricity generation process in MFCs occurs only if the overall reaction is thermodynamically favorable. This can be evaluated by calculating the Gibbs free energy (J) using the following equation:

$$\Delta G_r = \Delta G_r^0 + RT \ln(\Pi) \qquad \text{Eq. 2.1}$$

where ΔG_r (J) represents the Gibbs free energy for the determined conditions, ΔG_r^0 (J) is the Gibbs free energy measured under standard conditions (T=298.15 K, p=1 bar and 1M concentration for all the species involved), R is the universal gas constant (8.31447 j/(mol·K)), T (K) is the absolute temperature and Π is the reaction quotient so that the ratio of the activities of the products to those of the reactants (Logan, 2006).

The negative value of the Gibbs free energy is intended as the maximal theoretical work, W_{max} (J), derivable from the reaction and is related to the electromotive force, E_{emf} (V), as follows:

$$-\Delta G_r = W_{max} = E_{emf} \cdot Q = E_{emf} \cdot (n \cdot F) \qquad \text{Eq. 2.2}$$

with Q (C) representing the charge transferred during the reaction, as the product n is the number of electrons involved per reaction mol and F is the Faraday's constant (9.64853 x 10^4 C/mol) (Logan, 2006).

Rearranging the aforementioned equations, at standard conditions (Π=1), electromotive force can be calculated using the following expression:

$$E_{emf} = E^0_{emf} + \frac{RT}{nF} \ln(\Pi) \quad \text{Eq. 2.3}$$

The same equation can be utilized in order to calculate the theoretical half-cell potentials referred to reactions taking place at the anode or cathode electrode. These are generally reported relative to reference electrodes, such as the Standard Hydrogen Electrode (SHE), which exhibits a potential equal to zero at standard conditions.

The overall cell potential (E_{emf}) of MFCs can be expressed as:

$$E_{emf} = E_{cathode} - E_{anode} \quad \text{Eq. 2.4}$$

Hence, if the Gibbs free energy (*ΔG*) is negative the overall reaction can occur spontaneously and electricity can be generated by the MFC.

2.3 Electrochemical parameters

A microbial fuel cell is an electrical source and as any other electrical source, its performance can be described by electrochemical parameters such as cell voltage, power and current densities. Voltage (*E*) can be expressed as a function of the external load applied to the circuit (R_{ext}) and the current (*I*) using the first Ohm's law equation:

$$E = I \cdot R_{ext} \quad \text{Eq. 2.5}$$

Consequently, current can be calculated indirectly taking into account the voltage drop measured after that the external resistance is applied to the cell:

$$I = \frac{E}{R_{ext}} \quad \text{Eq. 2.6}$$

Power output, P (*W*), can be calculated using Eq. 2.7.

$$P = I \cdot E \quad \text{Eq. 2.7}$$

also expressed as:

$$P = \frac{E^2}{R_{ext}} \quad \text{Eq. 2.8}$$

Since the absolute value of power does not provide a comprehensive description of the efficiency of the system, conventionally power output is expressed as power density by normalizing by the electrode surface area (Logan, 2008).

14

Coulombic efficiency (*CE*) is another important indicator of MFC performances, which is defined as the ratio between the number of electrons recovered from the substrate as current with respect to the total equivalents incorporated within the organic matter and available for microbial oxidation (Logan, 2008). *CE* is calculated by Eq. 2.9 as follows:

$$CE = \frac{M \int_0^t I \, dt}{F \, b \, v_{an} \Delta c} \qquad \text{Eq. 2.9}$$

with *M* representing the molecular weight of the substrate; *F* is the Faraday's constant; *b* is the number of electrons exchanged per mol of substrate; v_{an} is the liquid volume in the anode compartment and Δc is the changes in substrate concentration over the time.

2.4   Energy losses in MFCs

When no current is flowing through the system, the resulting cell voltage is referred to as open circuit voltage (*OCV*). Theoretically, the *OCV* should equal the cell E_{emf} achieving a maximum MFC voltage around 1.1 V. However, in practice, the experimentally measured MFC voltage is significantly lower, with a maximum OCV obtainable of 0.8 V. Indeed, due to irreversible potential losses, the theoretical cell voltage (E_{emf}) provides a higher value compared to the actual cell potential. The difference between measured cell voltage and the E_{emf} is termed overpotential (Logan, 2006). Overpotentials can be categorized as activation losses, ohmic losses and mass transport or concentration losses (**Figure 2.2**).

When electrochemical reactions occurring at the electrode interphase are regulated by slow reaction kinetics, the activation energy has to be overcome for the reaction to occur (Du et al. 2007). This causes a non-linear voltage drop also termed activation losses (Kadier et al. 2016). The zone of activation overpotential corresponds to the low polarization region (**Figure 2.2 A**). Activation losses include the electron transfer from or to a reacting species at the electrode surface. Strategies to minimize activation losses include increasing anode electrode area, favoring anode-microorganism interaction, increasing working temperature and catalyst addition to the electrode surface (Kadier et al. 2016).

Ohmic losses observed in the medium polarization region (**Figure 2.2 B**), comprise the resistance to the electron and ion flow across the electrodes and the PEM, respectively and the resistance within the anodic and cathodic electrolyte. Several approaches can be adopted in order to limit ohmic losses. They comprise reducing the electrode distance, employing a low resistivity membrane and enhancing the conductivity of the electrolyte solutions (Logan, 2006).

Predominantly at high current density, substrate consumption is responsible of concentration losses **(Figure 2.2 C)**. In this case, the rate of mass transport to or

from the electrode of the species present within the bulk is limited, thus hindering current production (Logan et al. 2006).
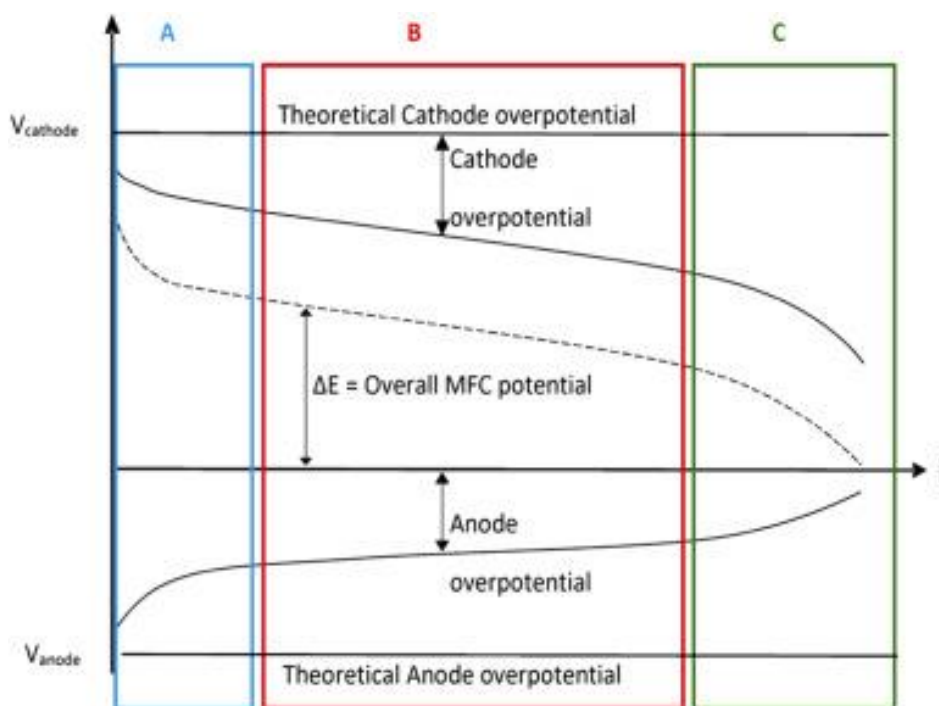
Figure 2.2 Schematic representation of anodic and cathodic polarization curves in a MFC system, compared to the theoretical profile (Kadier et al. 2016).

The following subchapter is an amended version of the already published chapter:

Pentassuglia, S., Agostino, V. and Tommasi, T. (2017). EAB—Electroactive Biofilm: A Biotechnological Resource. In: *Reference Module in Encyclopedia of Interfacial Chemistry: Surface Science and Electrochemistry, Elsevier* (Chapter 131461).

2.5   Electroactive biofilm

Biofilm can be described as a community of microbes where cells adhere to each other on a living or nonliving support within a self-produced matrix of extracellular polymeric substances (EPS) (Jamal et al. 2015; Flemming et al. 2016). Biofilm lifestyle turns out to be an efficacious survival strategy adopted by many microbes to cooperatively gain protection from hostile environmental factors such as the presence of antibiotics as well as predation and desiccation events (Bogino et al. 2013). Currently, biofilm is a topic of great scientific interest and it is receiving particular attention as biotechnological resource for energy and environmental applications. Notably, in nature some microbes are capable of generating electrical current by catalyzing the oxidation of organic matter with an electrode as an

external electron acceptor (anode). Some others instead utilize the electrode as sole electron reservoir (cathode) to perform electroreduction reactions (Bajracharya et al. 2016). In the former case this special kind of microorganisms are referred to as exoelectrogens whereas the second group comprises bacteria known as electrotrophs. In order to maximize the interaction with the electrode surface, both exoelectrogens and electrotrophs colonize and proliferate onto the electrode, forming the so-called EAB—electroactive biofilm. Due to the aim of this thesis, the following paragraphs mainly focus on bioanode, providing an overview of the most representative exoelectrogenic species and reviewing the current literature on anodic EET mechanisms.

2.5.1 Bioanode

In nature, bacteria have evolved strategies to interact with their surrounding environment gaining energy through microbial respiration, a cascade of biochemical redox reactions, based on electron transfer from an electron donor to an electron acceptor. In order to maximize the energy achieved, microorganisms regulate their metabolic pathways by selecting the electron acceptor with the highest potential available (Patil et al. 2012). Although electron acceptors present in microbial habitats are commonly soluble molecules (i.e. oxygen, carbon dioxide, nitrate, sulfate and formate), during respiration process some bacteria are able to reduce insoluble electron acceptors as well (Schroeder, 2007; Richter et al. 2012). In anoxic conditions a special class of microorganisms, known as dissimilatory metal-reducing bacteria (DMRB), has the biogeochemical ability to couple the oxidative degradation of organic matter with the reduction of solid electron acceptors, such as metals and minerals mainly containing Fe(III) and Mn(IV) oxides (Lovley, 1991). In this case microorganisms need to release electrons from their extracellular environment out of the cell (across the periplasm and beyond the cell membrane), to carry out the solid electron acceptor reduction. This mechanism is referred to as Extracellular Electron Transfer (EET). In MFCs exoelectrogens forming the so-called bioanode (**Figure 2.3**) exchange electrons with the anodic conductive surface via EET. Here, anode not only plays a structural role primarily providing a scaffold for biofilm adhesion, but it actively contributes to the biochemical processes working as a breathing tool.
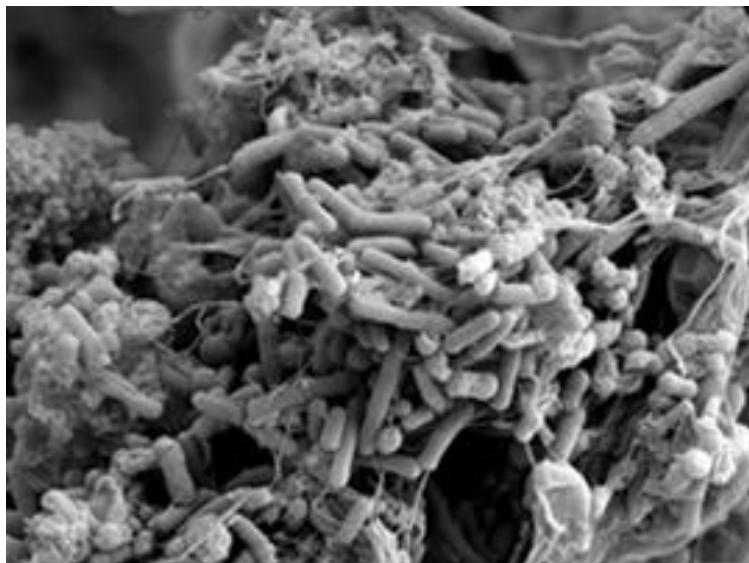
Figure 2.3 Field Emission-Scanning Electron Microscopy image (magnification at 20 kX) of anodic biofilm formed onto carbon felt electrode.

2.5.1.1 Representative exoelectrogens

Exoelectrogens can be isolated from several environmental samples, such as marine and freshwater sediments, rice-paddy soils, compost, and wastewater (Wang et al. 2019). Different names have been used to collectively define them and these include exoelectrogens, electricigens, anode-respiring bacteria, anodophilic microbes, etc. Electricigens represent a phylogenetically disparate category of microbes, whose members belong to different phyla such as α-, β-, γ- and δ-Proteobacteria, Firmicutes, Acidobacteria and Bacteroides (**Table 2.1**). *Geobacter* spp. and *Shewanella* spp. are the most promising anode-respiring bacteria. Over almost 30 years of research, *G. sulfurreducens* as well as *S. oneidensis* have been thoroughly studied, and hence, they became the current model system for investigating outward electron transfer dynamics. Bacteria of the *Geobacteracae* family are strictly anaerobic, Gram-negative microbes, populating iron-rich sedimentary environments (Lovley et al. 2011). *G. sulfurreducens* is considered one of the most efficient and successful catalyst in MFC technology because of its capability to readily recover nearly 100% of the electrons as electricity from acetate oxidation reaction (Nevin et al. 2008). *G. sulfurreducens* KN400 pure culture has been found able to produce one of the highest power densities with 3900 mW/m^2 (Yi et al. 2009). Beyond *G. sulfurreducens*, *G. metallireducens* is the first *Geobacter* species isolated and the most efficient in Fe(III)-oxide reduction (Lovley et al. 1993). In 2014, Sun et al. proposed another *Geobacter* species known as *G. anodireducens*. This bacterium was directly isolated from the anodic biofilm of a microbial fuel cell.

Shewanella spp. belong to the γ-proteobacteria phylum and are gram-negative and facultative anaerobes, able to respire a broad array of terminal electron acceptors,

such as iron and manganese oxides (Ong et al., 2014). Over the last few decades, about 20 Shewanella strains have been sequenced. For instance, recently a *S. oneidensis* MR-1 pure culture was proved to release a power density of 225 W/m^3 using an mL-scale MFC with a 3D nitrogen-doped graphene aerogel as anode material (Yang et al., 2016). The other prominent species, *S. putrefaciens* has been reported to yield a maximum power density of 4.92 W/m^3, in a single chamber MFC and in presence of $CaCl_2$ as anodic electrolyte (Pandit et al, 2014). However, with respect to *Geobacter* species, *Shewanella oneidensis* is generally less abundant in MFCs likely due to its inability of anaerobically metabolizing acetate (Logan et al. 2019).

Although the plethora of research studies has been focused on *Shewanella* and *Geobacter*, several other microorganisms have been identified as potential biocatalysts in MFCs. By now, 94 microbial species, principally including bacteria, have been assessed as electroactive and most likely more electrogenic species have not be discovered yet (Koch and Harnish, 2016). Some of the currently known exoelectrogens are listed in **Table 2.1**. As reported, the absolute majority of the electricigenic microorganisms are gram-negative, since their outer membrane allows intermembrane ET mechanisms, resulting in a higher electrical output. On the contrary, gram-positive produce less current than gram-negative, due to the presence of a cell envelope, which hinders EET (Semenec and Franks, 2015). Perhaps unexpectedly, the gram-positive *C. butyricum*, *B. subtilis*, *T. potens* and *T. ferriacetica* were found capable to directly interact with the anode electrode surface during electron transfer processes (Park et al. 2001; Nimje et al. 2012; Wrighton et al. 2011; Marshall and May, 2009). Additionally, many of the anode-respiring bacteria reported are DMRB (*Geobacter sp., Shewanella sp., Rhodoferax ferrireducens, Thermincola sp., Pseudomonas aeruginosa, Geothrix fermentan*s etc.). However, extracellular metal reduction is not a pre-requisite for electroactivity. Indeed, even bacteria not involved in metal biogeochemical reduction, such as *Ochrobactrum sp.*, are able to successfully perform EET when grown into the anodic chamber of MFCs.

Table 2.1 Most representative exoelectrogenic microorganisms. Table continues next page.

Class	Species	Features	Reference
δ-Proteobacteria	Geobacter sulfurreducens	Gram negative, strict anaerobic	Richter et al. 2008
δ-Proteobacteria	Geobacter metallireducens	Gram negative, strict anaerobic	Lovley et al. 1993
δ-Proteobacteria	Geobacter anodireducens	Gram negative, anaerobic	Sun et al. 2014
γ-Proteobacteria	Shewanella oneidensis	Gram negative, facultative anaerobic	Yang et al. 2016
γ-Proteobacteria	Shewanella putrefaciens	Gram negative, facultative anaerobic	Kim et al. 1999
γ-Proteobacteria	Pseudomonas aeruginosa	Gram negative, Aerobic-facultative anaerobic	Shen et al. 2014
γ-Proteobacteria	Pseudomonas putida	Gram negative, facultative anaerobic	Majumder et al. 2014
β-Proteobacteria	Rhodoferax ferrireducens	Gram negative, facultative anaerobic	Liu et al. 2007
γ-Proteobacteria	Aeromonas Hydrophila	Gram negative, facultative anaerobic	Li et al. 2017a
δ-Proteobacteria	Desulfovibrio desulfuricans	Gram negative, strict anaerobic	Kang et al. 2014
α-Proteobacteria	Rhodopseudomonas palustris	Gram negative, facultative anaerobic	Xing et al. 2008
γ-Proteobacteria	Klebsiella pneumoniae	Gram negative, facultative anaerobic	Yuvraj and Aranganathan, 2017
γ-Proteobacteria	Escherichia coli	Gram negative, facultative anaerobic	Liu et al. 2012

δ-Proteobacteria	Desulfovibrio alaskensis	Gram negative, strict anaerobic	Keller et al. 2014
Clostridia	Thermincola ferriacetica	Gram positive, strict anaerobic	Parameswaran et al. 2013
Clostridia	Thermincola potens	Gram positive, strict anaerobic	Wrighton et al. 2011
Holophagae (Acidobacteria)	Geothrix fermentans	Gram negative, strict anaerobic	Bond and Lovley, 2005
α-Proteobacteria	Ochrobactrum anthropic	Gram negative, facultative anaerobic	Wang et al. 2016
Bacilli	Bacillus subtilis	Gram positive, facultative aerobic	Nimje et al. 2012
Bacilli	Enterococcus faecalis	Gram positive, facultative anaerobic	Zhang et al. 2014
γ-Proteobacteria	Enterobacter cloacae	Gram negative, facultative anaerobic	Rasmussen and Minteer, 2015
γ-Proteobacteria	Citrobacter sp. SX-1	Gram negative, facultative anaerobic	Xu and Liu, 2011
γ-Proteobacteria	Raoultella electrica	Gram negative, facultative anaerobic	Kimura et al. 2014
Bacilli	Lysinibacillus sphaericus	Gram positive, facultative anaerobic	Nandy et al. 2013
Clostridia	Clostridium butyricum	Gram positive, strict anaerobic	Park et al. 2001

2.5.1.2 Pure vs. mixed-community anodic biofilm

Actually, although recognized as exoelectrogenic, several microbial species exhibit low electrochemical performances when employed as pure culture in MFCs (Logan, 2009). In general, it is worth noting that a mixed species biofilm outperforms pure culture biofilm in terms of power production. The highest current density values achieved so far derive from experiments using mixed cultures as inoculum, which were predominantly constituted by microorganisms of the genus *Geobacter* (Logan et al. 2019). Recently, a power density of 6400 mW/m^2 was reported by Oliot et al. (2017) using bioanodes formed in compost leachate. However, *G. sulfurreducens* pure culture biofilm constitutes an exception, because able to generate equivalent power amount than mixed biofilms, with a conductivity up to 5000 µS/cm (Li et al. 2016a). The strategy to use mixed community deriving from the enrichment of a natural or industrial inoculum (marine and freshwater soils, wastewater, active sludge) is reasonable since the employment of pure culture is definitely less cost-effective and not suitable for industrial applications. Instead, a mixed consortium-based anodic biofilm can be compared as an electric network where some bacteria take part as electron donors and others as electron acceptors (Patil et al, 2012). Within a multi-species biofilms, in fact, microbes establish close symbiotic relationships, allowing different metabolic pathways (ranging from anaerobic respiration to fermentation) to interact syntrophically, with the anode electrode serving as final electron acceptor (Semenec and Franks, 2015). This makes the biofilm more flexible toward external phenomena such as environmental parameters changes, system design, medium composition etc. However, a more biodiverse biofilm community does not necessarily results in higher MFC power output. It has been proved that co-cultures can exhibit greater electrical output than the respective pure strains thanks to mutualistic syntrophic interactions. On the other hand, it is also conceivable that competition or inhibition events can occur, negatively influencing electrochemical performance (Semenec and Franks, 2015). For instance, Bourdakos et al. (2014) analyzed the extracellular metabolites in air-cathode MFCs inoculated with *G. sulfurreducens* and *E. coli* co-culture, finding that co-culture MFC generated less power (63 mW/m^2) than a control MFC with a *G. sulfurreducens* pure culture (128 mW/m^2). The lower performances had been attributed to the inhibition effect of succinate produced in the co-culture. In general, even though mixed-culture usage reflects several advantages, when consortia are selected as inoculum, non-exoelectrogenic microbes may attach onto the anode surface otherwise colonized by EAMs, drastically diminishing biofilm electrical conductivity (Logan, 2009). So, preventing or minimizing non electroactive bacteria (i.e. methanogens, nitrate-reducer, aerobic microorganisms, H$_2$-scavenging bacteria, fermentative microorganisms) growth onto the anode as biofilm or into the anolyte solution as planktonic cells, may help to improve MFC performances (Borole et al., 2011).

2.5.1.3 EET from exoelectrogenic microbes to anode

EET—extracellular electron transfer process chiefly involves two key steps: first electron transfer from the inner to the outer membrane of the bacterial cell and then electron transfer from the outer membrane to extracellular electron acceptor (Fan and Xue, 2016). However, microbial envelope constitutes other than a physical barrier between cytoplasm and external environment, an electrical barrier, due to the presence of electrically nonconductive components (peptidoglycan, S-layer, etc.) (Shi et al. 2016). To overcome this limit, microorganisms have thrived gripping strategies to perform EET but how the electrons are shuttled from anode-respiring bacteria to electrode surface? Once reached the cell surface, electrons can take different routes, depending on the redox networks involved: (i) DET— direct electron transfer and (ii) MET—mediated electron transfer. A schematic representation of electron transfer mechanisms from microbes to anode is provided in **Figure 2.4**. The model systems, *G. sulfurreducens* and *S. oneidensis*, utilize similar approaches to transfer electrons to and across the outer membrane but differ for the pattern of redox protein employed. Moreover, whereas *Geobacter* requires electronic contact with solid-state electrode, *Shewanella* is capable of donating electrons to the anode without attaching on its surface, just synthesizing redox mediators then secreted into surrounding environment (Nealson and Rowe, 2016). In DET—direct electron transfer microbes attached onto anode surface directly transfer electrons to the electrode, using two main modalities (long-range and short-range EET). The long-range EET consists of electrons shuttling across the biofilm layers via electrically conductive protein-based pili (**Figure 2.4 A**), while the short-range EET occurs at the interphase microbes-electrode via a series of outer-membrane c-type cytochromes (OMCs) (**Figure 2.4 B**) (Patil et al. 2012). Studies with pure-culture of *G. sulfurreducens* strains have intensively contributed to elucidate DET dynamics. *G. sulfurreducens* genome has 111 genes encoding putative c-type cytochromes (c-Cyts), including OmcB, OmcE, OmcS, and OmcZ. Among all the OMCs listed, OmcZ plays a crucial role. It is loosely bound to the membrane surface and accumulates at the biofilm/electrode interface, acting as an "electrochemical gate", by driving electron exchange between microbes attached onto the electrode and anode surface (Inoue et al. 2010). The absence of OmcZ homologs in other *Geobacteraceae* member may explain why they exhibit lower current performance than *G. sulfurreducens* (Nevin et al. 2009). Beyond OMCs, outer-membrane multicopper protein (OmpB and OmpC) are expected to contribute in EET, but their role is still controversial. In *Shewanella* spp. electron transfer mechanism is reliant on MtrCAB–OmcA protein complex, which consists of both cytochromes and structural proteins, with MtrB (nonheme OM b-barrel protein) connecting the multiheme c-Cyts MtrA and MtrC (Patil et al. 2012). In *S. oneidensis* strain MR-1 MtrC deletion caused more than 50% decrease in electricity production (Coursolle et al. 2010). *Geobacter OMCs complex* and *Shewanella spp.* MtrCAB-OmcA complex, are not phylogenetically closed, meaning that they evolved independently (Shi et al. 2014).

Since short-range DET is limited to the nanometer scale, certain EABs produce a dense "grid of conductive pili" in order to extend DET distance and maximize electron exchange rate (Kumar et al. 2017). Today, the conductive properties of these proteinaceous structures are attracting a great interest in the field of bioelectronics materials (Tan et al. 2017). It has been challenged that long-range EET can occur according to two competing models: the electro hopping/tunneling, also known as super-exchange model, and the metallic-like conductivity model. The latter positively correlate pilus conductivity with the distribution of aromatic amino acids into the protein structure of the nanowire (Malvankar et al. 2015). On the other hand, according to electron hopping model the driving force for long-range EET lies on the intrabiofilm redox gradient established by multiheme cytochromes redox state (Harris et al. 2010). Driven by redox gradient, which is higher further from anode, electrons hop between OMCs packed close into pilus structure (Snider et al. 2012). Microbial nanowires were earlier discovered in *G. sulfurreducens* (Reguera et al. 2006). *G. sulfurreducens* pili (20 mm in length with a diameter of 3–5 nm) consist of assemblies of pilin monomers, a relatively small structural protein (Juàrez et al. 2009). Conversely, *S. oneidensis* nanowires lack the pilin-based structure and resemble protrusion of periplasm and external membrane, associated with vesicles, along which mainly MtrC and OmcA are localized (Pirbadian et al. 2014). Although the research efforts made so far largely contributed to postulate the above described models, there is no unanimous consensus on how microbial nanowires support EET.

As the biofilms grow, the number of microorganisms localized further away from electrode increases. Hence, many bacteria naturally secrete endogenous soluble shuttle molecules allowing the EET even at larger distances (**Figure 2.4 C**) (Sydow et al. 2014). The first evidence of self-secreted redox shuttle EET came in 1999 when *S. putrefaciens* was proposed as the first bacterium capable of catalyzing electrochemical reaction at anode electrode in MFCs, without addition of artificial mediators (Kim et al. 1999). Several redox mediators such as flavins (riboflavin and FMN), and phenazines (phenazine-1-carboxylate, pyocyanin, 1-hydroxy-phenazine, phenazine-1-carboxamide) have been detected in bioanodes. *S. oneidensis* (Marsili et al. 2008) and *P. aeruginosa* (Rabaey et al. 2005) represent the most extensively explored for MET understanding. In *S. oneidensis* MR-1, flavins play a double role, acting both as soluble electron shuttles in the anodic medium and as bound cofactors within the biofilm (Okamoto et al. 2014). The prominent role of soluble electron shuttles in *Shewanella* was demonstrated by Marsili et al (2008), who claimed a 75% reduction of current generation as with riboflavins removal. In its monolayer biofilm also *G. sulfurreducens* secretes riboflavins (Okamoto et al. 2014). Despite its contribution to MFC-electrochemical performance, MET is characterized by slow diffusive flux of shuttle molecules and, hence, high potential losses, in comparison with DET.

Exoelectrogens, beyond interacting with the electrode, may syntrophically exchange electrons with other microorganisms that act as metabolic partners, via

the so-called DIET-Direct Interspecies Electron Transfer (**Figure 2.4 D**). The redox compounds involved in DIET are biological components such as the pilus-associated OmcS and microbial nanowires, flagella, phenazines; and non-biological species like H_2, formate, magnetite, hematite, granular activated carbon (GAC), anthrahydroquinone-2,6-disulfonate (AHQDS) (Semenec and Franks, 2015). The first proof of DIET process was observed in a co-culture of *G. metallireducens* and *G. sulfurreducens* (Summers et al. 2010). To date several DIET experimental evidences have been provided but, taking into account the myriad of interspecies electron transfer possible, a deep investigation into the matter is required.

As claimed by Flemming and Wingender, "simply, there is no biofilm without an EPS matrix", which is described as "the house of biofilm cells" to highlight its significant role (Flemming and Wingender, 2010; Flemming et al. 2007). Extracellular Polymeric Substances consists of a hydrated high-molecular-weight mixture of polymers, primarily made up by polysaccharides, proteins, nucleic acids, lipids, humic substances, extracellularly secreted by microorganisms. Beyond serving as a scaffold, due to the presence of cytochromes and microbial nanowires encapsulated in, it has been speculated that EPS may contribute to charge electron transfer (Li et al. 2016b). Therefore, in order to ascertain its putative redox properties, valid methods to characterize EPS matrix redox species are required.
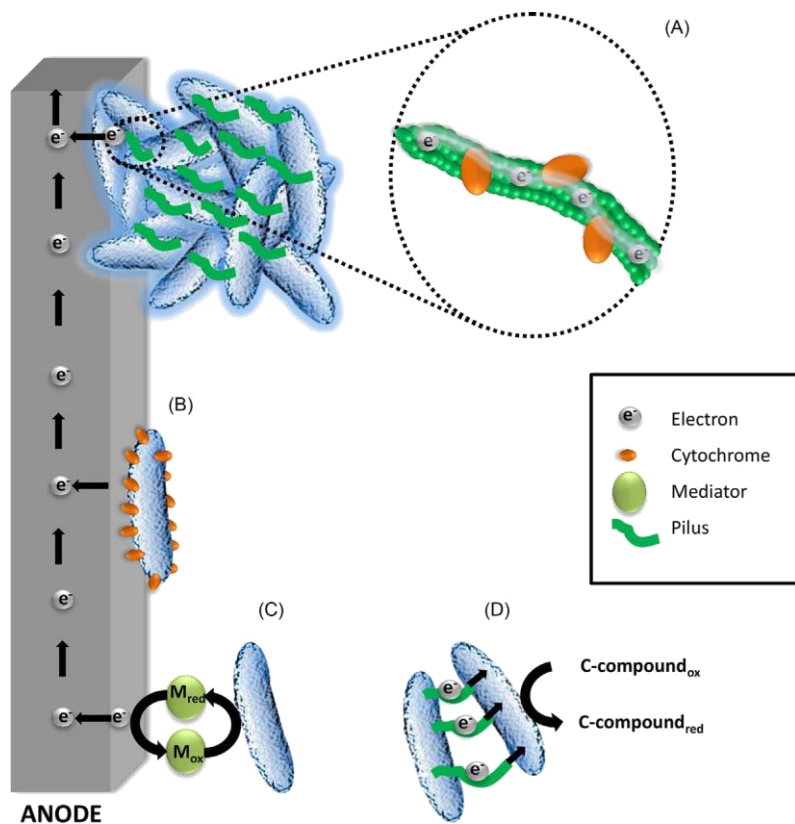
Figure 2.4 Schematic representation of electron transfer mechanisms from microbes to anode: DET via (A) microbial pili and (B) outer-membrane cytochromes; (C) MET mediated by soluble redox-shuttles; (D) DIET via microbial pili.

2.6   Practical applications of MFCs

Multiple and diverse applications have been proposed so far as demonstration of the potential practical value of MFC technology. Usually employed on large scale, MFCs have also been implemented in small-scale for portable applications (Santoro et al. 2017). An overview of the most representative MFC applications is provided below.

2.6.1 Bioelectricity production

MFCs have been described as energy transducers, which release electric energy as by-product of anaerobic respiration (Ieropolous et al. 2013). Hence, the primary and practical application of MFCs consists in bioelectricity generation. This technology is considered extremely innovative since is the only able to produce electricity directly from the oxidation of organic matter. Compared to conventional chemical fuel cell, electricity harvested from MFCs is not limited by the Carnot cycle and heat loss, thus allowing higher conversion efficiency (Ali et al. 2018). Rosenbaum and co-workers (2006) through the oxidation of formate using Pt-black as catalyst obtained a remarkably high CE of 97%. A power density of 3.6 W/m^2 was achieved using glucose as substrate (Rabaey et al. 2003). Recently, the highest value of power densities reached were 4.7 W/m^2 (Yang and Logan, 2016) and 6.4 W/m^2 (Oliot et al. 2017). Regarding Yang and Logan work, immobilization of a Fe-N-C co-catalyst on activated carbon significantly helped increasing the oxygen reduction reaction (ORR), thus resulting in higher electrochemical performances. Beyond, the implementation of novel materials, a further strategy aimed to enhance power output relies on assembly of multiple MFC units into a stacked configuration. A power of 258 W/m^3 was achieved by employing a stacked configuration composed by six units (Aelterman et al. 2006). However, even though over the last decade MFC power output has been increased by a number of orders of magnitude, many blockages are still present and several issues have to be tackled in order to ensure full-scale applications.

2.6.2 Wastewater treatment

An enormous advantage that compensates for the low power output is the possibility to employ MFCs for complementing the established wastewater treatment systems (Ieropolous et al. 2016; Santoro et al. 2017). Whereas conventional biological approaches for low-concentration wastewater treatment are not cost-effective and energy consuming, BESs can be considered as "self-powered wastewater treatment devices" (Roy et al. 2017). MFCs enable to recover up to nine-fold electrical power needed to treat the same amount of wastewater through conventional systems (Borjas et al. 2015). It has been estimated that during the

aeration of activated sludge 0.3 kW/(h·m^3) are consumed and additional pumping power is required during domestic wastewater treatment (Ali et al. 2018). Wastewater treatment by MFC also results in 50-90% less sludge to discard (Holzman, 2005). Additionally, a further advantage is represented by the capability of certain bacteria to remove sulfides. Different types of wastewater have been tested in MFCs ranging from domestic wastewater (Liu et al. 2004), brewery wastewater (Feng et al. 2008), effluents from hydrogen-producing bioreactors (Sharma et al. 2011) etc. MFCs were first applied to treat wastewater in 1991 (Habermann and Pommer, 1991). The first pilot scale with a volume of approximately 1 m^3, was installed in Yatala (Queensland, Australia) and led by the Advanced Water Mangement at the University of Queensland for brewery wastewater treatment (Logan, 2010). Lately, 1000 L modularized MFCs was employed for one year for real municipal wastewater treatment achieving 90% COD removal and up to 60 W/m^3 (Liang et al. 2018). A 98% removal of chemical oxygen demand was reported by Lu et al. (2017), using a 20 L MFC system operating with brewery wastewater for almost one year.

2.6.3 Bioremediation

Remediation involves both degradation of organic pollutants by the anode and reduction of inorganic compounds such as nitrate and uranium at the cathode electrode (Logan et al. 2008). The idea of utilizing biocathode for *in situ* nitrate bioremediation was first suggested by Gregory and co-workers in 2004, when by applying a potential of -0.5 V (vs Ag/Ag/cl) conversion of nitrate to nitrite was obtained using a *G. metallireducens* pure culture. Successively, Gregory and Lovley (2005) reported an 87% of U (IV) recovered on the electrode with a pure culture of *G. sulfurreducens*. Interestingly, *G. metallireducens* was also used for the oxidation of recalcitrant aromatic compounds such as benzoate (Bond et al. 2002) and toluene (Zhang et al. 2010). Recently, a 195 L-benthic MFC was employed as a novel method for river *in situ* restoration allowing sediment organic removal (Li et al. 2017b).

2.6.4 Water desalination

The worldwide water shortages have encouraged the research towards desalination approaches aimed to generate potable water from seawater. Seeking alternative and sustainable treatment technologies would allow reducing the dependency from the high energy-demanding techniques established so far (Roy et al. 2017). Interestingly, microbial desalination cells (MDCs) have been successfully employed with the aim to treat wastewater, simultaneously generating current and desalinating water (Cao et al. 2009). In MDCs desalination occurs due to the potential difference established between the two electrodes in a MFCs. Specifically,

the electrical potential gradient generated by the metabolic activity of exoelectrogens acts as driving force for ion transfer through a series of ion exchange membrane, thus resulting in water desalination. In MDCs, the standard MFC configuration is slightly modified by the addition of a third compartment placed between the anodic and cathodic chambers. The middle compartment is separated from the anode and the cathode, respectively through an anion exchange membrane (AEM) and a cation exchange membrane (CEM). When anodic microorganisms oxidize the organic matter electron and protons are generated; the anions present in the desalination chamber move to the anode whereas cations migrate to the cathode in order to keep charge neutrality. This increases the conductivity of anolyte and catholyte solutions, hence resulting in higher power production. Compared to conventional reverse osmosis (RO) technologies which are supposed to use 2.2 kWh to desalinate 1 m^3 of seawater, MDCs can generate 1.8 kWh by treating the same amount of seawater (Roy et al. 2017). The largest MDC used so far is a 105 L system, which achieved 9.2 kg $m^{-3}d^{-1}$ of salt removal by simultaneously generating 2A of current (Zhang and He, 2015).

2.6.5 Biosensor for environmental monitoring

Another prominent application of MFC technology is the water quality monitoring. Recently MFC-based biosensors have been proposed for toxic compound detection as well as biochemical oxygen demand (BOD) measurement. Advantages related to the use of MFC-based biosensor include the *in situ* and real-time monitoring as well as their economically-effectiveness. This novel approach relies on the fact that in MFCs the electrical signal generated strictly correlates to the metabolic activity of anodic biofilm; thus, changes in electrical output are exhibited in presence of any disturbance compound within the feed water. Notably, when the MFC-based sensor is exposed to a toxic compound, the inhibitory effect on metabolic activity reflects a decrease in current production. Therefore, transducers commonly used to translate the output in readable signal are not required. Due to the high sensitivity, MFCs can be employed as early warming signals (Bajracharya et al. 2016). Moreover, it has been reported that MFC used as BOD sensor can stably operate for over 5 years with not significant maintenance (Chang et al. 2004). Kim et al. (2007) first reported the use of MFC system for detection of heavy metals such as Pb and Hg, pesticides and polychlorinated biphenyls (PCBs).

2.6.6 Power supply for remote areas

Whilst the numerous experimental examples provided above, MFC technology is still in its infancy in terms of implementation in real world applications (Gajda et al. 2018). So far, this biotechnology has been considered more as a lab tool to deepen the knowledge on electromicrobiology. Hence, compared to other technologies, MFCs have received less investment (Santoro et al. 2017). The most

challenging hindrance is the low electrochemical performances intrinsically associated with MFCs (Ivars-Barcelò et al. 2018).

However, MFCs remain a potential and suitable option for powering low energy-demanding electronics. As an example, environmental monitoring is conventionally accomplished by the means of sensors and biosensors (Dewan et al. 2014). The majority of commercially available sensing-devices are generally powered by electrochemical batteries (e.g. lithium batteries) (Ivars-Barcelò et al. 2018). However, traditional batteries are characterized by a short shelf-life and environmental hazardous. Hence, when the sensor is operating in a remote area, periodic battery recharge or replacement becomes obviously challenging, also making the sensor network itself not financially sustainable (Dewan et al. 2014; Ivars-Barcelò et al. 2018). Attempts to provide self-sustainable power sources have been pursued so far. These alternative power-supplies should exhibit the following traits: i) produce power *in situ*; ii) renewable and reliable; iii) reduced human intervention and iv) cover typical power requirements (Dewan et al. 2014). Typical power requirements for sensors deployed in underwater environments (i.e. ultrasonic, infrared, barometric, piezoelectric, electrochemical, oxygen, conductivity and fluorescence sensors) range from 10 mW to 6 W. Similarly, ground sensors (magnetic, infrared or acoustic sensors) commonly employed for weather, volcano and habitat monitoring need from 1 mW to 6 W for their operation. Floating sensors are mainly utilized instead for underwater surveillance for naval/military purposes, ship navigation and sea surface water monitoring with power requirements ranging from 5.4 mW to 85 W. Batteries employed in remote sensors have an output voltage within the range of 1.2 to 12 V. For instance, four 12 V batteries are required for operating an underwater sensor for approximately 2-4 days (Dewan et al. 2014). Alternative power-sources include microbial fuel cells, solar cells, wind and hydroelectric energy. Up to now, numerous studies have been performed using MFCs as power sources for underwater (Donovan et al. 2013; Janani and Murugan, 2018; Reimers and Wolf, 2018), ground (Donovan et al. 2008) and floating sensors (Schievano et al. 2017). One of the first real practical applications is that of EcoBot-I, directly and entirely powered by MFCs (Ieropolous et al. 2003). Pragmatically, this robot used a refined fuel such as sucrose and chemical mediators added into the anolyte. These issues were successfully addressed with the advanced version EcoBot-II, which utilized unrefined insect biomass, natural mediators and air-cathode MFCs (Melhuish et al. 2006). Although extremely captivating, these early proof-of-concept examples did not actually exhibited truly energetic autonomy, since human intervention was still needed (Santoro et al. 2017). This goal was achieved instead by the implementation of EcoBot-III, proposed by Ieropolous's group in 2010. This robot was able to operate for 7 days using the power output released by 48 stacked MFCs. Further practical demonstrations include the charging of a Samsung mobile phone using stacked MFCs fed with urine (Ieropoulos et al. 2013). Four years later, the same research group reported the first urine-based smartphone charger, which allowed 1 h 45 min

phone call for every 3 h of charge time using a 6 modules MFC system as power source (Walter et al. 2017). Moreover, two small-scale MFCs (6.25 ml volume) were implemented as power source for a Texas Instruments Chronos digital wristwatch (Papaharalabos et al. 2013). A single red LED for internal lighting was directly connected to a novel ceramic MFC system, allowing its continuous operation over a 7-day period (Gajda et al. 2015). This particular experiment led to two pee power urinal field trials. The first was conducted at the UWE in Bristol, using 288 MFCs generating an average of 75 mW while the second one was performed during the Glastonbury Music Festival, employing 432 MFCs with a resulting power output of 300 mW (Ieropoulos et al. 2016). This is an interesting finding in the context of sanitation and public heath, since an autonomous waste-based power source is certainly beneficial for providing internal lighting (Ieropoulos et al. 2016). These experimental evidences highlight that MFCs are capable of offering long-term power supply and reducing operational costs and environmental risks (Ivars-Barcelò et al. 2018). In order to overcome limitations related to low power generation, nowadays many strategies are adopted. Beyond MFCs series and parallel configurations, power management systems (PMSs) allow intelligently controlling the energy distribution to the desired system (Dewan et al. 2014; Donovan et al. 2011). Ultra-capacitors are also employed with the aim to store the low energy deriving from MFC operation and adequately deliver it when the level of power output is enough to trigger sensor operation (Ivars-Barcelò et al. 2018). DC/DC converters augment and stabilize the electric potentials of MFCs (Schievano et al. 2017; Ewing et al. 2014), allowing to linearly scale up the power release as a function of the number of MFC units employed.

Considering applications in aquatic environment, sedimentary microbial fuel cells (SMFC) also referred to as benthic MFCs, have been widely exploited. In this configuration, the anode electrode is entirely buried in the anaerobic sediment while the cathode is immersed in the overlying water (river, sea, lake, groundwater etc) at the interphase with air (Roy et al. 2017). The first practical application was described in 2008 by Tender and co-workers who used a benthic MFC to power a meteorological buoy in river and salt marsh environments for over 7 months. A 30 m-long linear array of SMFCs was fabricated to power a seafloor magnetometer (Arias-Thode et al. 2017). This configuration results advantageous because water salinity increases conductivity between the electrodes. Additionally, natural organic matter is continuously and naturally renewed making the maintenance costs approaching to zero. However, the bottlenecks of using SMFC consists in high electrodes distance, which enhances the internal resistance, difficulty in providing continuous power and limited cathodic performance due to the low dissolved oxygen. In order to tackle these limitations, a new configuration called floating MFC has been proposed and experimentally validated in real environment (Schievano et al. 2017; Huang et al. 2012).

Chapter 3

Material and Methods

This chapter is an amended version of the already published manuscript:

Massaglia, G., Margaria, V., Sacco, A., Tommasi, T., **Pentassuglia, S.**, Ahmed, D., Mo, R., Pirri, C.F., Quaglio, M. (2018). *In situ* continuous current production from marine floating microbial fuel cells. *Applied Energy*, 230:78-85.

3.1 Characterization of synthetic solid-state electrolyte (SSE)

Synthetic solid-state electrolyte (SSE) composition is reported in **Table 3.1**.
SSE was prepared by dissolving the desired components in distilled and deionized water and the resulting solution was autoclaved at 121 °C for 15 minutes. 15 ml were poured into Petri dishes and left to solidify under horizontal-flow laminar hood. The SSE was plunged into 150 ml of sterile distilled and deionized water, under anaerobic conditions. A solution containing only 12.5 g/L of Agar was prepared and used as blank. Nutrient release from the SSE to the bulk solution was evaluated. With this aim, samples were withdrawn using sterile syringes and subjected to ionic conductivity and COD analysis. Ionic conductivity was measured using a conductivity probe CO 11 (VWR). COD analysis was performed by photometric determination (Photometer PF-12 Plus, Macherey-Nagel GmbH &Co, Germany) of Chromium (III) concentration after oxidation with potassium dichromate/sulfuric acid/silver sulfate and using Nanocolor kit (Test 0-28, Macherey-Nagel GmbH &Co, Germany). The samples were prepared according to manufacturer's instructions.

Table 3.1 Composition of the synthetic solid-state electrolyte (SSE).

Component	Amount (g/L)
CH_3COONa	20
NH_4Cl	12.4
Agar	12.5

3.2 General microbiology techniques

3.2.1 Inoculum source

Seawater and marine sediment used as inoculum were collected from the bay of La Spezia (Italy) at 3 m depth.

3.2.2 Enrichment procedures

For *in situ* pre-colonization enrichment commercial carbon felt (Soft felt SIGRATHERM GFA5, SGL Carbon) used as anode electrode was buried into the marine sediment within a plastic bottle and left at 3 m underwater for 1 month. With the aim to maximize biofilm formation, the felt was previously soaked in PBS containing 2.5 g/L of sodium acetate. The *in situ* enrichment was performed without the use of polarized electrodes.

According to the standard colonization enrichment protocol, the seawater sediment sample (bay of La Spezia, Italy) was enriched in 250 mL serum bottles with carbon felts placed in. Composition of the liquid medium is reported in **Table 3.2**. Cultures were subjected to three successive enrichment steps (10% v/v) for 1 month of total growth, at room temperature (21 ± 2 °C) and under gentle orbital shaking (150 rpm).

Table 3.2 Liquid medium composition.

Component	Amount (g/L)
CH_3COONa	2.5
NH_4Cl	0.75

The desired components were dissolved in seawater.

3.3 Experimental design

3.3.1 Laboratory tests

Validation of the *in situ* pre-colonization enrichment approach was performed during laboratory tests. For this purpose, MFCs were fabricated using anode electrodes prepared through (i) the novel *in situ* pre-colonization enrichment based on seawater sediment (referred to as *in situ* MFCs) and (ii) the standard enrichment approach (named standard MFCs), as described in Section 3.2.2. Three nominally identical MFCs for each biofilm enrichment procedure were assembled and placed in a bucket filled with seawater so that the cathodes were directly exposed to air whereas the anodes were entirely immersed into the seawater. The water level was maintained constant by refilling with seawater every 7 days, without adding extra nutrients. Laboratory tests were conducted at room temperature (21 ± 2 °C). The performance of the *in situ* MFCs was compared with that of the standard MFCs by electrochemical characterization conducted as outlined in Section 3.6.

3.3.2 *In situ* tests

Field tests were carried out in the Mediterranean Sea, in a bay near La Spezia (Italy), using a dedicated floating MFC-based set-up, sketched and described below (Section 3.4.2). The first field measurement campaign was carried out during

summertime, from July 22nd to September 18th, 2016 (58 days). For this campaign, six nominally identical MFCs were fabricated employing *in situ* pre-colonized electrodes and mounted in a black opaque enclosure. After the first experimental phase, MFCs were moved from the bay of La Spezia to the laboratory to be further characterized and successively four out of the six devices were re-used during the second measurement campaign. The second field measurement campaign was performed during late autumn/winter for a period of 45 days (from December 1st to January 15th, 2017). The electrochemical performance of the MFCs was monitored for a period of two months as in Section 3.6.

3.4 Set-up configuration

3.4.1 Single-chamber air cathode MFC

MFC prototype used is shown in **Figure 3.1**. The squared single-chamber MFCs with an open-air cathode configuration were fabricated by 3D printing technology (OBJET 30, Stratasys) using a polymeric UV-curable material (polymethyl-methacrylate, PMMA), as outlined in Massaglia et al. 2017. The MFC internal volume was 12.5 mL. The MFC modular design comprises an anode module, an inner module constituting the inner chamber and a cathode module (**Figure 3.1a**). As for the anodes, cathode electrodes were also made of commercial carbon felt, both having a nominal geometric area of 5.76 cm^2. Cathodes were modified by applying four polytetrafluoroethylene (PTFE) diffusion layers on the external side of the electrode (Massaglia et al. 2017). Ti wires were placed into the texture of carbon felt material and employed as current collectors. No catalyst layer was applied to the cathodes, allowing the spontaneous formation of an aerobic cathodic biofilm.

a)

b)
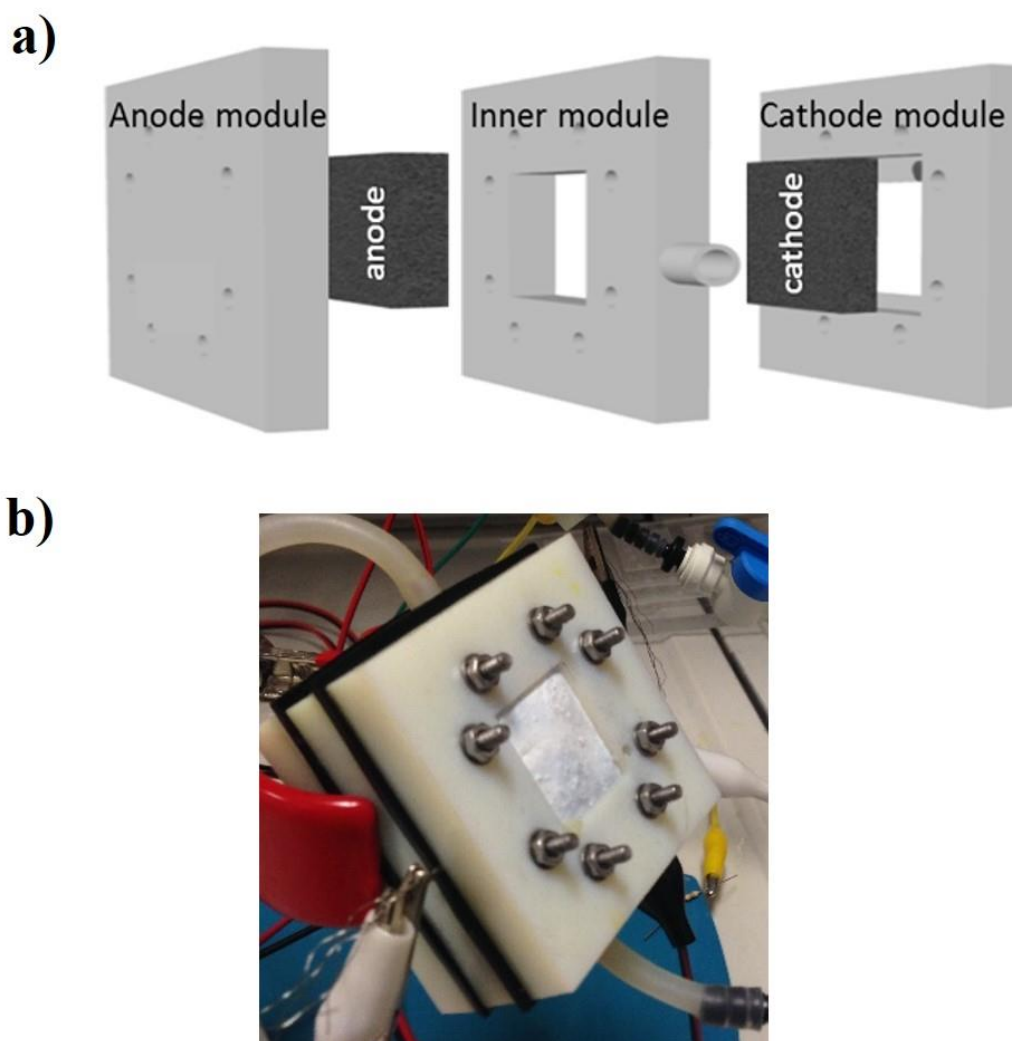
Figure 3.1 Representation of the single-chamber MFC used in the current study. Panels: a) schematic design of the modular device and b) picture of the MFC.

For each MFC, 6 mL of the SSE at a temperature equal to 50 °C (liquid state) were poured into a Petri dish until solidification. The agar-based SSE was then randomly broken and the resulting fragments located onto the anode surface, within the anodic module, as shown in **Figure 3.2**.
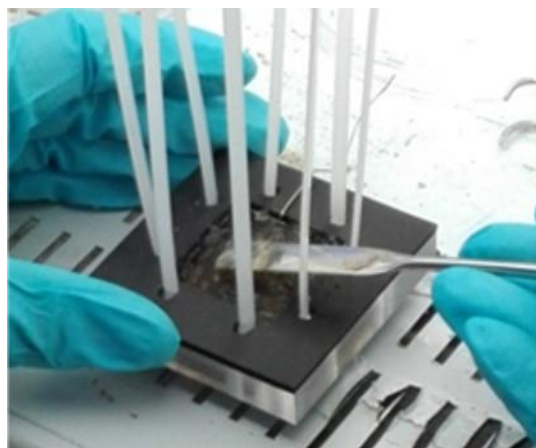
Figure 3.2 Positioning of the synthetic solid-state electrolyte (SSE) onto the anode electrode.

3.4.2 MFC-based floating system

During the on field experiments, MFCs were placed in a floating housing system, which was anchored at a distance of 2 m from the pier. A multipolar cable with protective outer shell (Igus CF9.02.12) (**Panel c)** in **Figure 3.3**) was used to electrically connect the cell outputs (cathodes and anodes) to the control room, where the data acquisition (**Figure 3.3a**) system was set-up. The latter consisted of a programmable relay board (Devantech ETH8020), a control board (Raspberry Pi 2 model B) and a modem. The relay board was equipped with eight data acquisition channels and different resistors, thus allowing the measurement of each MFC voltage over a fixed load. Voltage signals acquired by the different channels were transduced by analog/digital converters and sent to the modem through the control board. A custom software was developed to facilitate the remote acquisition of MFCs' voltage data and the programming of the relay board, using a PC or a smartphone connected to the internet. Inside the floating set-up (**Panel b)** in **Figure 3.3**), Ti wires corresponding to anode and cathode of each MFC were connected with the wires of the multipolar cable. A thermosetting resin was used to insulate the electrical connections. The resulting floating system (**Figure 3.3d**) was employed during the *in situ* tests.
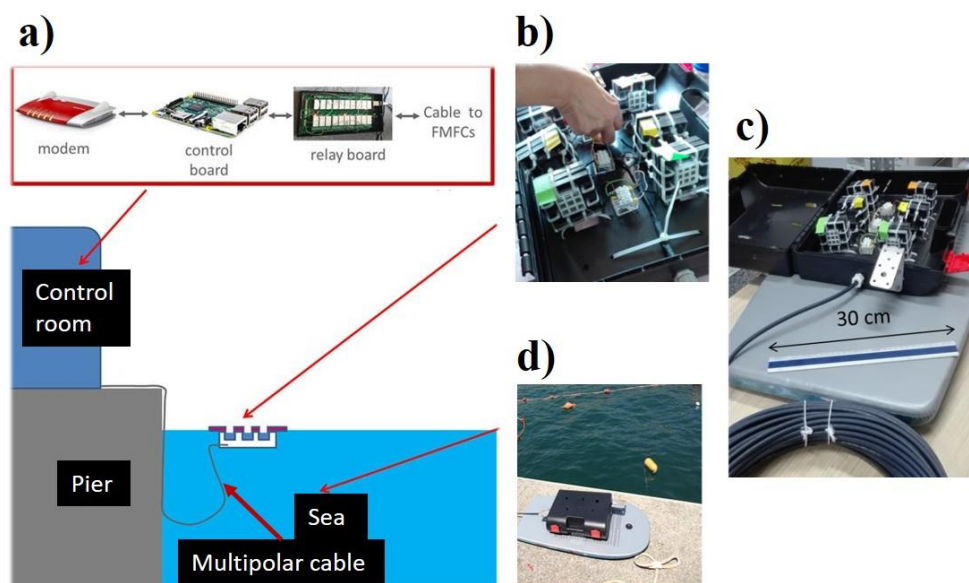
Figure 3.3 Representation of the set-up utilized during on field experiments in the bay of La Spezia (Italy). Panels: a) data acquisition system; b) internal view of the MFC-based floating set-up; c) assembled floating system connected with the multipolar cable; d) bottom view of the floating system before employment in seawater.

3.5 Environmental parameters monitoring

Throughout the on field investigations, seawater physicochemical parameters such as temperature, pH, conductivity, salinity and dissolved oxygen, were acquired using a Geoves SMx-485 multiparametric meter.

Table 3.3 Average physico-chemical parameters of seawater recorded during the two outdoor measurement campaigns.

Period	T (°C)	Conductivity (mS/cm)	Salinity	pH	Dissolved O$_2$ (mg/L)
Summer	26.6 ± 2.5	59.0 ± 2.9	38.1 ± 0.3	7.9 ± 0.3	8.7 ± 0.5
Winter	15.1 ± 2.0	38.3 ± 2.7	32.5 ± 0.6	8.3 ± 0.2	9.0 ± 0.5

3.6 Electrochemical techniques

3.6.1 Voltage monitoring (VM)

During tests performed in the laboratory, cell voltage across a 560 Ω resistor was monitored using an Agilent 34972A data acquisition unit, for around 40 days. 560 Ω resistor was also selected for the *in situ* experiments, during which voltage monitoring (VM) was carried out utilizing the data acquisition system above

described. The resulting current output was calculated by using Eq. 2.6. Current and power densities were calculated based on the cathode geometric area.

3.6.2 Electrochemical impedance spectroscopy (EIS)

EIS measurements were carried out using a BioLogic VSP potentiostat in 2-electrodes configuration, employing the external resistor method (Agostino et al. 2017), with a load of 560 Ω; the AC signal amplitude was 10 mV and it was performed over a frequency range of 10 mHz–20 kHz.

Chapter 4

Marine consortium provides continuous current production in Floating MFCs

This chapter is an amended version of the already published manuscript:

4.1 Introduction

When dealing with applications in aquatic environments, sedimentary microbial fuel cells (SMFCs) are usually exploited (Ewing et al. 2017). In this configuration, the anode is completely buried in sediment, which is rich in organic matter, while the cathode is suspended in overlying water (Song and Jiang, 2011). The anoxic conditions are preserved at the anode due to the presence of the sediment and the device can work for long time with low or null maintenance costs (Tender et al. 2008). Usually, SMFCs are characterized by large dimensions (Hong et al. 2009; Hsu et al. 2017), and thus, after deployment, they are used *in situ* (Zabihallahpoor et al. 2015). SMFCs were employed by Tender et al. to supply power to a meteorological buoy in river and salt marsh environments (Tender et al. 2008). Arias-Thode et al. fabricated a 30 m-long linear array of SMFCs to power a seafloor magnetometer for the detection of passing ship movements (Arias-Thode et al. 2017). Zhang and Angelidaki reported the use of a SMFC based on two pieces of bioelectrodes to remove nitrates and nitrites from eutrophic lakes (Zhang and Angelidaki 2012). Nevertheless, SMFCs are characterized by some disadvantages, including low operating voltages (Donovan et al. 2013), large ohmic losses due to a large distance between the electrodes (An et al. 2013), restricted dissolved oxygen availability which limits cathode performance (Wang et al. 2017) and difficulty in providing continuous power (Donovan et al. 2008). In order to overcome some of these limitations, floating MFCs (FMFCs) have recently been proposed for aquatic applications, either with wastewater (Martinucci et al. 2015) or seawater (Erable et al. 2013). This configuration is similar to an air cathode single-chamber MFC (Mateo et al. 2018), in which both electrodes share the same reactor volume, using oxygen from air for the reduction reaction at the cathode (Jannelli et al. 2017). Since FMFCs can float on the water surface, the cathode is directly exposed to air. Moreover, to limit the ohmic losses, the interelectrode distance is reduced. FMCFs with dimensions up to 0.3 m^2 were employed in the denitrification tank of a wastewater plant (Martinucci et al. 2015) and in a "floating garden" over a pond (Schivano et al. 2017), to power remote environmental sensors and data transmission devices. In all the works described above, the devices were immobilized in the environment in which they worked, either providing power to an external load or acting as water treatment elements. However, portability and small dimensions are strict requirements for several applications, for example when the device to be powered (sensor, instrumentation, etc.) is moving in the water or along its surface.

4.1.1 Aims of this study

The main objective of this work was to propose a novel and compact floating set-up, based on small-scale single-chamber MFCs, able to continuously produce electricity in real marine environment using seawater as fuel and electrolyte. This study represents the first application of small-scale FMFCs in a real marine environment, in view of a future exploitation as portable power sources for low-power sensors and devices. An alternative enrichment approach based on *in situ* pre-colonization of the anodic material was validated and compared to the conventional enrichment procedure. The devices were characterized in laboratory and in the bay of La Spezia (north of Italy), exploiting a dedicated set-up for data acquisition and transmission. Field tests were repeated twice during summer and winter, in order to identify potential effects of temperature on the microbial activity and consequently on MFCs' electrochemical performance. Additionally, for the first time the applicability of a synthetic solid-state electrolyte (SSE) was tested in real environment.

4.2 Results and discussion

4.2.1 SSE and nutrient release

In order to boost microbial metabolism, especially during the start-up phase, the anode electrode was used in conjunction with an agar-based synthetic solid-state electrolyte (SSE), containing CH_3COONa and NH_4Cl as carbon and nitrogen sources, respectively. Beyond providing nutrients required for bacterial growth, SSE allowed keeping the anode chamber partially anaerobic, serving as a physical filter for O_2. The implementation of SSEs in MFCs has already been demonstrated by our research group (Tommasi et al. 2016a). However, its applicability in real environment has not been tested so far. In the current study, the capability of the SSE of releasing nutrients was experimentally validated as outlined in Section 3.1. When release of nutrients from the SSE to the bulk solution occurs, this event results in measurable changes of composition and ionic conductivity of the aqueous solution. Hence, ionic conductivity and COD were selected as indicators of nutrient release. As displayed in **Figure 4.1**, the ionic conductivity of the solution containing the SSE sharply increased within 24 h, reaching a plateau after 3 days with a value around 16 mS/cm. Even though the observed profile clearly differed from that of the control SSE, to further confirm whether the depletion of carbonaceous nutrients in the SSE occurred, COD analysis of the bulk solution was conducted. A COD value of 5.6 g/L O_2 was measured after 3 and 23 days. The profile observed over the time is conceivable since in abiotic conditions no concentration gradient driving the diffusion of the desired species to the liquid phase is established. Moreover, COD was not detectable in the blank solution. This finding demonstrated that the

41

SSE structure with agar working as cross-linker, was not compromised over the course of the entire experiment. The contribution of agar as carbon source is conversely expected in real environment, due to the presence of agarolytic bacteria in both marine sediments and in seawater (Chi et al. 2012).
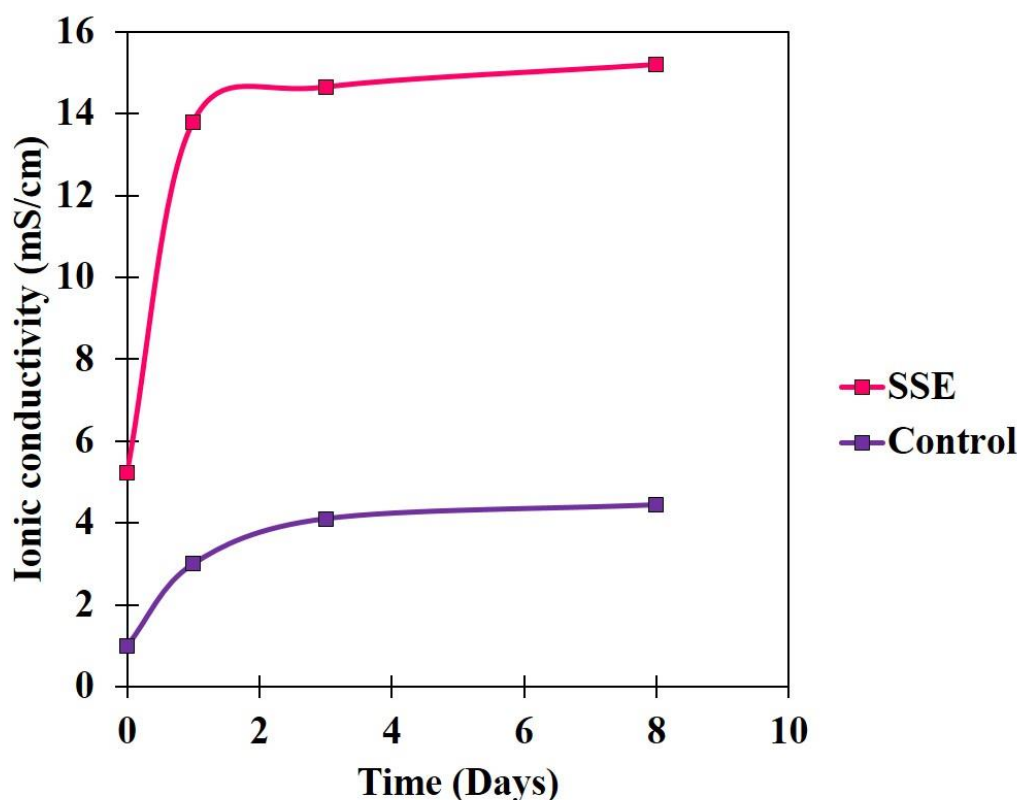
Figure 4.1 Profile of the ionic conductivity (mS/cm) of the solutions containing the synthetic solid-state electrolyte (SSE) and the control SSE.

4.2.2 Laboratory tests

To investigate the feasibility of the *in situ* pre-colonization enrichment approach for anode preparation, the performance of three *in situ* MFCs was compared with that of three standard MFCs. Results of the VM measurements over time are shown in **Figure 4.2**. During the first four days, after device start up, a substantial increment in electrical power production was observed for both types of cells, with maximum values of about 18 ± 2 mW/m^2 and 10 ± 3 mW/m^2 for standard and *in situ* MFCs, respectively (corresponding to 227 mA/m^2 and 178 mA/m^2). This initial rise of current density may be attributed to the presence of carbon and nitrogen sources in the SSE, which helps the biofilm metabolic activity (Tommasi et al. 2016a). Vice versa, the drop of current production observed around day 4 can likely be related to the depletion of nutrients within the SSE, consumed during the biofilm formation. Eventually, seawater was the only fuel source remaining,

containing a lower concentration of organic compounds with respect to the SSE. It is worth noting that starting from the sixth day, the electrochemical performance of *in situ* MFCs appeared to be higher with respect to standard MFCs. This behavior can be explained by considering that *in situ*-developed biofilms are accustomed to grow and proliferate in marine environment, using seawater as nutrient source; on the contrary, standard-enriched microorganisms need to be acclimated into the new environment, and their adaptability resulted to be lower. After 35 days, both kinds of devices exhibited quite constant power density values, equal to about 1.0 ± 0.3 mW/m^2 and 0.8 ± 0.1 mW/m^2 for *in situ* and standard MFCs, respectively; the corresponding current density values were 40 mA/m^2 and 33 mA/m^2.
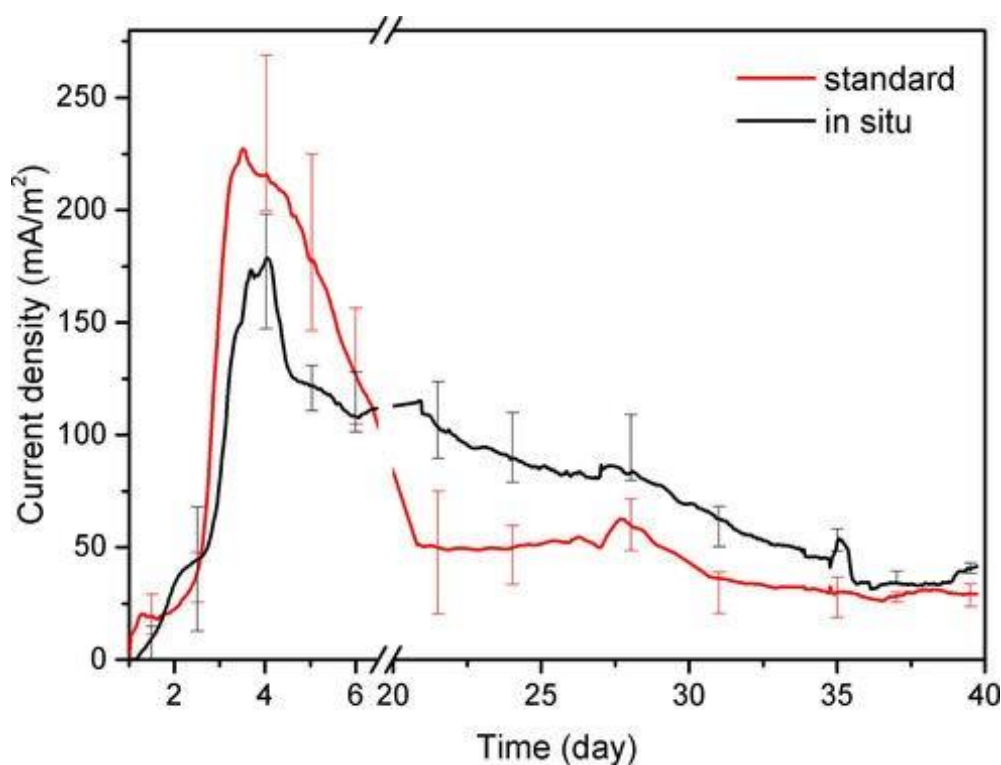
Figure 4.2 Current density as a function of time during the indoor tests for MFCs fabricated with anodes colonized with the two enrichment approaches. Each point is the average of data obtained from three nominally identical MFCs, and maximum and minimum values are reported as error bars. The break between days 7 and 20 was due to an electrical black-out.

The results of VM measurements were successfully confirmed by EIS analysis (Sacco, 2017; Manohar et al. 2008). Typical Nyquist plots related to the MFCs fabricated with anodes colonized with the two different methods are reported in **Figure 4.3**. Both impedance spectra exhibit two features, a high-frequency one (on the leftmost part of the graph) related to the cathode polarization, and a low frequency one, related to the anode (Tommasi et al. 2016b); no feature related to ionic diffusion was evidenced in these Nyquist plots, probably because it was masked by the large capacitive behavior characterizing the felt electrodes (Agostino

et al. 2017). As evident, both kinds of devices exhibit similar cathode resistance: this result was expected, since this electrode is identical in all the fabricated devices. On the contrary, *in situ* MFCs were characterized by slightly lower anodic resistances, in accordance with the above reported VM results. In order to quantitatively evaluate the internal resistances, impedance spectra were fitted through the equivalent electrical circuit shown in the inset. This comprises of: (i) a series resistance Rs related to the ohmic losses in the devices, (ii) a parallel combination of the charge transfer resistance R1 and the Helmholtz layer capacitance Q1 (fitted with a constant phase element (Hidalgo et al. 2015) accounting for the cathodic process and (iii) a parallel combination of the charge transfer resistance R2 and the Helmholtz layer capacitance Q2 accounting for the anodic process. The curves obtained through the fitting procedure are reported in **Figure 4.3**, superimposed over the experimental data. In agreement with the qualitative analysis above reported, series and cathodic resistances are quite similar for both kind of devices, while anodic resistances were found to be about 448 Ω and 500 Ω for *in situ* and standard MFCs, respectively. All of these results confirmed that our novel pre-colonization enrichment approach allowed obtaining anodic biofilms able to successfully be employed in MFCs without the need of any laboratory procedure. The latter, indeed, requires multiple steps to be carried out by the operator and involves the use of several reagents. Moreover, it requires the removal of the microbiota from its natural environment with possible effects on its composition. On the other hand, the novel enrichment approach presents various advantages: (i) it minimizes operator tasks, since it involves only the burial of the carbon electrodes in the sediment and their subsequent immersion in seawater; (ii) drastically reduces the use of reagents; (iii) leaves the microbiota in its natural environment. Therefore, *in situ* colonized electrodes were used during the subsequent tests.
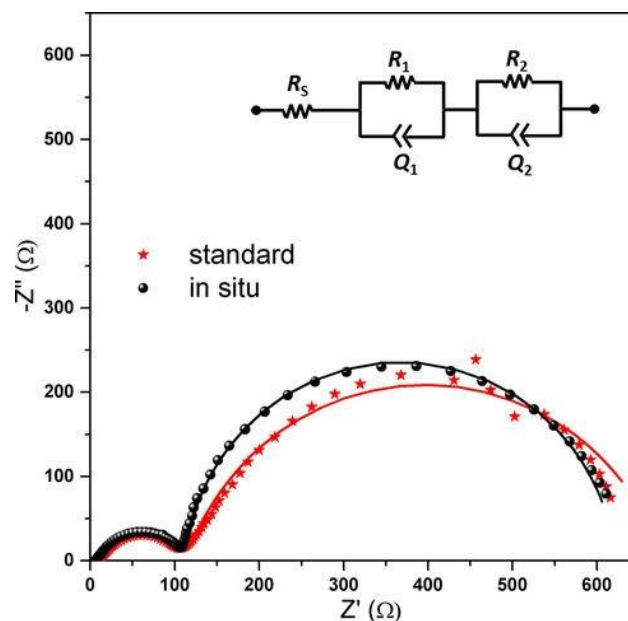
Figure 4.3 Typical impedance response (Nyquist plot) of MFCs fabricated with anodes colonized with the two enrichment approaches. The points are experimental data, while the lines are related to the fitting procedure performed using the circuit shown in the inset.

4.2.3 *In situ* experiments

As mentioned above, for the first field measurement campaign, six nominally identical FMFCs based on *in situ* pre-colonized anodes were fabricated, and their power production in real marine environment was evaluated during summertime over a period of two months. With the exception of two devices (MFC4 and MFC5, discussed below), the average current density produced by the remaining four cells is shown in **Figure 4.4**. During the first 15 days, these devices exhibit large current production, in agreement with the initial stage of the indoor tests. After this period, they were able to produce a stable output power of about 6 mW/m^2 (135 mA/m^2) until the end of the test. By comparing this value with the one obtained during laboratory experiments, it can be concluded that the continuous supply of "fresh" seawater, together with the movement of the floating system (which allows an effective fluid flow inside the devices), is responsible for the larger current production in marine environment. Interestingly, the effect of seawater temperature variation between daytime and night-time were observed. As reported in **Figure 4.5**, a variation of about ±50% was measured between 5:00 AM (minimum point) and 1:00 PM (maximum point). This effect was already observed in previous laboratory and in situ studies: Velasquez-Orta and coworkers found that among different environmental and design factors (salinity, temperature and external resistance), temperature presented a statistically significant effect on the current response (Velasquez-Orta et al. 2017); Ren et al. employed a miniaturized MFC to study the power production in various temperature ranges, finding an optimal condition with larger amount of cytochrome c contributing to extracellular electron transfer (Ren et al. 2017). Based on these outcomes, the variation of the current in **Figure 4.5** can be attributed to the influence of the external temperature on bacterial metabolism. However, it is worth noticing that the observed current density (and power) cycles are repeatable, leading to mean values which remain constant over time, as reported in **Figure 4.4**. Concerning the remaining two devices, their performance are also shown in **Figure 4.4** After the initial stage, MFC5 started experiencing some issues, which led to a sudden decrease of the current density at day 19. Moreover, starting from day 30, its performance abruptly fell down, and it was characterized by low power density values for all the remaining period of investigation (about 30 μW/m^2, corresponding to 9 mA/m^2). On the contrary, MFC4 suffered from electrical connection problems: due to these issues, the device was, cyclically, connected and disconnected to/from the external resistor load, thus the measured current values do not represent the actual power produced by this cell during the whole duration of the campaign.
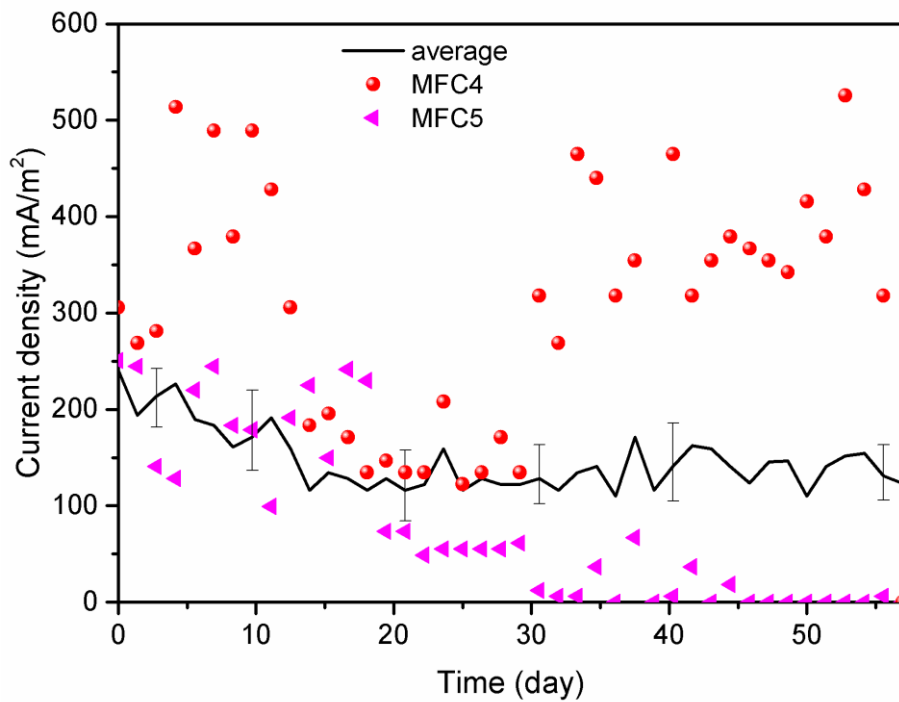
Figure 4.4 Current density as a function of time during the first campaign of outdoor tests for MFCs fabricated with *in situ* pre-colonization anodes: the continuous line represents the average value of 4 devices (MFC1, MFC2, MFC3 and MFC6) with maxima and minima reported as error bars, while the points are related to MFC4 and MFC5.
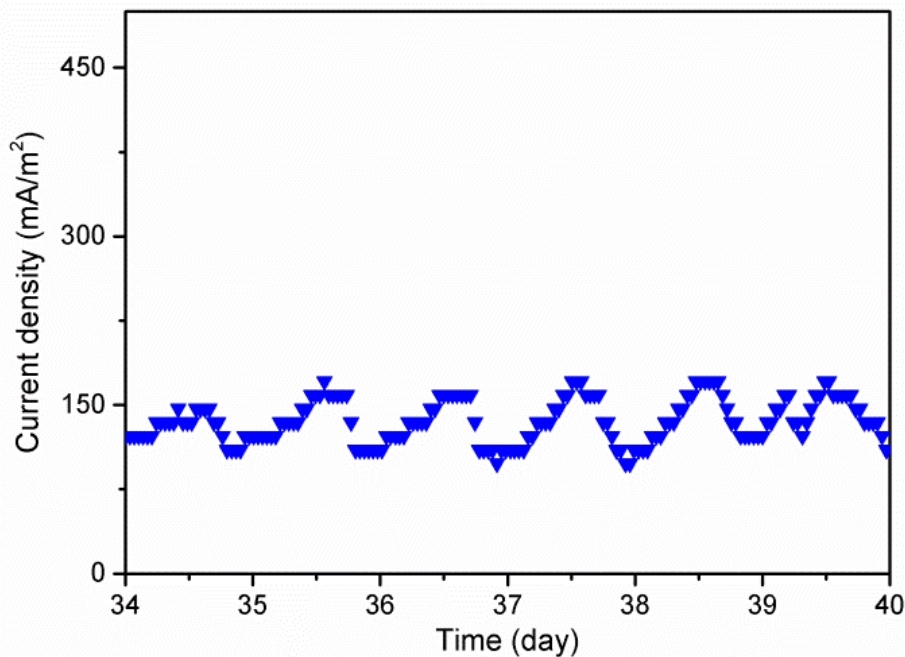
Figure 4.5 Current density as a function of time during six days of the first campaign of outdoor tests highlighting the effect of temperature on device performance.

46

After the end of the first campaign, in order to investigate the observed decay in MFC5 performance and to solve the connection problems of MFC4, all the six devices were transferred to laboratory. They were kept under VM and immersed in seawater at room temperature. Results of VM measurements showed that all the devices (including MFC5) gave a stable output of about 2 mW/m^2 (data not shown), in agreement with the indoor tests results no connection issues were evidenced for MFC4. Based on these results, two out of six devices (namely MFC1 and MFC2) were kept for further experiments that are out of the scope of this thesis, while the remaining four cells were selected to be mounted on the floating system for the second field measurement test. Results of the VM measurements associated to the second campaign are shown in **Figure 4.6**, with the exception of data related to MFC4, which once again suffered from connection problems. Therefore, current density values of this cell were not reliable and are not reported. From the analysis of this graph, a large power production for MFC5 can be seen during the first 15 days, followed by a rapid decrease to minimum values, similarly to what was observed during the first field campaign. On the contrary, the remaining two cells were able to produce a quasi-constant output for all the period of investigation. By comparing these results with those obtained during the first campaign, it can be concluded that no appreciable difference between the two seasons was evidenced concerning FMCFs' performance, despite about 10 °C temperature variation. The gradual temperature decrease between summer and winter allowed microorganisms to progressively adapt their metabolism to environmental temperature. On the contrary, the results observed during day/night cycle can be associated with a quick temperature change which did not allow a metabolic adjustment (Eriksson et al. 2002), similarly to what observed by Hall and coworkers (Hall et al. 2010).
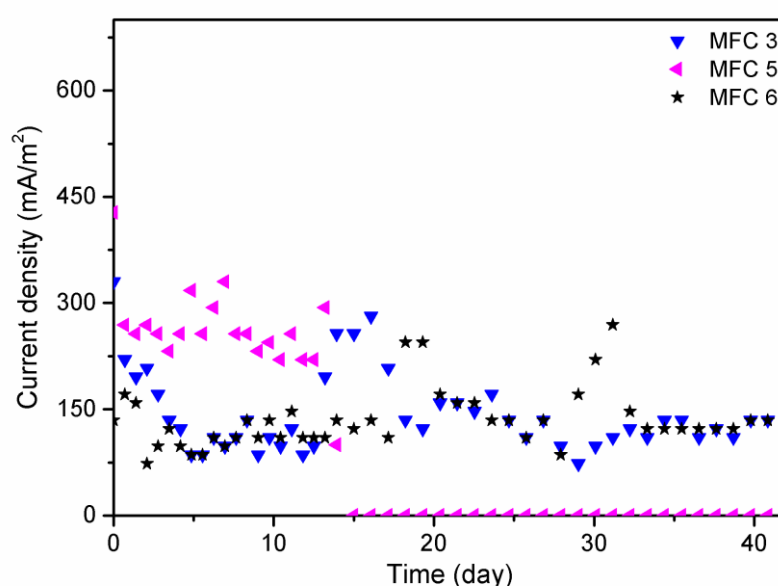
Figure 4.6 Current density as a function of time during the second campaign of outdoor tests for MFCs fabricated with in situ pre-colonization anodes.

The results of the two measurement campaigns demonstrated that small-scale FMFCs can efficiently produce electrical energy using seawater as fuel. This feature, combined with the low cost of the used materials (basically, carbon electrodes and polymeric housing set-up) and the ease of the anode colonization enrichment approach, makes the technological approach proposed in this work an effective way to design cheap and portable systems, which are able to harvest green and renewable energy from marine environment. So far, very few works reported current production using FMFCs in field marine environments (Erable et al. 2013; Huang et al. 2012). These works generally presented PEM-based large-volume devices. In Huang et al. (Huang et al. 2012), the membrane, which separates granular graphite anode and Pt-covered carbon fibers cathode, is arranged as a 4.5 L tube, and the cell is able to produce 4 mW/m^2; Erable et al. (Erable et al. 2013) employed titanium covered with iridium and tantalum oxides as anode, and stainless steel as cathode, obtaining 20 mW/m^2 using acetate and seawater as fuel. These power density values are in line or larger with respect to the one obtained in this work; however, it must be highlighted that expensive materials have been employed in the above reported papers (PEMs, cathode catalyst, Ir) and, in both cases, anodic biofilms were formed in laboratory and then transferred to the final device, thus implying additional costs. On the contrary, quite low power density values were obtained in laboratory experiments, with the exception of Song et al. (Song et al. 2010), which attained 311.2 mW/m^2 employing composite anode, Pt-covered carbon cathode, and glucose, macro and micronutrients as fuel.

Despite the relatively low values, power densities obtained in this work are nevertheless sufficient to provide power to small sensors and devices. As an example, Zhang et al. (Zhang et al. 2011), whose SMFCs were able to produce 2.2 mW/m^2, demonstrated the possibility to power a wireless temperature sensor employing a power management system (PMS) based on a supercapacitor to store the energy produced by MFCs. In the work of Gong et al. (Gong et al. 2011), a seawater oxygen sensor and an acoustic modem capable of routing data from the sensor itself (with power needed for the modem quiescent state equal to 3 mW) were powered through MFCs. In this case, the PMS was based on a 200 F supercapacitor and a backup battery. These examples suggest that, if coupled with an appropriate PMS, our FMFC system could be employed as a low-power source, especially when portability is essential. However, considering the malfunctioning of MFC4 and MFC5, the proposed technology and experimental set-up need to be optimized. As discussed before, during the field tests, MFC4 experienced electrical issues, which caused repeated connection/disconnection cycles to/from the external resistor load. The connection issue may be attributed to the field experimental setup, in particular to some failures of the relay board, which rendered the link between device and resistive load unstable. On the other hand, a different mechanism lies behind the observed behavior of MFC5. In this case, during both field campaigns, after an initial stage characterized by a current production of about 200 mA/m^2, its

performance substantially reduced (**Figures 4.4** and **4.6**). This feature could be explained by considering a mechanical failure between one of the electrodes and its current collector, induced by the seawater flow.

4.3   Conclusions

This work presents a cost-effective floating set-up for MFCs operating in a real marine environment. This set-up can be particularly beneficial when portability and small dimensions are required. An *in situ* pre-colonization enrichment approach of the anode electrode coupled with the exploitation of a solid-state electrolyte allowed releasing continuous current production from floating microbial fuel cells during two distinct field measurement campaigns, using seawater as the sole fuel. An average power density of 6 mW/m^2 was obtained during summertime and wintertime, with negligible seasonal effects although a water temperature difference of about 10 °C. Despite the observed connection issues, the floating MFC setup exhibited promising results.

Chapter 5

References

Aelterman, P., Rabaey, K., Verstraete, W., Pham, H. T. and Boon, N. (2006). Continuous electricity generation at high voltages and currents using stacked microbial fuel cells. *Environmental Science and Technology*. 40: 3388–3394.

Agostino, V., Ahmed, D., Sacco, A., Margaria, V., Armato, C. and Quaglio, M. (2017). Electrochemical analysis of microbial fuel cells based on enriched biofilm communities from freshwater sediment. *Electrochimica Acta*, 237: 133–143.

Ali, J., Sohail, A., Wang, L., Haider, M.R., Mulk, S. and Pan, G. (2018). Electro-microbiology as promising approach towards renewable energy and environmental sustainability. *Energies*, 11: 1822.

An, J., Kim, B., Nam, J., Ng, H.Y. and Chang, I.S. (2013). Comparison in performance of sediment microbial fuel cells according to depth of embedded anode, *Bioresource Technology*, 127: 138–142.

Arias-Thode, Y.M., Hsu, L., Anderson, G., Babauta, J., Fransham, R., Obraztsova, A., Tukeman, G. and Chadwick, D.B. (2017). Demonstration of the SeptiStrand benthic microbial fuel cell powering a magnetometer for ship detection. *Journal of Power Sources*, 356: 419–429.

Bajracharya, S., Sharma, M., Mohanakrishna, G., Benneton, X.D., Strik, D., Sarma, P.M. and Pant, D. (2016). An overview on emerging bioelectrochemical systems (BESs): Technology for sustainable electricity, waste remediation, resource recovery, chemical production and beyond. *Renewable Energy*, 98: 153-170.

Bogino, P.C., Oliva, M.M., Sorroche, F.G. and Giordano, W. (2013). The Role of Bacterial Biofilms and Surface Components in Plant-Bacterial Associations. *International Journal of Molecular Sciences*, 14: 15838–15859.

Bond, D.R., Holmes, D.E., Tender, L.M. and Lovley, D.R. (2002). Electrode-reducing microorganisms that harvest energy from marine sediment. *Science*, 295: 483-485.

Bond, D.R. and Lovley, D.R. (2005). Evidence for Involvement of an Electron Shuttle in Electricity Generation by *Geothrix fermentans*. *Applied and Environmental Microbiology*, 71: 2186–2189.

Borjas, Z., Ortiz, J., Aldaz, A., Feliu, J. and Esteve-Nùñez, A. (2015). Strategies for reducing the start-up operation of microbial electrochemical treatments of urban wastewater. *Energies*, 8: 14064-14077.

Borole, A. P., Reguera, G., Ringeisen, B., Wang, Z.W., Feng, Y. and Kim, B.H. (2011). Electroactive Biofilms: Current Status and Future Research Needs. *Energy and Environmental Science*, 4: 4813–4834.

Bourdakos, N., Marsili, E. and Mahadevan, R. (2014). A defined co-culture of *Geobacter sulfurreducens* and *Escherichia coli* in a membrane-less microbial fuel cell. *Biotechnology and Bioengineering*, 111: 709-718.

Cao, X., Huang, X., Liang, P., Xiao, K., Zhou, Y., Zhang, X. and Logan B.E. (2009). A new method for water desalination using microbial desalination cells. *Environmental Science and Technology*, 43: 7148–52.

Chang, I.S., Jang, J.K., Gil, G.C., Kim, M., Kim, H.J., Cho, B.W. and Kim, B.H. (2004). Continuous determination of biochemical oxygen demand using microbial fuel cell type biosensor. *Biosensor and Bioelectronics*, 19: 607-613.

Chi, W.J., Chang, Y.K. and Hong, S.K. (2012). Agar degradation by microorganisms and agar-degrading enzymes. *Applied Microbiology and Biotechnology*, 94: 917-30.

Cohen, B. (1931). The bacterial culture as an electrical half-cell. *Journal of Bacteriology*, 21: 18-19.

Coursolle, D., Baron, D.B., Bond, D.R. and Gralnick, J.A. (2010). The Mtr respiratory Pathway is essential for reducing flavins and electrodes in Shewanella oneidensis. *Journal of Bacteriology*, 192: 467-474.

Dewan, A., Ay, S.U., Karim, M.N. and Beyenal, A. (2014). Alternative power sources for remote sensors: a review. *Journal of Power Sources*, 245: 129-143.

Donovan, C., Dewan, A., Heo, D. and Beyenal, H. (2008). Batteryless, wireless sensor powered by a sediment microbial fuel cell. *Environmental Science and Technology*, 42: 8591–8596.

Donovan, C., Dewan, A., Peng, H., Heo, D. and Beyenal, A. (2011). Power management system for a 2.5 W remote sensor powered by a sediment microbial fuel cell. *Journal of Power Sources*, 196: 1171-1177.

Donovan, C., Dewan, A., Heo, D., Lewandowski, Z. and Beyenal, H. (2013). Sediment microbial fuel cell powering a submersible ultrasonic receiver: new approach to remote monitoring. *Journal of Power Sources*, 233: 79-85.

Du, Z., Li, H. and Gu, T. (2007). A state of the art review on microbial fuel cells: A promising technology for wastewater treatment and bioenergy. *Biotechnology advances*, 25: 464-482.

Erable, B., Lacroix, R., Etcheverry, L., Féron, D., Delia, M.L. and Bergel, A. (2013). Marine floating microbial fuel cell involving aerobic biofilm on stainless steel cathodes, *Bioresource Technology*, 142: 510–516.

Eriksson, S., Hurme, R. and Rhen, M. (2002). Low-temperature sensors in bacteria. *Philosophical Transaction of the Royal Society B*, 357: 887-893.

Ewing, T., Ha, P.T., Babauta, J.T., Tang, N.T., Heo, D. and Beyenal, H.(2014). Scale-up of sediment microbial fuel cells. *Journal of Power Sources*, 272: 311-319.

Ewing, T., Ha, P.T. and Beyenal, H. (2017). Evaluation of long-term performance of sediment microbial fuel cells and the role of natural resources. *Applied Energy*, 192: 490-497.

Fan, L.P. and Xue, S. (2016). Overview on Electricigens for Microbial Fuel Cell. *The Open Biotechnology Journal*, 10: 398-406.

Feng, Y., Wang, X., Logan, B.E. and Lee, H. (2008). Brewery wastewater treatment using air-cathode microbial fuel cells. *Applied microbiology and biotechnology*, 78: 873-800.

Flemming, H.C., Neu, T.R., Wozniak, D.J. (2007). The EPS Matrix: The "House of Biofilm Cells". *Journal of Bacteriology*, 89: 7945–7947.

Flemming, H.C. and Wingender, J (2010). The Biofilm Matrix. *Nature Reviews Microbiology*, 8: 623–633.

Flemming, H.C., Wingender, J., Szewzyk, U., Steinberg, P., Rice, S.A. and Kjelleberg, S. (2016). Biofilms: an emergent form of bacterial life. *Nature Reviews Microbiology*, 14: 563–575.

Gajda, I., Greenman, J., Melhuish, C. and Ieropoulos, I. (2015). Simultaneous electricity generation and microbially-assisted electrosynthesis in ceramic MFCs. *Bioelectrochemistry*, 104: 58-64.

Gajda, I., Greenman, J. and Ieropoulos, I.A. (2018). Recent advancements in real-world microbial fuel cell applications. *Current opinion in Electrochemistry*, 11: 78-83.

Gong, Y., Radachowsky, S.E., Wolf, M., Nielsen, M.E., Girguis, P.R. and Reimers, C.E. (2011). Benthic Microbial Fuel Cell as direct power source for an acoustic modem and seawater oxygen/temperature sensor system. *Environmental Science and Technology*, 45: 5047–5053.

Gregory, K.B., Bond, D.R. and Lovley, D.R. (2004). Graphite electrodes as electron donors for anaerobic respiration. *Environmental Microbiology*, 6: 596–604.

Gregory, K.B. and Lovley, D.R. (2005). Remediation and Recovery of Uranium From Contaminated Subsurface Environments With Electrodes. *Environmental Science and Technology*, 39: 8943–8947.

Habermann, W. and Pommer, E.H. (1991). Biological fuel cells with sulphide storage capacity. *Applied Microbiology and Biotechnology*, 35: 128–133.

Hall, E.K., Singer, G.A., Kainz, M.J. and Lennon, J.T. (2010). Evidence for a temperature acclimation mechanism in bacteria: an empirical test of a membrane-mediated trade-off. *Functional Ecology*, 24: 898–908.

Harris, H.W., El-Naggar, M.Y., Bretschger, O., Ward, M.J., Romine, M.F., Obraztsova, A.Y. and Nealson, K.H. (2010). Electrokinesis is a microbial behavior that requires extracellular electron transport. *Proceedings of the National Academy of Sciences of the United States of America*, 107: 326-331.

Hidalgo, D., Sacco, A., Hernández, S. and Tommasi, T. (2015). Electrochemical and impedance characterization of Microbial Fuel Cells based on 2D and 3D anodic electrodes working with seawater microorganisms under continuous operation, *Bioresource Technology*, 195: 139–146.

Holzman, D.C. (2005). Microbe power. *Environmental Health Perspectives*, 113: 754-757.

Hong, S.W., Chang, I.S., Choi, Y.S. and Chung, T.H. (2009). Experimental evaluation of influential factors for electricity harvesting from sediment using microbial fuel cell. *Bioresource Technology*, 100: 3029–3035.

Hsu, L., Mohamed, A., Ha, P.T., Bloom, J., Ewing, T., Arias-Thode, M., Chadwick, B. and Beyenal, H. (2017). The influence of energy harvesting strategies on performance and microbial community for sediment microbial fuel cells. *Journal of the Electrochemical Society*, 164: H3109–H3114.

Huang, Y., He, Z., Kan, J., Manohar, A.K., Nealson, K.H. and Mansfeld, F. (2012). Electricity generation from a floating microbial fuel cell. *Bioresource Technology*, 114: 308–313.

Ieropoulos, I., Melhuish, C. and Greenman J. (2003). Artificial metabolism: towards true energetic autonomy in artificial life. *Advances in Artificial Life*, 2801: 792-799.

Ieropoulos, I., Greenman, J., Melhuish, C. and Horsfield, I. (2010). EcoBot-III: a robot with guts. *Artificial Life XII*, 733-740.

Ieropoulos, I.A., Ledezma, P., Stinchcombe, A., Papaharalabos, G., Melhuisha, C. and Greenmanb, J. (2013). Waste to real energy: the first MFC powered mobile phone. *Physical Chemistry Chemical Physics*, 15: 15312-15316.

Ieropoulos, I.A., Stinchcombe, A., Gajda, I., Forbes, S., Merino-Jimenez, I., Pasternak, G., Sanchez- Herranza, D. and Greenmanab, J. (2016). Pee power urinal –microbial fuel cell technology field trials in the context of sanitation. *Environmental Science: Water Research and Technology*, 2: 336-343.

Inoue, K., Leang, C., Franks, A.E., Woodard, T.L., Nevin, K.P., Lovley, D.R.. (2010). Specific localization of the c-type cytochrome OmcZ at the anode surface in current-producing biofilms of *Geobacter sulfurreducens*. *Environmental Microbiology Reports*, 3: 211-217.

Ivars-Barcelò, F., Zuliani, A., Fallah, M., Mashkour, M., Rahimnejad, M. and Luque, R. (2018). Novel applications of Microbial Fuel Cells in Sensors and biosensors. *Applied Sciences*, 8: 1-16.

Jamal, M., Tasneem, U., Hussain, T. and Andleeb, S. (2015). Bacterial biofilm: its composition, formation and role in human infections. *Research and Reviews: Journal of Microbiology and Biotechnology*, 4: 1-14.

Janani, P. and Murugan, S.S. (2018). Implementation of sea sand in microbial fuel cell for an energy harvesting system using LTC for underwater applications. *Indian Journal of Geo Marine Sciences*, 47: 884-889.

Jannelli, N., Nastro, R.A., Cigolotti, V., Minutillo, M. and Falcucci, G. (2017). Low pH, high salinity: too much for microbial fuel cells? *Applied Energy*, 192: 543–550.

Juàrez, K., Kim, B.C., Nevin, K., Olvera, L., Reguera, G., Lovley, D.R. and Methè, B.A. (2009). PilR, a transcriptional regulator for pilin and other genes required for Fe(III) reduction in *Geobacter sulfurreducens*. *Journal of Molecular Microbiology and Biotechnology*, 16: 146-158.

Kadier, A., Kalil, M. S., Abdeshahian, P., Chandrasekhar, Mohamed, A., Azman, N.F., Longrono, W., Simayi, Y. and Hamid, A.A. (2016). Recent advances and emerging challenges in microbial electrolysis cells (MECs) for microbial production of hydrogen and value-added chemicals. *Renewable and Sustainable Energy Reviews*, 61: 501-525.

Kang, C.S., Eaktasang, N., Kwon, D.Y. and Kim, H.S. (2014). Enhanced current production by *Desulfovibrio desulfuricans* biofilm in a mediator-less microbial fuel cell. *Bioresource Technology*, 165: 27-30.

Keller, K.L., Rapp-Giles, B.J., Semkiw, E.S., Porat, I., Brown, S.D. and Wall, J.D. (2014). New model for electron flow for sulfate reduction in *Desulfovibrio alaskensis* G20. *Applied and Environmental Microbiology*, 80: 855-868.

Kim, B. H., Kim, H. J., Hyun, M. S., & Park, D. H. (1999). Direct electrode reaction of Fe(III)-reducing bacterium, Shewanella putrefaciens. *Journal of Microbiology and Biotechnology*, 9: 127-131.

Kim, M., Hyun, M.S., Gadd, G.M. and Kim, H.J. (2007). A novel biomonitoring system using microbial fuel cells. *Journal of Environmental monitoring*, 9: 1323-1328.

Kimura, Z., Chung, K.M., Itoh, H., Hiraishi, A. and Okabe, S. (2014). *Raoultella electrica* sp. nov., isolated from anodic biofilms of a glucose-fed microbial fuel cell. *International Journal of Systematic and Evolutionary Microbiology*, 64: 1384-1388.

Koch, C. and Harnisch, F. (2016). Is There a Specific Ecological Niche for Electroactive Microorganisms? *ChemElectroChem*, 3: 1282–1295.

Kumar, A., Hsu, L. H., Kavanagh, P., Barrière, F., Lens, P.N.L., Lapinsonnière, L., Lienhard, J.H.V., Schröder, U., Jiang, X. and Leech, D. (2017). The Ins and Outs of Microorganism–Electrode Electron Transfer Reactions. *Nature Reviews Chemistry,* 1: 1-13.

Li, C., Lesnik, K.L., Fan, Y. and Liu, H. (2016a). Redox Conductivity of Current-Producing Mixed Species Biofilms. PLoS One, 11: 1-14.

Li, S. W.; Sheng, G. P.; Cheng, Y. Y.; Yu, H. Q. (2016b). Redox Properties of Extracellular Polymeric Substances (EPS) From Electroactive Bacteria. *Scientific Reports*, 6: 39098.

Li, S.W., He, H., Zeng, R.J. and Sheng, G.P. (2017a). Chitin degradation and electricity generation by *Aeromonas Hydrophyla* in microbial fuel cells. *Chemosphere*, 168: 293-299.

Li, H., Tian, Y., Qu, Y., Qie, Y., Liu, J. and Feng, Y. (2017b). A pilot-scale benthic Microbial Electrochemical System (BMES) for enhanced organic removal in sediment restoration. Scientific Reports, 7:39802.

Liang P., Duan R., Jiang Y., Zhang X., Qiu Y. and Huang X. (2018). One-year operation of 1000-L modularized microbial fuel cell for municipal wastewater treatment. *Water Research*, 141: 1-8.

Liu, H., Ramnarayanan, R. and Logan, B.E. (2004). Production of electricity during wastewater treatment using a single chamber microbial fuel cell. *Environmental Science and Technology*, 38: 2281-2285.

Liu, Z.D., Du, Z.W., Lian, J., Zhu, X.Y., Li, S.H. and Li, H.R. (2007). Improving energy accumulation of microbial fuel cells by metabolism regulation using *Rhodoferax ferrireducens* as biocatalyst. *Letters in Applied Microbiology*, 44: 393-398.

Liu, J., Yong, Y.C., Song H and Li, C.M. (2012). Activation enhancement of citric acid cycle to promote bioelectrocatalytic activity of arcA knockout *Escherichia coli* toward high-performance microbial fuel cell. *ACS Catalysis*, 2: 1749-1752.

Logan, B.E., Hamelers, B., Rozendal, R., Schröder, U., Keller, J., Freguia, S., Aelterman, P., Verstraete, W. and Rabaey, K. (2006). Microbial Fuel Cells: Methodology and Technology. *Environmental Science and Technology*, 40: 5181-5192.

Logan, B.E. (2008) Microbial Fuel Cell. Hoboken, New Jersey: John Wiley and Sons, Inc.

Logan, B. E. (2009). Exoelectrogenic Bacteria That Power Microbial Fuel Cells. *Nature Reviews Microbiology*, 7: 375–381.

Logan, B. E. (2010). Scaling up microbial fuel cells and other bioelectrochemical systems. *Applied Microbiology and Biotechnology*, 85: 1665-1671.

Logan, B.E., Rossi, R., Ragab, A. and Saicaly, P.E. (2019). Electroactive microorganisms in bioelectrochemical systems. *Nature Reviews Microbiology*, 17: 307-319.

Lovley, D.R. (1991). Dissimilatory Fe(III) and Mn(IV). *Microbiology and Molecular biology review*s, 55: 259-287.

Lovley, D.R., Giovannoni, S.J., White, D.C., Champine, J.E., Phillips, E.J.P., Gorby, Y.A. and Goodwin, S. (1993). *Geobacter metallireducens* gen. nov. sp. nov., a microorganism capable of coupling the complete oxidation of organic compounds to the reduction of iron and other metals. *Archives of Microbiology*, 159: 336-344.

Lovley, D.R., Ueki, T., Zhang, T., Malvankar, N.S., Shrestha, P.M., Flanagan, K.A., Aklujkar, M., Butler, J.E., Giloteaux, L., Rotaru, AE., Holmes , D.E., Franks, A.E., Orellana, R., Risso, C. and Nevin, K.P. (2011). Geobacter: the microbe's electric physiology, ecology and practical applications. *Advances in Microbial Physiology*, 59: 1-100.

Lu, M., Chen, S., Babanova, S., Phadke, S., Salvacion, M., Mirhosseini, A., Chan, S., Carpenter, K., Cortese, R. and Bretschger, O. (2017). Long-term performance of a 20-L continuous flow microbial fuel cell for treatment of brewery wastewater. *Journal of Power Sources*, 356: 274–287.

Majumder, D., Maity, J.P., Tseng, M.J., Nimje, V.R., Chen, H.R., Chen, C.C., Chang, Y.F., Yang, T.C and Chen, C.Y. (2014). *International Journal of Molecular Sciences*, 15: 16772:16786.

Malvankar, N.S., Vargas, M., Nevin, K.P., Tremblay, P.L., Evans-Lutterodt, K., Nykypanchuk, D., Martz, E., Tuominem, M.T. and Lovley, D.R. (2015). Structural Basis for Metallic-Like Conductivity in Microbial Nanowires. MBio, 6:e00084–e00115.

Manohar, A.K., Bretschger, O., Nealson, K.H. and Mansfeld, F. (2008). The use of electrochemical impedance spectroscopy (EIS) in the evaluation of the electrochemical properties of a microbial fuel cell. *Bioelectrochemistry*, 72: 149–154.

Margaria V., Tommasi T., Pentassuglia S., Agostino V., Sacco A., Armato C., Chiodoni A., Schilirò T., Quaglio M. (2017). Effect of pH variations on anodic marine consortia in a dual chamber microbial fuel cell. *International Journal of Hydrogen Energy*, 43: 1820-1829.

Marshall, C. and May, H. (2009). Electrochemical evidence of direct electrode reduction by a thermophilic Gram-positive bacterium, *Thermincola ferriacetica. Energy and Environmental Science*, 2: 699-705.

Marsili, E., Baron, D.B., Shikhare, I.D., Coursolle, D., Gralnick, J.A. and Boond, D.R. (2008). *Shewanella* secretes flavins that mediate extracellular electron transfer. PNAS, 105: 3968–3973.

Martinucci, E., Pizza, F., Perrino, D., Colombo, A., Trasatti, S.P.M., Lazzarini Barnabei, A., Liberale, A. and Cristiani, P. (2015). Energy balance and microbial fuel cells experimentation at wastewater treatment plant Milano-Nosedo. *International Journal of Hydrogen Energy*, 40: 14683–14689.

Massaglia, G., Gerosa, M., Agostino, V., Cingolani, A., Sacco, A., Saracco, G., Margaria, V. and Quaglio, M. (2017). Fluid dynamic modeling for microbial fuel cell based biosensor optimization. *Fuel Cells*, 17: 627–634.

Mateo, S., Cañizares, P., Rodrigo, M.A. and Fernandez-Morales, F.J. (2018). Driving force of the better performance of metal-doped carbonaceous anodes in microbial fuel cells. *Applied Energy*, 225: 52–59.

Melhuish, C., Ieropoulos, I., Greenman, J. and Horsfield, I. (2006). Energetically autonomous robots: food for though. *Autonomous Robots*, 21: 187-198.

Nandy, A., Kumar, V., Kundu, P. P. (2013). Utilization of proteinaceous materials for power generation in a mediatorless microbial fuel cell by a new electrogenic bacteria *Lysinibacillus sphaericus* VA5. *Enzyme and Microbial Technology*, 53: 339-344.

Nealson, K.H. and Rowe, A.R. (2016). Electromicrobiology: Realities, Grand Challenges, Goals and Prediction. *Journal of Microbiology and Biotechnology*, 9: 595–600.

Nevin, K.P., Richter, H., Covalla, S.F., Johnson, J.P., Woodard, T.L., Orloff, A.L., Jia, H., Zhang, M. and Lovley, D.R. (2008). Power output and columbic efficiencies from biofilms of Geobacter sulfurreducens comparable to mixed community microbial fuel cells. *Environmental Microbiology*, 10: 2505–2514.

Nevin, K.P., Kim, B.C., Glaven, R.H., Johnson, J.P., Woodard, T.L., Mathè, B.A., Di Donato Jr, R.J., Covalla, S.F., Franks, A.E., Liu, A., and Lovley, D.R. (2009). Anode biofilm transcriptomics reveals outer surface components essential for high density current production in Geobacter sulfurreducens fuels cells. PLOSOne, 4: e5628.

Nimje, V.R., Chen, C.C., Chen, H.R., Chen, C.Y., Tseng, M.J., Cheng, K.C., Shih, R.C. and Chang, Y.F. (2012). A single-chamber microbial fuel cell without an air cathode. *International Journal of Molecular Sciences*, 13: 3933-3948.

Okamoto, A., Kalathil, S., Deng, X., Hashimoto, K., Nakamura, R. and Nealson, K.H. (2014). Cell- Secreted Flavins Bound to Membrane Cytochromes Dictate Electron Transfer Reactions to Surfaces With Diverse Charge and pH. *Scientific Report*, 4:5628.

Oliot, M. Etcheverry, L., Mosdale, A., Basseguy, R., Délia, M.L., Bergel., A. (2017). Separator electrode assembly (SEA) with 3-dimensional bioanode and removable air-cathode boosts microbial fuel cell performance. *Journal of Power Sources,* 356: 389–399.

Ong, W. K., Vu, T. T., Lovendahl, K. N., Llull, J.M., Serres, M.H., Romine, M.F. and Reed, J.L. (2014). Comparisons of *Shewanella* Strains Based on Genome Annotations, Modeling, and Experiments. *BMC System Biology*, 8:31.

Pandit S., Khilari S., Roy S., Pradhan D. and Das D. (2014). Improvement of power generation using *Shewanella putrefaciens* mediated bioanode in a single chambered microbial fuel cell: Effect of different anodic operating conditions. *Bioresource Technology*, 166: 451-457.

Pandit, S. and Das, D. (2018). Principles of microbial fuel cell for the power generation. In D. Das (Ed.), Microbial fuel cell, *Springer*, 21-41.

Pant, D., Bogaert, G.V, Diels, L. and Vanbroekoven, K. (2010). A review of the substrates used in microbial fuel cells (MFCs) for sustainable energy production. *Bioresource Technology*, 6: 1533-1543.

Papaharalabos, G., Greenman, J., Melhuish, C., Santoro, C., Cristiani, P., Li, B. and Ieropoulos, I. (2013). *International Journal of Hydrogen Energy*, 38: 11552-11558.

Parameswaran, P., Bry, T., Popat, S.C., Lusk, B.G., Rittman, B.E. and Torres, C.I. (2013). Kinetic, electrochemical, and microscopic characterization of the thermophilic, anode-respiring bacterium *Thermincola ferriacetica*, *Environmental Science and Technology*, 47: 4934-4940.

Park, H.S., Kim, B.H., Kim, H.S., Kim, H.J., Kim, G.T., Kim, M., Chang, I.S., Park, Y.K. and Chang, H.I. (2001). A novel electrochemically active and Fe(III)-reducing bacterium phylogenetically related to *Clostridium butyricum* isolated from a microbial fuel cell. *Anaerobe*, 7: 297-306.

Patil, S.A., Hägerhäll, C. and Gorton, L. (2012). Electron transfer mechanisms between microorganisms and electrodes in bioelectrochemical systems. *Bioanalytical Reviews*, 4: 159–192.

Pirbadian, S., Barchinger, S. E., Leung, K. M., Byun, H.S., Jangir, Y., Bouhenni, R.A., Reed, S.B., Romine, M.F., Saffarini, D.A., Shi, L., Gorby, Y.A., Golbeck, J.H. and El Naggar, M.Y. (2014). *Shewanella oneidensis* MR-1 Nanowires are Outer Membrane and Periplasmic Extensions of the Extracellular Electron Transport Components. PNAS, 111: 12883–88.

Potter, M.C. (1911) Electrical effects accompanying the decomposition of organic compounds. *Proceedings of Royal Society B*, 84: 260-276.

Rabaey K, Lissens G, Siciliano S, Verstraete W. (2003). A microbial fuel cell capable of converting glucose to electricity at high rate and efficiency. *Biotechnology Letters*, 25: 1531–1535.

Rabaey, K., Boon, N., Hofte, M., Verstraete, W. (2005). Microbial phenazine production enhances electron transfer in biofuel cells. *Environmental Science and Technology*, 39: 3401–3408.

Rasmussen, M. and Minteer, S.D. (2015). Long-term arsenic monitoring with an *Enterobacter cloacae* microbial fuel cell. *Bioelectrochemistry*, 106: 207–212.

Reguera, G., Nevin, K.P., Nicoll, J.S., Covalla, S.F., Woodard, T.L. and Lovley, D.R. (2006). Biofilm and nanowire production leads to increased current in *Geobacter sulfurreducens* fuel cells. *Applied and Environmental Microbiology.* 72: 7345–7348.

Reimers, C.E. and Wolf, M. (2018). Power from Benthic Microbial Fuel Cells drives Autonomous sensors and Acoustic modems. *Oceoanography*, 31: 98-103.

Ren, H., Jiang, C. and Chae, J. (2017). Effect of temperature on a miniaturized microbial fuel cell (MFC). *Micro and Nano Systems Letters,* 5:13.

Richter, H., McCarthy, K., Nevin, K.P., Johnson, J.P., Rotello, V.M. and Lovley, D.R. (2008). Electricity generation by Geobacter sulfurreducens attached to gold electrodes. *Langmuir*, 24: 4376-4379.

Richter K., Schicklberger M. and Gescher J. (2012). Dissimilatory reduction of extracellular electron acceptors in anaerobic respiration. *Applied and Environmental Microbiology*, 78: 913–921.

Rosenbaum, M., Schroder, U. and Scholz, F. (2006). Investigation of the electrocatalytic oxidation of formate and ethanol at platinum black under microbial fuel cell conditions. *Journal of Solid State Electrochemistry*; 10: 872-8.

Roy, S., Marzorati, S., Schievano, A. and Pant, D. (2017). Microbial Fuel Cells. In: Abraham, M.A. (Ed.), *Encyclopedia of Sustainable Technologies, Elsevier*, 245–259.

Sacco, A. (2017). Electrochemical impedance spectroscopy: fundamentals and application in dye-sensitized solar cells. *Renewable and Sustainable Energy Reviews*, 79: 814–829.

Santoro, C., Arbizzani, C., Erable, B., Ieropoulos, I. (2017). Microbial fuel cells: From fundamentals to applications. A review. *Journal of Power Sources*, 356: 225-244.

Schievano, A., Colombo, A., Grattieri, M., Trasatti, S.P., Liberale, A., Tremolada, P., Pino, C. and Cristiani, M. (2017). Floating microbial fuel cells as energy harvesters for signal transmission from natural water bodies. *Journal of Power Sources*, 340: 80–88.

Schröder, U. (2007). Anodic electron transfer mechanisms in microbial fuel cells and their energy efficiency. *Physical Chemistry Chemical Physics*, 9: 2619-2629.

Semenec, L. and Franks, A.E. (2015). Delving Through Electrogenic Biofilms: From Anodes to Cathodes to Microbes. *Bioengineering*, 2: 222–248.

Sharma, Y., Parnas, R., and Li, B. (2011). Bioenergy production from glycerol in hydrogen producing bioreactors (HPBs) and microbial fuel cells (MFCs). *International Journal Hydrogen Energy*, 36: 3853- 3861.

Shen, H.B., Yong, X.Y., Chen, Y.L., Liao, Z.H., Si, R.W., Zhou, J. and Zheng, T. (2014). Enhanced bioelectricity generation by improving pyocyanin production and membrane permeability through sophorolipid addition in *Pseudomonas aeruginosa*-inoculated microbial fuel cells. *Bioresource Technology*, 167: 490-494.

Shi, L., Fredrickson, J.K. and Zachara, J.M. (2014). Genomic analyses of bacterial porin-cytochrome gene clusters. *Frontiers in Microbiology*, 5:657.

Shi, L., Dong, H., Reguera, G., Beyenal, H., Lu, A., Liu, J., Yu, H.Q. and Fredrickson, J.K. (2016). Extracellular Electron Transfer Mechanisms Between Microorganisms and Minerals. *Nature Reviews Microbiology*, 14: 651–662.

Snider, R.N., Strycharz-Glaven, S.M., Tsoi, S.D., Erickson, J.S. and Tender, L.M. (2012). Long-range electron transport in *Geobacter sulfurreducens* biofilm is redox gradient-driven. PNAS, 109: 15467-15472.

Song, Y.C., Yoo, K.S. and Lee, S.K. (2010). Surface floating, air cathode, microbial fuel cell with horizontal flow for continuous power production from wastewater. *Journal of Power Sources*, 195: 6478–6482.

Song, T.S. and Jiang, H.L. (2011). Effects of sediment pretreatment on the performance of sediment microbial fuel cells, *Bioresource Technology*, 102: 10465–10470.

Summers, Z.M., Fogarty, H.E., Leang, C., Franks, A.E., Malvankar, N.S. and Lovley, D.R. (2010). Direct exchange of electrons within aggregates of an evolved syntrophic co-culture of anaerobic bacteria. *Science*, 330: 1413-1415.

Sun, D., Wang, A., Cheng, S., Yates, M. and Logan, B.E. (2014). *Geobacter anodireducens* sp. nov., an exoelectrogenic microbe in bioelectrochemical systems. *International journal of Systematic and Evolutionary Microbiology*, 64: 3485-3491.

Sydow, A., Krieg, T., Mayer, F., Schrader, J., Holtmann, D. (2014) Electroactive Bacteria—Molecular Mechanisms and Genetic Tools. *Applied Microbiology and Biotechnology*, 98: 8481–8495.

Tan, Y., Adhikari, R.Y., Malvankar, N.S., Ward, J.E., Woodard, T.L., Nevin, K.P. and Lovley, D.R. (2017). Expressing the *Geobacter metallireducens* PilA in *Geobacter sulfurreducens* yields pili with exceptional conductivity. mBio, 8:e02203-16.

Tender, L.M., Gray, S.A., Groveman, E., Lowy, D.A., Kauffman, P., Melhado, J., Tyce, R.C., Flynn, D., Petrecca, R. and Dobaro, J. (2008). The first demonstration of a microbial fuel cell as a viable power supply: powering a meteorological buoy, *Journal of Power Sources*, 179: 571–575.

Tommasi, T., Salvador, G.P. and Quaglio, M. (2016a). New insights in Microbial Fuel Cells: novel solid phase anolyte. *Science Reports*, 6:29091.

Tommasi, T., Sacco, A., Armato, C., Hidalgo, D., Millone, L., Sanginario, A., Tresso, E., Schilirò, T. and Pirri, C.F. (2016b). Dynamical analysis of microbial fuel cells based on planar and 3D-packed anodes. *Chemical Engineering Journal*, 288: 38–49.

Velasquez-Orta, S.B., Werner, D., Varia, J.C. and Mgana, S. (2017). Microbial fuel cells for inexpensive continuous in-situ monitoring of groundwater quality, *Water Research*, 117: 9–17.

Walter, X.A., Stinchcombe, A., Greenman, J. and Ieropoulos, I. (2017). Urine transduction to usable energy: A modular MFC approach for smartphone and remote system charging. *Applied Energy*, 192: 575-581.

Wang, G.H., Cheng, C.Y., Liu, M.H., Chen, T.Y., Hsieh, M.C. and Chung, Y.C. (2016). Utility of *Ochrobactrum anthropic* YC152 in a Microbial Fuel Cell as an early warning device for hexavalent Chromium determination. *Sensors*, 16: 1272.

Wang, C.T., Lee, Y.C., Ou, Y.T., Yang, Y.C., Chong, W.T., Sangeetha, T. and Yan, W.M. (2017). Exposing effect of comb-type cathode electrode on the performance of sediment microbial fuel cells. *Applied Energy*, 204: 620–625.

Wang, J., Deng, H., Wu, S.S., Deng, Y.C., Liu, L., Han, C., Jiang, Y.B. and Zhong, W.H. (2019). Assessment of abundance and diversity of exoelectrogenic bacteria in soil under different land use types. *Catena*, 172: 572-580.

Wrighton, K.C., Thrash, J.C., Melnyk, R.A., Bigi, J.P., ByrneBailey, K.G., Remi, J., Schi chnes, D., Auer, M., Chang, C.J. and Coates, J.D. (2011). Evidence for direct electron transfer by a Gram-positive bacterium isolated from a microbial fuel cell. *Applied Environmental Microbiology*, 77: 7633–7639.

Xing, D., Zuo, Y., Cheng, S., Regan, J.M. and Logan B.E. (2008). Electricity Generation by *Rhodopseudomonas palustris* DX-1. *Environmental Science and Technology*, 42: 4146-4151.

Xu, S. and Liu, H. (2011). New exoelectrogen *Citrobacter* sp. SX-1 isolated from a microbial fuel cell. *Journal of applied microbiology*, 111: 1108-1115.

Yang, W. and Logan, B.E. (2016). Immobilization of a metal-nitrogen-carbon catalyst on activated carbon with enhanced cathode performance in microbial fuel cells. *ChemSusChem*, 9: 2226-2232.

Yang, Y., Liu, T., Zhu, X., Zhang, F., Ye, D., Liao, Q. and Li, Y. (2016). Boosting power density of microbial fuel cells with 3D Nitrogen-doped graphene aerogel electrode. *Advanced Sciences*, 3:160097.

Yi, H., Nevin, K.P., Kim, B.C., Franks, A.E., Klimes, A., Tender, L.M. and Lovley, D.R. (2009). Selection of a variant of Geobacter sulfurreducens with enhanced capacity for current production in microbial fuel cells. *Biosensors and Bioelectronics*, 24: 3498-3503.

Yuvraj, C. and Aranganathan, V. (2017). Enhancement of voltage generation using isolated Dissimilatory Iron-Reducing (DIR) *Klebsiella pneumoniae* in Microbial Fuel Cell. *Arabian Journal for Science and Engineering*, 42: 65-73.

Zabihallahpoor, A., Rahimnejad, M. and Talebnia, F. (2015). Sediment microbial fuel cells as a new source of renewable and sustainable energy: present status and future prospects. RSC *Advances*, 5: 94171–94183.

Zhang, T., Gannon, S.M., Nevi, K.P., Franks, A.E. and Lovley, D.R. (2010). Stimulating the anaerobic degradation of aromatichydrocarbons in contaminated sediments by providingan electrode as the electrode acceptor. *Environmental Microbiology*, 12: 1111-1020.

Zhang, F., Tian and L. and He, Z. (2011). Powering a wireless temperature sensor using sediment microbial fuel cells with vertical arrangement of electrodes. *Journal of Power Sources*, 196: 9568–9573.

Zhang, Y. and Angelidaki, I. (2012). Bioelectrode-based approach for enhancing nitrate and nitrite removal and electricity generation from eutrophic lakes, *Water Research*, 46: 6445–6453.

Zhang, E., Cai, Y., Luo, Y. and Piao, Z. (2014). Riboflavin-shuttled extracellular electron transfer from *Enterococcus faecalis* to electrodes in Microbial Fuel Cells. *Canadian journal of microbiology*, 60: 753-759.

Zhang, F. and He, Z. (2015). Scaling up microbial desalination cell system with a post-aerobic process for simultaneous wastewater treatment and seawater desalination, *Desalination*, 360: 28-34.

Section 2

Gas fermenting *C. autoethanogenum* as prominent cell factory

Chapter 6

Introduction

6.1   An overview of biofuels

Fossil fuel reserves have been used as main energy source for many years (Rodionova et al. 2017). However, the deleterious global effects of their exploitation (increases of fuel prices, fossil fuel depletion and overwhelming environmental issues) have driven interest toward renewable energy sources (solar, wind, geothermal and biofuels) (Rasool and Hemalatha, 2016). Due to the great emphasis placed on bioenergy over the past decades, it has been estimated that it will account for around 20-30% of the overall primary energy worldwide by 2035 (IEA, 2013). With their dramatically reduced (or non-existent) carbon emissions into the atmosphere, biofuels represent a suitable alternative to fossil fuels (Elshahed, 2010). Collectively, biofuels (e.g. bioalcohol, biodiesel and biogas) are classified as any energy-enriched chemicals generated by using biomass as feedstock (Rodionova et al. 2017; Rasool and Hemalatha, 2016). The history of biological fuel is not restricted to recent decades. In 1898, German scientists demonstrated fermentative ethanol production from plant materials (Elshahed, 2010). At the start of the 20th century, with the attempt to produce rubber artificially, the chemist Weizmann discovered the ability of a new isolated culture (mainly *C. acetobutylicum*) to produce a large amount of a liquid, containing mostly ethanol and acetone (Dürre, 2007). This biochemical process was then termed ABE (Acetone-Butanol-Ethanol) fermentation (Dürre, 2007). Following ethanol fermentation, ABE became the second biggest example of biotechnology (Liew et al. 2013). During the World War I, acetone, initially a disregarded by-product, turned out to be useful for the production of cordite, the propellant of cartridges and shells (Dürre, 2007; Elshahed, 2010; Liew et al. 2013). Even though ABE made a comeback during the World War II, rising substrate prices with a concomitant drop in crude oil cost supplied from the Middle East, led to petrochemical fuel production gradually replacing ABE fermentation (Liew et al. 2013; Dürre, 2007). Successively, the oil crisis of 1973-1974 renewed the interest toward the field of biofuels (Elshahed, 2010). Depending on the biomass feedstocks used, biofuels are categorized into four generations. Traditionally, first generation biofuels are produced from agricultural crops containing starch (from wheat, barley, corn and potato) and sugars (from sugarcane and sugar beet), and oil seeds (IEA, 2010; Ho et al. 2014). Conversion of sugar-based biomass into ethanol involves the fermentation of hexose sugars (mainly glucose) by yeasts (*S. cerevisiae* or *Z. mobilis*) or genetically engineered microorganisms (Elshahed, 2010); conversely, when starch is used, an initial hydrolysis step to fermentable sugars is required, with energy consumption implications (Lin and Tanaka, 2006). Nowadays, first generation biofuels represent the majority of biofuels commercially available, with Brazil and USA producing more than 80% of the global supply (Bhatia et al. 2017; Chum et al. 2014). Even though first generation bioenergy has reached an advanced state with mature technologies, infrastructures and markets, environmental and socioeconomic limitations have emerged along with its deployment (Ho et al. 2014). In 2008, despite only 2% of the world's arable land having been employed

to cultivate biomass feedstocks for biofuel production (IEA, 2008), food commodity prices sharply increased, with sugar prices reaching a record of US$ 795.40/ton in 2011 (Aro, 2016). Additionally, in the same year the massive use of fertilizers in the United States had a dramatic impact on the environment (Elshahed, 2010). Taking into account all the implications of growing dedicated biomass, no significant benefits in terms of GHG emissions reduction are achieved (EASAC, 2012). Thus, due to ethical issues (food vs. fuel competition), first generation biofuels turned out to be unfit for replacing fossil fuels (Dutta et al. 2014). As a result, according to the New Policies Scenario, the use of biomass intended for first generation biofuels in total primary energy demand will be reduced to 3.9% by 2035 (IEA, 2013). The deployment of forest and agricultural wastes or non-food crops could be a solution to the crisis (Dutta et al. 2014). Second generation biofuels rely on the use of perennial plants growing on marginal, non-agricultural lands (Elshahed, 2010). Lignocellulosic biomass includes cereal straw, sugarcane bagasse, forest residues, organic components of municipal solid waste (MSW) and dedicated feedstocks such as vegetative grasses (Dutta et al. 2014). Since the whole plant can be used as raw material, less farmland is required for biomass production. Moreover, the possibility to simultaneously cultivate diverse types of crops makes the lignocellulosic material more cost effective, due to the minor amount of fertilizers needed (Priefer et al. 2017). However, whilst they appear more appealing than first generation, second generation biofuels still have their own shortcomings. Even if it represents one of the largest energy resources, lignocellulosic material is also the least utilized biological matter on earth (Bhatia et al. 2017). The major constraint of lignocellulosic feedstocks is their heterogeneous nature (combination of cellulose, hemicellulose and lignin), which makes them more difficult to be degraded by anaerobic microorganisms (Elshahed, 2010). Particularly lignin, which can account for 10-40% of plant biomass and for 25-35% of the total energy content, is responsible for the lignocellulosic biomass recalcitrance (Daniell et al. 2012; Elshahed, 2010; Sun and Cheng 2002). Hence, in order to fractionate the single components and give more accessibility to cellulose and hemicellulose, lignocellulosic feedstocks are first pretreated through physical (milling and irradiation), chemical (use of oxidizing agents or strong acids) or biological methods, and then hydrolyzed to release free sugars (Daniell et al. 2012; Bhatia et al. 2017; Ho et al. 2014). Although required, pretreatments can negatively affect microbial growth and fermentation itself by promoting the synthesis of toxic compounds that have to be removed from the hydrolysate through costly detoxification methods (Allen et al. 2010a). As an alternative solution, the so-called consolidated bioprocessing process (CBP) involves the use of cellulolytic microorganisms, able to carry out both hydrolysis of lignocellulosic biomass and fermentation of sugars (Liew et al. 2016a). Another disadvantage of lignocellulosic feedstocks relates to invasive species of plants or weeds, which if encouraged to grow, may damage the ecosystem (Elshahed, 2010). At the current stage, only a few commercial level plants for second generation biofuel production have been set up in countries such as Brazil, the U.S. and Italy (Bhatia et al. 2017). In an effort to

make this approach economically feasible, much more research work needs to be undertaken. Another widely explored strategy is the photosynthetic capture of CO_2 in microorganisms such as cyanobacteria and microalgae, which are referred to as third generation biofuels (Rodionova et al. 2017). Other than biodiesel and bioethanol, algal-based biofuels comprise biohydrogen and biomethane, where the latter can be used for transportation, electricity and heating production. The advantage of using algae over other approaches relies on their higher photosynthesis and growth rate compared to any other terrestrial plants, potentially doubling their biomass in 2-5 days. Additionally microalgae (e.g. *Botryococcus* and *Chlorella*) accumulate mainly lipids (up to 80% of their dry weight) suitable for biodiesel production, macroalgae and cyanobacteria (e.g. *Chlamydomonas* sp. and *Spirulina platensis*) mostly accumulate carbohydrates, adequate for bioethanol production (Costa and de Morais, 2011). Moreover, algae do not contain any lignin, thereby resulting in a higher hydrolysis efficiency and fermentation yields as well as lower costs. However, even third generation biofuels still have many drawbacks, comprising algal cultivation, production modes, design of photobioreactors and downstream treatments (Ho et al. 2014). The major limitation is the fact that biodiesel production mostly occurs during stress phases, when growth and biomass production are compromised, thus resulting in a reduction of the overall productivity (Aro, 2016). Steps toward a successful commercialization should include screening of promising algal strains, genetic manipulation of lipid and cellulose synthesis pathways as well as improvements in downstream separation processes (Ho et al. 2014). All the biofuel generations described so far use either biomass or wastes as feedstock, making their development on global scale strongly dependent on geographical location, and hence unfit for replacing fossil fuels (Aro 2016; Dutta et al. 2014). Fourth generation biofuels is an emerging approach that utilizes photosynthetic microorganisms (algae and cyanobacteria) as catalysts, enabling to harvest the solar energy and directly convert it into fuels, without a biomass phase. The revolutionary aspect is the application of synthetic biology, which although in its infancy, promises the construction of synthetic cellular factories and tailored microorganisms, to increase conversion efficiency for instance by enhancing their carbon entrapment capability. In addition to photobiological solar fuels, fourth generation also includes electrobiofuels, which can be generated by combining photovoltaic or inorganic water splitting with the innovative microbial electrosynthesis technology (Aro, 2016).

6.2   Fundamentals of Gas Fermentation

The capacities of the biofuel generations reviewed above are not keeping up with demand currently being met by conventional fuels. There are still several obstacles preventing biofuel commercialization and substrate price represents one of the main barriers, accounting for more than 45% of the fermentation process cost (Bhatia et al. 2017). The solution relies on the use of abundant and low cost gases as carbon and energy sources. In the process known as syngas fermentation, instead of being incorporated in lignocellulosic biomass, carbon from C1-based feedstocks

(CO and CO_2) can be directly assimilated by specific microbial chassis and converted into high value products, such as fuels and chemicals (Humphreys & Minton, 2018). Synthetic gas or syngas is a mixture of gases primarily containing CO (30-60%), H_2 (25-30%) and CO_2 (5-15%), which can be generated through gasification of virtually any carbonaceous material (Liew et al. 2013; Teixeira et al. 2018). Beyond pyrolysis/gasification of solid biomass or gasification of other organic matter such as municipal solid waste (MSW) and organic industrial wastes, C1 compounds can also be derived from the gasification of fossil sources (coal, petroleum, natural gas and peat coal) (Liew et al. 2016a; Bengelsdorf and Dürre, 2017). Alternatively, some industries such as steel mills, ferroalloy industries, refineries and chemical plants release large volumes of CO and/or CO_2 rich off-gases (Liew et al. 2013; Heijstra et al. 2017). As an example, in China, approximately 1.04 tons of carbon are emitted per ton of steel manufactured (IPCC, 2018). When biomass is used as starting material, the derived syngas is considered "green carbon"; alternatively syngas from fossil sources or derived products is referred to as "black carbon" (Bengelsdorf and Dürre, 2017) (**Figure 6.1**).
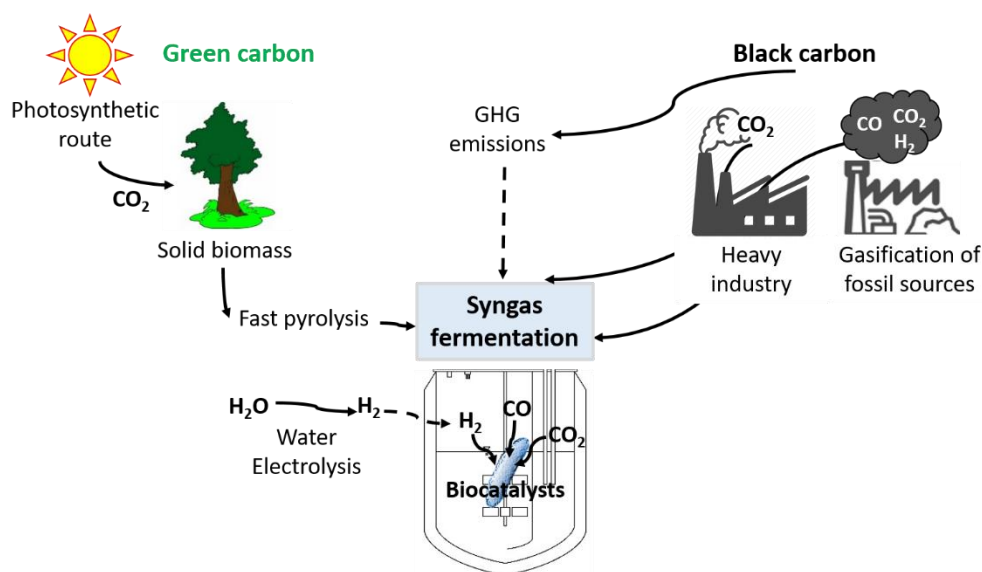
Figure 6.1 Overview of feedstocks available for syngas fermentation technology. Figure adapted from Bengelsdorf and Dürre, 2017**.**

Gas fermentation technology represents a hybrid thermochemical/biochemical platform, with the overall process mainly comprising four steps (Phillips et al. 2017; Liew et al. 2016a). During gasification, carbonaceous material is converted into gaseous intermediates in the presence of an oxidizing agent (air, steam or oxygen), elevated temperature (600-1000 °C) and pressure (>30 bar) (Griffin and Schultz, 2012; Breault, 2010). In addition to its main components (CO, H_2, CO_2 and N_2), the resulting gas streams also include: water vapor, methane (CH_4) and impurities such as tar, particulates, aromatic compounds as benzene (C_6H_6), toluene (C_7H_8),

naphthalene ($C_{10}H_8$), ethylene (C_2H_4); sulfur compounds such as hydrogen sulfide (H_2S), carbonyl sulfide (COS) and carbonyl disulfide (CS_2); halogens such as chlorine and hydrogen fluoride (HF), and potential inhibitors as ammonia (NH_3), hydrogen cyanide (HCN), oxygen (O_2) and nitrogen oxides (NO_X) (Liew et al. 2016a). The concentrations of these species vary depending on the gasification technique and on the feedstock composition (Xu et al. 2011). A key advantage of using gas-fermenting microorganisms is their capability of growing even in the presence of these impurities. However, some of these chemical species need to be removed. Hence, prior to fermentation, syngas requires minimal pre-treatments. Next, treated syngas is cooled down, compressed and then sparged into the bioreactor where fermentation can occur. Lastly, the desired products are separated from the fermentation broth by distillation, liquid-liquid extraction, gas stripping, adsorption, perstraction, pervaporation or vacuum distillation (Liew et al. 2016a). Currently gas fermentation is receiving considerable scientific attention; however, traditionally conversion of gas to liquid biofuels was achieved using the Fischer-Tropsch Process (FTP).

6.3 Gas Fermentation vs. Fischer-Tropsch Process (FTP)

Historically, synthetic gas generated from coal, natural gas or biomass, has been used as raw material in the Fischer-Tropsch Process (FTP). The FTP was developed by Franz Fischer and Hans Tropsch in the 1920s (Fischer and Tropsch, 1930), giving access to an industrial organic chemical process starting from simple inorganic molecules. The viability of FT technology across the world has been shaped by fluctuations in fossil fuel prices, with the exception of South Africa, where extremely cheap domestic coal favored the development of the FT industry (Schulz, 1999). FT synthesis is based on the catalytic polymerization and hydrogenation of CO to a mixture of hydrocarbons (linear paraffins and olefins) and oxygenates, which are successively hydrocracked to produce liquid fuels (Zhou et al. 2016; Teixeira et al. 2018). Like gas fermentation, FT relies on a preliminary gasification step, which confers both technologies the advantage of building block flexibility, allowing access to almost all the carbon contained within the biomass feedstock (including the recalcitrant lignin) and so avoiding partial conversion into fermentable sugars (Daniell et al., 2012). The thermochemical conversion of syngas occurs in the presence of metal catalysts such as iron, cobalt and ruthenium, using high reaction temperatures (150-350°C) and pressures (up to 30 bar) (De Klerk et al. 2013). Features in terms of selectivity, robustness and flexibility of the metal-catalyst used as well as the utilized operative conditions, result in high capital requirements and energy costs, thus limiting the feasibility of the process (Griffin and Schultz, 2012). Conversely, gas fermentation occurs at low temperature (typically 37°C) and atmospheric pressure, which is obviously more economically favorable (De Klerk et al. 2013). Crucially, metal catalyst-based technologies face

partial or permanent catalyst inactivation and poisoning by tars, sulphur and chlorine present in the gaseous mixture, thus requiring elevated gas pre-treatment costs (Köpke et al. 2011; Mohammadi et al. 2011). Vice versa, gas purity is not essential when biological catalysts are employed, due to the less sensitivity exhibited by microorganisms. However, compounds such as acetylene, NO_x and HCN are known to inhibit key enzymes, with cyanide able to bind carbon monoxide dehydrogenase (CODH), an essential enzyme of the Wood-Ljungdahl pathway (WLP) (discussed in detail below) (Anderson et al. 1993; Shima and Ataka, 2011; Ragsdale et al. 1983). Additionally, microbes can self-regenerate by using the fed gas as carbon and energy source and with the supplementation of low-cost media (Daniell et al. 2012). According to a study published by Griffin and Schultz (2012), conversion of syngas originating from woody biomass into ethanol via FT results in a 45% overall energy efficiency (energy in feedstock converted to final product), whereas 57% is obtained with gas fermentation. Furthermore, gas fermentation has lower CO_2 emissions and higher rates of carbon conversion, compared to the thermochemical approach (Griffin and Schultz, 2012). Moreover, syngas originating from non-uniform feedstocks (biomass and MSW) comprises variable amount of H_2 (1.2-7.3 mol %) (Boateng et al. 2007; Datar et al. 2004), thus hindering FT catalytic process, which ideally requires a $H_2:CO_2$ ratio of 2:1 (De Klerk et al. 2013). Therefore, before being thermochemically converted, syngas is subjected to a water-gas shift step, in order to extensively clean and optimize gas composition (Daniell et al. 2012). By contrast, gas fermentation has freedom to operate across a wide range of syngas component ratios, thus avoiding external gas-shift operation (Heiskanen et al. 2007). Another advantage over FT is the higher selectivity of biological catalysts, which helps increase desired product yields and reduce by-product formation, consequently simplifying downstream extraction processes (Abubackar et al. 2012; Griffin and Schultz, 2012). Finally, the irreversible nature of biological reactions leads to a near complete conversion efficiency (Liew et al. 2016a). Despite the several advantages reported, there are still some limitations with gas fermentation, which need to be tackled in order to bring this technology to a wider implementation.

6.4 Microbiology and biochemistry of gas fermentation

6.4.1 Acetogens

The capability of fixing inorganic and gaseous carbon such as CO and CO_2 into multicarbon compounds (autotrophy) is a prerequisite for gas fermenting microorganisms. C1-assimilating bacteria comprise the anaerobic acetogens, the aerobic chemoautotrophs, photoautotrophs and methanotrophs (Humphreys and Minton, 2018). This study is mainly focused on acetogenic anaerobic microorganisms, with special focus on *Clostridium autoethanogenum*. Acetogens play a key role in the global carbon cycle, being responsible for fixing about 20% of CO_2 on earth and producing a minimum of 10^{12} kg of acetate per year (Drake et

al. 2006; Tracy et al. 2012). They are ubiquitous in nature as they have been isolated from disparate ecosystems including soils, sediments, sewage sludge, feces, intestinal tracts of humans and animals, and industrial wastes (Daniell et al. 2012; Phillips et al. 2017). This special group of microbes is capable of growing chemoorganotrophically as well as autotrophically with H_2/CO_2 and/or CO as carbon and energy source, producing short-chain fatty acids and alcohols (Daniell et al. 2012; Henstra et al. 2007). Acetogens utilize the Wood-Ljungdahl pathway as a mechanism for reduction of CO_2 (and/or CO) to the intermediate Acetyl-CoA, energy conservation for growth and assimilation of CO_2 into the cell carbon. Within the 20 genera and 100 species of acetogens identified so far, *Acetobacterium* and *Clostridium* represent the best-characterized genera (Drake et al. 2008). Among them *C. aceticum* was the first to be isolated and characterized (Wieringa, 1940). These bacteria are extremely heterogeneous, including both Gram-positive and Gram-negative, alkaline and acidic microorganisms with various morphologies (rods, cocci and spirochetes) and optimal temperatures ranging from 5°C to 62°C (Phillips et al. 2017). **Table 6.1** provides an overview of some of the most noteworthy acetogens with their native substrates and products. Although in nature, only few bacteria are capable of growing solely on CO, due to inhibition effects on metalloproteins and hydrogenases, most acetogens can utilize CO as both a carbon and energy source (Liew et al. 2013). In contrast to CO, CO_2 as more oxidized carbon form, requires H_2 for its fixation. Regarding products, all acetogens produce acetic acid and, under autotrophic conditions, more than 90% of them produce solely acetate as their fermentation metabolite (homoacetogens) (Köpke et al. 2014). Homoacetogens include the well-studied *Acetobacterium woodii*, *Moorella thermoacetica* and *Clostridium aceticum* (Daniell et al. 2012). However, what makes acetogens particularly appealing is their native ability to synthesize a wide range of industrially relevant molecules such as ethanol and the C4 compounds 2,3-butanediol, butanol and butyrate (Humphreys and Minton, 2018). *Clostridium ljungdahlii* represents the first acetogen reported for its ability to produce ethanol from syngas (Tanner et al. 1993). Together with *C. ljungdahlii*, *C. autoethanogenum* recently gained much attention from the academic and industrial scientific community and so far these microorganisms are the most extensively studied in the field of gas-fermentation.

Table 6.1 Overview of some of the most representative acetogens. Adapted from *Liew et al. 2016a*.

Microorganism	Substrates	Products	T_{opt} (°C)	pH_{opt}	References
Acetobacterium woodii	H_2/CO_2, CO	Acetate	30	6.8	Genthner and Bryant, 1987
Acetonema longum	H_2/CO_2	Acetate, butyrate	30-33	7.8	Kane and Breznak, 1991
Alkalibaculum bacchi	H_2/CO_2, CO	Acetate, ethanol	37	8-8.5	Allen et al. 2010b
Eubacterium limosum	H_2/CO_2, CO	Acetate, butyrate	38-39	7.0-7.2	Genthner et al. 1981
Clostridium ljungdahlii	H_2/CO_2, CO	Acetate, ethanol, 2,3-BDO, lactate	37	6	Tanner et al. 1993
Clostridium autoethanogenum	H_2/CO_2, CO	Acetate, ethanol, 2,3-BDO, lactate	37	5.8-6.0	Abrini et al. 1994
Clostridium carboxidivorans (or *P7*)	H_2/CO_2, CO	Acetate, ethanol, butyrate, butanol, lactate	38	6.2	Liou et al. 2005
Clostridium aceticum	H_2/CO_2, CO	Acetate	30	8.3	Adamse, 1980
Clostridium ragsdalei (or *P11*)	H_2/CO_2, CO	Acetate, ethanol, 2,3-BDO, lactate	37	6.3	Köpke et al. 2011
Clostridium formicoaceticum	CO	Acetate, formate	37	NA*	Andreese et al. 1970
Clostridium difficile	H_2/CO_2, CO	Acetate, ethanol, butyrate	35-40	6.5-7.0	Rieu-Lesme et al. 1998
Moorella thermoacetica	H_2/CO_2, CO	Acetate	55	6.5-6.8	Pierce et al. 2008
Moorella thermoautotrophica	H_2/CO_2, CO	Acetate	58	6.1	Savage et al. 1986

*NA, Not Available

6.4.2 Wood-Ljungdahl pathway

In 1966, Lars G. Ljungdahl and Harland G. Wood elucidated the biochemistry and enzymology of the reductive Acetyl-CoA pathway, which is more commonly named Wood-Ljungdahl pathway (WLP), in recognition of its two pioneers. The model organism used was the thermophilic acetogen *Clostridium thermoaceticum*, now recognized as *Moorella thermoacetica* (Drake et al. 2006; Ljungdahl and Wood, 1969). WLP is even referred to as the carbon monoxide dehydrogenase/acetyl-CoA synthase (CODH/ACS) pathway, whereby the enzymatic complex CODH/ACS is a pivotal component for carbon fixation. Analysis of the transcript levels revealed that CODH/ACS is the highest expressed in *C. autoethanogenum* grown under autotrophic conditions (Köpke et al. 2011). As the simplest among autotrophic pathways, it has been speculated that WLP represents the first biochemical pathway on earth (Drake et al. 2006; Lindahl and Chang, 2001). Moreover, it is reported to be the most efficient non-photosynthetic carbon fixation pathway as well as the only non-cyclic CO_2 conversion metabolic route to Acetyl-CoA (Fast and Papoutsakis, 2012; Drake et al. 2008). It is also worth noting that WLP remains active even under heterotrophic growth conditions, thus allowing the recapture of the released CO_2 (Drake et al. 2006). Acetyl-coA pathway scheme is illustrated in **Figure 6.2**. It entails two branches, the methyl (sometimes referred to as the eastern) and the carbonyl (also referred to as western) branch. In presence of only CO, one molecule of gas can directly enter the carbonyl route. The CO_2 required for the methyl branch is generated instead from CO oxidation with concomitant ferredoxin reduction, in a CODH-mediated Water Gas Shift (WGS) reaction (Daniell et al. 2012). WGS reaction proceeds as follows:

$$CO + H_2O \rightarrow CO_2 + H_2 \; (\Delta G^{\circ\prime} = -20.1 \; kj/mol) \quad \text{Eq. 6.1}$$
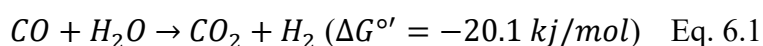
WGS reaction is responsible for the enormous flexibility exhibited by acetogens in terms of gas composition, allowing utilization of either CO or H_2 as an electron source. However, electrons generation from CO is thermodynamically more favorable. With a CO/CO_2 redox potential from -524 to -558 mV, CO is about 1000-fold more able to generate very low potential electrons compared to NADH, allowing reduction of ferredoxin and flavodoxin (Liew et al. 2013). Conversely, when grown on CO_2 as substrate, the CO is generated from CO_2 reduction via CODH in the carbonyl branch. As above reported, in this case reducing power derives from oxidation of molecular hydrogen that is used as substrate in hydrogenase-based reactions $(H_2 \rightarrow 2H^+ + 2e^-)$. In the methyl branch CO_2 is first reduced to formate by formate dehydrogenase. Then, formyl-THF-folate synthase catalyzes the condensation of formate with tetrahydrofolate (THF), forming 10-formyl-THF and consuming one molecule of ATP. Through a cascade of enzymatic reactions, 10-formyl-THF is reduced to methyl-THF. Next, the methyl group is transferred to a corrinoid-iron-sulfur-containing protein (CoFeSP) via the action of a B12-dependent methyltransferase. Finally, the methyl group resulting from the

eastern branch and the carbonyl moiety deriving from the western branch, are condensed with a coenzyme A group, via the bifunctional carbon monoxide dehydrogenase/acetyl-CoA synthase (CODH/ACS), thus generating the Acetyl-CoA intermediate (Liew et al. 2016a). The platform compound Acetyl-CoA serves as a precursor for cellular mass and product synthesis.

Conversion into acetate and ethanol occurs according to the following equations:

$$6CO + 3H_2O \rightarrow CH_3CH_2OH + 4CO_2 \ (\Delta G^{\circ\prime} = -224 \ kJ/mol) \qquad \text{Eq. 6.2}$$

$$4CO + 2H_2O \rightarrow CH_3COOH + 2CO_2 \ (\Delta G^{\circ\prime} = -175 \ kJ/mol) \qquad \text{Eq. 6.3}$$

$$3CO + 3H_2 \rightarrow CH_3CH_2OH + CO_2 \ (\Delta G^{\circ\prime} = -164 \ kJ/mol) \qquad \text{Eq. 6.4}$$

$$2CO + 2H_2 \rightarrow CH_3COOH \ (\Delta G^{\circ\prime} = -135 \ kJ/mol) \qquad \text{Eq. 6.5}$$

$$2CO + 4H_2 \rightarrow CH_3CH_2OH + H_2O \ (\Delta G^{\circ\prime} = -144 \ kJ/mol) \qquad \text{Eq. 6.6}$$

$$2CO_2 + 6H_2 \rightarrow CH_3CH_2OH + 3H_2O \ (\Delta G^{\circ\prime} = -104 \ kJ/mol) \qquad \text{Eq. 6.7}$$

$$2CO_2 + 4H_2 \rightarrow CH_3COOH + 2H_2O \ (\Delta G^{\circ\prime} = -95 \ kJ/mol) \qquad \text{Eq. 6.8}$$
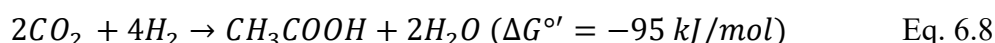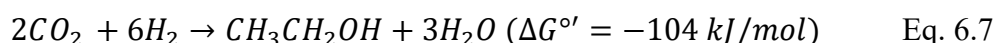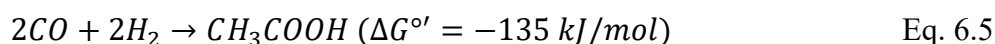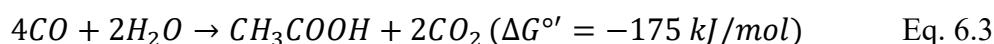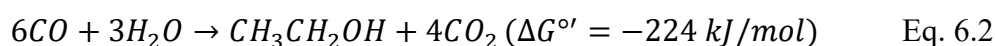
Acetate is obtained from Acetyl-CoA through the successive activity of two enzymes: phosphotransacetylase (Pta) and acetate kinase (Ack) (Daniell et al. 2012). As shown in **Figure 6.2**, in *C. autoethanogenum* and other acetogenic species (e.g. *C. ljungdahlii*, *C. ragsdalei* and *C. carboxidivorans*) biosynthesis of ethanol can occur via two distinct metabolic paths, both reliant on acetaldehyde as an intermediate. In the direct route, a two-step reduction reaction converts acetyl-CoA into acetaldehyde and then into ethanol via the action of the bi-functional aldehyde/alcohol dehydrogenase (AdhE), acetaldehyde dehydrogenase (Ald) and alcohol dehydrogenase (Adh). In the indirect route acetate is first reduced to acetaldehyde in a reaction catalyzed by aldehyde:ferredoxin oxidoreductase (AOR) (Liew et al. 2017).
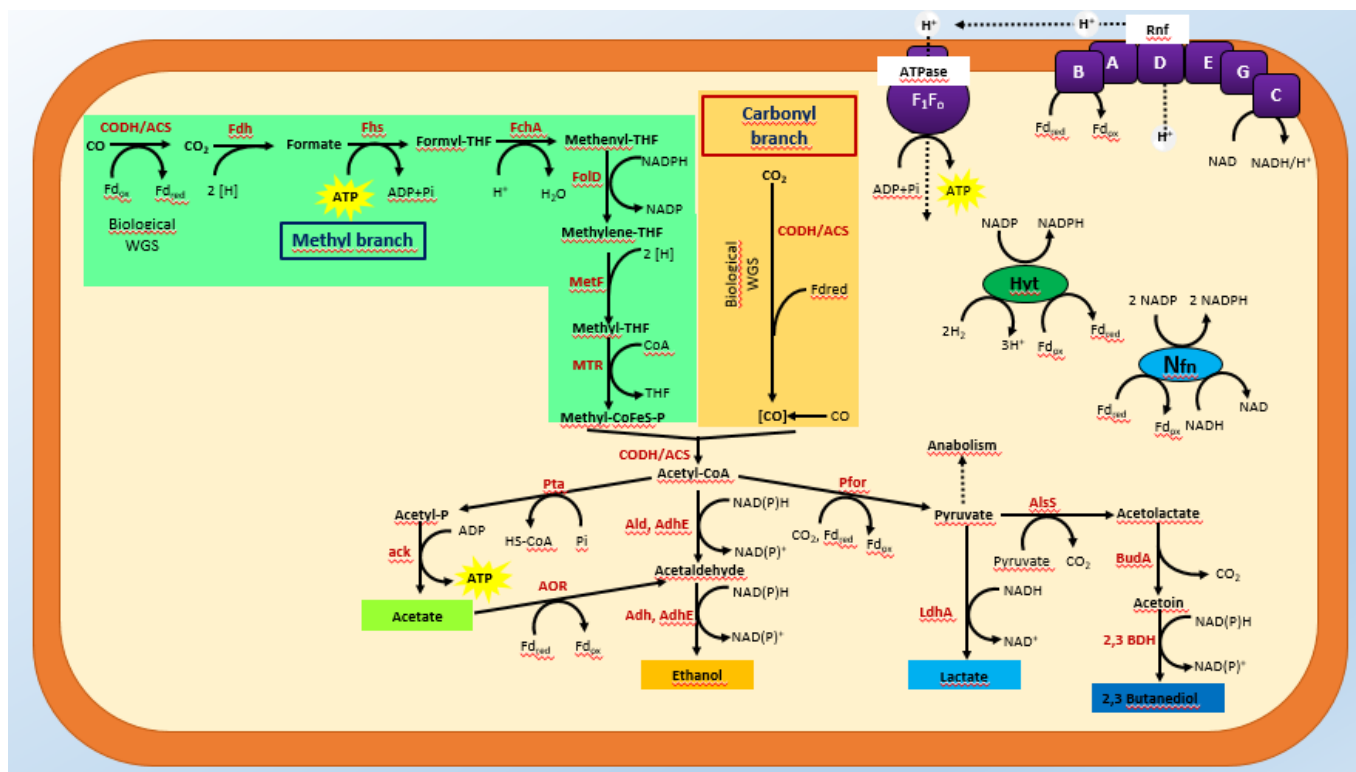
Figure 6.2 Overview of autotrophic metabolism in *C. autotoethaogenum*. Methyl and carbonyl branches of the Wood-Ljungdahl pathway are highlighted in green and yellow, respectively. CODH (carbon monoxide dehydrogenase); ACS (Acetyl-CoA synthase); Fdh (Formate dehydrogenase); Fhs (Formyl-THF ligase); FchA (Methenyl-THF cyclohydrolase); FolD (Methenyl-THF dehydrogenase); MetF (Methenyl-THF reductase); MTR (methyl transferase). CoFeSP (corrinoid iron sulphur protein). Fermentation metabolic pathway with native products (boxed). Pta (phosphotransacetylase), Ack (acetate kinase), AOR (aldehyde:ferredoxin oxidoreductase), AdhE (bi-functional aldehyde/alcohol dehydrogenase), Ald

(CoA-dependent acetaldehyde dehydrogenase), Adh (alcohol dehydrogenase), Pfor (pyruvate:ferredoxin oxidoreductase), AlsS (acetolactate synthase), BudA (acetolactate decarboxylase), 2,3-butanediol dehydrogenase (2,3-BDH), LdhA (lactate dehydrogenase). Energy conservation mechanism: Hyt (NADP-dependent electron bifurcating hydrogenase); Rnf (H^+-translocating ferredoxin: NAD^+-oxidoreductase); Nfn (NADH-dependent reduced ferredoxin:NADP oxidoreductase). Cofactors: Fd_{ox} (oxidized ferredoxin); Fd_{red} (reduced ferredoxin). Figure adapted from Liew et al. 2017; Bengelsdorf et al. 2013.

6.4.3 Energy conservation mechanisms

Although in literature the WLP is recognized as extremely efficient, the generation of Acetyl-CoA from CO_2 and H_2 has a negative energetic balance. As aforementioned, in the methyl branch CO_2 undergoes several reductive steps, including the activation of formate to formyl-tetrahydrofolate that consumes one mol ATP (**Figure 6.2**) (Henstra et al. 2007; Daniell et al. 2012; Liew et al. 2016a). In order to compensate for the invested metabolic energy, one mol ATP is gained during acetate synthesis in the reaction catalyzed by acetate kinase enzyme (**Figure 6.2**) (Henstra et al. 2007). Despite this mechanism of energy conservation via substrate-level phosphorylation (SLP), still no net ATP is gained (Daniell et al. 2012). Hence, additional energy must be provided. In order to overcome severe energy limitations, acetogens have developed unique strategies to support growth and fermentation, which combine ion-gradients and ATPase activity (Liew et al. 2016a; Dürre, 2017). These mechanisms are schematically shown in **Figure 6.2**. Net ATP gain is achieved through the membrane-associated ferredoxin-NAD: oxidoreductase complex (Rnf) and F_1F_0 ATP synthase (Mock et al. 2015). Briefly, it can be speculated that Rnf energetically couples ferredoxin to the NAD pool, with a highly reduced-ferredoxin/NAD^+ ratio resulting an essential condition for conservation energy mechanism to occur (Biegel et al. 2011). Rnf extrudes either protons or sodium ions via oxidation of reduced ferredoxin coupled with NAD^+ reduction, thus creating a transmembrane electrochemical gradient (Liew et al. 2016a; Biegel and Muller, 2010). Consequently, the built up gradient acts as a driving force for ADP phosphorylation through the F_1F_0 ATP synthase (Biegel and Muller, 2010). The Rnf complex is not ubiquitous in acetogens and in some species such as *C. autoethanogenum* the mechanism described above is proton-dependent rather than strictly sodium-dependent like in *A. woodii* (Mock et al. 2015; Liew et al. 2016a). Recently novel energy conserving systems have been identified in some acetogens such as *C. autoethanogenum*. These include the electron-bifurcating and NADP dependent [Fe-Fe]-hydrogenase (Hyt) and the NADH-dependent reduced ferredoxin:NADP oxidoreductase (Nfn) (Liew et al. 2016a). The activity of these key mechanisms along with the presence of the aldehyde:ferredoxin oxidoreductase (AOR) enable some acetogens (i.e. *C. autoethanogenum*, *C. ljungdahlii*, *C. ragsdalei*, *C. carboxidivoran* and *C. coskatii*) to produce more reduced metabolites such as ethanol, 2,3-BDO or butanol (Liew et al. 2016a; Mock et al. 2015).

6.4.4 *Clostridium autoethanogenum*

Clostridium autoethanogenum was first isolated in 1994 from rabbit feces by its ability to utilize CO (Abrini et al. 1994). It is a Gram-positive, strict-anaerobic and motile microorganism, resembling a rod-like shape. *C. autoethanogenum* grows optimally at 37°C and pH within 5.8-6 (**Table 6.1**). Despite being described as a spore forming microbe, the phenomenon of sporulation has not been

experimentally highlighted yet (Piatek, 2017). With the same arrangement and sequence in the Wood Ljungdahl operon and 99% similarity in 16S rRNA sequences, *C. autoethanogenum* is phylogenetically indistinguishable from its closest-relative *C. ljungdahlii* (Humphreys et al. 2015; Köpke et al. 2011). A full genome version was published in 2014 (Brown et al. 2014) but further improvements were provided later by the means of manual annotations and Sanger sequencing to assess putative SNPs (Humphreys et al. 2015). Moreover, recently a multi-omic investigation including transcriptome, metabolome and proteome analysis of *C. autoethanogenum* has been conducted and included in a publication by Marcellin and co-workers (Marcellin et al. 2016). To date, *C. autoethanogenum* constitutes a prominent microbial factory, particularly robust and effective in fermenting CO and CO_2 to acetate, ethanol, lactate and 2,3-BDO (Liew et al. 2016a). *C. autoethanogenum* is also able to grow heterotrophically using fructose and xylose (Brown et al. 2014). This model gas fermenting acetogen is already deployed at industrial scale. LanzaTech, the most advanced company in the gas-fermentation field, has developed a proprietary process reliant on *C. autoethanogenum* in strategy for conversion of steel mill off-gases (Humphreys and Minton, 2018).

6.5   Current commercialization status

Many entrepreneurial initiatives have been undertaken toward commercialization, reflected by the sharp increase in the number of scientific articles published as well as patent filings. To date, mainly three companies (Ineos Bio, Coskata and LanzaTech) have approached commercialization of gas fermentation technology, by employing pilot and demonstration plants for production of low-carbon fuels and chemicals in acetogens (Liew et al. 2016a). Among them, LanzaTech is the most advanced in scaling-up gas fermentation process, cooperating with more than 40 international partnerships in both private and academic sector. The first patents in the field of gas fermentation were filed by Prof. J.L. Gaddy of University of Arkansas (USA), who in 2003 founded Bioengineering Resources Inc (BRI), the pioneer company exploring the syngas-to-bioethanol process. In 2008, BRI was acquired by the multinational chemical INEOS and rebranded as INEOS Bio (Daniell et al. 2012; Liew et al. 2013). INEOS Bio relied on an 8 million gallon per year (Mgy) semi-commercial facility, employing *C. ljungdahlii* as biocatalyst and using lignocellulosic biomass and MSW as feedstocks (Liew et al. 2016a). It ceased to operate in 2016, primarily due to high concentrations of hydrogen cyanide in syngas (Teixeira et al. 2018). Coskata was created in 2006 in USA. In 2009 it started operating a demonstration plant using syngas first from wood biomass and MSW and then from reformed CH_4 (Teixeira et al. 2018). However, this company went out of business in 2015 with no further scale-up, when its technology was inherited by Synata Bio (Daniell et al. 2012; Liews et al. 2016a). Lanzatech was launched in New Zealand in 2005 and nowadays

it has undertaken the most commercially advanced approach for ethanol production, using a proprietary strain of *Clostridium autoethanogenum* and CO-rich steel mill off gases as substrate (Daniell et al. 2012; Humphreys and Minton, 2018). It has been estimated that with a full potential scale-up of LanzaTech facilities over the Europe, a production of 104 Mgy would displace 1.6 million barrels of fossil fuel-derived gasoline (Liew et al. 2016a). LanzaTech has cooperated with two steel Chinese companies, BaoSteel and Shougang Steel, for the construction of steel mill-based plants (Daniell et al. 2012). In 2015, together with ArcelorMittal and Primetals Technologies, LanzaTech set up a corporation in order to construct a large-scale facility for ethanol production in Ghent (Belgium) (Bengelsdorf and Dürre, 2017). Further commercial-scale ethanol projects, currently under development, include the utilization of different feedstocks such as ferroalloy off-gases in South Africa, refinery off-gases in India and gasified biomass in California, in cooperation with Swayana, IndianOil and Aemetis, respectively (Teixeira et al. 2018). LanzaTech is also investing in 2,3-BDO synthesis process. Given its industrial relevance, 2,3-BDO is reasonably receiving much attention as precursor of rubber and nylon, insecticides and pharmaceuticals (Marcellin et al. 2016; Teixeira et al. 2018). Additionally, since 2011 LanzaTech is focused on industrial-scale production of isobutylene in partnership with Global Bioenergies (Teixeira et al. 2018).

6.6 Approaches improving Gas fermentation technology

Advantages over conventional metal catalyst–based processes have been extensively discussed before; though gas fermentation platform also faces technical and economic bottlenecks that must be overcome to fully exploit its potentiality at commercial level.

Gas-to-liquid mass transfer represents the major barrier. Gaseous species such as H_2 and CO are sparingly soluble in the aqueous fermentation broth, with a solubility at 293 K and 1 atm pressure of 1.6 mg/L and 28 mg/L, respectively, compared to 900 g/L for the traditional glucose (Teixeira et al. 2018; Liew et al. 2016a). Hence, gas-to-liquid mass transfer becomes the rate-limiting step at high cell concentration. When either biomass concentration or CO consumption are too low the process is kinetically limited. Both these rate-limiting conditions negatively affect CO-bioconversion and process yield (Ungerman and Heindel 2007; Abubackar et al. 2012). Considering their key role as carbon source (CO) and/or reducing equivalents (CO and H_2) source, these main components of syngas mixture require constant replenishment in the fermentation media (Phillips et al. 2017). Several strategies to enhance gas-liquid mass transfer have been pursued and will be further discussed.

Other drawbacks include slow bacterial growth rate, medium costs, low product yields and product recovery (Liew et al. 2013). With the aim to circumvent these limitations, on-going research is mainly focusing on optimization of reactor

configuration, fermentation medium and operative conditions, as well as on the implementation of genetic engineering tools. An overview of these concepts will be provided in the next paragraphs.

6.6.1 Reactor design

One strategy of addressing issues related to mass transfer is the optimization of reactor design. Improvements in the design of industrial-scale bioreactors aim for high biomass concentrations, homogeneous mixing systems and high volumetric mass transfer coefficients (Ungerman & Heindel, 2007). Gas-liquid volumetric mass transfer coefficient, denoted as $k_L a$ (h^{-1}), is a reliable parameter to compare mass transfer rates among different reactor configurations as it describes the hydrodynamic conditions within the bioreactor (Munasinghe & Khanal, 2010). Essentially, it represents the efficiency of gas delivery to the system (Liew et al. 2016a). $k_L a$ can be determined as follows:

$$\frac{dc}{dt} = k_L a \, (c^* - c) \qquad \text{Eq. 6.9}$$

where c is the dissolved gas concentration in the liquid bulk at time t and c^* is its saturation concentration at the gas-liquid interface. As predicted by the Henry's law, the concentration of a gas species in the interface liquid is at equilibrium with its partial pressure within the gas bulk. As an example for CO:

$$C_{CO} = y_{CO} \, \frac{P_T}{H_{CO}} \qquad \text{Eq. 6.10}$$

where y_{CO} is the gas phase molar fraction of CO, P_T is the total pressure applied and H_{CO} is the Henry's law constant determined for CO (Phillips et al. 2017). Even if low volumetric mass transfer coefficient ($K_L a$) is responsible of limited substrate bioavailability within the bulk solution, on the other side, high concentrations of CO dissolved in the media would inhibit hydrogenases activity, thus lowering fermentation performance (Bertsch and Müller, 2015; Heijstra et al. 2017). With this concept in mind, reactor design proves challenging.

The majority of the academic research on gas fermentation has been accomplished using bench-top scale continuous stirred tank reactors (CSTRs) (**Figure 6.3a**). Their wide utilization is due to an excellent mixing as well as homogeneous distribution of gaseous substrate and temperature along the entire system (Liew et al. 2016a; Asimakopoulos et al. 2018). In CSTRs, the power input of the impeller generally is increased with the attempt to promote bubble breakup and, hence, enhance gas-liquid interfacial area available for mass transfer (Drzyzga et al. 2015). Baffled impellers mechanically shear gas bubbles, thus the resulting finer bubbles show reduced rising velocity while increased retention time in the fermentation

broth (Liew et al. 2013; Munasinghe and Khanal, 2010). k_La for CO over 100 h^{-1} can be obtained in CSTRs by setting high agitation rates, using microspargers as well as improving impeller design (Chen et al. 2015). Ungerman and Heindel (2007) tested alternative impeller geometries, concluding that a dual Rushton-type impeller improved mass transfer rate without substantial increases in power draw, but when an axial flow impeller was fixed on the top the highest k_La per unit power input ($k_La\ P_g^{-1}$) was reached. However, this set-up is not economically appealing and may irreversibly compromise the bacterial culture (Drzyzga et al. 2015). With the attempt to achieve homogeneous mixing of gases, alternative low-energy consuming systems have been examined (Teixeira et al. 2018). Hollow fiber membrane reactors (HFMRs) rely on cell immobilization onto the membrane with cell forming a biofilm or being trapped in pores (Wilkins and Atiyeh, 2011). This configuration has the advantage to provide high specific surface area. However, long-term mass transfer and fouling issues, caused by biofilm formation at high biomass concentration, strongly limit membrane-based bioreactors application (Asimakopoulos et al. 2018). Currently, bubble column reactors (BCRs) (**Figure 6.3b**) are considered promising candidates for industrial-scale gas fermentation, since they are characterized by good heat and mass transfer efficiencies, resulting in reduced capital and energy costs (Liew et al. 2013). Here, gas mixing is obtained through gas sparging, otherwise achieved with mechanical agitation in CSTRs. In BCRs the gas mixture, supplied from the bottom, is distributed in the liquid volume of the column via convective flows, thus ensuring longer gas-liquid contact times. Due to metabolic gas uptake, the substrate decreases as the gas flows up, creating a density gradient across the column (Asimakopoulous et al. 2018; Chen et al. 2015). Consequently, spatially different growth environments form within the column, making BCRs more difficult to optimize compared to CSTRs. Recently, a spatiotemporal metabolic model has been proposed and validated for BCRs, and this may be a step toward industrial-scale design (Chen et al. 2018). Another option is represented by trickle bed reactors (TBRs) (**Figure 6.3c**), where a packed bed column allows biofilm formation, with gas flowing co-currently or counter-currently respect to the liquid (Asimakopoulous et al. 2018). Similar to BCRs, no mechanical agitation is needed (Liew et al. 2013). This set up reduces the liquid resistance to mass transfer since the gaseous phase is in contact with a thin liquid layer (Devarapalli et al. 2017). Lastly, bioreactors in series have also been employed, where each unit was operated with recirculation driven by diverse liquid phase densities and pressures (Teixeira et al. 2018).
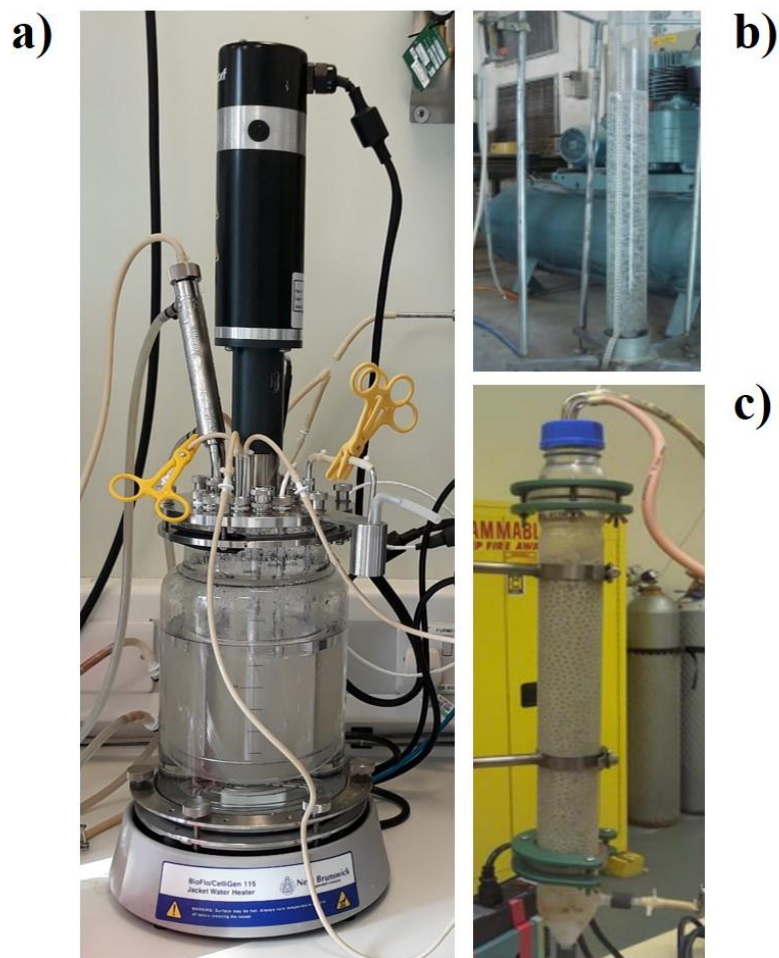
Figure 6.3 Bioreactor configurations for gas-fermentation. Panels: a) stirred tank reactor (STR) (This study); b) bubble column reactor (BCR) (Habobi and Turki, 2008) and c) trickle bed reactor (TBR) (Devarapalli, 2017).

6.6.2 Process parameters

The adjustment of process parameters such as pH, temperature, pressure, gas composition and flow rates can either improve or compromise acetogens' metabolic activity and, hence, gas fermentation performances. It has been abundantly reported that fermenting bacteria rearrange their metabolism toward solventogenesis to mitigate the negative effects of pH drop, occurring during acidogenesis phase (Daniell et al. 2012). Indeed, acetic acid is a weak organic acid, which in its undissociated state is lipophilic and penetrates through bacterial membranes. Consequently, H^+ ions are conducted along the transmembrane gradient, resulting in internal pH decrease. When internal pH decreases, the effect of external pH is magnified, causing a physiological stress that is circumvented by producing solvents (Overmann, 2006; Ahmed et al. 2006). Therefore, controlling pH of the fermentation broth throughout the overall process is beneficial. Whereas setting optimal pH (**see Table 6.1**) increases biomass yield and thus acetate synthesis, product selectivity (ethanol/acetate ratio) is reduced (Abubackar et al. 2016). Most

studies published so far demonstrated that decreasing pH helps to channel carbon into ethanol and other highly reduced products rather than acetate. Abubackar and his co-workers (Abubackar et al. 2012) conducted a batch-bottle experiment with *C. autoethanogenum,* showing a 200% enhancement in ethanol production, when both pH and Yeast Extract (YE), were lowered from 5.75 to 4.75 and from 1.6 to 0.6 g/L, respectively. Similarly, the same research group found a 143.5% reduction in ethanol production compared to acetate at pH 5.75, while an opposite trend was observed at pH 4.75 with *C. autoethanogenum* grown in a continuous CO-fed bioreactor (Abubackar et al. 2015a). Moreover, with a pH equal to 4.75, no accumulation of acetate was detected compared to pH 6 (Abubackar et al. 2015b). A further solution envisages a two-stage system, where the first bioreactor is set at higher pH in order to promote bacterial growth, whereas solventogenesis is triggered in the second unit by lowering pH (Gaddy and Clausen, 1992; Richter et al. 2013). Alternatively, Abubackar et al. (2016) recently applied cyclic pH shifts from high pH (5.75) to low pH (4.75) within the same bioreactor, allowing *C. autoethanogenum* to keep consuming CO and converting the endogenous acetate into ethanol. Conflicting results were reported instead by Cotter et al. (Cotter et al. 2009), who reached a higher biomass and ethanol titer with a *C. ljungdahlii* grown at pH 6.8 compared to 5.5. Inconsistency of these results may be determined by differences in operative conditions, strain and substrate used.

In an effort to maximize overall gas fermentation performances, temperature represents another key factor as it influences gaseous substrate solubility, inoculum growth rate, and hence metabolite productivity. As outlined in **Table 6.1**, acetogens are predominantly mesophilic with temperatures ranging from 30°C to 40°C; however, harnessing thermophiles would offer several advantages, including a reduction in cooling pre-treatment costs, less contamination risks as well as higher metabolic and diffusion rates (Bengelsdorf and Dürre, 2017; Henstra et al. 2007). Considering that Henry's law constant is a temperature dependent parameter (Wieland et al. 2015), the more temperature increases the less gas solubilizes into the liquid bulk. However, the resulting lower viscosity of the fermentation broth may improve mass transfer rate from gas to liquid (Daniell et al. 2012). In contrast to pH, few studies have investigated the effects of temperature on gas fermentation. Among them, Kundiyana et al. (2011) achieved higher ethanol titers in *Clostridium ragsdalei* setting a temperature at 32°C instead of its standard incubation temperature of 37°C. The authors speculated that the metabolite profile observed resulted from an enhancement of CO molar concentration and, thus of reducing equivalents in the medium (Kundiyana et al. 2011).

Although pH is a prerequisite for solventogenesis to occur (Gottschal and Morris, 1981), many parameters may interactively induce this metabolic shift. It has been speculated that, beyond reflecting the reduction and oxidation properties of the environment, redox potential (or oxidoreduction potential-ORP) of fermentation broth is an excellent indicator of cellular growth and metabolism (Kim, 1988). Hence, manipulating redox potential could be a promising approach to redistribute metabolic fluxes toward desired products, where a surplus of

reducing equivalents is responsible of solvent production (Meyer, 1986; Liu et al. 2017). Several approaches can be implemented to alter redox potential such as media supplementation with reductants or oxidants agents (See section 6.6.3) or adjustment of gas composition used to sparge fermentation broth. In the latter case, gases such as CO tends to reduce redox potential (Liu et al. 2017).

Composition of the gas entering the bioreactor also dictates product yield and selectivity. As mentioned before, during autotrophic growth, CO and H_2 act as energy sources for fixing CO_2 into reduced products but when H_2 is not present only 1/3 of the carbon available as CO can be converted into ethanol (Eq. 6.1) (Hurst and Lewis, 2010). Valgepea et al. (Valgepea et al. 2017) recently provided the first quantitative analysis of the impact of H_2 supplementation on acetogenic cultures grown on CO. The authors concluded that H_2 addition into the inlet gas is beneficial in terms of biomass and ethanol yield.

Once selected the desired gas mixture composition, inlet partial pressure of each gas species has to be optimized as well. The concentration of gases dissolved into the broth directs the thermodynamic of reactions and the kinetic rates (Phillips et al. 2017). The partial pressure of each gaseous component can be calculated using Eq. 6.11. As an example for CO:

$$p_{CO} = y_{CO}P_T \qquad \text{Eq. 6.11}$$

By substituting Eq. 6.10 into Henry Law's and then applying it to the liquid-mass transfer expression (Eq. 6.8), the resulting equation is:

$$\frac{dc_i}{dt} = K_{L,CO}aH_{CO}(p_{CO}^G - p_{CO}^L) \qquad \text{Eq. 6.12}$$

Where $p_{CO}^G - p_{CO}^L$ represents the driving force, so that the difference in CO partial pressure. By increasing the headspace partial pressure of CO, CO_2 and/or H_2, higher gas saturation levels and enhanced gas liquid mass transfer can be achieved (Drzyzga et al. 2015; Oswald et al. 2018). Some works published so far assessed the effects of partial pressure on gas fermentation. One of the first studies was conducted on *C. ljungdahlii* by Vega et al. (1989). When initial p_{CO} and p_{H_2} were increased beyond 2.5 bar absolute pressure, inhibition effects were encountered with a resulting retarded exponential phase. Conversely, a culture of *C. carboxidivorans P7* was subjected to different p_{CO} ranging from 0.35 to 2 atm. The authors found that increasing p_{CO} resulted in higher biomass concentration, with 440% increase in maximum cell density and ethanol productivity at p_{CO} of 2 atm (Hurst and Lewis, 2010). Similarly, in *C. autoethanogenum* higher ethanol yield was reached by increasing pressure up to 1.6 bar during batch bottle assays (Abubackar et al. 2012).

Another potential approach aimed to increase gas solubility, is the use of over-pressurized bioreactor. Gaddy and co-workers (2007) reported the highest ethanol productivity (360 g/L·d) with a *C. ljungdahlii* culture grown at 1.7-2 bar pressure.

However, lately, the same strain was cultivated on CO_2 and H_2 in a 2.5 L batch stirred-tank reactor at absolute pressure of 7 bar. The authors demonstrated that, despite the high pressure applied, no significant changes in product yield were observed (Oswald et al. 2018). Moreover, gas compression at industrial level is not economically feasible; hence, new strategies have to be pursued.

6.6.3 Medium optimization

From a commercial perspective due to the large volume used, optimizing medium composition is imperative to save operating costs and make the bioprocess scale-up economical affordable. Plus CO and/or CO_2 + H_2, acetogens need vitamins, trace metals, minerals and reducing agents to support their metabolic activity (Liew et al. 2013). Some of these supplements are not good candidates for commercial scope, due to their unsustainable costs. For instance, buffering reagents such as morpholinoethanesulfonic acid (MES) can account for approximately 97% of the final cost of the media. Cheap undefined supplements such as cotton seed extract (CSE) or corn steep liquor have been investigated to substitute for vitamins (Kundiyana et al. 2010; Saxena and Tanner, 2012). CSE with a cost of 0.91 $/Kg results definitely economically advantageous compared to YE 183 $/kg (Kundiyana et al. 2010). Literature about the effects of YE on CO-fermentation is controversial. Some experimental evidences of the benefits of YE utilization on ethanol selectivity have been provided. Xu et al. (Xu et al. 2017) achieved the highest ethanol concentration by increasing YE concentration up to 1 g/L. Conversely, Abubackar et al. (2012) reported a 200% ethanol increasing, by lowering the YE up to 0.6 g/L. However, works on *C. autoethanogenum* using medium lacking YE have been also reported in literature (Valgepea et al. 2017, 2018). Metal co-factors are also essential components. For instance, the addition of nickel, a cofactor of CODH and ACS enzymes, was found to improve CO fixation (Ragsdale, 2009). Additionally, reducing agents (e.g. sodium sulphide, cysteine-HCl, methyl viologen and potassium ferricyanide) are required in order to establish a low redox potential environment, which favors solvents production by increasing intracellular NADH concentration (Liew et al. 2013).

6.6.4 Genetic manipulation in Clostridium spp.

Besides manipulation of culture conditions and optimization of bioreactor configuration, a further step toward gas-fermentation commercialization is the rational design of improved gas-fermenting bacteria. Combining these approaches offers a great aid to overcome the bottlenecks above discussed, making gas-fermentation technology more competitive on a cost perspective (Drzyzga et al. 2015). The next section is intended to provide a brief overview of the genetic tools available so far in *Clostridium* spp., giving more emphasis on the genome editing techniques utilized in the current study.

6.6.4.1 Overview of available genetic tools

Over the past decade, with the advent of cheap and reliable DNA sequencing technologies, the genetic composition of C1-fermenting bacteria has become more accessible. Whereas only a single acetogen had been sequenced up until 2010, multiple genome sequences have been ascertained in the past few years (Daniell et al. 2012). Notably, whole genome sequence and genome-scale models (GEMs) have been provided for the industrial relevant acetogens, *C. autoethanogenum* and *C. ljungdahlii* (Liew et al. 2016a). However, it is worth noting that acetogens are recalcitrant hosts for genetic manipulation, and their genetic inaccessibility makes these microorganisms still challenging to work with (Liew et al. 2016a). The slow doubling-times and the adverse culturing conditions have negatively influenced the development of solid molecular biology tools (Heijstra et al. 2017). Notably, as Gram-positive bacteria, the thickness of peptidoglycan within the cell wall plus the presence of native CRISPR systems or restriction-modification systems (methyl transferase and nucleases), have dramatically hampered the establishment of reliable protocols for introducing foreign DNA into cells (Liew et al. 2016a; Pyne et al. 2014). However, this step is a pre-requisite for genetic engineering of microorganisms. Today, electroporation and conjugation represent the most routinely used methods to accomplish DNA transfer into cells (Heijstra et al. 2017). Electroporation is a donor-cell independent approach, which offers several advantages such as simplicity, scalability and high reproducibility (Liew et al., 2016a). Additionally, it exhibits a high transformation efficiency up to 1.7×10^4 CFU/μg DNA for *C. ljungdahlii* (Leang et al. 2013). Electro-competent cell preparation is tedious but it can help further increasing transfer frequencies by implementing some strategies including pre-treatments with cell weakening agents, variations of electrical parameters and use of special buffers (Minton et al. 2016). Alternatively, when physical contact between the so-called donor-cell (regularly *E. coli*) and the recipient microorganism (*Clostridium*) occurs, DNA can be also transferred via conjugation. The advantage of conjugation is that the incoming DNA is transported as single strand, hence circumventing the recipient's restriction systems (Heijstra et al. 2017; Jennert et al. 2000). Unlike *C. ljungdahlii*, that is more genetically malleable and can be transformed through both procedures, *C. autoethanogenum* is capable of receiving DNA only via conjugation (Liew et al. 2017; Mock et al. 2015; Nagaraju et al. 2016). Before transformation, plasmids have to be suitably customized by inserting all the components required for propagation and selection in both hosts and recipients. In this regard, a significant contribution was made by Heap et al. (Heap et al. 2009), who constructed a standardized modular system for *Clostridium-E. coli* shuttle plasmids having Gram-positive and Gram-negative replicons, for maintenance in *Clostridia* and *E. coli*, respectively, plus the *traJ* gene for conjugation.

When genetic tools were still underdeveloped and generating inactivated mutants was still challenging, antisense RNA (asRNA) strategies were used to down-regulate target genes (Tummala et al. 2003). Here, complementary binding between

the asRNA and target mRNA prevents translation by blocking ribosome-binding site (RBS) interactions. First mutagenic tools developed for clostridia were reliant on intron-based gene inactivation mechanism (Liew et al. 2016a). These were mainly typified by ClosTron technology, which enables site-directed genetic disruption using the efficient and specific retrohoming mechanism of Mobile Group II introns (Joseph et al. 2018). Initially developed by Sigma-Aldrich and designated as TargeTron™, successively it was specifically tailored to *Clostridium* species by the research group of Professor Nigel Minton from the University of Nottingham, and thus renamed ClosTron (Liew et al. 2013). The ease of use, efficiency and reproducibility made ClosTron the most extensively applied genetic tool in clostridia, including *C. autoethanogenum* (Marcellin et al. 2016; Mock et al. 2015). However, like other insertional mutagenesis approaches, ClosTron may be affected by polar effects on downstream open reading frames (ORFs), which can potentially distort phenotypical analysis (Ehsaan et al. 2016; Kuehne et al. 2011). Additionally, multiple gene mutants cannot be created via ClosTron (Kuehne et al. 2011) and possibility of intron excision from the target gene cannot be ignored neither (Clauwers et al. 2016). Alternative techniques based on homology recombination (HR) have been evolved in an attempt to construct in-frame mutations. Among them, Allele-Coupled Exchange (ACE) technology (see section 6.6.4.2) has been formulated by the same research group that had previously developed ClosTron. Beside reverse genetic, with regard to forward engineering, generation of random mutant libraries can be achieved through transposon mutagenesis (Liew et al. 2016a). An exhaustive roadmap for an in-depth understanding of how to implement the aforementioned genetic procedures, is outlined in (Minton et al. 2016). Today, the revolutionary CRISPR/Cas9 is receiving enormous attention from the scientific community. The powerful CRISPR-based editing tool allows creating insertions, deletions or scar-less single-nucleotide mutations in a single-step, with high specificity and versatility (Jiang et al. 2013). A detailed description is provided in below.

6.6.4.2 Homologous recombination (HR) and Allele-Coupled Exchange (ACE)

Homologous recombination is a natural mechanism that ensures genetic diversity within a bacterial population, through the recombination occurring between two DNA sequences sharing high nucleotide identity. This native ability is exploited to target specific genes residing in the genome by either disruption (knock-out) or insertion (knock-in) (Nakashima and Miyazaki, 2014) Unlike yeasts and naturally competent bacteria, clostridia cannot be efficiently transformed with linear DNA so plasmid DNA is used instead (Heap et al. 2012). Plasmid design for HR-based methodologies envisages the inclusion of a homology cassette containing DNA fragments homologous to the flanking regions of the target DNA locus. As plasmid DNA is circular, if single crossover occurs, the plasmid will entirely integrate within the host's chromosome, resulting in an unstable conformation that can potentially revert to wild type. If the second recombination event happens at the

other homology arm (HA), the desired double crossover mutants will be generated. This circumstance is rare since it results from two HR events in the same cell or lineage (Heap et al. 2012; Minton et al. 2016). In order to promote the isolation of double crossover mutants from single crossover cells, a wide number of counter-selection markers located on the plasmid backbone have been developed so far (Heap et al., 2012). These include *upp* (uracil phosphoribosyltransferase) (Croux et al. 2016), *mazF* (*E.coli* toxin) (Al-hinai, Fast, & Papoutsakis, 2012), *codA* (cytosine deaminase) (Cartman et al. 2012) and *pyrE/pyrF* (orotate phosphoribosyltransferase) (Heap et al. 2012). However, selecting an efficient counter-selection marker and the optimal conditions to use it can be a laborious task (Heap et al. 2012). Rather than employing a plasmid-borne counter-selection marker to screen for the second recombination event, Heap et al. (2012) developed an alternative method called Allele-Coupled Exchange (ACE), which is reliant on two principles: a) activation/inactivation of gene(s) resulting in a selectable phenotype and b) use of asymmetrical homology arms to dictate the order of recombination events. As demonstrated by the insertion of the whole phage lambda genome (48.5 kB) into C. *acetobutyilicum* chromosome, ACE technology allows the incorporation of heterologous DNA into the genome, with no limits on size or complexity (Heap et al. 2012). ACE technology application in microorganisms of *Clostridium* genus is well-established (Joseph et al. 2018), so that several studies are reported in literature, including works on *C. acetobutyilicum* (Ehsaan et al. 2016; Heap et al., 2012), *C. difficile* (Ng et al., 2013), *C. sporogenes* (Zhang et al. 2015a) as well as *C. autoethanogenum* (Liew et al. 2017). The system is conceived so that once the plasmid is integrated into the chromosome after single crossover, during the desired second recombination event the plasmid-borne allele becomes coupled to an allele located on the genome, leading to the creation of a new selectable allele (Ehsaan et al. 2016).

Although heterologous DNA insertion via ACE can take place in diverse genetic loci, the most used exemplification of this procedure involves the native *pyrE* gene (Ehsaan et al. 2016). *pyrE* gene encodes orotate phosphoribosyltransferase enzyme, which catalyzes the conversion of the pyrimidine intermediate orotic acid into orotidine 5'-monophosphate (OMP), during *de novo* pyrimidine biosynthesis (Ng et al. 2013; Boeke et al. 1987). The same enzyme converts 5 fluoro-orotate (FOA), analogue of orotic acid, into 5-fluoroorotidine monophosphate (5-FOMP), subsequently converted to 5-fluorouridine monophosphate (5-FUMP), instead of UMP (Boeke et al. 1987). Misincorporation of fluorinated nucleotides into nucleic acids causes toxicity and consequently is lethal to the cell (Boeke et al. 1987). Due to its pivotal metabolic role, *pyrE* is essential when exogenous pyrimidines are not provided (Ng et al. 2013). As a result, *pyrE* deficient mutants are uracil auxotrophs and exhibit resistance to FOA (FOA[R]). Therefore, *pyrE* can be employed as positive/negative selection marker (Ng et al. 2013).

As described in Heap et al. 2012, a *pyrE*-deficient mutant is needed prior to whether perform clean in-frame deletion or insertion within the host's genome. For this purpose, the construction of a special allele exchange cassette, incorporating a long

HA (1200 bp) corresponding to the region immediately downstream *pyrE* and a much smaller HA (300 bp) internal region of *pyrE* (omitting the 3' end), is required. Due to its greater size, the long HA directs the first recombination event (plasmid integration) following which *pyrE* still maintains its integrity. Since the vectors utilized comprise an antibiotic resistance gene (generally the chloramphenicol/thiamphenicol-resistance marker *catP*), the integrants have a growth advantage over those clones in which plasmid remains autonomous into the cytoplasm. Hence, single crossover clones result in larger and faster-growing colonies after exposed to thiamphenicol (Tm) (Minton et al. 2016). The second crossover event at the shorter homology arm results in *pyrE* truncation (Δ*pyrE*) and so plasmid excision. Double-cross mutants can be selected for by supplemented media with FOA and uracile. As follows, in *pyrE* negative strain the wild-type *pyrE* allele has been replaced with a mutant version lacking about 300 bp at the 3' end. Now a heterologous *pyrE* gene can be employed as counter-selection marker, leading to restoration of FOA sensitivity.

Once the *pyrE* deficient strain has been constructed, this serves as a background for ACE mutant construction. As shown in **Figure 6.4a**, for in-frame deletion of the target gene, equal sized homology arms (flanking the chromosomal locus of the target gene) are spliced together and ligated into the plasmid, forming the KO cassette. Beyond resistance marker and defective replicon, a heterologous functional copy of *pyrE* needs to be included. Initiation of homologous recombination can occur indistinctly at one of the two HAs. The successfully isolated integrants are subjected to antibiotic selection, and can be carried forward to the next selection step by the inclusion of FOA, whose addition allows the counter selection against the functional orthologous *pyrE* located on the plasmid backbone. ACE can be implemented also for gene insertion with the concomitant repair of *pyrE* locus, as shown in **Figure 6.4b**. In this instance, an ACE correction vector is designed so that a heterologous cargo is located between the *pyrE* homology regions. When the *pyrE* minus strain is transformed with the ACE correction vector, the *pyrE* allele is restored back to wild type. As previously described, single crossover mutants are first selected for by supplementing media with Tm whereas double crossover cells can be isolated plating on media lacking uracil. Indeed, once *pyrE* locus has been correctly repaired by replacement of the defective allele, the auxotroph strain is become back to prototrophy. No false positives can emerge with this procedure since reestablishment of prototrophy can just occur by the means of ACE-mediated substitution of the truncated allele with a wild-type version. ACE methodology offers also the possibility to complement a mutant strain at an appropriate gene dosage, by cloning a functional wild type copy of the knocked out gene, either under the control of its native promoter or of a strong promoter, in the latter case resulting in gene overexpression. This approach is often useful to assess mutant phenotype. The straightforward procedure described, made ACE chromosomal complementation certainly advantageous over conventional plasmid-based approach, requiring continuous antibiotic addition to ensure plasmid maintenance instead (Minton et al. 2016).
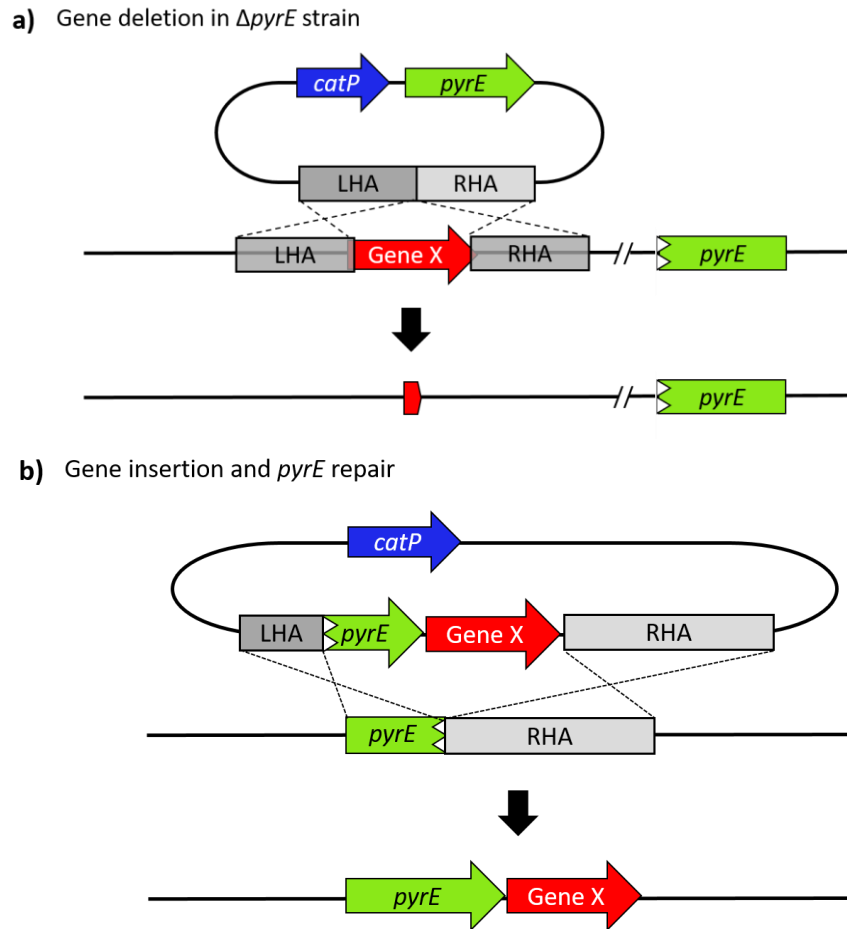
Figure 6.4 Schematic representation of Allele-Coupled Exchange (ACE) procedure. a) For in-frame deletion of target gene (Gene X), a plasmid incorporating homology arms flanking chromosomal locus of the target gene, and a heterologous *pyrE* gene, is transformed in a Δ*pyrE* strain. Homology recombination (dotted line) occurs at one of the HA and the single crossover mutants are selected for by thiamphenicol inclusion. Double crossover mutants are then isolated using 5-FOA. b) Insertion of target gene at the *pyrE* locus and concomitant *pyrE* restoration can be achieved using an ACE correction vector carrying a heterologous cargo between the *pyrE* homologous regions. Single crossover clones can be selected for by supplementing media with thiamphenicol whereas double crossover mutants can be identified on media lacking uracile.

6.6.4.3 CRISPR-based genome editing

Lately, the addition of CRISPR-Cas machinery in the genome-engineering toolbox, has noteworthy augmented the capability of tailoring genome and programming gene expression in both prokaryotes and eukaryotes. CRISPR is an acronym for Clustered Regularly Interspaced Short Palindromic Repeat. In prokaryotes, CRISPR in tandem with its CRISPR-associated (*Cas*) proteins constitute an RNA-guided adaptive immunity system, conferring resistance against invasive DNA

elements such a phages and conjugative plasmids (Marraffini & Sontheimer, 2010). CRISPR loci contain a series of repeated elements (CRISPR repeats) interposed by variable spacers (CRISPR spacers), and are typically flanked by *cas* genes, encoding the enzymatic machinery responsible for foreign DNA cleavage (Barrangou and Marraffini, 2014; Jiang et al. 2013). CRISPR loci have been found in approximately 45% of bacteria and in almost 90% of archeal species (Marraffini and Sontheimer, 2010). Although identified in 1987 (Ishino et al. 1987), their biological function remained elusive until 2005, when the variable spacers were found to share homology with genomes of phages and other mobile elements (Barrangou and Marraffini, 2014). CRISPR-Cas systems are grouped into five major types, each having individual structural and functional characteristics. Among them, the type II CRISPR system with its single Cas9 effector protein, native to the pathogen *Streptococcus pyogenes* (spCRISPR-Cas9), is the most well-described so far as well as the first cleverly implemented for genome editing purpose (Bruder et al. 2016; Joseph et al. 2018).

CRISPR-based immune system acts via three conserved steps (**Figure 6.5**). Initially, exogenous DNA uptake from an infecting agent triggers the so-called acquisition (or adaptation phase). During this stage, short fragments of DNA homologous to the invading nucleic acid are incorporated as new spacers into the CRISPR locus located in the host's chromosome, with the recruitment of Cas proteins (Makarova et al. 2011). This process makes the resulting CRISPR arrays an authentic immune "memory" (Bruder et al. 2016). Successively, in the expression stage also referred to as CRISPR RNA (crRNA) biogenesis, the repeat-spacer array is first transcribed in a long precursor transcript (pre-crRNA) and then processed into small interfering crRNAs. The crRNAs will define now the CRISPR targets (also called protospacers). During the last step, termed targeting or interference, the crRNA drives Cas endonuclease to the DNA target. While crRNA binds to the complementary target sequence that matches the spacers, the Cas protein performs the nucleolytic cleavage of the target homologous sequence within the proto-spacer sequence, thus degrading the invading DNA. The presence of a sequence motif located immediately downstream of the target region termed protospacer-adjacent motif (PAM), is critical to ensure recognition by the Cas-RNA complex and for the cleavage to occur (Barrangou and Marraffini, 2014; Jiang et al. 2013; Makarova et al. 2011). The PAM consensus sequence depends on the type of Cas protein. Specifically, spCas9 recognizes a PAM of 5'-NGG-3' (where N can be any nucleotide) (Tian et al. 2017).
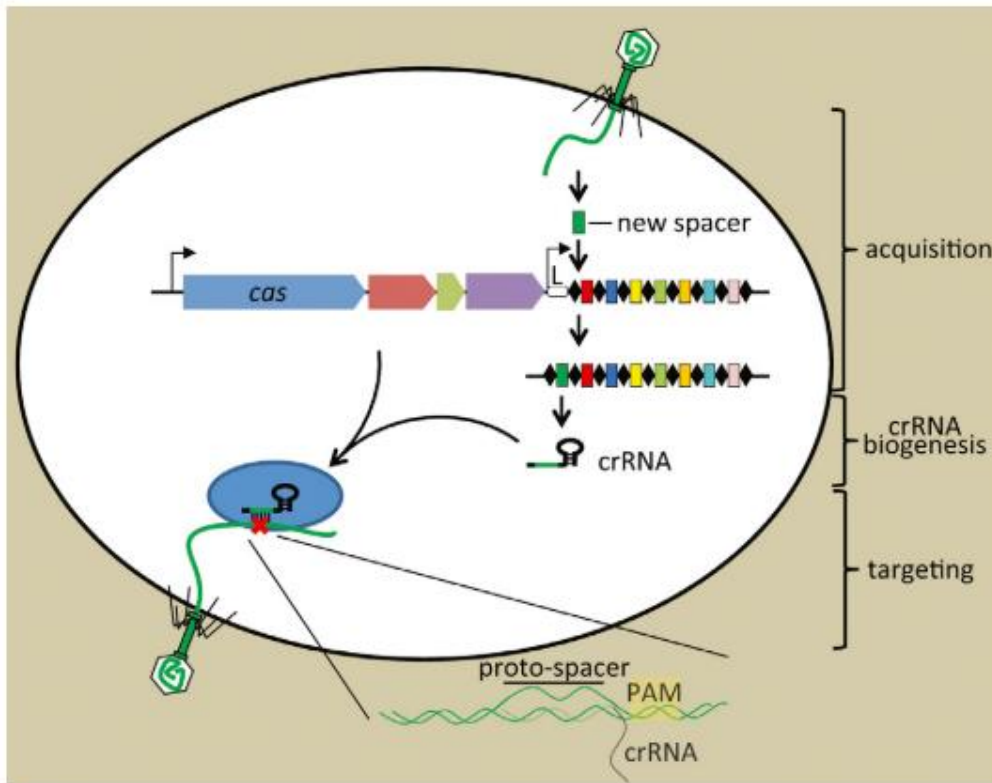
Figure 6.5 Three steps of CRISPR –based immunity: new spacers deriving from the invading agent are inserted into the CRISPR array. During crRNA synthesis, nuclease Cas processes a CRISPR precursor transcript, to generate small crRNAs. During targeting phase, the annealing between crRNA spacer and target DNA sequence promotes the cleavage of the invading DNA (Sampled from Barrangou and Marraffini, 2014).

Regarding the most commonly used type II system, the mature crRNA forms a hybrid complex with a trans-activating RNA (tracrRNA), which then guides Cas9 to hybridize with the foreign DNA (Bruder et al. 2016). In adapting CRISPR-Cas9 system into a genetic tool, a single chimeric RNA (sgRNA) with features of both tracrRNA and crRNA, have been constructed, thus simplifying system design (Huang et al. 2016; Y. Wang et al. 2016). The single guide RNA (sgRNA) is designed to target a 20 bp sequence immediately adjacent to PAM (Joseph et al. 2018). Hence, by replacing the sgRNA sequence with a sequence of interest, Cas9 endonuclease activity can be easily redirected to the gene of choice (Huang et al. 2016). Following this principle, multiple guide sequences can be gathered together as a single CRISPR array to enable the simultaneous editing of multiple chromosomal loci, as recently reported in *E. coli* (Jiang et al. 2015).

As illustrated in **Figure 6.6**, if one wants to precisely delete a desired gene by the means of CRISPR-Cas9, the editing plasmid has to incorporate a homology cassette, Cas9 coding sequence and a sgRNA targeting the gene of interest. Whilst in eukaryotes the double strand break (DSB) introduced by Cas9 is repaired by non-homologous end joining mechanism (NHEJ), in prokaryotes DNA repair is mediated by homologous recombination as explained above (Nagaraju et al. 2016).

Consequently, CRISPR-Cas9 system works as counter-selection tool allowing accurate selection of successful homologous recombination events while discriminating non-mutant clones by targeting the wild-type sequence (Joseph et al. 2018). Indeed, Cas9 DSB cut is not prone to repair and it consequently would prove lethal for wild type cells, whereas clones harboring the edited chromosome are able to survive.
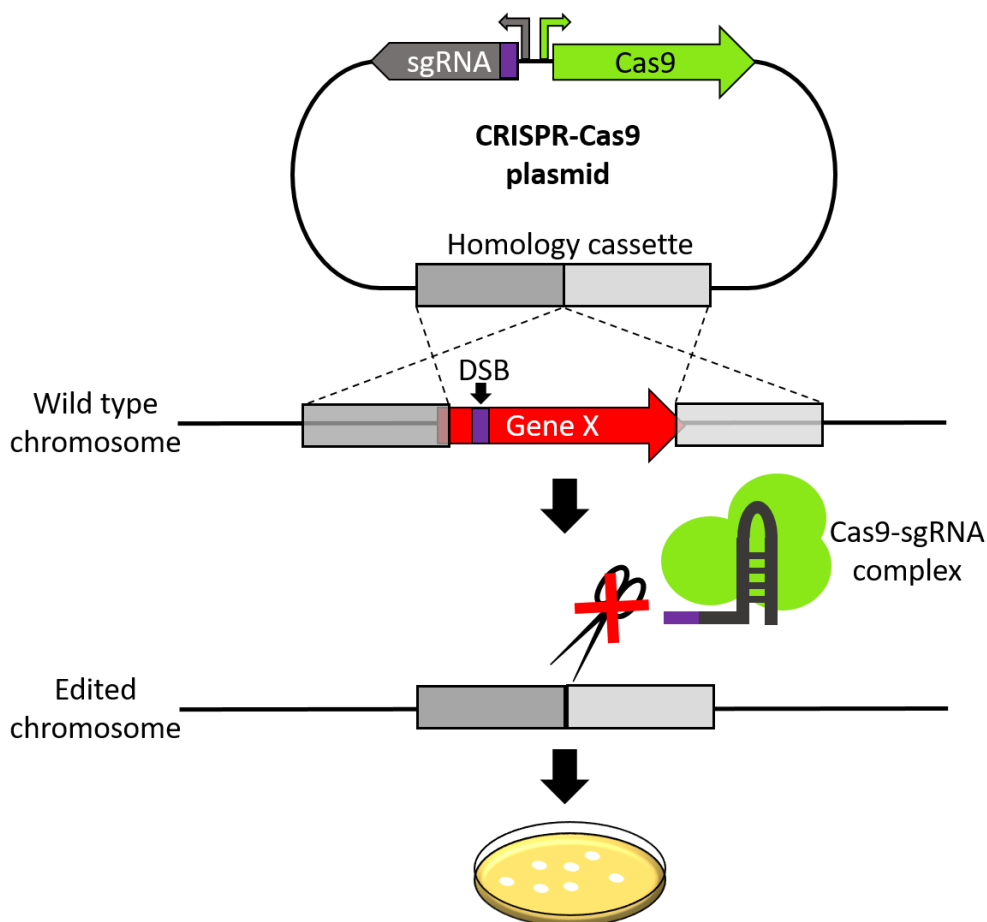
Figure 6.6 Schematic representation of CRISPR/Cas9 system for target gene deletion. CRISPR-Cas9 editing plasmid incorporate the Cas9 coding sequence, single guide RNA (sgRNA) and the homology cassette as editing template. Homologous recombination events are indicated by the dotted lines.

Applications of CRISPR-Cas9 methodology have been reported so far in *C. autoethanogenum* (Nagaraju et al. 2016), *C. ljungdahlii* (Huang et al. 2016), *C. acetobutylicum* (Li et al. 2016), *C. beijerinckii* (Li et al. 2016) and *C. saccharoperbutylacetonicum* (Wang et al. 2018). In spite of the numerous benefits over other techniques, there are still some challenges with CRISPR-Cas9 engineering. For instance, the constitutive expression of heterologous Cas9 from *S. pyogenes* may result deleterious, because of the inability of the host to repair double strand break, as a consequence of the supposed lack of non-homologous end joining (NHEJ) mechanism as well as low HR frequencies (Xu et al. 2015). Issues related

to toxicity of constitutively heterologous cas9 expression can be addressed by the use of an inducible promoter (Nagaraju et al. 2016; Wang et al. 2016). Another strategy consists of introducing the *cas9* gene and the sgRNA separately, by using a two-plasmid system. This approach allows circumventing the unsuccessful attempts to insert large fragments but two transformation steps need to be performed (Wasels et al. 2017). Furthermore, construction of a modified Cas9 known as Cas9 nickase was developed in order to mitigate the detrimental effects of DSBs. Two nickase versions, containing the inactivating point mutations D10A or H840A, are capable of introducing single-strand nicks instead of DSBs within the target DNA (Jinek et al., 2012). Xu et al. (Xu et al. 2015) proved that single-nick-triggered HR (SNHR), based on the use of Cas9 nickase, allows a single-step deletion generation in *C. cellulolyticum,* while lethal effects were found in the use of the wild-type Cas9 in this strain. Additionally, up to 100% editing efficiency was reached in *C. beijerinckii* and *C. acetobutylicum* by the use of Cas9 nickase version (Li et al. 2016). Moreover, the employment of native CRISPR-Cas system has been proposed as further strategy by Pyne et al. (Pyne et al. 2016). The authors were the first to harness endogenous type I-B CRISPR-Cas based machinery in *C. pasteuriaunum*, achieving 100% deletion efficiency compared to 25% reached with the *S. pyogenes* Cas9. Similarly, *C. autoethanogenum* genome possesses eight *cas* genes of type I-B, while no endogenous CRISPR machinery was found in *C. ljungdahlii* (Brown et al. 2014). This feature could be advantageous in terms of industrial application

6.6.4.4 Examples of successful metabolic engineering of *C. autoethanogenum* and *C. ljungdahlii*

The ideal gas-fermenting catalyst should exhibit the following peculiarities: high biomass density, efficient substrate consumption, high solvent tolerance, low aero-inhibition, asporogenous, enhanced fermentation product yield and selectivity (Liew et al. 2013). These traits can be selected for by the means of the continuous progresses made in synthetic biology and metabolic engineering field, which have opened up new avenues toward the creation of customized biocatalysts. Metabolic engineering studies that seek to enhance solvent production have extensively been reported. For instance, by genetically inactivating the native *aor2* or *adhE* genes with in-frame deletions, approximately 180% more ethanol was produced in *C. autoethanogenum* compared to the control strain (Liew et al. 2017). Earlier, Kopke et al. (2013) achieved 79% more ethanol using a *C. autoethanogenum* mutant with the competing 2,3-BDO metabolism inactivated through acetolactate decarboxylase gene (*budA*) deletion. Targeted gene-disruption strategy has been also implemented to assess the function of key genes. Relevant insight was provided by the functional genomic studies performed by Leang et al. (Leang et al. 2013). The authors observed a redirection of carbon and electron flow toward acetate with a corresponding 6-fold ethanol decrease in *C. ljungdhalii* carrying *adhE1*

chromosomal deletion. Additionally, incorporation of synthetic pathways has also been demonstrated in acetogens. Heterologous butanol pathway from *C. acetobutylicum* was successfully integrated in *C. ljungdahlii* and *C. autoethanogenum* (Kopke and Liew, 2011). Experimental evidences of enhanced solvent tolerance have also been documented. For instance, when genes encoding chaperones GroEL and GroES were overexpressed in order to prevent protein misfolding, *C. autoethanogenum* mutant outperformed the wild type strain during growth on steel mill gas in presence of high amount of ethanol (Simpson et al. 2011). Interestingly, broadening metabolites portfolio beyond the native products constitutes an attractive route to explore. Particularly, products separable with the same distillation technologies used for ethanol result economically appealing since minimum modifications to downstream processes are required (Liew et al., 2016a). In *C. autoethanogenum* product spectrum has already been expanded toward butanol (Kopke and Liew, 2011), acetone and isoproponol (Kopke et al. 2012), 3-Hydroxypropionate (Kopke and Chen, 2013), MEK (Mueller et al. 2013), isoprene and mevalonate (Chen et al. 2013). An alternative route aimed to increase solvent synthesis relies on the control of expression of genes involved in redox homeostasis. Notably, disruption of the *rex* gene coding a redox-sensitive transcriptional repressor has been proved to enhance solvent production in many clostridia (See Chapter 8). However, this avenue has not been explored yet in gas-fermenting microbes.

Chapter 7

Material and Methods

7.1 Bacterial strains and plasmids

7.1.1 Bacterial strains

Details of all bacterial strains used in this study are listed in **Table 7.1**.

Table 7.1 Bacterial strains used in this study. Abbreviations: *E. c.* = *Escherichia coli*; *C. a.* = *Clostridium autoethanogenum*; DSMZ = Deutsche Sammlung von Mikroorganismen und Zellkulturen.

Strain	Description	Source/Reference
E. c. DH5 Alpha (C2987)	Plasmid cloning and storage strain	New England Biolabs (NEB)
E. c. "sExpress"	NEB Express *E. coli* strain carrying R702 conjugative plasmid	Dr C. Woods (Uni. of Nottingham)
C. a. JA1-1 DSM10061	Wild type strain	DSMZ
C. a. Δ*rex*	*rex* deletion strain	This study
C. a. Δ*rex*Δ*pyrE*	*rex* deletion and *pyrE* truncation strain	This study
*C. a. rex**	Strain with *rex* complementation downstream of *pyrE* locus	This study

7.1.2 Plasmids

Plasmids that were either created or obtained in this study are reported in **Table 7.2**.

Table 7.2 Plasmids used in this study.

Strain	Description	Source/Reference
pMTL-CRISPR-Cas9	Construction of gene deletion strain	Dr C. Humphreys (Uni. of Nottingham)
pMTL-CRISPR-Cas9_*rex*	Construction of Δ*rex* strain	This study
pMTL-CRISPR-Cas9_*pyrE*	Construction of Δ*pyrE* strain	Dr C. Humphreys (Uni. of Nottingham)
pMTL-CH23	*pyrE* repair and gene insertion plasmid	Dr C. Humphreys (Uni. of Nottingham)
pMTL-CH23_*rex*	Chromosomal complementation of *rex* gene and concomitant *pyrE* repair	This study

7.2 General Microbiology methods

7.2.1 Antibiotics

Antibiotics used in the current study are reported in **Table 7.3**. When antibiotics are mentioned in the text, refer to **Table 7.3** for the working concentrations.

Table 7.3 Antibiotics used in this study. Abbreviations: *E. c. = Escherichia coli*; *C. a. = Clostridium autoethanogenum*.

Antibiotic	Dissolved in	Working conc. (µg/ml)	
		E. c.	*C. a.*
Chloramphenicol	Ethanol (100%)	25	
D-cycloserine	H_2O		250
Thiamphenicol	Ethanol (50%)		7.5

7.2.2 Culture conditions

Escherichia coli strains were cultivated aerobically in LB (Lysogeny Broth) medium, whose composition is listed in **Table 7.4**. Liquid cultures were typically gown in a shaking incubator at 225 rpm and at 37°C whereas solid agar LB plates were incubated in a static incubator at 37°C. For selection, LB was supplemented with chloramphenicol (Cm). For recovery step, SOC media (**Table 7.5**) was used when higher transformation efficiency was required.

Clostridium autoethanogenum strains were grown anaerobically at 37°C in a MG1000 Mark II Anaerobic Work Station (Don Whitley Scientific Ltd) operating with a gas mixture composed of 80% N_2, 10% H_2 and 10% CO_2. Strains were cultivated in YTF (Yeast-Tryptone-Fructose) (**Table 7.6**) or in PETC-MES media (**Table 7.10**). For selection, appropriate antibiotics such as thiamphenicol (Tm) and D-cycloserine (D-Cyc) were added to both liquid media or agar plates. Prior to their use, liquid media and agar plates were intentionally left in the anaerobic cabinet overnight and 4 hours, respectively, to ensure anaerobicity.

7.2.3 Growth media

All the media reported below were generally sterilized by autoclaving at 121°C for 20 minutes. Supplements to media were filter sterilized. For solid media, 15 g/L of Bacteriological Agar was added. All chemicals were purchased from Sigma-Aldrich, unless otherwise specified.

Table 7.4 LB (Lysogeny Broth) medium.

Component	Amount (g/L)
Tryptone	10
Yeast extract	5
NaCl	5

Table 7.5 SOC medium.

Component	Amount (g/L)
Tryptone	20
Yeast extract	5
$MgSO_4$	4.8
Dextrose	3.603
NaCl	0.5
KCl	0.186

Table 7.6 YTF (Yeast Typtone Fructose) medium.

Component	Amount per 1L
Yeast extract	10 g
Tryptone	16 g
Fructose	10 g
NaCl	0.2 g
Acidic trace element solution (1000x)	1 ml
Basic trace element solution (1000x)	1 ml
B-Vitamin stock solution (1000x)	1 ml

Adjust the pH to 5.8 using HCl.

Table 7.7 Acidic trace element solution (1000x)**.**

Component	Amount per 1 L
HCl	50 mM
H_3BO_3	100 mg
$MnCl_2 \cdot 4H_2O$	230 mg
$FeCl_2 \cdot 4H_2O$	780 mg
$CoCl_2 \cdot 6H_2O$	103 mg
$NiCl_2 \cdot 6H_2O$	602 mg
$ZnCl_2$	78 mg
$CuSO_4 \cdot 5H_2O$	50 mg
$AlK(SO_4)_2 \cdot 12H_2O$	50 mg

Table 7.8 Basic trace element solution (1000x).

Component	Amount per 1 L
NaOH	10 mM
Na_2SeO_3	58 mg
Na_2WO_4	53 mg
$Na_2MbO_4 \cdot 2H_2O$	52 mg

Table 7.9 B-Vitamin stock solution (1000x).

Component	Amount (mg/L)
p-aminobenzoate	114
Riboflavin	104
Thiamine	200
Nicotinate	206
Pyridoxin	510
Pantothenate (calcium)	104
Cyanocobalamin	78
d-biotin	22
Folate	48
Lipoate/thioctic acid	50

Adjust the pH to 7.8.

Table 7.10 PETC-MES medium.

Component	Amount per 1 L
NH_4Cl	1g
KCl	0.10 g
$MgSO_4 \cdot 7H_2O$	0.20 g
KH_2PO_4	0.20 g
$CaCl_2$	0.02 g
NTA- Nitriolotriacetic Acid	0.05 g
$Fe(SO_4)2(NH_4)_2 \cdot 6H_2O$	0.05 g
CH_3COONa	0.25 g
MES	20 g
Trace metal 100x	10 ml
Wolfe's vitamin solution 100x	10 ml
Resazurin (2 g/L)	0.5 ml

Adjust the pH to 5.8 using NaOH.

Table 7.11 Trace metal solution (100x).

Component	Amount per 1 L
NTA- Nitriolotriacetic Acid	2 g
$MnSO_4 \cdot H_2O$	1 g
$Fe(SO_4)_2(NH_4)_2 \cdot 6H_2O$	0.8 g
$CoCl_2 \cdot 6H_2O$	0.2 g
$ZnSO_4 \cdot 7H_2O$	0.2 mg
$CuCl_2 \cdot 2H_2O$	0.02 g
$NaMoO_4 \cdot 2H_2O$	0.02 g
Na_2SeO_3	0.02 g
$NiCl_2 \cdot 6H_2O$	0.02 g
$Na_2WO_4 \cdot 2H_2O$	0.02 g

Table 7.12 Wolfe's vitamin solution (100x).

Component	Amount (mg/L)
Biotin	4
Folic acid	4
Pyridoxine hydrochloride	10
Thiamine·HCl	10
Riboflavin	10
Nicotinic acid	10
Calcium D-(+)-pantothenate	10
Vitamin B12	0.2
p-Aminobenzoic acid	10
Thioctic acid	10

After preparation, PETC-MES medium was boiled and immediately placed on ice while sparging with N_2 to favor O_2 escape. The sparged medium was stored into the anaerobic cabinet to fully reduce for approximately 3-4 days, avoiding addition of carbon sources until inoculation.

Table 7.13 Bioreactor medium.

Component	Amount for 1.5 L
$MgCl_2 \cdot 6H_2O$	0.750 g
$CaCl_2 \cdot 2H_2O$	0.555 g
KCl	0.225 g
NaCl	0.180 g
85% H_3PO_4	0.570 ml
NH_4Cl	1.50 g
Metal mix 1	1.50 ml
Metal mix 2	0.30 ml
Tungsten solution	0.30 ml
Resazurin (2 g/l)	0.750 ml

Table 7.14 Metal mix 1.

Component	Amount (g/L)
$FeCl_2 \cdot 4H_2O$	19.35
$NiCl_2 \cdot 6H_2O$	1.19
$ZnCl_2$	0.69

Table 7.15 Metal Mix 2.

Component	Amount (g/L)
$CoCl_2$	2.38
HBO_4	0.62
$MnCl_2 \cdot 4H_2O$	1.98
$NaMoO_4 \cdot 2H_2O$	2.42
Na_2SeO_3	1.73

Table 7.16 Tungsten solution.

Component	Amount (g/L)
$Na_2WO_4 \cdot 2H_2O$	3.29

7.2.4 Bacterial strain storage and recovery

E. coli strains were stored by adding 15% *(v/v)* glycerol to the bacterial culture or using the Microbank^{TM} Bacterial and Fungal preservation system tubes provided by Pro-Lab Diagnostics. *Clostridial* stocks were created by adding 15 % *(v/v)* of dimethylsulfoxide (DMSO) to the bacterial suspension into 2 ml cryogenic screw-cap vials. Gently mixed, the tubes were then stored at -80°C (Innova® U725) without being snap-frozen. Cryoprotectants were filter sterilized before use. Recovery of stored samples was performed by scraping the frozen stock off with a sterile loop or resuspending a bead into the media.

7.2.5 Preparation of chemically competent *E.coli* cells

Preparation of chemically competent *E. coli* cells was performed using the following procedure: i) sub-culture 1 ml of an over-night culture into 100 ml of LB broth in a sterile conical flask and incubate at 37°C and 225 rpm in a rotary shaking; ii) when OD_{600} reaches 0.4-0.6, place the flask on ice for 10 min; iii) aliquot the culture into 50 ml falcon tubes; iv) spin down at 4000 rpm for 10 minutes in a refrigerated centrifuge at 4°C; v) discard supernatant and re-suspend the cell pellets in 10 ml sterile, ice-cold $CaCl_2$ (100 mM) with 20% *(v/v)* glycerol, leaving on ice for 15 min; vi) repeat steps iv) and v) but re-suspending bacterial pellets in 500 μL of $CaCl_2$; vii) aliquot in pre-chilled micro-centrifuge tubes and stored at -80°C.

7.2.6 Chemical transformation of competent *E.coli* cells

Chemically competent *E. coli* cells were transformed as follows: i) take out from the -80°C freezer a vial of chemically competent *E. coli* cells and thaw on ice for approximately 20-30 min; ii) add 1-3 μL of plasmid DNA into 40 μL of competent cells and gently mix by flicking the bottom of the tube a few times; iii) incubate the mixture on ice for 30 min; iv) heat shock the cell mixture at 42°C for 20-30 sec and then put the tube back on ice for 5 min; v) for cell recovery, add 500 μL of either LB or SOC media and incubate the mixture in a 37°C shaking incubator for 1h; vi) plate 100 μL of transformation mixture onto LB agar plates supplemented with Cm, and then incubate at 37°C overnight.

7.2.7 Conjugation

Plasmids were transferred into *C. autoethanogenum* via conjugation using *E. coli* sExpress (**Table 7.1**) as donor strain, carrying both the R702 conjugative plasmid and the plasmid of interest. The protocol was as follows: i) re-suspend the donor plasmid in 5 ml of LB, supplemented with chloramphenicol and incubate at 37°C overnight in a shaking incubator (225 rpm); ii) spin 1 ml of donor plasmid bacterial suspension for 3 min at 4000 rpm, then discard the supernatant; iii) wash with PBS to remove residual chloramphenicol; iv) centrifuge at 3000 rpm for 3 min and discard the supernatant; v) transfer the tube into the anaerobic cabinet and add 200 µL of a *C. autoethanogenum* culture grown for 2-3 days in YTF to the *E. coli* pellet; vi) spot the bacterial suspension onto non selective YTF agar plates previously degassed; vii) after 24 h, recollect the sample by adding 600 µL of sterile and anaerobic PBS, and plate onto selective YTF agar plates, containing thiamphenicol, to select for the desired plasmid and D-cycloserine to counter-select the *E. coli* donor.

7.3   Molecular Biology methods

7.3.1 Extraction of plasmid DNA from *E. coli*

Plasmid DNA was isolated from *E. coli* cultures grown overnight in LB media, supplemented with chloramphenicol as selection marker. Plasmid recovery was performed using Monarch® plasmid mini-prep Kit (NEB) according to the supplier's instructions.

7.3.2 Extraction of genomic DNA from *C. autoethanogenum*

Genomic DNA (gDNA) from *C. autoethanogenum* was routinely extracted using the GenElute™ Bacterial Genomic DNA Kit (Sigma-Aldrich), including the lysozyme lysis step for Gram-Positive bacteria preparation as per manufacturer's instructions.

7.3.3 Analysis of extracted DNA

When required, extracted plasmid DNA and gDNA samples were quantitatively and qualitatively analyzed using NanoDrop™ Lite spectrophotometer (ThermoFisher Scientific). Sample concentration was measured at 260 nm whereas the 260/280 nm ratio was selected to assess sample purity.

7.3.4 Polymerase Chain Reaction (PCR)

Polymerase Chain Reactions (PCRs) were routinely performed using the TProfessional Trio thermocycler by Biometra. SensoQuest Gradient Thermal Labcycler by Geneflow was occasionally used, when determination of the optimum annealing temperature was required. PCRs were carried out in a reaction volume of 20 μL according to the supplier's instructions. Q5® High-Fidelity DNA Polymerase (NEB) was utilized for amplification of fragments successively used for cloning steps and for mutant confirmation, while DreamTaq Green PCR Master Mix (Thermo Scientific™) was utilised for Colony PCR applications when lower fidelity was acceptable. An example of conventional PCR program used is reported in **Table 7.17**.

Table 7.17 Standard PCR program used in this study.

PCR step	Temp. (°C)	Time (min:sec)	
Initial denaturation	98*	00:30	
Denaturation	98	00:20	
Annealing	**	00:30	30 cycles
Elongation	72	***	
Final elongation	72	10:00	
Hold	15	-	

* 95°C for DreamTaq Green PCR Master Mix.

** Annealing temperature depends on primers selected.

*** 1 min per 1 kb.

7.3.4.1 Splicing by Overlapping Extension (SOEing) PCR

SOEing PCR served as method to construct the homology cassette required for deletion mutant construction, by amplifying and splicing together the left homology arm (LHA) and the right homology arm (RHA) of the target gene. The flanking regions were joined together by using primers with homologous sequences added to the 5' ends. Thus, two primers, designated as *rex*LHA_R1 and *rex*RHA_F1 (Appendix, **Table 12.1**), were designed comprising about 20 bp upstream from the target gene (including the stop codon) and 20 nucleotides downstream from the target gene (including the start codon), respectively. Initially, two independent PCR reactions were set up in order to amplify the HAs: *rex*LHA_F1 and *rex*LHA_R1 were used as forward and reverse primers for the LHA; while, the RHA was separately amplified using *rex*RHA_F1 and *rex*RHA_R1. Fragments separated on agarose gel were then used as template in the final PCR reaction, combining *rex*LHA_F1 and *rex*RHA_R1 to generate a full length product (Thornton, 2016). The overall PCR reactions mentioned were performed using Q5® High-Fidelity DNA polymerase.

7.3.4.2 Colony PCR

To set-up Colony PCRs, single colonies were picked from the plate using a sterile loop and swirled in 20 µL of sterile dH$_2$O. Then, 1 µL of the suspension of lysed bacteria was used as template along with 10 µL of DreamTaq Green PCR Master Mix, 1.5 µL of each primer and 6 µL of dH$_2$O.

7.3.4.3 Oligonucleotide primers

Oligonucleotide primers used throughout this study were purchased from Sigma-Aldrich. A complete list of the primers used is provided in Appendix, section 12.1.

7.4 Cloning techniques

7.4.1 Restriction enzyme digestion

For restriction enzyme digestion of plasmid DNA, restriction buffers and enzymes were purchased from NEB and used following manufacturers' protocols. Restriction digestion was generally performed in a volume of 10 µL with 1 µL of DNA, by incubating the reaction mix at 37°C for 1h. The restriction endonucleases used throughout this study and their cleavage sequence are reported in appendix, **Table 12.2**. Either single or double digestion was performed in CutSmart buffer, for which all the enzymes used have 100% activity.

7.4.2 Treatment with Antarctic Phosphatase (AnP)

The linearized plasmid DNA was treated with Antarctic phosphatase (NEB), which catalyzes the dephosphorylation of 5' and 3' ends, thus preventing backbone recircularization. Both phosphatase and Antarctic Phosphatase reaction buffer (NEB) were added directly into the digestion mix reaction, and subsequently incubated at 37° for 1h. The enzyme was irreversibly inactivated at 80°C for 2 min.

7.4.3 Ligation

Ligation reaction was performed using a ratio of 1:3, digested backbone to the insert of interest. T4 DNA ligase and T4 DNA ligase buffer were purchased from NEB. Ligation mixture reaction was incubated at room temperature for 1h and, successively used for *E. coli* transformation as previously outlined.

7.4.4 Hi-Fi assembly

Hi-Fi DNA or Gibson assembly cloning kit provided by NEB was used to assemble two or multiple DNA fragments. sgRNA oligonucleotides insertion into

CRISPR-Cas9 vector was achieved by mixing 10μL of each sgRNA stock with 25μL of NEB Buffer 2.1 and brought to 250 μL with sterile H_2O. Then, the resulting mix was combined with the CRISPR-Cas9 backbone previously digested with SalI restriction enzyme, in a ratio of 1:1 insert: vector. 10μL NEBuilder® HiFi DNA Assembly Master Mix, containing exonuclease, polymerase and DNA ligase, were successively added in the same tube and the reaction volume made up to 20 μL with H_2O. The reaction mix was incubated in the thermocycler at 50°C for 60 min and then used to transform competent *E. coli* cells.

7.4.5 Gel electrophoresis

DNA fragments were separated on 1% *(w/v)* agarose gels prepared by dissolving agarose powder in Tris-Acetate-EDTA (TAE) buffer (40 mM Tris, 1 mM EDTA and 0.1% Glacyal acetic acid). DNA detection was achieved using SYBR Safe DNA Gel stain (Invitrogen by ThermoFisher Scientific). Before loading DNA on the gel, DNA sample and gel loading dye purple (6X) (NEB) were mixed thoroughly. Electrophoresis was run at 100 V for around 30-45 min, using 'OgeneRuler 1kb plus DNA ladder (ThermoFisher Scientific) as marker. Bands were visualized using either a Syngene UltraBright blue-light transilluminator (Syngene) or an Odyssey® Fc imaging system (LI-COR).

7.4.6 Purification of DNA from agarose gel

The desired bands were excised from the agarose gel and target DNA fragments were purified using Monarch® DNA Gel Extraction Kit (NEB) following the manufacturer's instructions.

7.4.7 DNA sequencing

DNA sequencing of plasmids and PCR-purified products was conducted by Eurofin Genomics, either requesting or providing primers to the company.

7.5 Construction of *C. autoethanogenum* mutants

7.5.1 Construction of knock-out strains

Construction of *C. autoethanogenum* strain carrying *rex* gene deletion was achieved using a CRISPR-Cas9 genome editing tool developed within the Synthetic Biology Research Centre (SBRC) of the University of Nottingham. Plasmid pMTL-CRISPR-Cas9 was donated by Dr C. Humphreys (Uni. of Nottingham) and modified to host the appropriate homology cassette and the sgRNA targeting the desired gene. To achieve the desirable homologous recombination around the *rex*

ORF, the homology cassette generated by SOEing PCR (See section 7.3.4.1) was cloned into the CRISPR-Cas9 vector, using AscI and AsiSI restriction sites. Multiple independent KO strains were generated using three unique CRISPR-Cas9 plasmids, carrying a separate 20-nt single guide RNA (sgRNA) with discrete targeting locus within the *rex* gene. These strains are referred to as Δ*rex* sg1, Δ*rex* sg2 and Δ*rex* sg3. Each sgRNA was inserted into the vector using Hi-Fi assembly procedure as above described. The presence of *catP* cassette into the plasmid confers resistance to both chloramphenicol and thiamphenicol, thus allowing amplification in both *E. coli* and *C. autoethanogenum*. After plasmid propagation in *E. coli* Dh5 alpha, the constructed plasmid referred to as pMTL-CRISPR-Cas9_*rex*, was transformed into *E. coli* sExpress, successively employed in conjugation step. Delivery of the editing plasmid into *C. autoethanogenum* was performed via conjugation as previously outlined. After conjugation occurred, transconjugants grown onto YTF agar plates supplemented with Tm and D-cyc, were inoculated in 3 ml YTF medium for approximately 3/5 days, in order to induce plasmid loss. Successively, serial dilutions were plated onto YTF agar plates and the appeared colonies then restreaked onto both YTF and YTFTC agar plates. After 3/5 days of incubation, only colonies visible onto YTF and not onto YTFTC agar plates, lost the plasmid. PCR screening of the *rex* locus was performed using the primer *rex*ScrF1, F2 and R1, reported in appendix, **Table 12.1**. Thus, the PCR-amplified fragments were extracted and sequenced to further confirm the deletion of *rex* ORF.

Construction of Δ*rex*Δ*pyrE* strains was achieved using the pMTL-CRISPR-Cas9_*pyrE* plasmid donated by Dr. C. Humphreys (Uni. of Nottingham). pMTL-CRISPR-Cas9_*pyrE* was used to transform the Δ*rex* sg1 strain. The selection for desired double crossover event was carried out as above described for *rex* KO mutant. Double KO mutants were screened for by PCR using ACE *pyrE*_FSP and ACE *pyrE*_RSP and the amplicons sent for Sanger sequencing.

7.5.2 *rex* mutant complementation

For *rex* gene complementation, plasmid pMTLCH23 was donated by Dr. C. Humphreys (Uni. of Nottingham) and suitably modified by cloning the coding sequence of the *rex* gene within the *pyrE* allele repair cassette. Insertion of *rex* gene was performed using Hi-Fi assembly procedure (Section 7.4.4). First *rex* ORF was amplified using primers rexHiFi_F1 and rexHiFi_R1 reported in appendix, **Table 12.1**, using *C. autoethanogenum* gDNA as template. Primers were designed so that *rex* native promoter was omitted while maintaining its own RBS. The resulting ACE complementation vector was transformed in Δ*rex*Δ*pyrE* strain via conjugation. After conjugation, colonies arisen on selective YTFTC agar plates were inoculated into 3 ml YTF supplemented with Tm and, after 3/5 days, plated onto PETC agar plates lacking uracil and supplemented with casein amino acid (1.5 g/L), to select for prototrophyc colonies. Screening of both restoration of *pyrE* locus

and *rex* complementation was carried out by PCR using primer ACE *pyrE*_FSP and ACE *pyrE*_RSP.

7.6 Phenotypic characterization

7.6.1 CO-fermentation in serum-flasks

The constructed strains including the deletion mutant (Δrex sg1) and the complemented mutant (*rex** sg1) were phenotypically characterized and compared to *C. autoethanogenum* wild type (WT) strain. Fermentation experiments were conducted in 50 ml PETC-MES in 250 ml serum flasks. Once resazurin contained in the media indicated anaerobic conditions, serum bottles were placed into the anaerobic cabinet overnight to remove residual oxygen. The day after, 50 ml PETC-MES were aliquoted into each flask, sealed with butyl-rubber stoppers and aluminum crimps to preserve anaerobicity, and sent for autoclaving. Before inoculation, 500 µL of 50 mM Na_2S were injected in each flask using sterile syringes, in order to further reduce the media. Due to the presence of the resazurin redox indicator a color change from orange to yellow was observed. Successively, serum bottles were inoculated in sterile and anaerobic conditions with 2% of inoculum. For inoculum preparation, first bacterial stocks were revived in 3 ml YTF and after approximately 3 days subcultured in 3 ml PETC-MES supplemented with fructose (10 g/L) and cysteine (0.25 g/L). Immediately after inoculation, serum flasks were over-pressurized with 1 bar of pure CO using a gas-exchange station (Anaerobe Gaswisselsysteem GW6400, GR Instruments B.V.). Afterward, serum bottles were incubated in a static incubator at 37°C and in horizontal position to maximize gas-liquid interface. This first step is referred to as CO adaptation phase, which was required to accommodate for CO consumption. To set up the experiment the seed-culture grown on CO was next subculture into three flasks, following the same procedure above described. Cultures were grown for approximately 10 days with two time-points per day. Samples were withdrawn using a sterile syringe through the pre-sterilized rubber stopper and subjected to optical density measurements at 600 nm (OD_{600}) (Section 2.8.1) and solvent analysis with HPLC (Section 2.6.1). Changes in headspace gas pressure were monitored twice a day using a DPG 110 hand-held pressure gauge (Omega Engineering, USA).

7.6.2 CO-fermentation in stirred tank reactor (STR)

7.6.2.1 Bioreactor set-up

Experiments comparing *rex* deletion mutant (Δrex sg1) and its complemented strain (*rex** sg1) to *C. autoethanogenum* WT, were performed in triplicate using a BioFlo®/CelliGen® 115 benchtop bioreactor (New Brunswick, Eppendorf), with a nominal volume of 2L and an initial volume of 1.5 L. Composition of bioreactor

media is given in **Table 7.13**. An overall scheme of the gas fermentation set-up used is provided in **Figure 7**. The stirred-tank reactor (STR) was operated in semi-batch mode, with batch liquid medium and continuous gas supply. Bioprocess parameters such as ORP, pH, temperature and agitation were constantly monitored and/or controlled using BioCommand Batch Control Software (New Brunswick, Eppendorf). Specifically, ORP values were acquired by the Pt4805-DPAS-SC-K8S probe (Mettler-Toledo) connected to the multi-parameter M300 analytical transmitter (Mettler-Toledo), and then transferred to the software, via the NBS Analog Input/Output manual (New Brunswick, Eppendorf). pH was monitored using a 405-DPAS-SC-K8S probe (Mettler-Toledo). pH was controlled within the range of 5-5.9, through the operation of peristaltic pumps. Depending on the base or acid assignment, peristaltic pumps performed the addition of 2 M NaOH or 10% H_2SO_4, respectively, when the pH value recorded was below or above the desired range. To ensure reliability of measurements, pH was also recorded offline and pH probe was calibrated every 48 h with a pHmeter Mettler-Toledo FiveEasy. Temperature was maintained at 37°C through either a water jacket or an heater plate, and measured using a Resistance Temperature Detector (RTD), accommodated into a thermowell. Broth culture agitation was provided by a direct-drive motor, located on the headplate. The agitation system comprised also a dual six-blade Rushton-type impeller, oriented onto the agitation drive shaft, so that distance from the bottom of the head plate of the lower and the upper impeller, was 20 cm and 15 cm, respectively. The bioreactor was also equipped with a baffle assembly. Bioreactor was continuously fed with a gaseous mixture containing 25% CO and 75% N_2 (*v/v*), at a flow rate of 80 ml/min using a thermal mass flow controller SmartTrack® 100 (Sierra). Before entering the bioreactor, gas inlet was sterilized by passing through a MTGR85010 0.22 µm filter (Millipore™). Gas was sparged at the bottom of the vessel using a sparger with gassing frit diameter of 1.5 mm. The exhausting gases, mainly N_2, CO, CO_2 and H_2, from the bioreactor were passed through a chilled-water condenser. The inlet and outlet ports of the exhaust condenser were connected through silicone tubing to the recirculating chiller (Isotemp, FisherScientific), kept at 10°C. Both inlet gas and off-gases were analyzed by a micro gas chromatographer (490 MicroGC, Agilent) (see section 2.6.2), every 4 hours and 20 minutes, respectively. A column filled with 70 cm of water generated a backpressure in order to direct the off-gases to the microGC. Marprene tubing (Watson-Marlow) were utilized for both gas (d_i=6.4 mm) and liquids (d_i=1.6) supplied. In case of foam formation, about 20 µL of antifoam 204 (Sigma-Aldrich) was manually injected through the inoculum port using a sterile syringe.
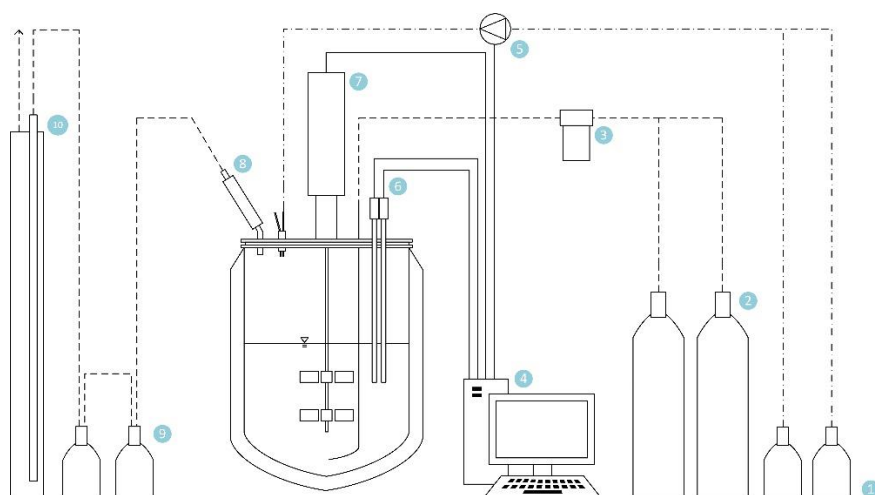
Figure 7 Schematic representation of the semi-batch fermentation set-up used in this study. (1) Acid/base solutions; (2) N_2 and CO cylinders; (3) Mass flow controller; (4) Control station; (5) Pumps; (6) pH and Redox probes; (7) Rotor; (8) Chilled-water condenser (9) Water-trap bottles; (10) Water column.

7.6.2.2 Inoculation procedure

Before proceeding with inoculation, bioreactor was bubbled with N_2 for at least 3 days, in order to create strict anaerobic conditions within the vessel. During the inoculation procedure, bioreactor media was supplemented with cysteine (0.17 g/L), sodium acetate (0.25 g/L), yeast extract (0.33 g/L) and 2ml of 1000X B-vitamin solution. Specifically, B-vitamin solution was added after all the other mentioned components, when pH was increased to 3.5 to avoid precipitation. pH was successively adjusted to 4.5-5 before inoculation. CO sparging into the bioreactor was started about 1 hour before inoculation at initial low agitation (200 rpm), to prevent achieving toxic CO concentration dissolved in the media. Bioreactor was inoculated with 150 ml inoculum (prepared as described in Section 2.5.1) in late exponential phase and with a headspace pressure within the range of 0.7-0.5 bar. When OD_{600} reached a value higher than 0.35, agitation program was activated so that agitation was automatically increased by 10 rpm every 4 hours, from 200 rpm up to 600 rpm in order to increase CO gas-to liquid mass transfer. Additionally, 50 mM Na_2S (Flow rate=1.7 ml/h) solution was supplied at that point until the end of the fermentation.

7.6.2.3 Liquid sampling

Liquid samples for OD_{600} and HPLC analysis were withdrawn twice a day. First, 5 ml were removed from the bioreactor sampling tube and discarded as waste; successively, the sample was collected into a 15 ml falcon tube. Pressure inside the vessel allowed sampling without the use of any syringe, just by pushing out the broth as soon as the sampling tube was un-clumped, thus maintaining the anaerobic conditions. After sampling, 1 ml of culture was centrifuged at 15000 rpm for 1

minute and cell-free supernatant stored at -20°C in a screw-cup tube, until HPLC analysis.

7.6.2.4 Calculation of fermentation parameters

Growth analysis

Growth profile was obtained by measuring the optical density (OD) of the culture at 600 nm (OD_{600}) with a Jenway 7505 spectrophotometer, using sterilized H_2O as blank. Whether the value exceeded 0.6 Abs, samples were diluted in H_2O and vortexed before measuring. For more accuracy, measurements were carried out in triplicate. OD_{60} was used to determine the Dry Cell Weigth (gDCW/L) using the following equation:

$$DCW = OD_{600} \times K \qquad \text{Eq. 7.1}$$

assuming a correlation-coefficient (K) of 0.21 (Valgepea et al. 2018).
The kinetic of the bacterial growth was estimated by calculating the specific growth rate μ (1/h). μ was graphically determined by plotting the growth curve in a logarithmic scale and then calculating the slope of the linear part corresponding to the exponential growth phase. The specific growth rate μ is inversely correlated to the doubling time (t_d) (h) as follows:

$$t_d = \frac{ln2}{\mu} \qquad \text{Eq. 7.2}$$

Carbon monoxide (CO) up-take

The grams of CO up-taken were calculated using the ideal gas law:

$$pV = RnT \qquad \text{Eq. 7.3}$$

where V is the volume (L) calculated as difference between the CO inlet (CO_{IN}) and CO outlet (CO_{OUT}), using the microGC data, integrated in the interval of time occurring between each sampling event; R is the gas constant (0.0821 L atm/mol K); n is the number of mole of CO; T is the temperature (310.15 K). The total pressure (p) was calculated adding to the atmospheric pressure, the back pressure generated by the water column (p_{wc}) as follows:

$$p_{wc} = \rho\, g\, h \qquad \text{Eq. 7.4}$$

with ρ representing the water density; g is the acceleration of gravity; h is the height of the water column (0.7 m).

Fermentation product analysis

The effectiveness of the process was investigated by calculating parameters including the volumetric productivity (p) for each product, using the following formula:

$$p = \frac{g\ (Product)}{V \cdot h} \qquad \text{Eq. 7.5}$$

Product yield (Y_p) was calculated as:

$$Y_p = \frac{g\ (Product)}{g_{CO}} \qquad \text{Eq. 7.6}$$

Carbon mass balance was performed for each growth product including acetate, ethanol, lactate, 2,3-BDO, CO_2 and biomass as fraction of C-mol product from total C-mol CO. Total carbon recovery was determined as the ratio of summed C-mol products to total C-mol CO. Total C-mol of CO were calculated by integrating CO mass flow over time. The carbon fraction of cysteine, YE and acetate supplemented during inoculation procedure was neglected.

7.7 Analytical methods

7.7.1 HPLC-High Performance Liquid Chromatography

For the HPLC analysis, samples were thawed on ice and then 300 μL of supernatant diluted in an equal volume of internal standard solution (50 mM valeric acid in 0.005 M H_2SO_4) and vortexed thoroughly. The solution obtained was successively filtered through a 0.22 μm regenerated cellulose syringe filters (Whatman Spartan Syringe Filter, GE Healthcare Life Sciences), directly into an HPLC vial with 300 μl insert and split cap. Same procedure was followed for blank and standard solutions, prepared in purified ELGA H_2O, selecting the range of metabolite concentration expected. Concentration of fermentation metabolites (ethanol, acetate, 2,3-BDO and lactate) was determined using a Dionex UltiMate 3000 System (ThermoScientific™) equipped with a Refractive Index (RI), operated at 35°C, and a Diode Array (UV-VIS 210 nm) as detectors. Aminex HPX-87H (300 mm x 7.8 mm; 9 μm particle size) (BIO RAD) was used as column, and kept at 35°C with a run-time of 55 minutes. An aqueous solution of 0.005 M H_2SO_4 prepared in purified ELGA H_2O was used as mobile phase, with a flow rate of 0.5 ml/min. Chromatograms were analyzed by Chromeleon 7 Chromatography Data System Software (ThermoScientific™).

7.7.2 Gas chromatography

Gas analysis, specifically inlet and outlet gases, was conducted using the 490 Micro GC-Gas Chromatograph by Agilent, equipped with a thermal conductivity detector (TCD and a dual channel cabinet, including 10 m Molsieve 5Å (MS5 Å) and 10 m PoraPLOT Q (PPQ) columns, both on Argon as gas carrier. H_2, CO and N_2 were separated using the MS5 Å, set at 100°C and 200 kPa and provided with a backflush to vent option (backflush time 6 s). The injector was kept at 100°C and a sampling time of 90 s was selected. CO_2 was detected with PPQ column kept at

80°C and 150 kPa. The injector was kept at 80°C and a sampling time of 60 s was selected. Injection time was set at 40 ms for both columns. The data were collected throughout the whole duration of the fermentation by an Agilent data system such OpenLAB EZChrom Edition.

7.8   Microscopy observation

Bacterial culture samples were observed under a phase contrast microscope (Nikon Eclipse Ci-E microscope). The microscopy analysis was performed in order to ensure no contaminants were present and to phenotypically confirm microbial shape and size, presence of dividing, elongated and debris cell.

7.9   Bioinformatic methods

Oligonucleotide primers were designed with the aid of UGENE software using the complete annotated genome sequence of *C. autoethanogenum* DSM 10061 (Humphreys et al. 2015) as template. Oligo analysis values (Tm, GC%, secondary structure and primer dimer) were verified by the oligonucleotide sequence calculator OligoEvaluator™ (Sigma-Aldrich). NEBuilder® Assembly Tool was used to design Hi-Fi assembly primers. CRISPR sgRNAs were designed using the online research platform Benchling (Benchling Inc. USA), which provides sgRNA target location, specificity and efficiency. Benchling was also employed for plasmid construction, DNA sequence alignment and DNA sequencing results and plasmid maps visualization. Nucleotide or protein similarity was evaluated using the algorithm provided by NCBI, Basic Local Alignment Search Tool (BLAST), comparing either nucleotide or amino-acids sequences to a database of sequences. Multiple protein alignment was performed using Clustal Ω. Candidate Rex-regulated operons were identified using RegPrecise (Novichkov et al. 2010) and Virtual Footprint (Münch et al. 2005).

Statistical data analysis and graphical representation of results were performed using Microsoft Excel 2010 (Microsoft, USA). For scheme composition either Microsoft Power Point 2010 (Microsoft, USA) or Microsoft Visio were used.

Chapter 8

Investigation of Redox-sensing transcriptional repressor Rex in *C. autoethanogenum*

8.1   Introduction

8.1.1 Redox homeostasis and fermentation

The strict correlation between metabolic activities and redox homeostasis cannot be neglected in alcohol producing microbial cell factories. Indeed, fermentative metabolic pathways mostly include reactions, which depend on the pool of cofactors such as NADH, NADPH and ferredoxin (Zhao et al. 2017). Environmental redox potential strongly reflects the net balance of reducing equivalents established within cells, whose changes in turn can affect signal transduction, synthesis of DNA and RNA, protein synthesis and enzyme activation (Liu et al. 2017). Hence, controlling either external or intracellular redox potential could be an effective route to alter and redistribute metabolic fluxes toward target products (Kracke et al. 2016; Liu et al. 2017). As previously discussed (Section 6.6.2), extracellular ORP can be controlled by energy input, gas sparging or redox reagent supplementation. However, concerning the latter approach, the use of additional reagents could interfere with the bioprocess and it is not cost effective for industrial-level fermentations (Liu et al. 2017). Moreover, many endeavors have been undertaken so far with the aim to enhance cofactor availability as well as to manipulate the affinity of redox enzymes to their cofactors (Zhao et al. 2017). An innovative approach was recently proposed by Kracke and co-workers (2016), who demonstrated in *C. autoethanogenum* a significant shift in carbon flux toward lactate and 2,3-BDO by applying a small electrical input using a bio-electrochemical system. Furthermore, genetic manipulation targeting genes coding enzymes catalyzing the redox reaction itself or regulators modulating pathways at the transcriptional level was also adopted. The latter approach includes the genetic engineering of redox-sensitive transcriptional regulator *rex*, recently found to play a key role in solventogenic shift in *C. acetobutylicum* (Zhang et al. 2014). Knowledge acquired to date on Rex regulator has made this repressor a potential target to modify the solvent profile.

8.1.2 Rex-redox sensing transcriptional repressor

Rex is a key bacterial regulator which acts as a redox state indicator by directly sensing changes in the *in vivo* NADH/NAD$^+$ ratio and consequently modulates metabolic pathways at a transcriptional level (Brekasis and Paget, 2003; Zheng et al. 2015). The crystal structure of the Rex protein from *Thermus aquaticus* (McLaughlin et al., 2010; Sickmier et al., 2005), *Thermus thermofilus* (Nakamura et al. 2007), *Bacillus subtilis* (Wang et al. 2008), *Streptococcus agalactiae* (PDB-Protein Data Bank, accession number 3KET) and *Thermoanaerobacter ethanolicus* (Zheng et al. 2014) has been determined both in complex with cofactors and/or DNA operator and without bound ligand. Rex has a dimeric organization with two

modular subunits, each comprising an N-terminal winged helix DNA-binding domain and a Rossmann-fold within its C-terminal domain, involved in dinucleotide incorporation and subunit dimerization (McLaughlin et al. 2010; Ravcheev et al. 2012). How Rex operates has been elucidated and the envisaged molecular mechanism involves ligand-dependent conformational changes triggered by fluctuations of NADH/NAD$^+$ ratio rather than by NADH itself (Brekasis and Paget, 2003; McLaughlin et al. 2010). When NADH binds to the C-terminal domain, Rex assumes a closed conformation and subsequently, its DNA recognition motifs are tightly packed so as to hinder Rex binding to the operator site (Ravcheev et al. 2012; Y. Zheng et al. 2015). Thus, Rex dissociation from DNA induces the transcription of downstream target genes (Hu et al. 2016). Release of NADH allows Rex to assume a flexible open conformation and then bind DNA to the N-terminal domain. In summary, in presence of low NADH/NAD$^+$ ratio Rex interacts with the target sites and represses expression of genes involved in NADH reoxidation, while elevated level of NADH causes the displacement of Rex from DNA sites and the consequent derepression of its target genes (McLaughlin et al. 2010). Although both reduced and oxidized forms of the pyridine dinucleotide bind to the Rex repressor, Wang et al. (2008) demonstrated in *B. subtilis* a 20000 times higher affinity for NADH than NAD$^+$. However, the increasing of NAD$^+$ affinity by a factor of 30 upon DNA binding, suggested a positive allosteric coupling between DNA binding and NAD$^+$ binding. Additionally, both NADH and its phosphorylated state NADPH affect Rex DNA binding activity, but the latter is less effective (Brekasis and Paget, 2003).

Rex is universal but not ubiquitously present in bacteria (Ravcheev et al. 2012). Even if Rex belongs to a conserved family widely distributed among Gram-positive bacteria, its homologues appear to be absent in the genome of Gram-negative microorganisms (Brekasis and Paget, 2003; Sickmier et al. 2005; L. Zhang et al. 2014). Furthermore, the presence of Rex does not correlate to the aerobic/anaerobic metabolism (Brekasis and Paget, 2003; Ravcheev et al. 2012). First identified in the aerobic *Streptomyces coelicolor* (Brekasis and Paget, 2003), the crystal structure has recently been released for the obligate anaerobic *Thermoanaerobacter ethanolicus*, revealing significant variations compared to aerobes, in terms of structure and DNA operator sequences (Zheng et al. 2014).

Ravcheev et al. (2012) investigated candidate Rex-binding DNA motifs in 119 genomes from 11 bacterial taxonomic groups. This comparative genomic analysis revealed that the transcriptional regulator Rex is significantly conserved across distantly related taxonomic groups, but a remarkable variability in terms of Rex regulon functions emerged. Notably, compared to the common consensus (TTGTGAANNNNTTCACAA) identified in model microorganisms such as *B. subtilis* and *S. coelicor*, Clostridia constitute an exception with a consensus (TTGTTAANNNNTTAACAA) deviating in two nucleotides at positions 5 and 14 (Ravcheev et al. 2012; Zhang et al. 2014). Alterations of the T5 and A14 nucleotides achieved by site-directed mutagenesis in *C. acetobutylicum* induced a reduction of

Rex affinity to the mutated binding site, revealing that those nucleotides highly conserved in Clostridia, play a key role in Rex binding to the operator sites (Zhang et al. 2014). Reconstruction of Rex regulons performed by Zhang et al. (2014) showed that in all the 11 analyzed clostridial species, including the well-characterized *C. acetobutylicum*, Rex controls genes involved in fermentation, mainly encoding enzymes that catalyze reactions consuming NADH or other reducing equivalents such as ferredoxin. In *C. kluyveri* an electrophoretic mobility shift assay (EMSA) demonstrated that Rex formed protein-DNA complexes with the promoter region of genes involved in carbon and energy metabolism (Hu et al. 2016). In *C. pasteurianum* 47 putative Rex boxes were identified, including fermentative target genes (Schwarz et al. 2017). Interestingly, the presence of a putative Rex-binding site upstream of the Wood-Ljungdahl pathway gene cluster was found in acetogens such as *C. carboxidivorans*, *C. ljungdahlii* and *C. autoethanogenum*, suggesting that Rex may regulate CO/CO_2 fixation (Zhang et al. 2014). This finding makes the *rex* gene a promising target to enhance product yield in syngas fermentation.

8.1.3 Aim of this study

The aim of this study was to assess if the redox-sensing transcriptional repressor Rex, encoded by a gene annotated as CLAU_1540 in the genome of *Clostridium autoethanogenum*, shares similarities with other well-described Rex proteins. With the same purpose, prediction of putative Rex-binding sites within *C. autoethanogenum* genome was conducted. As a result, *rex* was chosen as target for metabolic engineering study. Thus, a *rex* knock out mutant (Δ*rex*) and *rex* complemented strain (*rex**) were constructed by the means of CRISPR-Cas9 and ACE methodology, respectively. This experimental step aimed to elucidate the role of *rex* in gas fermentation in this industrially relevant microbial chassis.

8.2   Results and discussion

8.2.1 *In silico* analysis of *C. autoethanogenum* Rex

In *C. autoethanogenum* genome a 633 bp open reading frame CLAU_1540 encodes a protein annotated as "Redox-sensing transcriptional repressor Rex". The primary protein sequence of Rex comprises 210 amino acids. In order to identify potential similarities with well-described Rex proteins, a BLAST search was conducted by querying Rex protein sequences from other species against *C. autoeth anogenum* DSM 10061 genome (taxID:1341692). The query coverage and identity percentage are reported in **Table 8.1**. The protein showed the highest identity (86%) when compared to its homologues in *C. kluyveri* (CKL_0453), followed by *C.*

pasteurianum (77%) (CLPA_c28640), *C. acetobutylicum* (76%) (CA_C2713) and *C. beijerinckii* (72%) (Cbei_0320). Not surprisingly, *C. autoethanogenum* Rex shares lower sequence identity with Rex in model species such as the strict-anaerobe *T. ethanolicus* (TheetDRAFT_0450), the aerobic microorganisms *S. coelicolor* (SCO3320) and *T. aquaticus* (Taq_4998) as well as the facultative anaerobe *B. subtilis* (BSU05970).

Table 8.1 Results obtained in protein BLAST searches.

Organism	Query coverage (%)	Identity (%)	Reference
C. acetobutylicum ATCC 824	98	76	L. Zhang et al. 2014
C. kluyveri DSM 555	100	86	Hu et al. 2016
C. pasteurianum DSM 525	97	77	Schwarz et al. 2017
C. beijerinckii NCIMB 8052	98	72	L. Zhang et al. 2014
S. coelicolor A3(2)	77	38	Brekasis and Paget, 2003
B. subtilis 168	93	34	Gyan et al. 2006
T. aquaticus YT-1	95	38	Due and Pene, 1999
T. ethanolicus JW200	92	63	Zheng et al. 2014

As revealed by the multiple sequence alignment provided in **Figure 8.1**, the protein sequence shows within its C-terminus (residues 91-96) a conserved Gly-rich Rossman-fold motif (GXGXXG) corresponding to the sequence GAGNIG in all the Clostridium species selected. This domain is common among dinucleotide binding proteins and is responsible for pyridine nucleotide binding and subunit dimerization. At the N-terminus, the winged helix motif (GXXGXXGXGY), required for DNA-binding, is also conserved starting from residue G57. Moreover, the conserved Asp residue, reported to discriminate NAD(H) from its phosphorylated form by the interaction with the adenosine 2' hydroxyl group (Sickmier et al. 2005), is present at position D117, corresponding to D126 and D112, in Rex sequences from *S. coelicolor* and *T. aquaticus* respectively. Conserved sequence features include also some key residues (S47, Q51, W175, V193 and L195), which in the Rex sequence of the obligate-anaerobe *T. ethanolicus* were found to differ from that of aerobe Rex-family members (Zheng et al. 2014).

```
T.ethanolicus    ---------MSKKTIVSMAVIRRLPRYHRYLEELLKNDVKRISSRELSEKMGVTASQIRQ     51
C.beijerinckii   ---------MEKHKNISMAVIKRLPKYHRYLEELMKNEVDRISSKELGEKIGFTASQIRQ     51
C.pasteurianum   ------MQQLEKKKNISMAVIKRLPKYHRYLNELVNNEVDRISSKELSEKIGFTASQIRQ     54
C.acetobutylicum ---------MDKKKNISMAVIRRLPKYHRYLEELLKSDVDRISSKELSEKIGFTASQIRQ     51
C.autoethanogenum---------MDKKKNISMAVIKRLPKYHRYLMDLMKNDVDRISSKELSEKIGFTASQIRQ     51
C.kluyveri       ---------MDKKKDISMSVIKRLPKYHRYLGNLMRNDVDRISSKELSEKIGFTASQIRQ     51
B.subtilis       --------MNKDQSKIPQATAKRLPLYYRFLKNLHASGKQRVSSAELSDAVKVDSATIRR     52
S.coelicolor     MATGRAHRPATRSRGIPEATVARLPLYLRALTALSERSVPTVSSEELAAAAGVNSAKLRK     60
T.aquaticus      ------------MKVPEAAISRLITYLRILEELEAQGVHRTSSEQLGELAQVTAFQVRK     47
                         :   :.   **   *   *   *          **  :*.     . :   :*:
```

```
T.ethanolicus    DLNNFGGFGQQGYGYNVEELYNNLTKILGLDKTYNTIIIGAGNLGQAIANYTSFEKSGFN   111
C.beijerinckii   DLNCFGDFGQQGYGYNVKELYTQISAILGLDRGYEAALVGAGNIGQAVSNYSRFENLGFK   111
C.pasteurianum   DLNCFGDFGQQGYGYNVKDLHYQICNILGITKDYETIIVGAGNIGQAIANYTNFQKMGFK   114
C.acetobutylicum DLNCFGDFGQQGYGYNVKDLSREVDNILGLTKMYNTIIIGAGNIGQAIANYSRFEKIGFR   111
C.autoethanogenum DLNCFGDFGQQGYGYNVGELYGQICNILGLTKTYRTVIIGAGNIGQAIANYSRFEKIGFR   111
C.kluyveri       DLNCFGDFGQQGYGYNVSELYSQMCNILGLTKVYRTVIIGAGNIGQAISNYIGFEKLGFE   111
B.subtilis       DFSYFGALGKKGYGYNVDYLLSFFRKTLDQDEMTDVILIGVGNLGTAFLHYNFTKNNNTK   112
S.coelicolor     DFSYLGSYGTRGVGYDVEYLVYQISRELGLTQDWPVVIVGIGNLGAALANYGGFASRGFR   120
T.aquaticus      DLSYFGSYGTRGVGYTVPVLKRELRHILGLNRKWGLCIVGMGRLGSALADYPGFGE-SFE   106
                 *:. :*   * :* **   *    .    *.  .   ::* *.:* *. .*     . .
```

```
T.ethanolicus    LKGIFDINPRLFGLKIRDVEVMDVETVEDFIARNKIDIGILCIPKDNAQYTADRLVRAGI   171
C.beijerinckii   ITAIFDANPKLIGMKIRDVEIMDIDEMESVLEEHKIDIGIICPRKNAQVVADELIRGGV   171
C.pasteurianum   TNAIFDINPKLFGLKIRDIEIYDIDYLEPFLQKNPIDIATISVPPKNAQSVCDILVKNGV   174
C.acetobutylicum LKAIFDINPKLIGLKIQDVEVRDVDNIDGFLQKNKIDIGIICVPSKNAQKVCDIIVKNNV   171
C.autoethanogenum LEAIFDINPKLIGIRIRDIEIRDIDYLDDYLKENSIDIGVICVPNNAQKVCDILVKNKV   171
C.kluyveri       LRAIFDINPKLIGISIRDIEIRDIDYLGDYLRENVIDIGIICVPSNNGQKVCNILVKNGV   171
B.subtilis       ISMAFDINESKIGTEVGGVPVYNLDDLEQHVKDES--VAILTVPAVAAQSITDRLVALGI   170
S.coelicolor     VAALIDADPGMAGKPVAGIPVQHTDELEKIIQDDGVSIGVIATPAGAAQQVCDRLVAAGV   180
T.aquaticus      LRGFFDVDPEKVGRPVRGGVIEHVDLLPQRVP-GRIEIALLTVPREAAQKAADLLVAAGI   165
                  :* :     *   :  .  : .::  :        :.. *   .*    : ::   :
```

```
T.ethanolicus    KAIWNFSPIDLKVPDDVILENVHLSDSLFTVSYRLNEEELFKKLKGETAKIDG-------   224
C.beijerinckii   RAIWNFAPVDLVVPDHVKVENVHLSESLLTLIYLLNESES----------------   211
C.pasteurianum   KGIWNFAPVDLIAPADVMVENVHLSESLLTLTCLMNKTI-----------------   213
C.acetobutylicum NGIWNFAPVDLMTPENVIVENVHLSESLLTLSCLLQEVNKSRD----------------   214
C.autoethanogenum KGIWNFAPVDLVTPEDIKIENVHLSDSLLTLTCLLNDID-----------------   210
C.kluyveri       KGIWNFAPVDLIVPEDVKVENVHLSDSLLTLSCLLNDIE-----------------   210
B.subtilis       KGILNFTPARLNVPEHIRIHHIDLAVELQSLVYFLKHYSVLEEIE----------------   215
S.coelicolor     TSILNFAPTVLNVPEGVDVRKVDLSIELQILAFHEQRKAGEEAAADGAAPPVAARKQQRS   240
T.aquaticus      KGILNFAPVVLEVPKEVAVENVDFLAGLTRLSFAILNPKWREEMMG-------------   211
                  .* **:*   *  .*    :  :.::.:      *  :
```

```
T.ethanolicus    ------------------   224
C.beijerinckii   ------------------   211
C.pasteurianum   ------------------   213
C.acetobutylicum ------------------   214
C.autoethanogenum ------------------   210
C.kluyveri       ------------------   210
B.subtilis       ------------------   215
S.coelicolor     TGSADQGPDGDVPAVMPA   258
T.aquaticus      ------------------   211
```

Figure 8.1 Multiple sequence alignment (Clustal ω) of representative members of the Rex family. Conserved sequence features are framed as follows: Rossman-fold motif (GXGXXG) in blue and winged helix motif (GXXGXXGXGY) in red. The conserved Asp (D) residue is indicated by the green star. (For interpretation of amino acid colors refer to https://www.ebi.ac.uk/Tools/msa/clustalo/).

Hypothetical Rex binding sites in *the C. autoethanogenum* genome were identified using "Virtual Footprint" web tool (Münch et al. 2005), which was run with a position weight matrix (PWM) downloaded from the RegPrecise database (Novichkov et al. 2009) and based on previously determined Rex binding sites in Clostridia. Consensus sequences used were from a selection of Clostridia spp. ('5-

TTGTTANNNNNNTAACAA-3') and genomes from the Clostridiaceae order ('5-TTGTTAANNNNNTTAACAA-3'), reported in Ravcheev et al. (2012). **Table 12.4** (Appendix, section 12.4) shows the complete list of the target genes potentially preceded by a Rex-binding site. As a result, a total of 57 hypothetical Rex boxes and 76 genes putatively regulated by Rex were identified. The reconstruction of Rex regulons has been already conducted by Zhang and co-workers (2014). Using a comparative genomic approach, the authors claimed that a conserved set of regulons existed in at least 6 out of the 11 analyzed clostridial species. This species-specific cluster included genes involved in hydrogen production, tricarboxylic acid cycle, nitrate and sulfite reduction as well as fermentation. Regarding fermentation genes, Rex was predicted to regulate *adhA* (encoding an alcohol dehydrogenase) in *C. ljungdahlii* (CLJU_c18470), *C. carboxidivorans* (Ccarb_1085) and *C. beijerinckii* (*adhA*: Cbei_2181; *adhA2*: Cbei_1722). Cbei_1722 and Cbei_2181 encode enzymes catalyzing the reaction for primary alcohol production (ethanol and butanol) and were found to be up regulated during the shift from acidogenesis to solventogenesis in *C. beijerinckii* (Wang et al. 2012). According to this finding, within the *C. autoethanogenum* genome the 18-bp palindromic Rex-binding consensus sequence was found upstream of three genes encoding enzymes of unknown specificity but classified as an iron-containing alcohol dehydrogenase (CLAU_3861; CLAU_3514) and a Zn-dependent alcohol dehydrogenase (CLAU_3619). Protein BLAST search was performed in order to confirm genome annotations. Particularly, the product of CLAU_3861 showed high amino acid sequence identity with that of CLJU_c18470 (99%), Ccarb_1085 (81%), Cbei_1722 (75%) and Cbei_2181 (74%). Moreover, according to Zhang et al. (2014), *adhE2* (bifunctional alcohol/aldehyde dehydrogenase) is preceded by a Rex-binding box in *C. acetobutylicum* and *C. carboxidivorans* while is not a Rex-target gene in *C. beijerinckii*. Like *C. beijerinckii, C. autoethanogenum adhE2* is not classifiable as putative Rex target gene. Furthermore, Rex was predicted to regulate genes coding the transport protein L-lactate permease (CLAU_0239) and the D-lactate dehydrogenase (CLAU_0235). However, several *ldh* genes are present in *C. autoethanogenum* and as revealed by transcriptome analysis conducted by Henstra et al. (manuscript in preparation), CLAU_0235 mRNA level was substantially lower than that of other *ldh* in *C. autoethanogenum* grown on gas, suggesting that it may not play a pivotal role in lactate metabolism. Interestingly, a potential Rex-binding box has been also identified upstream the Acetolactate Synthase (CLAU_0388), which catalyzes the conversion of pyruvate to acetolactate in the 2,3-BDO pathway (**Figure 6.2**). Similarly to *C. kluyveri* (Hu et al., 2016), *C. pasteurianum* (Schwarz et al., 2017) and *T. saccharolyticum* (Zheng et al. 2018), 12 out the 76 identified genes were themselves transcriptional regulators, implying that Rex may be involved in a complex transcriptional regulatory network. Interestingly, Rex has also been proven to interact with its own promoter in a negative autoregulation mechanism, already suggested for *S. coelicolor* (Brekasis and Paget, 2003), *C. kluyveri* (Hu et al. 2016) and *C.*

pasteurianum (Schwarz et al. 2017). A similar mechanism was discussed in Ravcheev et al. (2012) identified in 51 out of 119 genomes analyzed. However, no putative Rex-binding box was identified immediately upstream of the *rex* gene in the genome of *C. autoethanogenum*. Additionally, as already described in Zhang et al. (2014), the WLP may potentially be regulated by Rex. In accordance with these results, a putative Rex-binding box was found within the promoter region of *codH*-Carbon monoxide dehydrogenase (CLAU_1579) and *fhs*-Formate-tetrahydrofolate ligase (CLAU_1576) in *C. autoethanogenum*.

In summary, the achieved results denoted that the protein encoded by *rex* gene in *C. autoethanogenum* may have similar functions of other well-described Rex proteins. Additionally, the identification of putative Rex-binding boxes within the promoter region of interesting genes such as alcohol dehydrogenases, lactate dehydrogenases, acetolactate synthase as well as genes playing an essential role in the formation of acetyl-coA during CO/CO_2 fixation (*codH* and *fhs*), makes *rex* an attractive target for a metabolic engineering study.

8.2.2 Development of *C. autoethanogenum* mutants

8.2.2.1 Construction of the *rex* deletion strain

Most research conducted so far on the redox-sensing transcriptional repressor Rex in clostridial species has been mainly focused on *in silico* analysis and consequently, on implementation of specific assays for assessing putative binding sites located in the target genome. Even though these studies gave an insight of the role played by Rex in transcriptional regulation, validation of the identified regulons is only attainable through construction of *rex* knock-out (KO) mutants combined with their phenotypic characterization. In undertaking this task, in the current project deletion of *C. autoethanogenum rex* gene was successfully achieved using a CRISPR/Cas9 genome editing tool developed within the SBRC (Uni. of Nottingham). The resulting *rex* knock-out strain is indicated in the text as Δ*rex*. CRISPR/Cas9 methodology was preferred over other established approaches since faster to generate mutants and generally requires less screening. Conversely, as mentioned above, ClosTron technology can cause potential insertional mutation which may have polar effects on adjacent genes. Additionally, ACE method due to multiple single colony selection stages, may give rise to acquisition of SNPs at other locations in the genome. So far, *rex*-deficient mutants have been only generated in the well-charaterized *C. acetobutylicum* (Wietzke and Bahl, 2012; Zhang et al. 2014), *C. bejerinckii* (Zhang et al. 2014) and *C. pasteurianum* (Schwarz et al. 2017), using either TargeTron or Allele-coupled exchange methodology. However, as previously discussed, intron-based approaches such as TargeTron merely disrupt a gene rather than entirely deleting it. Therefore, because of unintended polar effects, the enzyme encoded by the disrupted gene partially remains active with a residual activity depending on the insertion site and on gene's properties (Wang et al. 2015).

The followed experimental procedure is extensively outlined in materials and methods chapter (Section 7.4.1). Detailed description of CRISPR/*Cas9* plasmid used is provided in Ingle et al. (manuscript undergoing peer review) and plasmid map is showed in **Figure 8.2**. The selected plasmid contained the following components: i) the 4.1 kb *cas*9 gene native to *Streptococcus pyogenes,* responsible of double strand cleavage of target DNA; ii) the target-specific single guide RNA (sgRNA) expression cassette and iii) the homology arms (HAs) cassette serving as the *rex* editing template. The utilized plasmid also comprised the origins of replication for Gram-positive (*repH*) and Gram-negative (*ColE1*) bacteria as well as the chloramphenicol acetyltransferase gene *catP*, conveying chloramphenicol/thiamphenicol resistance. All these components were confined to a single plasmid with a total size of ≃11 kb, which was henceforth termed pMTL-CRISPR-Cas9_*rex*.
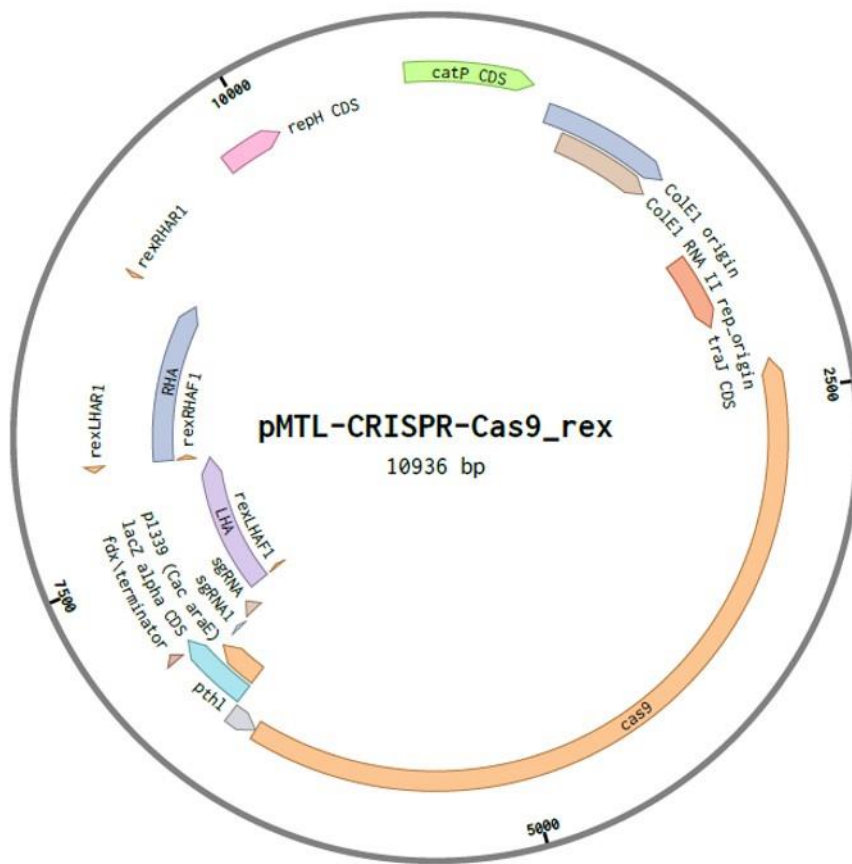
Figure 8.2 Plasmid map of pMTL-CRISPR-Cas9_*rex* vector.

As first step toward mutant generation, the homology cassette was generated by SOEing-PCR (Section 7.3.4.1) and the resulting fragment was then ligated with the plasmid, both previously digested with AscI and AsiSI restriction enzymes. Although genome editing can occur even using short HAs (Xu et al. 2015), some instances reported in the literature confirmed that the longer the region of homology

on the donor, the higher the likelihood that homologous recombination events occur (Joseph et al. 2018). Li et al. (Li et al. 2016) obtained a 100% effectiveness of mutant generation using HAs with a size greater than 0.5 kb. Likewise, in *C. acetobutylicum* higher efficiency was achieved by using 1kb HAs instead of 500bp (Bruder et al. 2016). Based on these observations, a size of ≃1kb was deliberately chosen for both left and right HAs. Next, the 20-nt RNA-guide sequence was inserted into the plasmid (before digested with SalI restriction enzyme) using HiFi-assembly method (Section 7.3.5.4). Single guide RNAs play a pivotal role, targeting the CRISPR associated endonuclease (Cas9) to a genomic DNA sequence flanked by the so-called PAM-protospacer adjacent motif (3'-NGG) via Watson–Crick base pairing (Jinek et al. 2012). Its function makes the sgRNA of prime importance for CRISPR-Cas9 successful workability. Indeed, during genome editing experiments high percentage of false positives can arise due to weak sgRNA expression, hence contributing to the presence of wild-type contamination within the population (Guo et al. 2018). In order to enhance the success rate of mutant construction, three-unique CRISPR-Cas9 plasmids, each carrying a separate sgRNA with a discrete targeting locus within the *rex* gene were constructed, hence generating multiple independent KO strains. Interestingly, a more accurate algorithm has been proposed recently, to predict highly effective sgRNAs specifically for bacterial genome engineering application (Guo et al. 2018), since so far algorithms based on mammalian cell datasets were commonly employed. In the current work, sgRNA sequences were selected using Benchling's CRISPR gRNA scoring tool, based on the *Rule Set 2 score* algorithm (Doench et al. 2016). The sgRNA sequences together with their unique binding sites are reported in the Appendix, **Table 12.3**. The sgRNA1 and sgRNA3 targeted a genomic sequences which are next to each other, with an overlap of two nt; while the sgRNA2 is annealed to a DNA region which is closer to the RHA.

The constructed plasmids were validated by Sanger sequencing with the aim to ascertain the correct HA and sgRNA cassettes. Successively, each confirmed plasmid was conjugated into *C. autoethanogenum* wild type strain using *E. coli* sExpress donor (Woods, et al., manuscprit undergoing peer review), carrying the plasmid of interest plus the conjugative plasmid R702. The plasmid R702 is located autonomously into the host (Minton et al. 2016) and enables the horizontal transfer of non-conjugative plasmid into Gram-positive bacteria (Williams et al. 1990). In order to promote DNA transfer, *C. autoethanogenum* was generally conjugated when the bacterial culture reached the exponential phase following the procedure explained in Section 7.2.7. Transconjugants harboring the editing plasmid were selected for by Tm supplementation. Among colonies capable of surviving the induced selection, desired double crossover mutants, restreaked to non-selective YTF plates, were screened by colony PCR. Primers (*rex* ScrF1; *rex* ScrR1) were designed to flank the HAs and anneal to the chromosome, and so that a 2288 bp and 2904 bp fragments would be amplified from the mutant and the wild type genotype, respectively. However, independently from the sgRNA sequence employed, a

significant number of colonies analyzed showed a mixed population, evidenced by the presence of both mutant and wild type bands (Data not shown). These data suggested that Cas9-mediated DNA cleavage might not be 100% efficient at this stage. The observed profile might be attributed to a heterogeneous distribution of either Cas9 protein or sgRNA in the population. A similar outcome was achieved in *ctf* and *pyrE* deletion experiments conducted in *C. ljungdahlii*. This issue was easily addressed with the observation that a prolonged incubation with active complex Cas9-sgRNA allows the entire conversion to mutants (Huang et al. 2016). Therefore, WT colonies were subcultured onto selective YTF plates and half of them were selected for the double crossover event. Again, the majority of the colonies analyzed appeared to be mixed population but one band showed the expected size (Data not shown). Thus, the latter was inoculated into YTF broth with the aim to promote plasmid loss and 72 hours culture was serially diluted and plated onto non-selective plates. Once colonies appeared, they were repeatedly streaked onto both YTF and YTFTC, to verify thiamphenicol sensitivity resulting from plasmid curing. As a final verification, the *rex* locus was amplified by PCR with extracted gDNA as a template and gel bands were purified and sent for Sanger sequencing. Gel imaging showed in **Figure 8.3** confirmed the entire removal of wild type background contamination together with the outright deletion of *rex* ORF. As above mentioned, the same procedure was carried out for all the three sgRNA and the confirmed *rex* KO clones were stored under the designation of Δ*rex*-sg1, Δ*rex*-sg2 and Δ*rex*-sg3.

In the literature, CRISPR/Cas9–based editing strategies have already been implemented in *C. autoethanogenum* (Nagaraju et al. 2016). In contrast to what is shown in the current study, Nagaraju and co-workers (2016) argued that controlled expression of Cas9 together with a constitutive sgRNA expression is required for CRISPR-Cas9 machinery to efficiently operate in *C. autoethanogenum*. In this case, a tetracycline-inducible promoter (tet3no) was harnessed to control the expression of the endonuclease, resulting in the increasing of the editing efficiency up to >50%. Similarly, in *C. beijerinckii* and *C. saccharoperbutylacetonicum cas9* gene was placed under the control of a lactose-inducible promoter (Wang et al 2016; Wang et al. 2017). By contrast, in the current study the strong promoter of thiolase gene (CA_C2873) (P_{thl}) from *C. acetobutylicum* was chosen to drive the constitutive expression of *cas*9. However, it is essential that not only the endonuclease but also the sgRNA is well expressed under the growth conditions used (Huang et al. 2016). Thus, in this study the strong promoter of genes encoding for a sugar-proton symporter (CA_C1339) (ParaE) from *C. acetobutylicum*, was used to control the expression of the sgRNA. P_{thl} and ParaE were tested in CRISPR-Cas9-mediated genome editing experiments by β-galactosidase activity assay in the closely related *C. ljungdahlii* and both the constitutive promoters used showed much greater activity compared to other non-inducible heterologous promoters selected, P_{ptb} and P_{adc} (Huang et al. 2016).
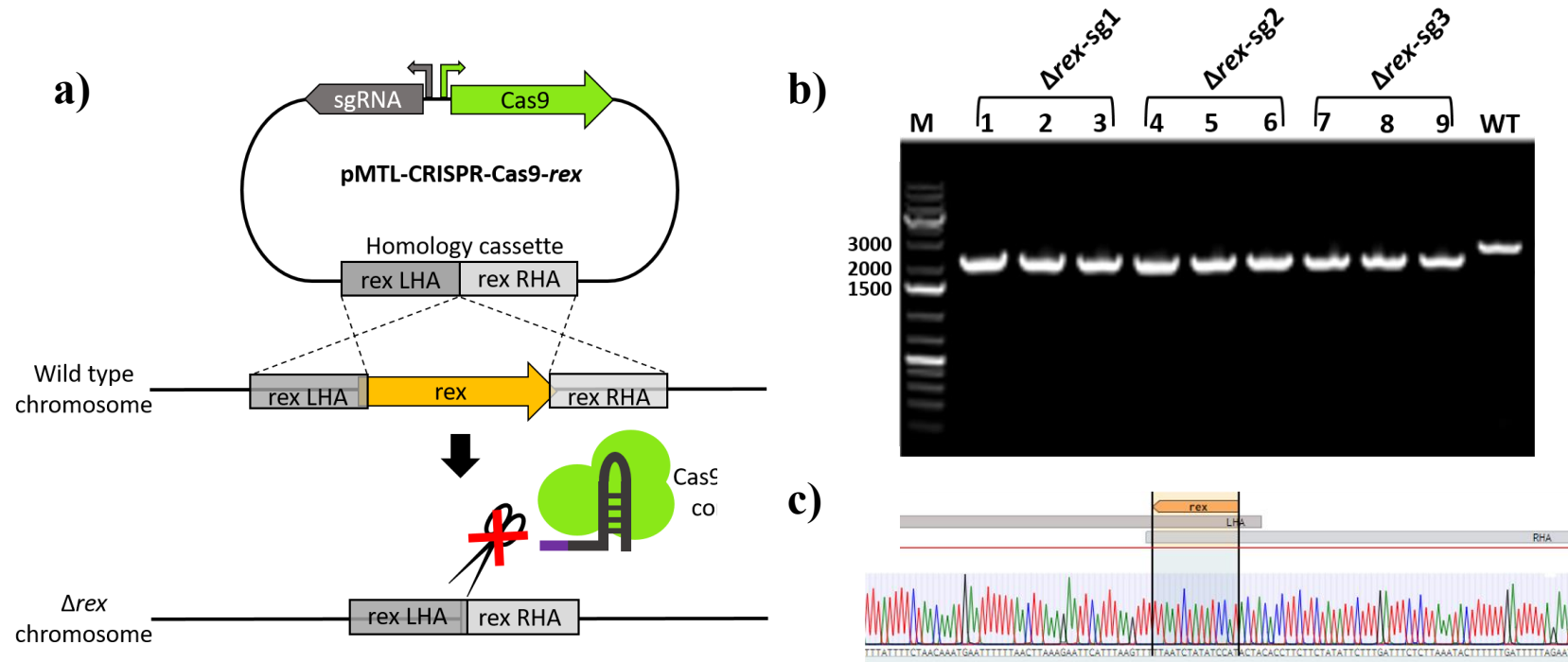
Figure 8.3 CRISPR-Cas9 procedure and results achieved. Panels: a) Schematic representation of CRISPR/Cas9 procedure; b) PCR screening of the *rex* KO mutants. The 2.2 kb and 2.9 kb represent the *rex* deleted and Wild-Type (WT) strains, respectively. M (Marker); c) sequencing results confirming *rex* gene deletion.

8.2.2.2   Generation of the Δ*rex*Δ*pyrE* strain

Bacteria subjected to intense stress such as genetic manipulation may spontaneously accumulate mutations within their genome. Notably, during subculturing experiments, if single colonies are selected the chance to select for SNPs (spontaneously occurred within the population) increases (Humphreys et al. 2015). Moreover, as mentioned before, even though CRISPR/Cas9 system offers tremendous advantages for genome editing, cleavage of unintended loci with similar sequences may occur, thus causing off-target mutations (Zhang et al. 2015b). Considering this, for a faithful interpretation of *rex* deletion effects, chromosomal complementation was performed. As explained in Section 6.6.4.2, a Δ*pyrE* background was required and hence *pyrE* locus was disrupted in the Δ*rex* strains. In *C. autoethanogenum* genome CLAU_1436 open reading frame comprises 573 nucleotides and is annotated as *pyrE*. Deletion of *pyrE* in the previously constructed *rex* KO mutant (Δ*rex*-sg1) was achieved by CRISPR-Cas9 editing technique. Plasmid pMTL-CRISPR-Cas9_*pyrE* was donated by Dr C. Humphreys (Uni. of Nottingham).

The plasmid backbone comprised the same basic features already described for pMTL-CRISPR-Cas9_*rex*, with the difference in the homology arms sequences and in the guide targeting region, designed to recombine with the *pyrE* locus, instead. Specifically, the LHA (1033 bp) sequence consisted in the region located immediately downstream of CLAU_1436 (partially including the gene CLAU_1435) plus 21 nucleotides of the *pyrE* 3'end. The RHA (942 bp) comprised part of the *pyrE* sequence (204 pb at 5' end) and 738 bp upstream of the starting codon, partially including the ORF of *pyrD*. The so designed homology cassette recombined with the homologous region within the chromosomal DNA, causing a 348 bp deletion. The selection for desired double crossover event was carried out by following the same workflow, outlined in the above paragraph and largely discussed in Section 7.4.1. Genomic DNA was extracted from candidates double KO colonies and used as template for PCR screening with *pyrE* flanking primers, ACE *pyrE*_FSP and ACE *pyrE*_RSP. Expected band sizes were 2059 bp for the wild type allele and 1711 bp for the mutant allele. Bands exhibiting the right size (**Figure 8.4**) were gel purified and sent for Sanger sequencing. Confirmed double knock out strains were stored and hereafter referred to as Δ*rex*Δ*pyrE*.
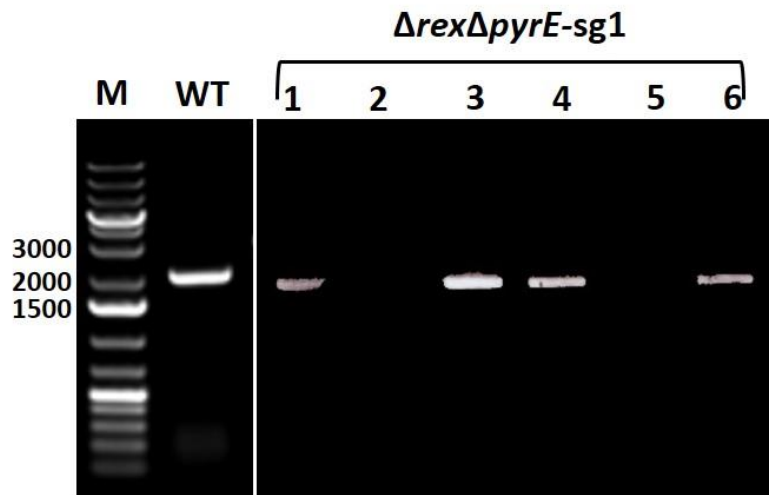
Figure 8.4 PCR screening of the *pyrE* locus. The 2 kb and 1.7 kb represent the WT and the *ΔrexΔpyrE* strains, respectively. M (Marker).

8.2.2.3 Restoration of *pyrE* locus and *rex* gene complementation

With the aim to assess whether the phenotypic profile resulting from *rex* deletion strictly correlates to the chromosomal gene modification rather than to potential off-target effects, it was pertinent to complement *rex* gene at the *pyrE* locus via ACE. ACE-based chromosomal complementation was chosen due to its straightforward procedure compared to plasmid-based complementation, which instead required antibiotic selection pressure for plasmid retention. Thus, the double knock-out *ΔrexΔpyrE* was used as recipient strain and conjugated with the complementing vector pMTL-CH23_*rex*. Plasmid pMTL-CH23_*rex* was developed using the pMTL-CH23 backbone donated by Dr. C. Humphreys (Uni. of Nottingham). A detailed description of the pseudo-suicide vector pMTLCH23 is provided in Annan et al. (manuscript undergoing peer review).
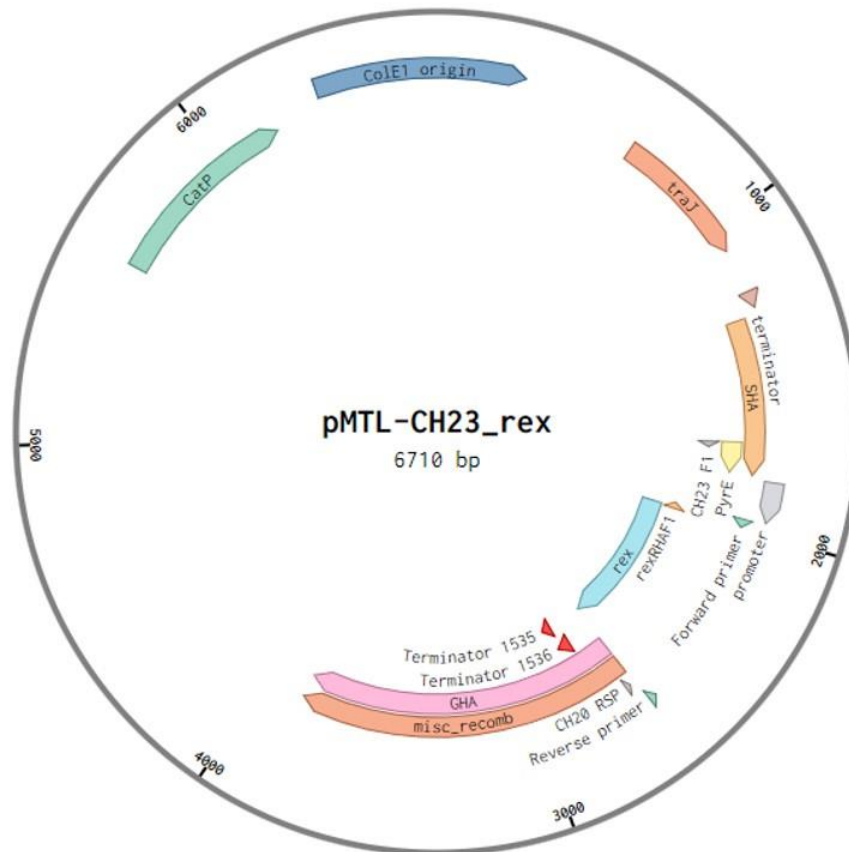
Figure 8.5 Plasmid map of the complementing vector pMTL-CH23_*rex*.

The *pyrE* repair cassette comprised two asymmetric homology arms, in order to dictate the order of homology recombination events (Ng et al. 2013). The short homology arm (SHA) was 524 bp long whereas the great homology arm (GHA) was 1212 nucleotides in length. The shorter fragment included the entire *pyrE* locus (CLAU_1436), truncated at its 5' end, with 49 nucleotides missing. The longer HA comprised the DNA region residing immediately behind the stop codon of *pyrE* gene plus the entire coding sequence of CLAU_1435. ACE is reliant on replication defective plasmids: in the case of pMTL-CH23, the Gram-positive pCB102 replicon native to *C. butyricum* was used (Minton et al. 2016; Minton and Morris, 1981). pCB102 in *C. acetobutylicum* was demonstrated to be the least stable in terms of segregation into daughter cells compared to the other three (pBP1, pCD6 and pIM13) replicons available in the pMTL80000 series (Heap et al. 2009). Between the two regions of homology, the plasmid incorporated a lacZα multiple cloning site (MCS), which can be excised and replaced with a cargo gene. ACE complementation approach provides two routes: the cargo gene can be overexpressed under the control of a strong promoter. Alternatively, a native promoter can drive the expression of the target gene, thus ensuring an appropriate gene dosage (Ng et al. 2013). Complementation of *rex* gene in *C. pasteurianum* by ACE revealed that, whilst the *rex* gene was introduced at the *pyrE* locus under the

control of its native promoter, unexpectedly the phenotype observed suggested an increase of *rex* expression levels. The authors attributed this finding to a *rex* deregulation due to the lack in the cloned sequence of a putative Rex-binding box located 340 bp upstream of the *rex* start codon, which might be responsible for *rex* transcriptional regulation (Schwarz et al. 2017). The absence in *C. autoethanogenum* of a Rex-binding site within the *rex* promoter or upstream in a region discreetly close to it, made the selection of promoter not limiting. Thus, the promoter-less and functional wild type copy of *C. autoethanogenum rex* together with its natural ribosome binding site (RBS) were cloned into the complementing vector (pMTL-CH23), under the control of P_{thl}. Indeed, increasing the gene dosage by *rex* gene overexpression might be helpful to more confidently attribute the observed phenotypic features to the genotypic modification introduced. The first attempts in *rex* cloning comprised the basic ligation protocol, preceded by restriction digestion with NheI/SpeI restriction enzymes. However, several failures were obtained by following the standard ligation procedure, because NheI/SpeI generated compatible ends and thus, either the plasmid religated without any insert or the insert could be incorporated in the wrong direction. To overcome this issue, a HiFi assembly method was developed as an alternative to restriction/ligation assembly. First the *rex* ORF was amplified using primers *rex*HiFi_F1 and *rex*HiFi_R1 reported in appendix, **Table 12.1**, and *Clostridium autoethanogenum* gDNA as template. The right size amplicon (663 bp) was gel purified and introduced into the pMTL-CH23 backbone through HiFi-assembly. The primers were designed so that the SpeI as well as the NheI restriction sites were incorporated respectively upstream and downstream of the *rex* coding sequence. The resulting vector was transformed into *E. coli* Dh5α, extracted and then confirmed by both enzymatic digestion and Sanger sequencing. Successively, the final plasmid pMTL-CH23_*rex* was transferred from *E. coli* sExpress donor into *C. autoethanogenum* Δ*rex*Δ*pyrE* via conjugation. As already described, the first recombination event is directed by the longer HA. The whole plasmid integrates into the genome of the host (single crossover), so allowing the plasmid to replicate under the control of the bacterial chromosome replication machinery. Since the plasmid is defective in the Gram-positive replicon, integrant cells showed a growth advantage compared to cells with a plasmid in an autonomous state, which instead do not easily tolerate the presence of antibiotic (Tm). Thus, larger and faster growing colonies were restreaked onto selective YTF plates. The following step consisted of selection for the desired double crossover event by plating on to media lacking uracil. Spontaneously occurring double crossover events can involve either the long or the short homology arm. In the latter scenario, the *pyrE* allele is restored to wild type and uracil prototrophy is reestablished, allowing the strain to grow without uracil (Minton et al., 2016; Ng et al. 2013). Thus, colonies found to be growing on selective plates were picked and inoculated in 3 ml YTF with Tm added. After 3/5 days, the bacterial culture was diluted and plated on PETC agar plates comprising 1.5 g/l casein amino acid hydrolysate without uracil supplementation.

Subsequently, plasmid loss was verified by plating out onto both YTF and YTFTC plates. Colonies resulting sensitive to thiamphenicol were screened for successful double crossover event by PCR with ACE *pyrE*_FSP and ACE *pyrE*_RSP primers, using genomic DNA as template. Consequently, *pyrE* restoration occurred in tandem with the *rex* gene insertion, the amplicon size was expected to be $\simeq$2.7 kb. **Figure 8.6**, confirmed successfully isolation of complementation strains, indicated as *rex**sg1.
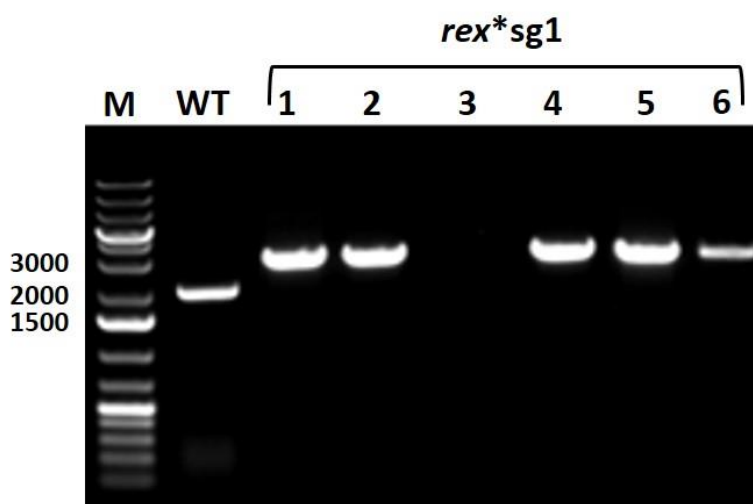
Figure 8.6 PCR screening of the *pyrE* locus. The 2 kb and 2.7 kb represent the WT and the *rex* complemented (*) strains, respectively. M (Marker).

8.3 Conclusions

In the current chapter, *in silico* analysis was conducted in order to investigate potential similarities between *C. autoethanogenum* Rex and other representative members of Rex family. This preliminary data illustrated that CLAU_1540 in *C. autoethanogenum* codes for a protein, which shares 86%, 76% and 77% identity with the well-described Rex-repressor in *C. kluyveri*, *C. acetobutylicum* and *C. pasteurianum*, respectively. Furthermore, these findings were confirmed by multiple sequence alignment, which highlighted the presence of conserved domains within the amino acid sequence. Interestingly, genes involved in CO/CO_2 fixation such as *codH*-carbon monoxide dehydrogenase (CLAU_1579) and *fhs*- formate-tetrahydrofolate ligase (CLAU_1576) were identified among the putative Rex-regulons, along with the *alsS*-acetolactate synthase (CLAU_0388) and a putative iron-containing alcohol dehydrogenase (CLAU_3861). This outcome corroborates the idea of a potential role of Rex in regulation of the Wood-Ljungdahl pathway gene cluster. Thus, to elucidate the role of Rex in regulation of fermentative pathways, *rex* gene (CLAU_1540) was deleted from *C. autoethanogenum* genome. Multiple independent KO strains were constructed using three unique CRISPR-Cas9 plasmids, each carrying a separate sgRNA with discrete targeting locus within

the *rex* gene. This to our knowledge is the first time that gene coding for the transcriptional repressor Rex has been knocked out in an acetogenic chassis microorganism, such as *Clostridium autoethanogeum*. Moreover, studies conducted so far on *rex* deletion implemented ACE or intron-based editing strategies. Hence, the use of a Cas9-mediated genome editing tool instead, made this work further innovative. Whilst CRISPR-Cas9 allows the construction of outright and clean gene deletion compared to other techniques, it is not exempt from the acquisition of SNPs which are common to any technique involving isolations of single colonies from a bacterial population. Therefore, with the aim to validate whether the phenotypic profile resulting from *rex* deletion strictly correlates to the introduced genetic modification, the *rex* gene was complemented at the *pyrE* locus via ACE. Notably, expression of *rex* gene was driven by a strong promoter P_{thl}, in order to induce a gene overexpression. Mutants and wild type strains were then phenotypically characterized in serum bottles as well as in a stirred-tank bioreactor, using CO as carbon and energy source. These achievements will be discussed and illustrated in the next chapter.

Chapter 9

Phenotypic characterization of *C. autoethanogenum rex* mutants

9.1 Introduction

Physiological evidence supporting the involvement of the Rex repressor protein in regulation of fermentative pathways has already been observed in microorganisms belonging to the clostridium genus (**Table 9.1**). Originally, the first confirmation was provided by two independent studies on *C. acetobutylicum* where *rex* was proved to play a relevant role in the redox-dependent solventogenic shift (Wietzke and Bahl, 2012) as well as in fermentation metabolite formation and oxidative stress tolerance (Zhang et al., 2014). Notably, Zhang et al. (2014) showed that deletion of the *rex* gene resulted in the up-regulation of 17 target genes (*adhE2*, *ldh*, *thlA*, *crt-bcd-etfBA-hbd*, *asrTABC*, *nadABC* and *ptb-buk*), encoding enzymes catalyzing fermentation reactions, NAD biosynthesis and sulfite reduction. Later, a *C. pasteurianum* mutant strain harboring a deletion in the *rex* gene was phenotypically characterized using either glucose or glycerol as the carbon source, and higher butanol production was observed compared to the wild type strain (Schwarz et al. 2017). Despite the aforementioned studies' contribution to understanding the Rex regulation system, current research on Rex is still narrow. Efforts undertaken thus far sought to investigate Rex activity only under heterotrophic growth conditions. Even though no conspicuous changes in redox carrier concentrations (including $NADPH/NADP^+$ ratio) have been detected between heterotrophic and autotrophic conditions in *C. autoethanogenum*, NAD^+ concentrations were shown to be higher in cells grown on gas (Marcellin et al. 2016). Taking into account this finding, and the fact that Rex controls genes encoding enzymes catalyzing NADH-consuming reactions, a *rex* gene deletion may entail divergent phenotypes whether the microorganism is cultured under autotrophic or heterotrophic conditions. Furthermore, the role of Rex has never been elucidated in acetogenic bacteria, where it perhaps carries out important functions in fermenting C1 gas. Indeed, as already mentioned, the identification of putative Rex-binding sites residing upstream of the WLP operon in the acetogens *C. carboxidivorans*, *C. ljungdahlii* and *C. autoethanogenum*, has inspired the hypothesis that Rex may act as regulator in the autotrophic CO/CO_2 fixation (Zhang et al., 2014). In accordance with what speculated by Zhang and co-workers (2014), bioinformatic analysis illustrated in Chapter 8, revealed that in *C. autoethanogenum* Rex may control the expression of genes such as *CodH* and *fhs,* responsible for Acetyl-CoA formation from CO.

Due to the strict correlation existing between autotrophic carbon, energy and redox metabolism, fluctuations in intracellular redox state (coupled with changes in $NAD(P)H/NAD(P)^+$ ratio) should reflect the metabolic route into which carbon is channeled (Valgepea et al. 2017). As expected, biosynthesis of reduced metabolites implies the depletion of reduced cofactors and, hence a more oxidized intracellular redox state in the ABE-fermenting *C. acetobutylicum* (Amador-Noguez et al. 2011). Inconsistent results were obtained in the gas-fermenting *C. ljungdahlii*, where redox

state was not clearly more oxidized during solventogenesis, as reported by Richter et al. (Richter et al. 2016). A similar trend to that displayed in *C. acetobutylicum* was recognized instead in *C. autoethanogenum* grown in a steady-state chemostat on syngas (Valgepea et al. 2017). Notwithstanding, since the collected transcriptomic data revealed that transcript levels measured for Rex were surprisingly low and inalterable, the authors suggested that Rex may not play a key role in the maintenance of redox homeostasis in clostridia. However, in a recently published review on *C. autoethanogenum* (Norman et al. 2018), this statement was negated. The authors claimed that, due to its allosteric mechanism (Wang et al. 2008) the absence of changes in Rex transcript levels in response to redox state poise conditions does not correlate with its inactivation. Consequently, *rex* gene inactivity can be reasonably supposed only if *rex* genes were self-regulated but, as shown in Chapter 8, no Rex-binding operators were found within *rex* promoter in *C. autoethanogenum* genome. Moreover, RNA-seq transcriptomic data performed during pH and gas-shift experiments on a CO-fed cultures grown in CSTR exhibited variations in *rex* RNA levels (Henstra et al., manuscript in preparation). In light of the controversial interpretations reported in literature, question concerning Rex role in *C. autoethanogeum* remains still unanswered. Reliable statements can be made only by properly examining the phenotypical effects of *rex* deletion in this gas-fermenting microbe.

9.1.1 Aim of this study

The purpose of this chapter is to address the unsolved question about the potential role of the Rex protein in regulating WLP pathway in the acetogen *C. autoethanogenum*. In undertaking this task, the constructed *rex* knock-out (Δ*rex*) and chromosomally complemented *rex* (*rex**) strains were characterized in order to display potential phenotypic discrepancies compared to the wild type strain. With this aim growth profiles alongside liquid and gaseous metabolite analysis were performed, initially in small-scale batch fermentation and successively in bioreactor operated with batch liquid and continuous gas supply. Finally, carbon-mass balance was conducted for all the three analyzed strains to evaluate carbon flow distribution during bioreactor fermentation experiments.

Table 9.1 Overview of previous works reported in literature on *rex* deletion (Δ*rex*) mutants in Clostridium spp.

Microorganism	Substrate	Operation mode	Relevant characteristics*	Reference
C. acetobutylicum ATCC 824	Glucose	Batch (serum flasks)	▪ Comparable growth rate ▪ Increased ethanol and butanol production ▪ Decreased acetone, butyrate and H_2 production ▪ No difference in acetate synthesis ▪ Overall higher pH values ▪ Earlier solventogenic shift ▪ Sensitivity to oxidative stress	Wietzke and Bahl, 2012; Zhang et al. 2014
C. beijerinckii NCIMB 8052	Glucose	Batch (serum flask)	▪ No appreciable alteration of fermentation product spectra	Zhang et al. 2014
C. pasterurianum DSM 525	Glycerol	Batch (Bioreactor)	▪ Comparable growth rate ▪ Higher lactate and butanol production ▪ Slightly lower acetate, butyrate and 1,3PDO production ▪ Equivalent ethanol production	Schwarz et al. 2017
	Glucose	Batch (Bioreactor)	▪ Slower growth rate ▪ Equivalent acetate production ▪ Increased ethanol and butanol generation	

*Relevant phenotypic characteristics found in Δ*rex* strain compared to the WT.

9.2 Results and discussion

During CRISPR-Cas9 genome editing experiments (outcomes displayed in Chapter 8) multiple independent KO strains designated as Δ*rex*-sg1, Δ*rex*-sg2 and Δ*rex*-sg3 were constructed using three unique plasmids, carrying a separate sgRNA, each targeting a unique locus within the gene of interest. Due to potentially diverse degrees of efficiency, different sgRNA sequences were implemented with the attempt to enhance mutant generation success rate. Once the mutants were isolated, one of them (Δ*rex*-sg1) was randomly selected as representative *rex* knock-out strain. To explore the effects of *rex* gene deletion and overexpression, the desired strains (Δ*rex* and *rex**) were subjected to phenotypical characterization and the resulting fermentation profiles compared to that of the wild type strain.

9.2.1 Batch fermentation experiments

As preliminary investigation, small-scale fermentation tests were conducted in batch using serum flasks over-pressurized with 1 bar CO, as the sole carbon and energy source (Methods outlined in Section 7.5.1). Before inoculation (2% *v/v*), PETC medium (**Table 7.10**) was supplemented with Na_2S used as both a reducing agent and sulphur source. Inoculation took place when seed-cultures reached mid-exponential phase with an OD_{600} value approaching 0.5 and a headspace pressure close to 0.6 bar. The inoculum was generally observed under microscope to suitably select for a viable bacterial population, deliberately avoiding cultures enriched in debries and elongated cells (**Figure 9.1**).
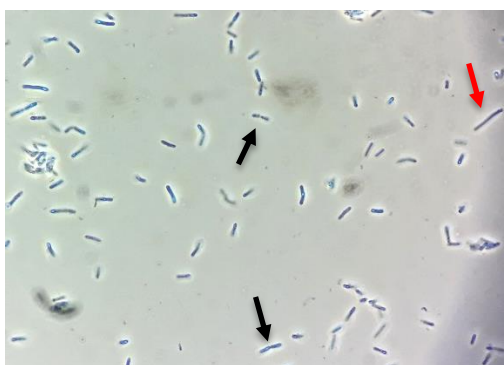
Figure 9.1 Phase contrast microscope imagine of *C. autoethanogenum* wild type strain (100x magnification). Arrows point to dividing (black) and elongated (red) cells.

Taking into account the well-known inhibition effects of CO on most of Fe-Fe hydrogenases even at relatively low concentration (Wang et al. 2013), pre-cultures were previously accommodated to CO usage, thus allowing microorganisms to gradually switch from heterotrophic to autotrophic metabolism. Growth profile,

headspace pressure changes as well as metabolite spectra were reconstructed through 20 time points at which samples were collected, until the initial CO was exhausted and optical density indicated that a stationary phase had been reached.

9.2.1.1 Growth profile and gas consumption analysis
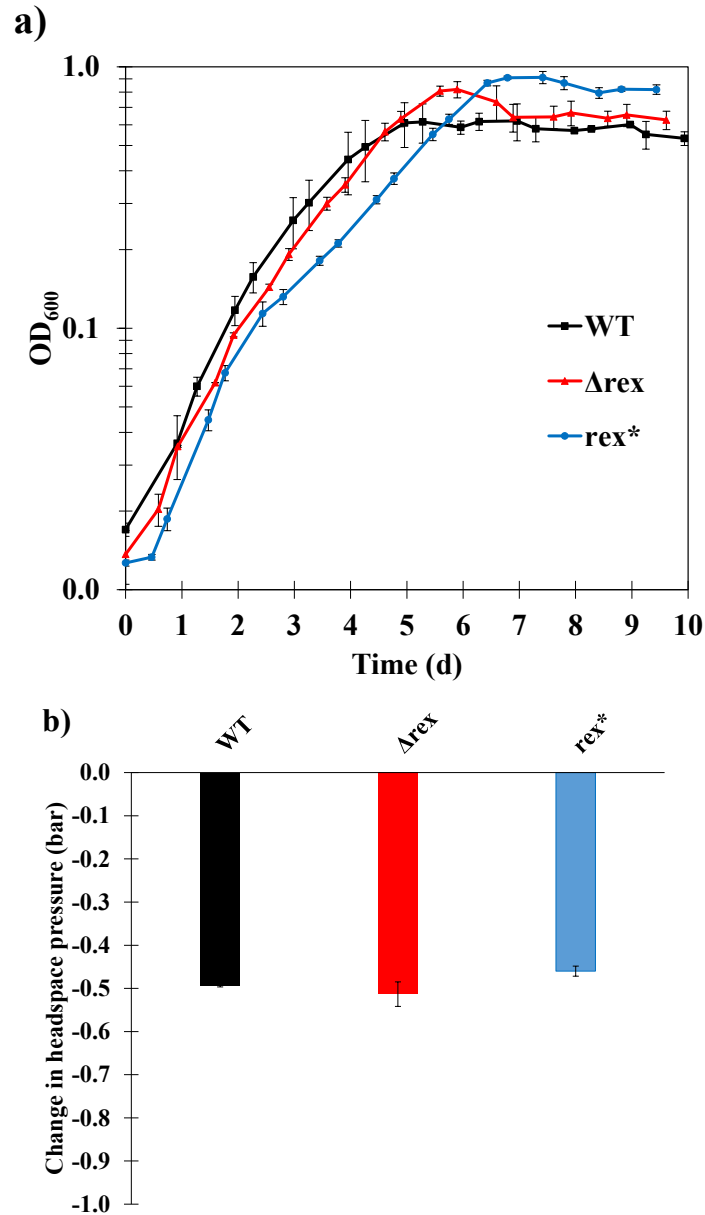
Figure 9.2 Batch fermentation experiments of *C. autoethanogenum* WT, *rex* deletion (Δ*rex*) and *rex* complementation (*rex**) strains grown on CO (1 bar overpressure). Panels: a) Growth profile based on OD_{600} measurements; b) Changes in headspace pressure from start to the end-point, normalized to the blank (un-inoculated bottle). Data is shown as the average of bio-triplicates for each strain. Error bars indicate standard error of the mean (s.e.m).

Since maintenance of intracellular redox homeostasis is crucial to support growth and metabolism, considering the physiological role played by Rex, it was expected that its absence would have determined growth discrepancies. Bacterial growth graphs with an average time course of 10 days are illustrated in **Figure 9.2a**. Focusing on the wild type and on the Δrex mutant, the optical density curves peaked after 7 and 6 days, reaching OD_{600} values of 0.62 ± 0.1 and 0.82 ± 0.06, respectively. Furthermore, concerning the KO strain, transition to the stationary phase occurred approximately after 134 hours, similarly to the WT, which required 127 h. However, since no statistically significant variations in growth were observed across the two strains, it can be speculated that deletion of *rex* ORF did not substantially alter growth on CO. This result is in accordance with the majority of the works conducted on Rex in clostridia and listed in **Table 9.1**.

Having chromosomally incorporated the *rex* gene at the *pyrE* locus, the resulting complementation strain (*rex**) was also characterized to assess whether the fermentation product profile was altered. As during the construction of *rex** the native promoter was replaced by the strong promoter P_{thl}, resulting in gene overexpression, the complementation strain was not necessarily expected to revert back to WT phenotype. As shown in **Figure 9.2a**, *rex** exhibited a slightly slower growth compared to the control strain and Δrex, also showed a prolonged lag-phase. This behavior was highly reproducible, since it was observed even during the gas-adaptation step. Unlike the WT and the KO strain, *rex** strain did not readily accommodate for CO metabolism (Data not shown). Shift to the stationary phase occurred after nearly 154 h. However, once the *rex** culture approached the stationary phase, it remained at higher OD_{600} with the maximum value measured of 0.91 ± 0.05.

Bacterial culture growth was monitored by microscopy, performed primarily during the start-up phase of the experiment, thus ascertaining size, shape and motility of cells. No irregularities were identified among all the analyzed strains (Data not shown).

In silico analysis performed previously revealed that *rex* might modulate fixation of CO and CO_2 during Wood-Ljungdahl metabolic pathway. Therefore, in order to validate this hypothesis and identify potential differences in terms of gas consumption, headspace gas analysis took place over the course of the growth assay. On this occasion, only headspace gas pressure was routinely monitored, whereas compositional gas analysis was carried out during bioreactor fermentation tests. As outlined in Materials and Methods, before beginning each experiment, flasks were stored in the anaerobic cabinet with a gas atmosphere containing also CO_2 (10%) and H_2 (10%), which hence contributed to the headspace composition. The gas metabolizing *C. autoethanogenum* is able to utilize CO_2 and H_2 under either autotrophic or heterotrophic/mixotrophic growth conditions, in the latter case by reassimilating a large amount of CO_2 released from fructose metabolism into Acetyl-CoA (Liew et al. 2016b). However, as already discussed, due to its lower

energy content, utilization of CO_2 as carbonaceous substrate is thermodynamically less favorable than CO (Liew et al. 2017). Thus, in the current study it was assumed that only CO was assimilated as a carbon and energy source.

The recorded data are graphically represented in **Figure 9.2b** as change in headspace pressure between the start and the end-point of the autotrophic growth experiment. The wild type and *rex* deletion strain were capable of reducing the same extent of headspace pressure with the following values: WT=-0.49 ± 0.01 bar and Δ*rex*= -0.51 ± 0.03 bar. A slightly smaller amount of gas was utilized by *rex**, with 0.46 ± 0.01 bar of gas consumed. Additionally, *rex* gene over-expression caused a retarded CO consumption against the WT and the *rex* knock out mutant (Data not shown), a phenomenon responsible for the extended lag phase mentioned before.

9.2.1.2 Fermentation product profile

Characterization of the fermentation phenotype was accomplished by quantifying metabolites produced over the course of the entire experiment. HPLC data (**Figure 9.3a-d**) included the main fermentation products acetate and ethanol as well as the C4 compounds, lactate and 2,3-BDO. **Figure 9.3a** shows that, regardless of the bacterial strain type, acetate concentration regularly dropped within the first two days of the test. Indeed, during the inoculation procedure acetate synthesized by the seed-culture was carried into the new batch, where acetate was converted into ethanol via the indirect metabolic route, catalyzed by AOR enzyme. Net acetate production started earlier in both WT and Δ*rex* than the complementation strain, reaching a final titer value of 3 ± 0.1 g/L and 3.4 ± 0.2 g/L, respectively. The delay in acetate production observed in *rex** justified the prolonged lag phase showed in the growth curve. Indeed, although acetate is considered an unwanted by-product, acetogens harvest energy for growth during acetate biosynthesis, by generating ATP via substrate level phosphorylation (Henstra et al. 2007; Liew et al. 2017). However, when the *rex* gene was overexpressed, as with growth, acetate concentration adjusted to the Δ*rex* level, with a final titer of 3.4 g/L ± 0.1. The concentrations reached by *rex* mutants were only marginally higher compared to the WT to speculate any role of Rex repressor in regulation of genes involved in acetate producing pathway.

Originally, the current project envisaged relevant high ethanol output for the deletion strain, due to the remarkable selectivity shift toward solvent production reported in other *rex* deficient Clostridium species (**Table 9.1**). For instance, disruption of *rex* gene in *C. acetobutylicum* resulted in enhanced alcohol (ethanol and butanol) to acetone ratio (from 2.7 to 4.8) (Zhang et al. 2014). Notably, the prominent increased in ethanol production was proved to directly correlate to *rex* inactivation, since a 160-fold increase in *adhE2* mRNA level was found in the mutant strain (Zhang et al. 2014). Conversely, in this study no substantial changes in ethanol concentration were observed between WT and Δ*rex* (**Figure 9.3b**). A reasonable explanation for this could be that no Rex-binding box was identified

upstream the bifunctional acetaldehyde/ethanol dehydrogenase *adhE2* (appendix, **Table 12.4**), suggesting that Rex does not directly regulate ethanol synthesis in *C. autoethanogenum*. Unexpectedly *rex** displayed higher ethanol titers, with a peak occurring around day 7. However, due to the high ethanol data variation reflected by the large error bars, no reliable conclusions can be made. Seemingly, ethanol curves profiled a similar trend across all the analyzed strains, with different phases occurring. As in accordance with Abubackar and co-workers (Abubackar et al. 2015a), no typical shift from acidogenesis to solventogenesis was observed. Initially, most of the ethanol was generated from acetate conversion, as reported above. Subsequently, the ethanol decrease suggested an opposite conversion of ethanol into acetate; this reaction is also feasible but the reason why this event occurred remains an unanswered question. Then, ethanol peaked and sharply lowered reaching a plateau. The drop in ethanol production matched with the end of CO-uptake as well as with the transition to the stationary phase.

Beside ethanol and acetate, *Clostridium autoethanogenum* is able to synthesize lactate and 2,3 BDO, when grown on CO as sole source of carbon and energy (Köpke et al. 2011). These two pyruvate-derived metabolites are generally released in small traces and due to their low concentration, they are not easily detectable. (Köpke et al. 2011) demonstrated that genes responsible of 2,3 BDO and lactate metabolism were already slightly upregulated during mid-late exponential phase but the massive upregulation occurred in stationary growth phase, when the pH of the environment drops as a consequence of acidogenesis and when a surplus of reducing equivalents takes place. Based on observations made on the Rex molecular mechanism, metabolic pathways controlled by Rex should be upregulated even in presence of low $NADH/NAD^+$ ratio, hence resulting in enhanced product formation. According to bioinformatics results shown in Chapter 8, in *C. autoethanogenum* the potential derepression of genes coding acetolactate synthase enzyme (AlsS) as well as lactate transporter and lactate dehydrogenase (LDH), could logically be expected to increase 2,3 BDO and lactate bioproduction, respectively. Augmented lactate synthesis was reported in Δ*rex*-*C. pasteurianum* strain grown on glycerol (Schwarz et al. 2017) whereas unexpectedly, the same deletion in *C. acetobutylicum* did not affect lactate synthesis although the *ldh* gene exhibited a Rex-binding box (Zhang et al. 2014). As shown in **Figure 9.3c-d**, the absence of a functional copy of *rex* encoding gene in *C. autoethanogenum* alters the fermentation pattern, by redirecting carbon fluxes toward 2,3 BDO and lactate. WT and *rex* KO mutant simultaneously started producing 2,3 –BDO but as with growth, Δ*rex* exceeded WT levels reaching a final titre up to 83% higher. With respect to lactate, 17-fold higher concentration was observed in Δ*rex,* compared to the WT and *rex** strains.
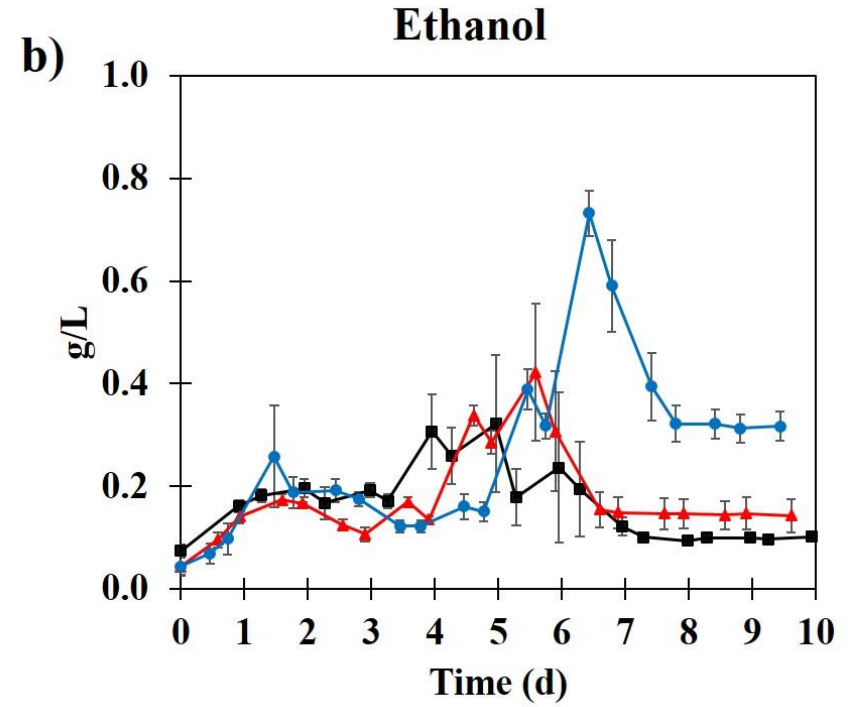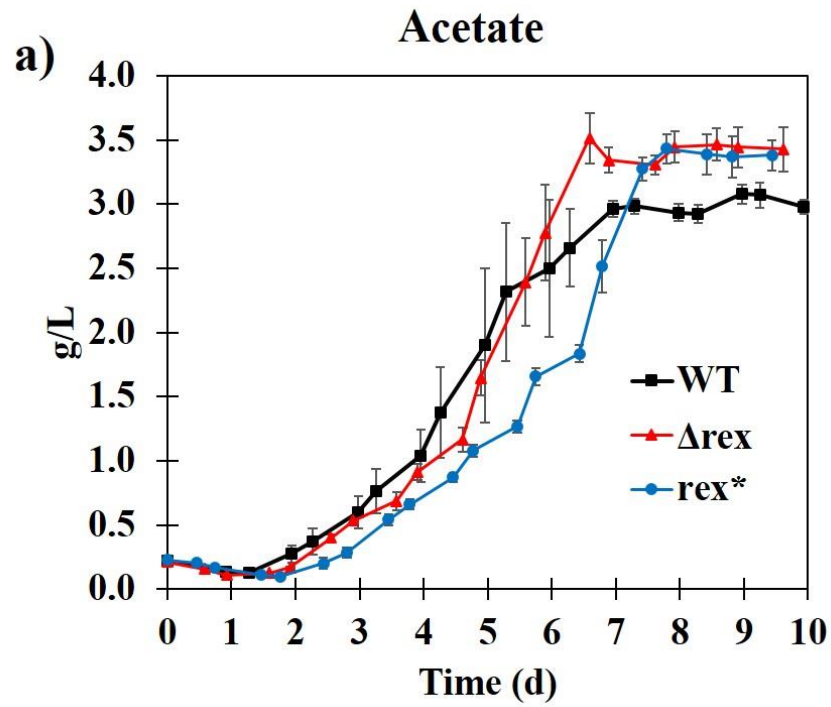
Figure continues next page.

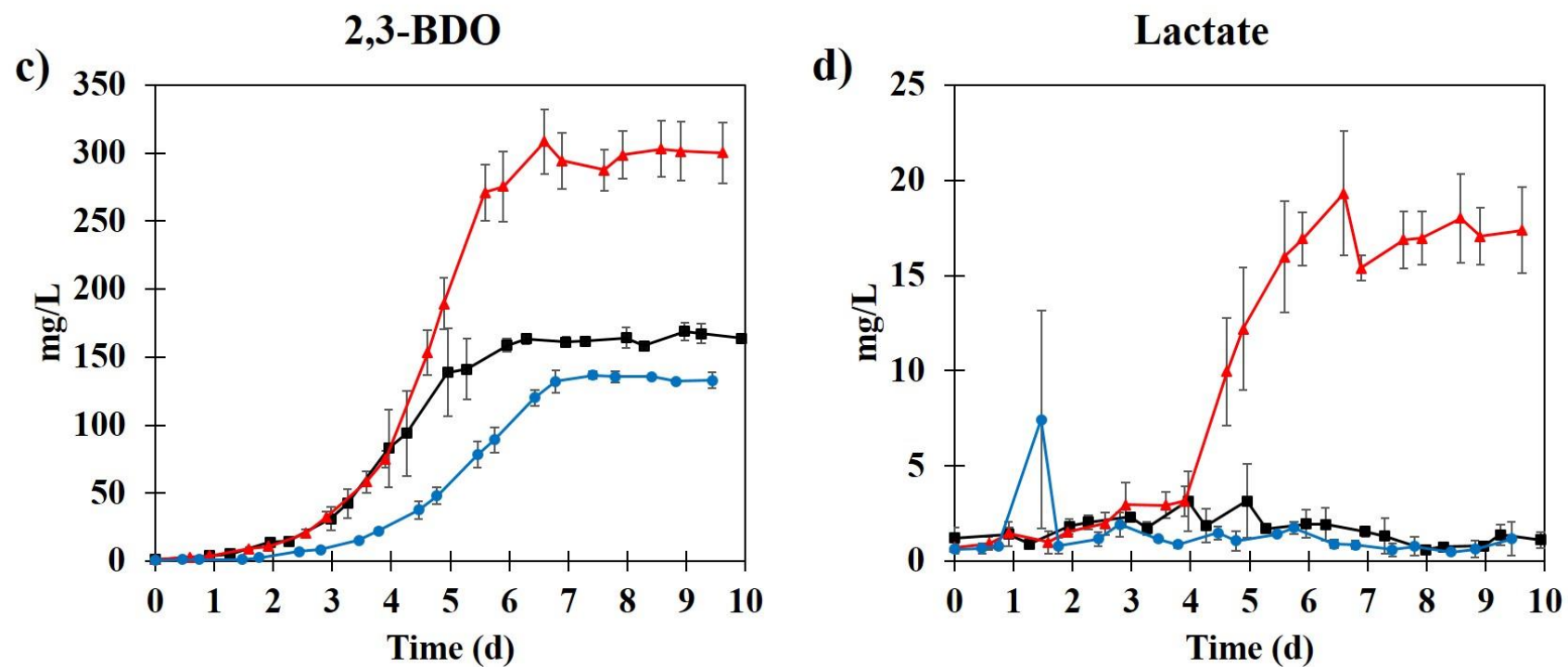**Figure 9.3** Batch fermentation product profile of *C. autoethanogenum* WT, *rex* deletion (Δ*rex*) and *rex* complementation (*rex**) strains grown on CO (1 bar overpressure). Panels: a) Acetate profile; b) Ethanol profile; c) 2,3-BDO profile; d) Lactate profile. Metabolites were quantified by HPLC. Data are shown as the average of bio-triplicates for each strain. Error bars indicate standard error of the mean (s.e.m).

9.2.2 Fermentation in Continuous CO-fed Bioreactor

Small-scale fermentation in serum-bottles is a time and resource-saving approach that allows the simultaneous screening of different cultivation conditions (Hegner et al. 2017). However, even though it represents a suitable option for culture maintenance, unstable conditions in terms of pH, redox potential, substrate supply, biomass and metabolite concentrations, make serum-flask performances not always transferable to bioreactor (Hegner et al. 2017; Phillips et al. 2017). Curiously, Xu et al. (Xu et al. 2017) proposed a novel gas-cultivation system, simply consisting of a gas–sampling bag. Although safer and cheaper compared to traditional bioreactors, its applicability is limited to strain screening or metabolomics research. Vice versa, bioreactor fermentation is more compatible with industrial conditions. Hence, the preliminary investigations conducted in batch flasks was integrated with further fermentation experiments in a stirred tank bioreactor.

C. autoethanogenum WT strain together with the constructed mutants (Δ*rex* and *rex**) were grown chemolithoautotrophically in a stirred-tank bioreactor operated in semi-batch mode with batch liquid and continuous CO supply (20 ml/min) for approximately 15 days. For reliable comparison, fermentation tests were performed in triplicate for each strain. The operative conditions selected are detailed in Section 7.5.2. Briefly, each bioreactor was inoculated (10% *v/v*) with a CO-adapted seed culture in mid-exponential phase. Bioreactor temperature was maintained at 37° and pH controlled within a range of 5-5.9 by addition of 2M NaOH or 10% H_2SO_4. A minimum pH of 5 was selected to prevent acid crash during acidogenesis whereas a threshold of pH 5.9 prevented to exceed the optimal pH value reported for *C. autoethanogenum*. Based on considerations made before about Yeast Extract, attempts aiming to omit YE were undertaken but turned out unsuccessful (Data not shown). Then, a low concentration of YE (0.33 g/L) was used to supplement bioreactor media in order to aid bacterial growth. Moreover, Cysteine was added to further reduce the media, together with acetate and B-vitamins. Each test started with a constant and low agitation regime (200 rpm) to avoid CO high partial pressure into the vessel, which would increase gas to liquid mass-transfer and hence CO gas solubilized into the media (Munasinghe and Khanal, 2010), potentially lethal at low biomass concentration. When a pH decrease along with increase in OD_{600} was observed, agitation speed was gradually and automatically increased up to 600 rpm. Semi-batch mode was preferred over batch mode to establish non-carbon limited growth regimes, which are reported to favor ethanol production (Mohammadi et al. 2011). Continuous mode operation was avoided due to time constraints. Additionally, this approach may allow observing solvent profiles over a wide range of CO supply conditions, which may give more chance of identifying the desired phenotype.

9.2.2.1 Effects on fermentation pH and Redox state

A further advantage over serum-flask fermentation relies on the constant monitoring and/or control of fermentation parameters offered by bioreactors. A representative fermentation profile of automatically recorded process parameters (temperature, pH, redox and agitation) can be found in appendix, section 12.5. **Figure 9.4** shows pH and redox state (ORP) trends observed for all the analyzed strains throughout the duration of the entire experiment.

Redox state strictly correlates to the external pH, with the ORP becoming less negative with pH decreasing (Abubackar et al. 2015a). Additionally, electron flux and thus redox state is crucial in terms of product pattern and yield in clostridia (Desai et al. 1999), with an increase in reducing equivalents such as NAD(P)H generally triggering solvent formation (Wietzke and Bahl, 2012). Therefore, ORP serves also as microbial growth and metabolic activity indicator during fermentation (Liu et al. 2017).
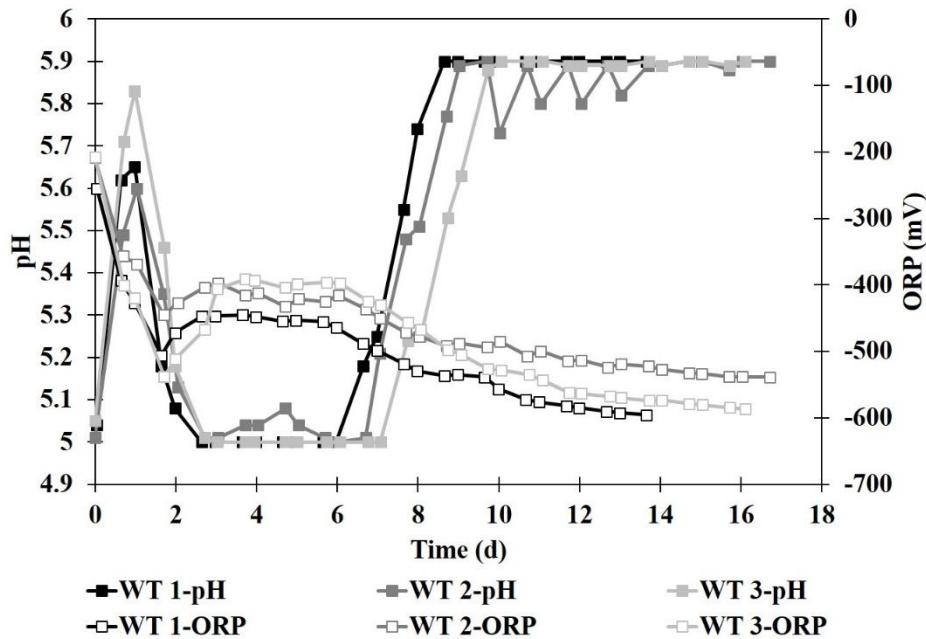
Figure continues next page.
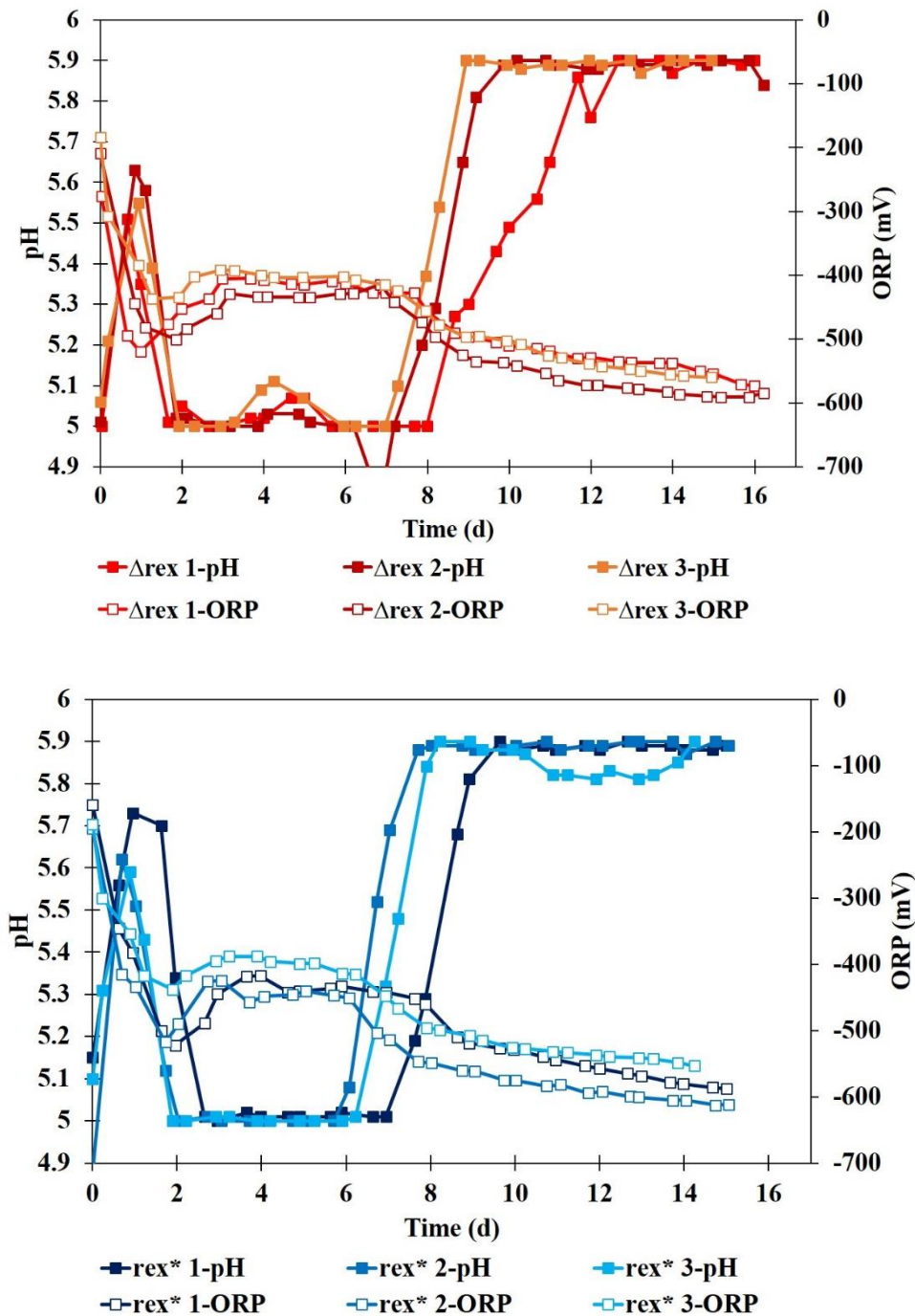
Figure 9.4 Redox potential-ORP (mV) and pH profile regularly acquired from the start to the end-point of the experiments. pH and ORP (mV) values were recorded automatically respectively by pH and redox probes located into the vessel.

As shown in **Figure 9.4**, similarly in all the three strains, pH started rising within 24-48 h after inoculation due to several factors, including assimilation of acetate supplemented and H_2S deriving from sulphur species (Na_2S and Cysteine) being stripped from the broth. Later, if bacterial culture suitably adapted to the new environment, since growth is coupled with acetate production, the acetate

144

extracellularly released sharply lowered pH of the media. Following a specular trend, after an initial sharp drop attributed to the reduced state of the inoculum, redox increased. Indeed, during acidogenesis redox arose due to the intracellular accumulation of NADH cofactors (Grupe and Gottschalk, 1992). Microorganisms kept releasing acids and due to the pH control set, pH stabilized with a pH value of 5, avoiding acid crash and making redox reaching a plateau. The shift toward solventogenesis phase led pH to go up and consequently ORP to decrease.

Studies conducted in *C. acetobutylicum* (Wietzke and Bahl, 2012) and in *C. pasteurianum* (Schwarz et al. 2017) displayed an overall increase of pH in the *rex* minus strains. As illustrated in **Figure 9.4**, a slight pH increase consistently occurred across all the Δ*rex* replicates around day 4-5. This phenomenon overlapped with a slowing down in acetate generation reflected in the slope of acetate curve (See below). In accordance, when *rex* was overexpressed, *C. autoethanogenum* did not show a similar behavior. Hence, it could be speculated that this event was determined by acetate reassimilation. However, a spike in pH was also displayed by WT 2. Some temporary issues related to NaOH pump activity caused instead a pH drop in Δ*rex* 2.

9.2.2.2 Growth profile analysis

Growth profile is illustrated in **Figure 9.5**. As demonstrated in other Δ*rex* clostridium species, no substantial differences were detected between the three strains, with cultures reaching the same maximum OD_{600} value (**Table 9.2**). The only appreciable difference is the slower growth rate exhibited by *rex* complemented strain resulting in a doubling time (T_d) of 31.5 ± 5.3 h (μ=0.02 ± 0.004 h^{-1}). This finding corroborated the outcome previously displayed for batch-bottle assays discussed above. In general, relatively long doubling times have been reported for gas-consuming bacteria when grown in batch operation mode (Richter et al. 2013), while a doubling time of 5 hours was reported for *C. autoethanogenum* grown on CO in a continuous cell culture (Mock et al. 2015). Surprisingly, the same authors found a 15 h T_d when the same culture was cultivated in batch mode on fructose as source of carbon, hence confirming the potentiality of this acetogen in gas fermentation.
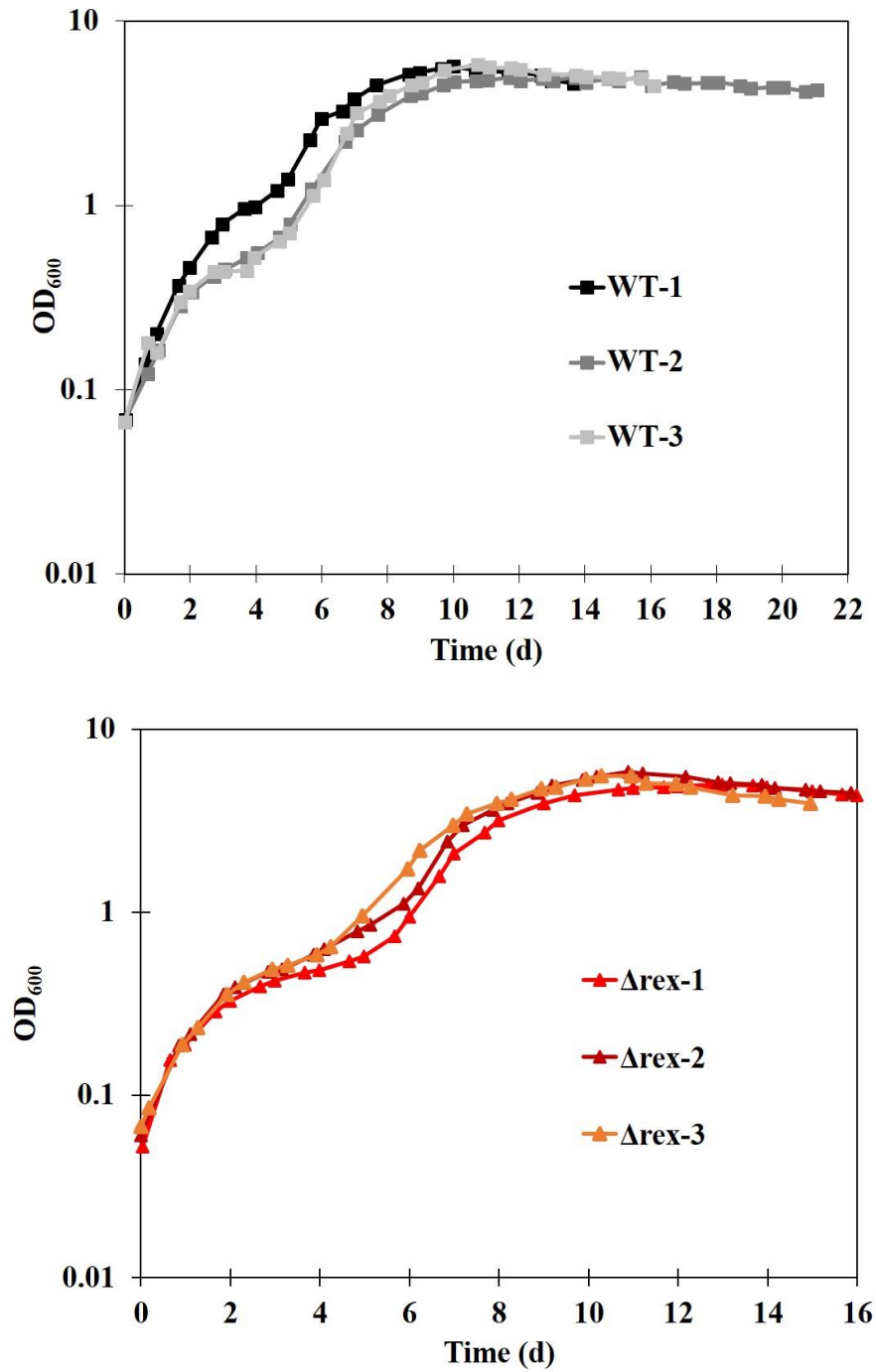
Figure continues next page.

Figure 9.5 Growth profile of the wild type (WT), rex knock-out mutant (Δrex) and chromosomally *rex* complemented (*rex**) strains, grown in bioreactor with continuous CO supply. Experiments were conducted in triplicate for all the three strains.

Table 9.2 Growth parameters of WT, Δrex and *rex** strain fermentations. Data are given as the average $\pm$ sem from bio-triplicates for each strain.

Strain	Max OD$_{600}$	μ (h^{-1})	Td (h)
WT	5.5 ± 0.3	0.03 ± 0.003	25.1 ± 2.5
Δrex	5.5 ± 0.3	0.03 ± 0.003	26.2 ± 2.9
rex*	5.5 ± 0.0	0.02 ± 0.004	31.5 ± 5.3

9.2.2.3 Fermentation metabolite profiling

In order to ascertain experimentally whether the genetic modifications introduced in *C. autoethanogenum* affected CO-metabolism, fermentation products were examined. Performances were compared across the analyzed strains by estimating volumetric productivity and product yield of acetate, ethanol, lactate and 2,3-BDO. Product yields were calculated based on CO consumed as outlined in Section 7.8.

Metabolite profiling did not reveal compelling metabolic changes compared to the control wild type strain. The wild type, Δrex and *rex** displayed acetate peak concentrations of 3.3 ± 0.4 g/L, 3.6 ± 0.5 g/L and 3.2 ± 0.4 g/L, reached after 158

± 7 h, 177 ± 7 h and 151 ± 9 h (**Figure 9.6**). At these time points, acetate productivities were 23.4 ± 3.6 mg/L· h, 21.6 ± 1.8 mg/L· h and 23.3 ± 2.3 mg/L· h, for the WT, Δ*rex* and *rex**, respectively (**Figure 9.10**). In accordance the resulting acetate yields showed similar values among the three strains (WT= 0.18 ± 0.02 g/g$_{CO}$, Δ*rex*=0.18 ± 0.01 g/g$_{CO}$ and *rex**=0.17 ± 0.04 g/g$_{CO}$).

Since regarding ethanol no distinct profile emerged during batch-fermentation tests, this further investigation was carried out also with the aim to clarify potential effects of the *rex* deletion on ethanol biosynthesis, but similar to acetate, no substantial differences appeared. **Figure 9.10** referred to productivity values measured after ~300h of operation. Apparently, solely *rex** strain showed a reduced ethanol productivity (51.1 ± 2.5 mg/L· h) against the WT (59.7 ± 1.4 mg/L· h) while *rex* deletion did not reflect substantial variations (Δ*rex*=56.7 ± 6.7 mg/L· h). Ethanol yields were 0.21 ± 0.003 g/g$_{CO}$, 0.20 ± 0.009 g/g$_{CO}$ and 0.19 ± 0.017 g/g$_{CO}$, respectively for wt, Δ*rex* and *rex**. At these time points ethanol concentration values were 18.2 ± 0.5 g/L, 16.3 ± 1.3 g/L and 15.4 ± 0.6 g/L, for the WT, Δ*rex* and *rex**, respectively (**Figure 9.6**). However, it is also worth noting that, as for serum-flask experiments, major variability was found in ethanol data compared to other metabolite, particularly with reactors operating at 600 rpm (see *rex**-2). This phenomenon could be linked to volatile nature of ethanol and hence to potential stripping effects.
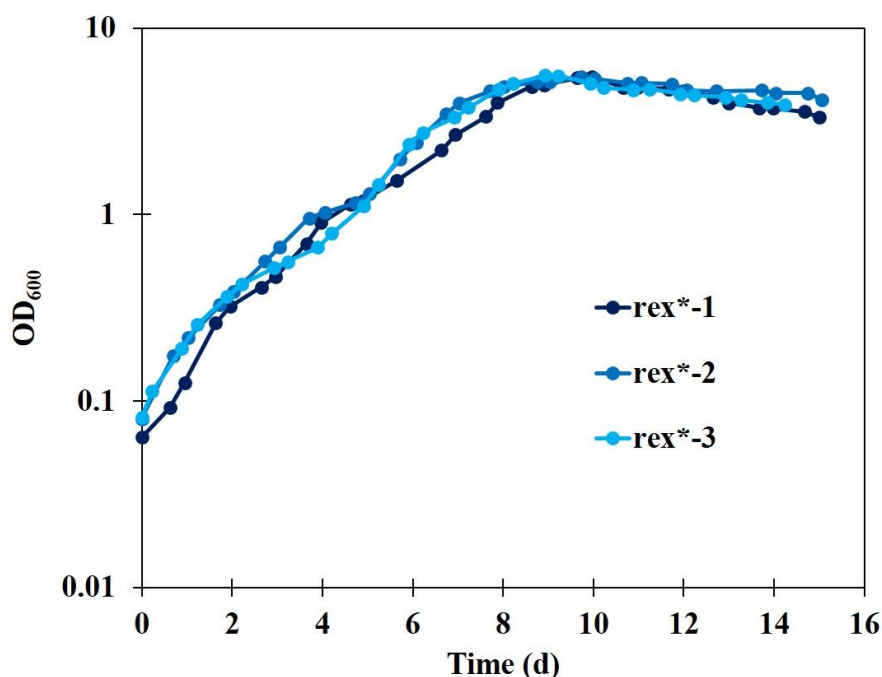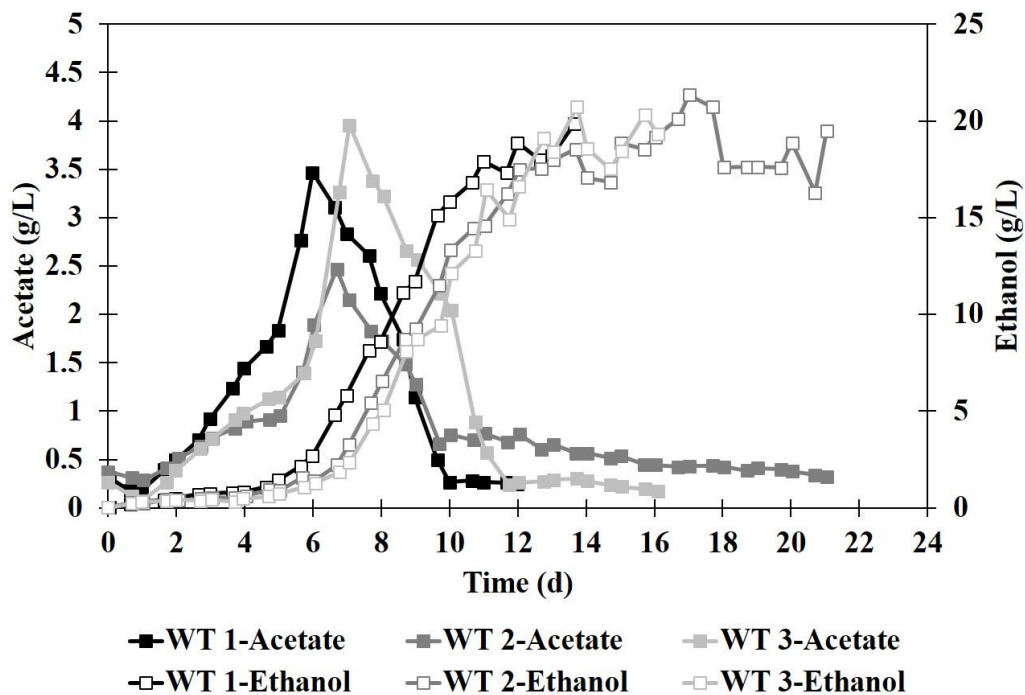

Figure continues next page.

Figure 9.6 Acetate and ethanol profile of the wild type (WT), *rex* knock-out mutant (Δ*rex*) and chromosomally *rex* complemented (*rex**) strains, grown in bioreactor with continuous CO supply. Experiments were conducted in triplicate for each single strain.

Even if no substantial differences were highlighted by comparing mutant and wild type cultures, all the tested bacterial strains exhibited a biphasic behavior when continuously fed with CO, not distinguishable instead during CO-batch assays. It has been reported that as for ABE fermentation, in acetogens solventogenesis is

149

triggered by the amount of acetate present rather than by the up regulation of alcohol producing enzymes (Martin et al. 2016). An explanation for this behavior can be that stressed conditions deriving from high acetate concentration induced metabolism rearrangement toward ethanol synthesis, allowing bacteria to get rid of the extra reducing equivalents (Molitor et al. 2016). Hence, it could be speculated that the observed phenotype may reflect the CO inhibition effect, which leads cultures to reassimilate acetate, with the resulting increase in pH (**Figure 9.4**), in order to withstand the adverse conditions. Clearly, since ethanol concentrations started increasing concurrently with acetate drop (**Figure 9.6**), this profile suggested that ethanol was not produced by the direct conversion of acetyl-CoA to acetaldehyde, and then to ethanol via the bifunctional acetaldehyde/ethanol dehydrogenase AdhE2, but rather the AOR-mediated metabolic route was mainly undertaken. Generally, this is beneficial since according to thermodynamic and stoichiometric calculations, during growth on CO, ethanol production via the AOR path is more profitable yielding 1.875 ATP/mol ethanol while 1.375 ATP are generated using the conventional route (Mock et al. 2015). Since acetate is considered an undesirable by-product which makes downstream process distillation more complicated (Martin et al. 2016), the observed selectivity toward ethanol is a desired profile.

Moreover, in disagreement with the study conducted by Wietzke and Bahl (2012), where *rex* deletion in *C. acetobutylicum* caused an earlier solvent (ethanol and butanol) production, solventogenesis phase occurred later in Δ*rex* compared to the WT (**Figure 9.7**).
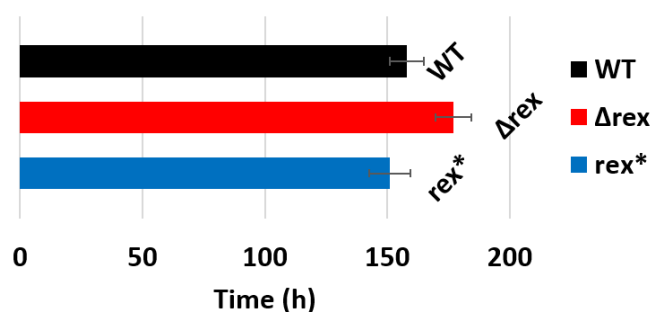
Figure 9.7 The histogram represents the duration from the starting point to the acetate peak. The results are reported as the average of the triplicate for each strain. Error bars are represented as standard error of the mean (s.e.m.).

Focusing the attention on the wild type performance, the maximum ethanol productivity achieved over the course of the fermentation was 63.8 ± 2.3 mg/L· h. This value is higher than the 58 mg/L· h ethanol productivity reported by Martin et al. (2016) with a two-stage continuous system consisting of a CSTR and a bubble column reactor, operating with syngas (60% CO, 35% H_2 and 5% CO_2) and cell recirculation. Conversely, under the same conditions, the closest-relative *C.*

ljungdahlii outperformed *C. autoethanogenum* reaching 301 mg/L· h of ethanol productivity. The value obtained in the current study is far lower than what reported in some previously published works. For instance, an ethanol productivity of 940 mg/L· h was reported by Wang et al. (Wang et al. 2013) for a continuous *C. autoethanogenum* culture grown on syngas (42% CO, 20% CO_2, 36% N_2 and 2% H_2). Additionally, 1.3 g/L· h were reached with *C. autoethanogenum* cultivated in a CSTR using H_2/CO_2 (Mock et al. 2015). These discrepancies are not surprising considering the intrinsic benefits related to continuous operation mode whereby no nutrient depletion occurs and steady state can be reached by cultures. However, when fairly compared to other works performed in semi-batch mode, the results produced are significantly higher. So far, works have been published by Abubackar and co-workers with *C. autoethanogenum* grown in a 1.2 L bioreactor operated with batch liquid and continuously fed with pure CO. In Abubackar et al. (Abubackar et al. 2015a) a maximum ethanol concentration of 0.35 g/L was achieved whereas later, the same group reported a final ethanol titer of 7.1 g/L by performing cyclic pH shift (Abubackar et al. 2016). In the current study, a maximum ethanol concentration of 20 g/L was recorded for the wild type strain. The higher value could be explained by different working conditions adopted throughout the experiment. As previously discussed, parameters such as temperature, gas flow-rate and speed agitation can affect gaseous substrate bioavailability within the fermentation broth. As a result, when higher CO partial pressures are used, ethanol generation is favored (Munasinghe and Khanal, 2010). Therefore, most likely the low concentration of CO solubilized into the liquid phase derived from the lower temperature (30°C vs. our 37°C), CO flow rate (15 ml/min vs. our 20 ml/min) and agitation speed (250 rpm vs. up to 600 rpm) selected in the experiments conducted by Abubackar et al.

The minor metabolites lactate and 2,3-BDO were also analyzed and the HPLC results are illustrated in **Figure 9.8 and 9.9**. In light of the successful outcome achieved during serum-flask fermentation, enhancement in lactate and 2,3-BDO was assumed to occur. Surprisingly, metabolite profiles deviated from the expectations. In all the studied strains a drastic drop in 2,3-BDO production occurred along with starting in lactate synthesis. This event might be interpreted as a preference to initially channel electrons into 2,3-BDO instead of lactate.
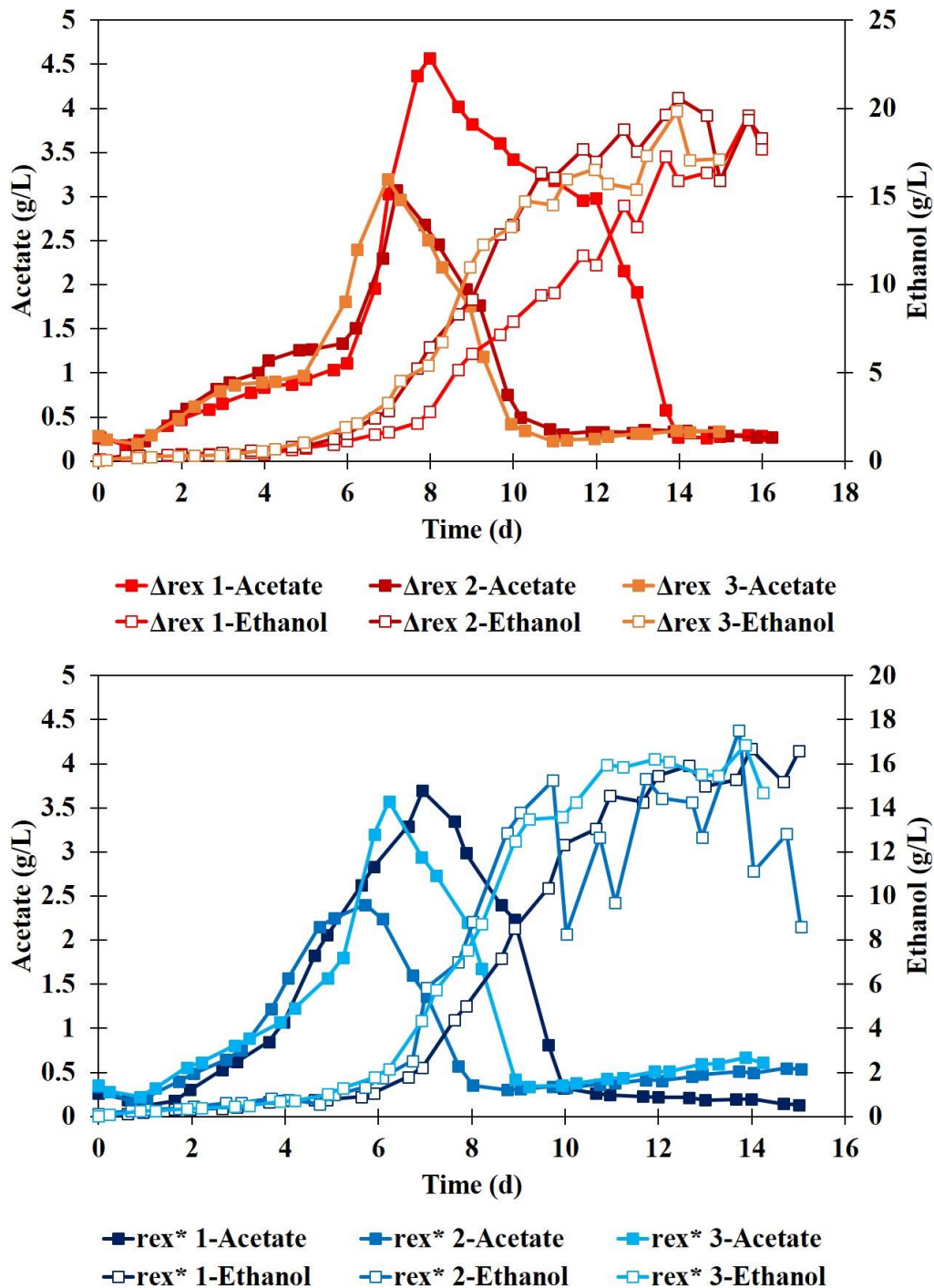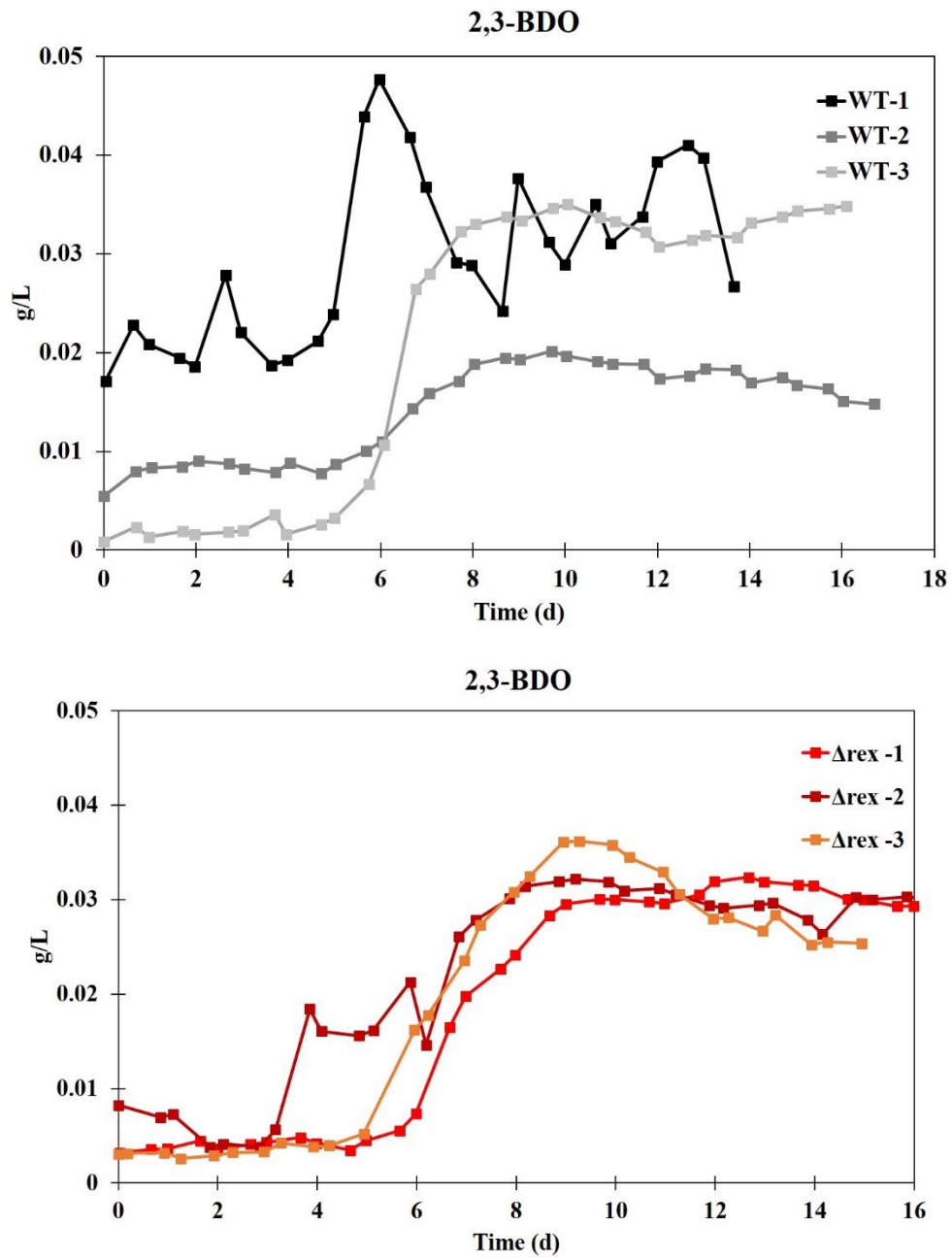
2,3-BDO

2,3-BDO

Figure continues next page.
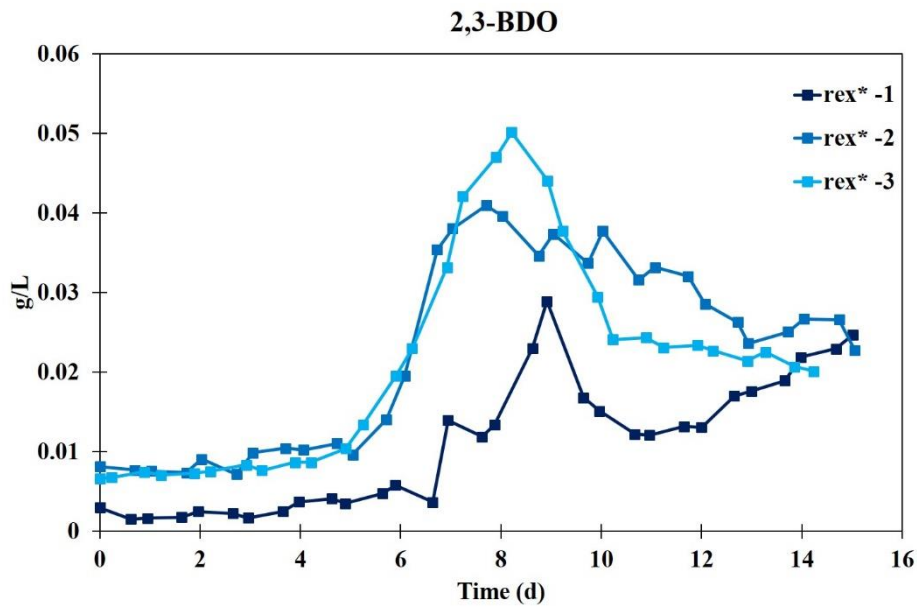
Figure 9.8 2,3-BDO profile of the wild type (WT), rex knock-out mutant (Δrex) and chromosomally *rex* complemented (rex*) strains, grown chemolithotrophically in a stirred-tank bioreactor operated in semi-batch mode with batch liquid and continuous CO supply (flow rate-20 ml/min). Experiments were conducted in triplicate for all the three strains.

As shown in **Figure 9.9**, lower lactate productivity was achieved by Δ*rex* against the control strain. However, due to the large error bars represented variations in *rex** experiments and the generally low values detected, no reliable conclusions can be made. Indeed, since this behavior is not related to any genotype but occurred indistinctly for each strain, the reason could be related to the CO different conditions. Since, both the pyruvate-derived metabolites are generally produced when substrate started to be limiting, during mid-late exponential phase, most likely the effect of deletion seen in batch is hidden in continuous-CO conditions.
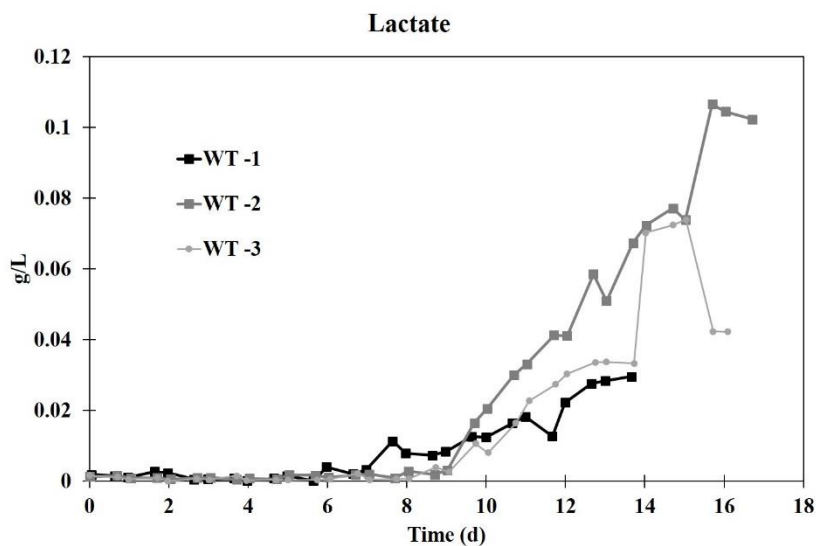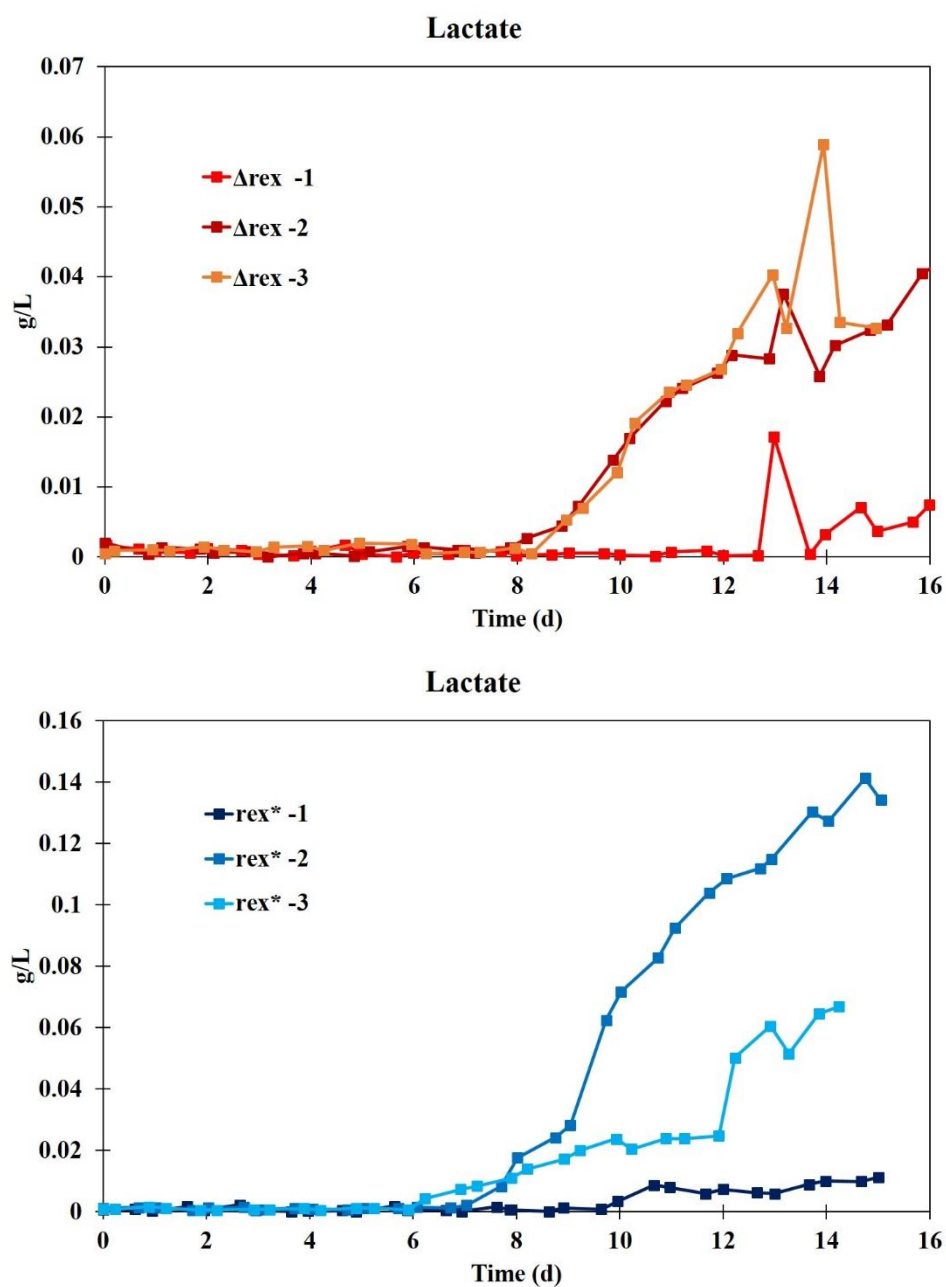
Figure 9.9 Lactate profile of the wild type (WT), rex knock-out mutant (Δrex) and chromosomally *rex* complemented (rex*) strains, grown chemolithotrophically in a stirred-tank bioreactor operated in semi-batch mode with batch liquid and continuous CO supply (flow rate-20 ml/min). Experiments were conducted in triplicate for all the three strains.

In agreement with the results shown in the current study, whilst derepression of *rex* target genes (*pflBA*, *adhA*, *adhA2*, *thlA*, *thlA2*, *crt-bcd-etfBA-hbd*, *ptb-buk*, *butA*, *fld- Cbei_4318*, *hydB*) was confirmed in *rex* deficient *C. beijerinckii,* no metabolic changes could be appreciated (L. Zhang et al., 2014). The authors concluded that a feasible explanation relies on the natural rigidity of electron distribution through solvent formation and hydrogen synthesis pathways in the solventogenic *C. beijerinkii*. Concerning *C. autoethanogenum*, it can be speculated that when CO is

154

continuously supplied, *rex* inactivation and its overexpression did not substantially alter the fermentation product profile. A reliable explanation cannot easily be provided since Rex is involved in a complex regulatory network. Moreover, the absence of Rex studies in autotrophically grown bacteria, makes it somewhat hard to compare with what has been reported in literature so far. Indeed, the use of different carbon sources may affect the downstream solvent production. For instance, some differences were identified depending on using glycerol or glucose as substrate in *C. pasteurianum rex* deficient strain. Indeed, utilization of different carbon sources implies different amount of reducing equivalents and thus diverse effects on metabolic pathways.
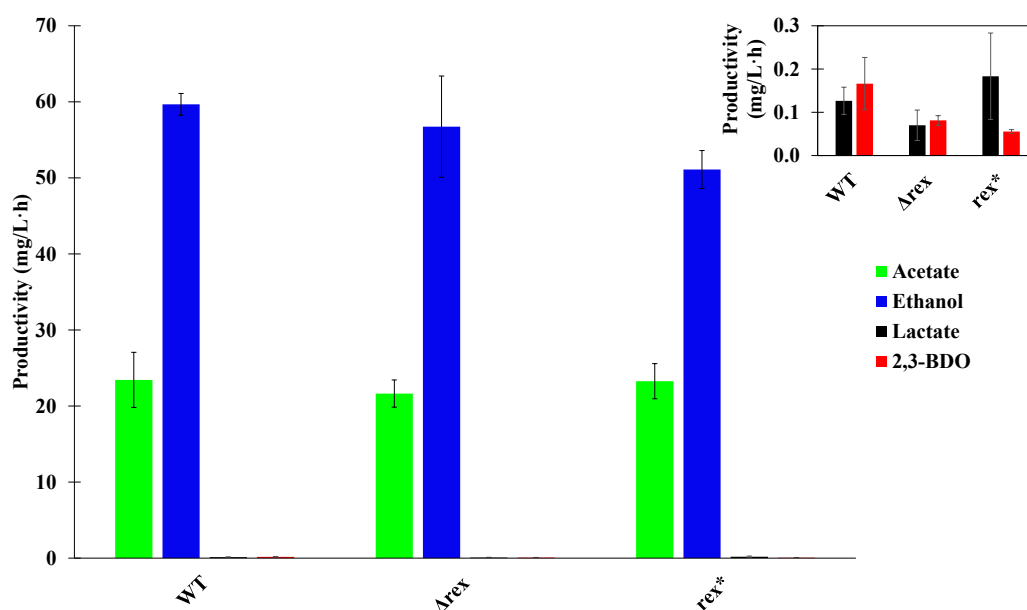
Figure 9.10 Productivity (mg/L·h) of ethanol and acetate. The inset shows the zoom of 2,3-BDO and lactate productivities. Data is reported as the average of each triplicate and error bars are represented as standard error of the mean (s.e.m.). Acetate productivity is referred to the peak time point, whereas all the others were calculated at ~300 h.

9.2.2.4 Fermentation gas analysis

Carbon monoxide serves as source of carbon and energy in the Wood-Ljungdahl pathway. When acetogens such as *C. autoethanogenum* assimilate CO, during its oxidization extra reducing equivalents are generated through the reversible water gas shift reaction (Valgepea et al. 2018). Hence, according to WGS equation (Eq. 6.1), during autotrophic growth on CO, beyond the main products ethanol and acetate, and the small amount of lactate and 2,3-BDO synthesized, molecular H_2 and CO_2 are also released. The control and mutant cultures were subjected to gas analysis. The CO entering the bioreactor as well as the outgoing gases H_2, CO_2 and the metabolically bypassed CO were systematically monitored. A representative gas profile is illustrated in **Figure 9.11**, where a typical growth profile is also shown

as confirmation of the existing correlation between CO consumption and bacterial growth.
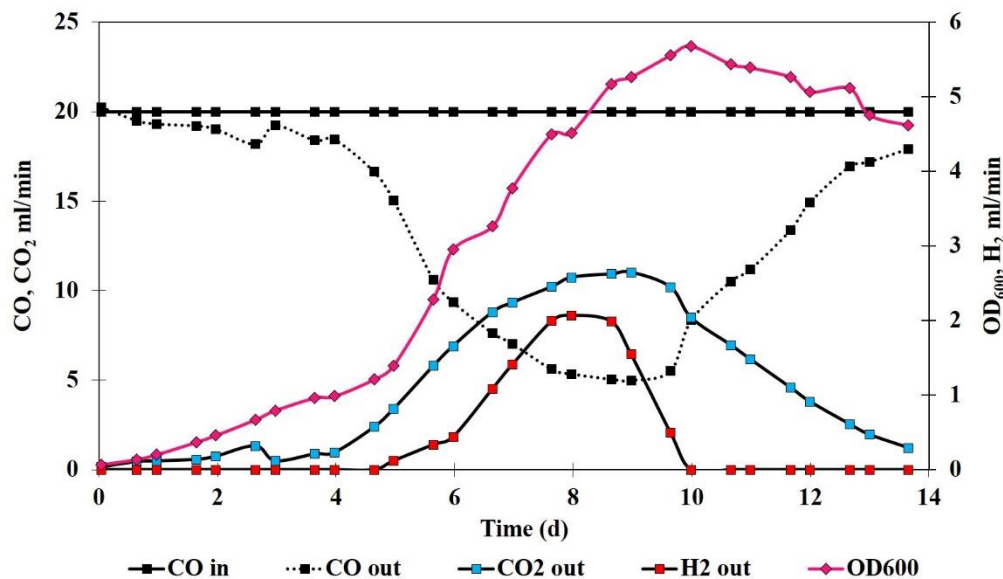
Figure 9.11 Changes in gas flow-rates calculated using micro GC-data and growth profile (OD600). Data is refereed to *C. autoethanogenum* wild type (WT 1) as representative strain. Inlet and outlet gas analysis was conducted by sampling every 4 h and 20 minutes, respectively.

As shown, CO_2 and H_2 evolution started in correlation with CO consumption by the bacterial cultures and successively dropped when CO utilization gradually decreased with the culture approaching stationary phase. Although CO_2 and H_2 can be utilized as carbon and energy sources respectively, due to the thermodynamic limitations discussed before, the amount produced cannot be considered as potentially utilizable, because pure CO is continuously fed into the system. Hence, cultures were presumed to consume CO only.

Since hydrogen production is also regulated by intracellular redox state and it competes with solvent synthesis for the electrons, in the *rex*-defective *C. acetobutylicum* an increase in alcohol production resulted in significantly reduced H_2 production (Hatch and Finneran, 2008; Wietzke and Bahl, 2012). However, no specific response in terms of H_2 generation was detected in Δ*rex* and *rex* C. autoethanogenum* strains compared to the control (Data not shown).

9.2.2.5 Mass balance analysis of carbon

In order to experimentally verify the theoretical stoichiometric calculations of metabolite yields, carbon mass balance was performed individually for each strain at the end of the fermentation process. Quantification of the inlet carbon content was performed by integrating the mass flow of CO measured throughout the entire fermentation. Off-gas analysis allowed an estimation of the amount of carbon

exiting the system as CO_2. For more accurate calculations, beyond the fermentation products (acetate, ethanol, 2,3-BDO and lactate), biomass was also included. As shown in **Figure 9.12**, carbon mass balance confirmed that no differences in terms of carbon distribution existed between the Δ*rex* and *rex** strains, when compared to the wild type.

When H_2 is not present within the gaseous mixture, CO fixation into ethanol proceeded by the Eq. 6.2, inevitably leads to dissipation of 2/3s of carbon as CO_2 (Wilkins and Atiyeh, 2011). Conversely, with the aid of hydrogenase activity converting H_2 in H^+ and e⁻, H_2-CO co-utilization generates a greater amount of reducing equivalents, hence saving more CO for conversion into ethanol. Valgepea et al. (2018) compared fermentation performances of *C. autoethanogenum* cultures grown on pure CO and CO plus H_2. As consequence of H_2 supplementation, only 17% of carbon was lost as CO_2 with a 4-fold increase of carbon flux channeled into ethanol whereas 61% of carbon was dissipated as CO_2 when solely CO was fed. The experimental data achieved in this study was extremely close to theoretical estimation provided by Wilkins and Atiyeh, 2011. Approximately 67-68% of the incoming carbon exited the vessel as CO_2. In *C. autoethanogenum* wild type and *rex* deficient strains, around $24 \pm 1\%$ and $23 \pm 1\%$ of initial carbon was converted into ethanol whereas a very low amount of carbon (not graphically visible) remained as pyruvate-derived products and acetate. This value is reliable since calculations are referred to the end point, when almost all the acetate available got converted into ethanol. At the end of the fermentation, carbon recovery calculated for the WT and Δ*rex* accounted for $93 \pm 2\%$ and $93 \pm 1\%$, respectively. Similarly, carbon recovery values of 93% and 92% resulted instead from *rex**-1 and *rex**-3, while 82% carbon recovery was calculated for *rex**-2. This low percentage has to be attributed to issues in ethanol measurements as demonstrated in both **Figure 9.12** and **9.6**. Since carbon recovery generally deviated from 100%, the unidentified portion of carbon might be reasonably attributed to ethanol stripped from the fermentation broth, especially at high rotation speed.
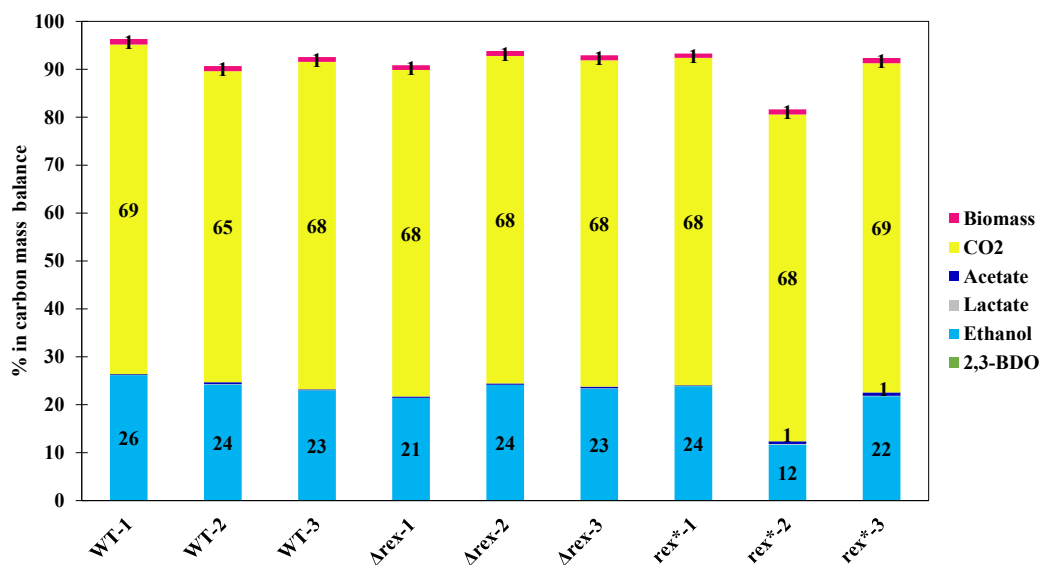
Figure 9.12 Carbon mass balance analysis at the end of fermentation for each biological triplicate of the wild type (WT), *rex* deletion (Δ*rex*) and chromosomally *rex* complemented (*rex**) strains, grown in semi-batch mode with batch liquid and continuous CO supply. Carbon mass balances were normalized to 100%.

9.3   Conclusions

This study represents the first attempt in the literature to explore the role of the redox sensing transcriptional repressor Rex in autotrophic metabolism of an acetogen, such as *C. autoethanogenum*. In order to investigate whether inactivation of the *rex* gene altered the fermentation metabolite spectrum, *rex* deletion (Δ*rex*) and complementation (*rex**) strains were phenotypically characterized and compared to the control strain (WT). The experimental data collected showed that Rex modulates the synthesis pathways of lactate and 2,3-butanediol, with *rex* deficient strain exhibiting 83% increase in 2,3-BDO and a final concentration of lactate 17-fold higher than the WT, during CO-batch cultivation. Conversely, no substantial metabolic changes across the strains were observed during non-carbon limited conditions, when cultures were cultivated in semi-batch mode with batch liquid and continuous CO supply. Cultures, which were continuously fed with CO, exhibited a biphasic behavior, not distinguishable during CO-batch tests, with a clear shift from acidogenesis to solventogenesis, suggesting that ethanol was mainly produced by the AOR-mediated metabolic route rather than by the conventional direct pathway. The observed phenotype may reflect the stressed conditions deriving from CO inhibition, which leads bacteria to rearrange their metabolism by reassimilating acetate and converting it into ethanol, to withstand the adverse conditions. However, as validated by *in silico* analysis, Rex is involved in a complex regulatory network and this makes the results more challenging to interpret. Moreover, the lack of previous studies involving Rex in autotrophically

grown bacteria, makes it somewhat difficult to compare this study with what has been reported in literature so far. Results obtained from the carbon mass balance calculations confirmed that no differences in terms of carbon distribution were present between the strains. Moreover, this data was in perfect agreement with the theoretical estimation provided by Wilkins and Atiyeh (2011), showing a 67-68% of carbon dissipation as CO_2 during ethanol formation. Consequently, approximately 23% of the initial carbon was incorporated into ethanol. Focusing on *C. autoethanogenum* wild type, with a maximum ethanol concentration of ~20 g/L achieved, its fermentation performance significantly outperforms other previously published studies operating under similar fermentation conditions. As general conclusion, the observation of *rex* involvement in 2,3-BDO synthesis emerged during batch-bottle assays, is an attractive finding, which should inspire further investigations in light of the great attention this compound is currently gaining. Conversely, it would appear that *rex* is not a valuable target for metabolic engineering studies seeking to enhance ethanol production in *C. autoethanogeum*.

Chapter 10

References

Abrini, J., Naveau, H. and Nyns, E.J. (1994). *Clostridium autoethanogenum,* sp. nov., an anaerobic bacterium that produces ethanol from carbon monoxide. Archives of Microbiology, 161: 345–351.

Abubackar, H.N., Veiga, M.C. and Kennes, C. (2012). Biological conversion of carbon monoxide to ethanol: Effect of pH, gas pressure, reducing agent and yeast extract. *Bioresource Technology*, 114, 518–522.

Abubackar, H.N., Veiga, M.C. and Kennes, C. (2015a). Ethanol and acetic acid production from carbon monoxide in a clostridium strain in batch and continuous gas-fed bioreactors. *International Journal of Environmental Research and Public Health*, 12: 1029–1043.

Abubackar, H.N., Veiga, M.C. and Kennes, C. (2015b). Carbon monoxide fermentation to ethanol by *Clostridium autoethanogenum* in a bioreactor with no accumulation of acetic acid. *Bioresource Technology*, 186: 122-127.

Abubackar, H.N., Fernández-Naveira, Á., Veiga, M.C. and Kennes, C. (2016). Impact of cyclic pH shifts on carbon monoxide fermentation to ethanol by *Clostridium autoethanogenum. Fuel*, 178: 56–62.

Adamse, A.D. (1980). New isolation of Clostridium aceticum. Antonie Van Leeuwenhoek, *Journal of Microbiology*, 46: 523–531.

Ahmed, A., Cateni, B.G., Huhnke, R.L. and Lewis, R.S. (2006). Effects of biomass-generated producer gas constituents on cell growth, product distribution and hydrogenase activity of *Clostridium carboxidivorans* P7T. *Biomass and Bioenergy*, 30: 665–672.

Al-Habobi N.A. and Turki, A.A. (2008). Image Processing To Determine Mass Transfer Coefficient for. *Distribution*. The 1 stRegional Conference of Eng. Sci. NUCEJ Spatial ISSUE, 11, 263–269.

Al-hinai, M.A., Fast, A.G. and Papoutsakis, E.T. (2012). Novel System for Efficient Isolation of Clostridium Double-Crossover Allelic Exchange Mutants Enabling Markerless Chromosomal Gene deletions and DNA integration, *Applied and Environmental Microbiology*, 78: 8112–8121.

Allen, S. A., Clark, W., McCaffery, J. M., Cai, Z., Lanctot, A., Slininger, P. J., Liu, Z. L.,

Gorsich, S.W. (2010a). Furfural induces reactive oxygen species accumulation and cellular damage in *Saccharomyces cerevisiae*. *Biotechnology for Biofuels*, 3, 2.

Allen, T.D., Caldwell, M. E., Lawson, P. A., Huhnke, R. L. and Tanner, R. S. (2010b). *Alkalibaculum bacchi* gen. nov., sp. nov., a CO-oxidizing, ethanol-producing acetogen isolated from livestock-impacted soil. *International Journal of Systematic and Evolutionary Microbiology*, 60: 2483–2489.

Amador-Noguez, D., Brasg, I.A., Feng, X.J., Roquet, N. and Rabinowitz, J.D. (2011). Metabolome remodeling during the acidogenic-solventogenic transition in *Clostridium acetobutylicum*. *Applied and Environmental Microbiology*, 77: 7984–7997.

Anderson, M. E., DeRose, V. J., Hoffman, B. M., and Lindahl, P. A. (1993). Identification of a cyanide binding site in CO dehydrogenase from Clostridium thermoaceticum using EPR and ENDOR spectroscopies. JACS. 115: 12204–12205.

Andreese, J.R., Gottscha, G. and Schlegel, H. G. (1970). *Clostridium formicoaceticum* nov spec - Isolation, description and distinction from *Clostridium aceticum* and *Clostridium thermoaceticum*. *Archives of Microbiology*, 72: 154-174.

Annan, F.J. and Henstra, A. Engineering of vitamin prototrophy in *Clostridium ljungdahlii* and *Clostridium autoethanogenum* (submitted).

Aro, E.M. (2016). From first generation biofuels to advanced solar biofuels. *Ambio*, 45, 24–31.

Asimakopoulos, K., Gavala, H.N., and Skiadas, I.V. (2018). Reactor systems for syngas fermentation processes: A review. *Chemical Engineering Journal*, 348: 732–744.

Barrangou, R. and Marraffini, L. A. (2014). CRISPR-cas systems: Prokaryotes upgrade to adaptive immunity. *Molecular Cell*, 54: 234–244.

Bengelsdorf, F.R. and Dürre, P. (2017). Gas fermentation for commodity chemicals and fuels. *Microbial Biotechnology*, 10: 1167–1170.

Bertsch, J. and Müller, V. (2015). Bioenergetic constraints for conversion of syngas to biofuels in acetogenic bacteria. *Biotechnology for Biofuels*, 8: 210.

Bhatia, S.K., Kim, S.H., Yoon, J.J., and Yang, Y.H. (2017). Current status and strategies for second generation biofuel production using microbial systems. *Energy Conversion and Management*, 148: 1142–1156.

Biegel, E. and Muller, V. (2010). Bacterial Na+-translocating ferredoxin:NAD+ oxidoreductase. *Proceedings of the National Academy of Sciences*, 107: 18138-18142.

Biegel, E., Schmidt, S., González, J.M. and Müller, V. (2011). Biochemistry, evolution and physiological function of the Rnf complex, a novel ion-motive electron transport complex in prokaryotes. *Cellular and Molecular Life Sciences*, 68: 613–634.

Boateng, A., Banowetz, G., Steiner, J., Barton, T., Taylor, D., Hicks, K., El-Nashaar, H. and Sethi, V.K. (2007). Gasification of Kentucky bluegrass (Poa pratensis l.) straw in a farm-scale reactor. *Biomass and Bioenergy*, 31:153–161.

Boeke, J.D., Trueheart, J., Natsoulis, G., Fink, G.R. (1987). 5-Fluoroorotic acid as a selective agent in yeast molecular genetics. Methods in Enzymology, 154: 164–175.

Breault, R.W. (2010). Gasification processes old and new: a basic review of the major technologies. Energies 3, 216–240.

Brekasis, D. and Paget, M.S. (2003). A novel sensor of NADH / NAD + redox poise in Streptomyces coelicolor A3(2). *EMBO Journal*, 22: 4856-4865.

Brown, S.D., Nagaraju, S., Utturkar, S., De Tissera, S., Segovia, S., Mitchell, W., Land, M.L., Dassanayake, A. and Köpke, M. (2014). Comparison of single-molecule sequencing and hybrid approaches for finishing the genome of *Clostridium autoethanogenum* and analysis of CRISPR systems in industrial relevant Clostridia. *Biotechnology for Biofuels*, 7:40.

Bruder, M.R., Pyne, M.E., Moo-Young, M., Chung, D.A. and Chou, C.P. (2016). Extending CRISPR-Cas9 technology from genome editing to transcriptional engineering in the genus Clostridium. *Applied and Environmental Microbiology*, 82: 6109–6119.

Cartman, S.T., Kelly, M.L., Heeg, D., Heap, J.T. and Minton, N.P. (2012). Precise Manipulation of the *Clostridium difficile* Chromosome Reveals a Lack of Association between the tcdC Genotype and Toxin Production. *Applied and Environmental Micobiology*, 78: 4683–4690.

Chen, W., Liew, F., and Koepke, M. (2013). Recombinant Microorganisms and Uses Therefor. US20130323820. Washington, DC: U.S. Patent and Trademark Office.

Chen, J., Gomez, J.A., Höffner, K., Barton, P.I. and Henson, M.A. (2015). Metabolic modeling of synthesis gas fermentation in bubble column reactors. *Biotechnology for Biofuels*, 8: 1–12.

Chen, J., Daniell, J., Griffin, D., Li, X. and Henson, M.A. (2018). Experimental testing of a spatiotemporal metabolic model for carbon monoxide fermentation with *Clostridium autoethanogenum*. *Biochemical Engineering Journal*, 129: 64–73.

Chum, H.L., Warner, E., Seabra, J.E., Macedo, I.C. (2014). A comparison of commercial ethanol production systems from Brazilian sugarcane and US corn. *Biofuels, Bioproducts and Biorefining*, 8: 205-223.

Clauwers, C., Vanoirbeek, K., Delbrassinne, L., Michiels, C. W. (2016). Construction of Nontoxigenic Mutants of Nonproteolytic Clostridium botulinum NCTC 11219 by Insertional Mutagenis and Gene Replacement. *Applied and Environmental Microbiology*, 82: 3100-3108.

Costa, J. A.V. and de Morais, M.G. (2011). The role of biochemical engineering in the

production of biofuels from microalgae. *Bioresource Technology*, 102, 2–9.

Cotter, J.L., Chinn, M.S. and Grunden, A.M. (2009). Influence of process parameters on growth of *Clostridium ljungdahlii* and *Clostridium autoethanogenum* on synthesis gas. *Enzyme and Microbial Technology*, 44: 281–288.

Croux, C., Nguyen, N.P., Lee, J., Raynaud, C., Saint-Prix, F. Gonzales-Pajuelo, M., Meynial-Salles, I. and Soucaille, P. (2016). Construction of a restriction-less, marker-less mutant useful for functional genomic and metabolic engineering of the biofuel producer *Clostridium acetobutylicum*. *Biotechnology for Biofuels*, 2: 9-23.

Daniell, J., Köpke, M. and Simpson, S. D. (2012). *Commercial biomass syngas fermentation. Energies*, 5:12.

Datar, R.P., Shenkman, R.M., Cateni, B.G., Huhnke, R.L. and Lewis, R.S. (2004). Fermentation of biomass-generated producer gas to ethanol. *Biotechnology and Bioengineering*, 86: 587–594.

De Klerk, A., Li, Y. W. and Zennaro, R. (2013). Greener Fischer-Tropsch Processes for Fuels and Feedstocks. Weinheim: John Wiley & Sons, Inc.

Desai, R.P., Harris, L.M., Welker, N.E. and Papoutsakis, E.T. (1999). Metabolic Flux Analysis Elucidates the Importance of the Acid-Formation Pathways in Regulating Solvent production by *Clostridium acetobutylicum*. *Metabolic Engineering*, 1: 206-213.

Devarapalli, 2017. Analysis of trickle-bed reactor for ethanol production from syngas using *Clostridium ragsdalei.* PhD thesis.

Devarapalli, M., Lewis, R. and Atiyeh, H. (2017). Continuous Ethanol Production from Synthesis Gas by *Clostridium ragsdalei* in a Trickle-Bed Reactor. *Fermentation*, 3:23.

Doench, J.G., Fusi, N., Sullender, M., Hegde, M., Vaimberg, E.W., Donovan, K.F., Smith, I., Tothova, Z., Wilen, C., Orchard, R. Virgin, H.W., Listgarten, J. and Root, D.E. (2016). Optimized sgRNA design to maximize activity and minimize off-target effects of CRISPR-Cas9. *Nature Biotechnology*, 34: 184–191.

Drake, H. L., Küsel, K. and Matthies, C. (2006). Acetogenic prokaryotes. In *The Prokaryotes: An Evolving Electronic Resource for the Microbiological Community*, eds M. Dworkin, S. Falkow, E. Rosenberg, K.-H. Schleifer, and E. Stackebrandt (New York: Springer), 354–420.

Drake, H. L., Gössner, A.S. and Daniel, S.L. (2008). Old acetogens, new light. *Annals of the New York Academy of Sciences*, 1125, 100–128.

Drzyzga, O., Revelles, O., Durante-rodríguez, G., Díaz, E., García, J.L. and Prieto, A. (2015). New challenges for syngas fermentation : towards production of biopolymers, 90: 1735-1751.

Du, X.H. and Pene, J.J. (1999). Identification, cloning and expression of p25, an AT-rich

DNA-binding protein from the extreme thermophile, *Thermus aquaticus* YT-1. Nucleic Acids Research, 27: 1690–1697.

Dürre, P. (2007). Biobutanol: An attractive biofuel. *Biotechnology Journal*, 2: 1525–1534.

Dürre, P. (2017). Gas fermentation – a biotechnological solution for today's challenges. *Microbial Biotechnology*, 10: 14–16.

Dutta, K., Daverey, A. and Lin, J.G. (2014). Evolution retrospective for alternative fuels: First to fourth generation. *Renewable Energy*, 69: 114–122.

EASAC, 2012. The current status of biofuels in the European Union, their environmental impacts and future prospects. *EASAC Policy Report* 19.

Ehsaan, M., Kuit, W., Zhang, Y., Cartman, S.T., Heap, J.T., Winzer, K. and Minton, N.P. (2016). Mutant generation by allelic exchange and genome resequencing of the biobutanol organism *Clostridium acetobutylicum* ATCC 824. *Biotechnology for Biofuels*, *9*: 4.

Elshahed, M.S. (2010). Microbiological aspects of biofuel production: Current status and future directions. *Journal of Advanced Research*, 1: 103–111.

Fast, A.G. and Papoutsakis, E.T. (2012). Stoichiometric and energetic analyses of non-photosynthetic CO_2-fixation pathways to support synthetic biology strategies for production of fuels and chemicals. *Current Opinion in Chemical Engineering*, 1: 380–395.

Fischer, H. and Tropsch (1930). Process for the production of paraffin-hydrocarbons with more than one carbon atom. U.S. Patent 1,746,464.

Gaddy, J.L. and Clausen, E.C. (1992). *Clostridium ljungdahlii,* an anaerobic ethanol and acetate producing microorganism. US Patent No. 5,173,429.

Gaddy, J. L., Dinesh, K.A., Ko, C.W., Phillips, J.R., Basu, R., Wikstrom, C.V. and Clausen, E. (2007). Methods for Increasing the Production of Ethanol from Microbial Fermentation. US7285402.Washington, DC: U.S. Patent and TrademarkOffice.

Genthner, B.R., Davis, C.L. and Bryant, M.P. (1981). Features of rumen and sewage sludge strains of *Eubacterium limosum*, a methanol- and H_2-CO_2-utilizing species. *Applied and Environmental Microbiology*, 42: 12–19.

Genthner, B.R.S. and Bryant, M.P. (1987). Additional characteristics of one-carbon-compound utilization by *Eubacterium limosum* and *Acetobacterium woodii*. *Applied and Environmental Microbiology*, 53: 471–476.

Gottschal, J. and Morris, J. (1981). The Induction of Acetone and Butanol Production in Cultures of *Clostridium acetobutylicum* by Elevated Concentrations of Acetate and Butyrate. FEMS *Microbiology Reviews*, 12: 385-389.

Griffin, D.W. and Schultz, M.A. (2012). Fuel and Chemical Products from Biomass Syngas: A Comparison of Gas Fermentation to Thermochemical Conversion Routes. *Environmental Progress and Sustainable Energy*, 31:219:224.

Grupe, H. and Gottschalk, G. (1992). Physiological events in Clostridium acetobutylicum during the shift from acidogenesis to solventogenesis in continuous culture and presentation of a model for shift induction. *Applied and Environmental Microbiology*, *58*: 3896–3902.

Guo, J., Wang, T., Guan, C., Liu, B., Luo, C., Xie, Z., Zhang, C and Xing, X.H. (2018). Improved sgRNA design in bacteria via genome-wide activity profiling. *Nucleic Acids Research*, 46: 7052–7069.

Gyan, S., Shiohira, Y., Sato, I., Takeuchi, M. and Sato, T. (2006). Regulatory loop between redox sensing of the NADH/NAD+ratio by Rex (YdiH) and oxidation of NADH by NADH dehydrogenase Ndh in Bacillus subtilis. *Journal of Bacteriology*, 188: 7062–7071.

Hatch, J.L. and Finneran, K.T. (2008). Influence of reduced electron shuttling compounds on biological H_2 production in the fermentative pure culture *Clostridium beijerinckii*. *Current Microbiology*, 56: 268–273.

Heap, J.T., Pennington, O.J., Cartman, S.T. and Minton, N.P. (2009). A modular system for Clostridium shuttle plasmids. *Journal of Microbiological Methods*, 78: 79–85.

Heap, J.T., Ehsaan, M., Cooksley, C.M., Ng, Y.K., Cartman, S.T., Winzer, K. and Minton, N.P. (2012). Integration of DNA into bacterial chromosomes from plasmids without a counter-selection marker. *Nucleic Acids Research*, 40: e59.

Hegner, R., Koch, C., Riechert, V. and Harnisch, F. (2017). Microbiome-based carboxylic acids production: from serum bottles to bioreactors. *RSC Advances*, 7: 15362–15371.

Heijstra, B. D., Leang, C. and Juminaga, A. (2017). Gas fermentation: Cellular engineering possibilities and scale up. *Microbial Cell Factories*, 16:60.

Heiskanen, H., Virkajarvi, I. and Viikari, L. (2007). The effects of syngas composition on the growth and product formation of *Butyribacterium methylotrophicum*. *Enzyme and Microbiology Technology*, 41: 362–367.

Henstra, A.M., Sipma, J., Rinzema, A. and Stams, A.J. (2007). Microbiology of synthesis gas fermentation for biofuel production. *Current Opinion in Biotechnology*, 18: 200–206.

Ho, D.P., Ngo, H.H., and Guo, W. (2014). A mini review on renewable sources for biofuel. *Bioresource Technology*, 169: 742–749.

Hu, L., Huang, H., Yuan, H., Tao, F., Xie, H. and Wang, S. (2016). Rex in *Clostridium kluyveri* is a global redox-sensing transcriptional regulator. *Journal of Biotechnology*, 233: 17–25.

Huang, H., Chai, C., Li, N., Rowe, P., Minton, N. P., Yang, S., Jiang, W. and Gu, Y. (2016). CRISPR/Cas9-Based Efficient Genome Editing in *Clostridium ljungdahlii,* an Autotrophic Gas-Fermenting Bacterium. *ACS Synthetic Biology*, 5: 1355-1361.

Humphreys, C.M., McLean, S., Schatschneider, S., Millat, T., Henstra, A.M., Annan, F.J., Breitkopf, R., Pander, B., Piatek, P., Rowe, P., Wichlacz, A.T., Woods, C., Norman, R., Blom, J., Goesman, A., Hodgman, C., Barret, D., Thomas, N.R., Winzer, K. and Minton, N.P. (2015). Whole genome sequence and manual annotation of *Clostridium autoethanogenum*, an industrially relevant bacterium. *BMC Genomics*, 16: 1–10.

Humphreys, C.M. and Minton, N. P. (2018). Advances in metabolic engineering in the microbial production of fuels and chemicals from C1 gas. *Current Opinion in Biotechnology*, 50, 174–181.

Hurst, K.M. and Lewis, R.S. (2010). Carbon monoxide partial pressure effects on the metabolic process of syngas fermentation. *Biochemical Engineering Journal*, 48: 159–165.

IEA, International Energy Agency, 2008. From 1st to 2nd generations of biofuel technologies, overview of current industry and RD&D activities. IEA/OECD, Paris.

IEA, International Energy Agency, 2010. Sustainable production of second-generation biofuels: potential and perspectives in major economies and developing countries. IEA/OECD, Paris.

IEA, International Energy Agency, 2013. World Energy Outlook 2013. IEA/OECD, Paris.

Ingle, P. and Minton, N. Generation of a fully erythromycin-sensitive strain of *Clostridioides difficile* using a novel CRISPR-Cas9 genome editing system. (submitted).

IPCC-Intergovernmental Panel on Climate Change, Iron and Steel (2018). Available: http://www.ipcc.ch/publications_ and_data/ar4/wg3/en/ch7s7-4-1.html.

Ishino, Y., Shinagawa, H., Makino, K., Amemura, M. and Nakatura, A. (1987). Nucleotide sequence of the iap gene, responsible for alkaline phosphatase isoenzyme conversion in *Escherichia coli*, and identification of the gene product. *Journal of Bacteriology*, 169: 5429–5433.

Jennert, K.C., Tardif, C., Young, D.I. and Young, M. (2000). Gene transfer to *Clostridium cellulolyticum* ATCC 35319. *Microbiology*, 146: 3071–3080.

Jiang, W., Bikard, D., Cox, D., Zhang, F. and Marraffini, L. A. (2013). CRISPR-assisted editing of bacterial genomes. *Nature Biotechnology*, 31: 233–239.

Jiang, Y., Chen, B., Duan, C., Sun, B., Yang, J. and Yang, S. (2015). Multigene Editing in the Escherichia coli Genome via the CRISPR-Cas9 System. *Applied and Environmental Microbiology*, 81: 2506-2514.

Jinek, M., Chylinski, K., Fonfara, I., Hauer, M., Doudna, J.A. and Charpentier, E. (2012). A Programmable Dual-RNA – Guided DNA Endonuclease in Adaptive Bacterial

Immunity. *Science,* 337: 816–821:

Joseph, R.C., Kim, N.M. and Sandoval, N.R. (2018). Recent developments of the synthetic biology toolkit for Clostridium. *Frontiers in Microbiology*, 9: 1–13.

Kane, M.D. and Breznak, J. A. (1991). *Acetonema longum* gen nov SP-nov, an H_2/CO_2 acetogenic bacterium from the termite, *Pterotermes occidentis*. Archives of Microbiology, 156:91–98.

Kim, J.R. Bajapai, R. and Iannotti, E.L. (1988). Redox Potential in Acetone-Butanol fermentations. *Applied Biochemistry and Biotechnology*, 18: 175-186.

Köpke, M. and Liew, F. M. (2011). Recombinant Microorganism and Methods of Production Thereof. US 2011/0236941 A1. Washington, DC: U.S. Patent and Trademark Office.

Köpke, M., Mihalcea, C., Liew, F. M., Tizard, J. H., Ali, M. S., Conolly, J. J., Al-Sinawi B. and Simpson, S.D. (2011). 2,3-Butanediol production by acetogenic bacteria, an alternative route to chemical synthesis, using industrial waste gas. *Applied and Environmental Microbiology*, 77: 5467–5475.

Köpke, M., Simpson, S., Liew, F. M., and Chen, W. (2012). Fermentation Process for Producing Isopropanol Using a Recombinant Microorganism. US20120252083 A1. Washington, DC: U.S. Patent and Trademark Office

Köpke, M. and Chen, W. Y. (2013). Recombinant Microorganisms and Uses Therefor. US20130323806.

Köpke, M., Nagaraju, S., and Chen, W. (2013). Recombinant Microorganisms and Methods of Use Thereof. US20140206901. Washington, DC: U.S. Patent and Trademark Office.

Köpke, M., Gerth, M.L., Maddock, D.J., Mueller, A.P., Liew, F.M., Simpson, S.D., and Patrick, W.M. (2014). Reconstruction of an acetogenic 2,3-butanediol pathway involving a novel NADPH-dependent primary-secondary alcohol dehydrogenase. *Applied and Environmental Microbiology*, 80: 3394–3303.

Kracke, F., Virdis, B., Bernhardt, P.V., Rabaey, K. and Krömer, J.O. (2016). Redox dependent metabolic shift in *Clostridium autoethanogenum* by extracellular electron supply. *Biotechnology for Biofuels*, 9: 249.

Kuehne, S.A., Heap, J.T., Cooksley, C.M., Cartman, S.T. and Minton, N. P. (2011). ClosTron-mediated engineering of Clostridium. *Methods in Molecular Biology*, 765: 389-407.

Kundiyana, D.K., Huhnke, R.L., Maddipati, P., Atiyeh, H.K. and Wilkins, M.R. (2010). Feasibility of incorporating cotton seed extract in Clostridium strain P11 fermentation medium during synthesis gas fermentation. *Bioresource Technology*, 101: 9673–9680.

Kundiyana, D.K., Wilkins, M.R., Maddipati, P. and Huhnke, R.L. (2011). Effect of

temperature, pH and buffer presence on ethanol production from synthesis gas by "*Clostridium ragsdalei.*" *Bioresource Technology*, 102: 5794–5799.

Leang, C., Ueki, T., Nevin, K.P. and Lovley, D.R. (2013). A Genetic system for *Clostridium ljungdahlii*: A chassis for autotrophic production of biocommodities and a model homoacetogen. *Applied and Environmental Microbiology*, 79: 1102–1109.

Li, Q., Chen, J., Minton, N.P., Zhang, Y., Wen, Z., Liu, J., Yang , H., Zeng, Z., Ren, X., Yang, J., Gu, Y., Jiang, W. and Yang, S. (2016). CRISPR-based genome editing and expression control systems in *Clostridium acetobutylicum* and *Clostridium beijerinckii*. *Biotechnology Journal*, 11: 961-972.

Liew, F.M., Kopke, M., and Dennis, S. (2013). Gas Fermentation for Commercial Biofuels Production. *Liquid, Gaseous and Solid Biofuels - Conversion Techniques*. IntechOpen, Chapter 5.

Liew, F.M., Martin, M.E., Tappel, R.C., Heijstra, B.D., Mihalcea, C. and Köpke, M. (2016a). Gas Fermentation-A flexible platform for commercial scale production of low-carbon-fuels and chemicals from waste and renewable feedstocks. *Frontiers in Microbiology*, 7:694.

Liew, F.M., Henstra, A.M., Winzer, K., Köpke, M., Simpson, S. D. and Minton, N.P. (2016b). Insights into CO_2 Fixation Pathway of *Clostridium autoethanogenum* by Targeted Mutagenesis. *MBio*, 7: e00427-16.

Liew, F., Henstra, A.M., Köpke, M., Winzer, K., Simpson, S.D. and Minton, N. P. (2017). Metabolic engineering of *Clostridium autoethanogenum* for selective alcohol production. *Metabolic Engineering*, 40: 104–114.

Lin, Y. and Tanaka, S. (2006). Ethanol fermentation from biomass resources: Current state and prospects. *Applied Microbiology and Biotechnology*, 69: 627–642.

Lindahl, P.A. and Chang, B. (2001). The evolution of Acetyl-CoA Synthase. *Origins of Life and Evolution of Biospheres*, 31: 403–434.

Liou, J.S., Balkwill, D.L., Drake, G.R. and Tanner, R.S. (2005). *Clostridium carboxidivorans* sp. nov., a solvent-producing clostridium isolated from an agricultural settling lagoon, and reclassification of the acetogen *Clostridium scatologenes* strain SL1 as *Clostridium drakei* sp. nov. *International Journal of Systematic and Evolutionary Microbiology*, 55: 2085–2091.

Liu, C.G., Qin, J.C. and Lin, Y.H. (2017). Fermentation and Redox Potential. *Fermentation Processes*, 23–42.

Ljungdahl, L.G., and Wood, H.G. (2003). Total Synthesis of Acetate From CO_2 by Heterotrophic Bacteria. *Annual Review of Microbiology*, *23*: 515–538.

Makarova, K.S., Haft, D.H., Barrangou, R., Brouns, S.J.J., Charpentier, E., Horvath, P.,

Moineau, S., Mojica, F.J.M., Wolf, Y.I., Yakuin, A.F., van der Oost, J. and Koonin, E.V. (2011). NIH Public Access, 9:467–477.

Marcellin, E., Behrendorff, J. B., Nagaraju, S., Detissera, S., Segovia, S., Palfreyman, R.W., Daniell, J., Licona-Cassani, C., Quek, L., Speight, R., Hodson, M.P., Simpson, S.D., Mitchell, W.P., Köpke, M. and Nielsen, L.K. (2016). Low carbon fuels and commodity chemicals from waste gases-systematic approach to understand energy metabolism in a model acetogen. *Green Chemistry*, 18: 3020–3028.

Marraffini, LA. and Sontheimer, E.J. (2010). CRISPR interference: RNA-directed adaptive immunity in bacteria and archaea. *Nature Reviews Genetics*, 11: 181–190.

Martin, M.E., Richter, H., Saha, S. and Angenent, L.T. (2016). Traits of selected Clostridium strains for syngas fermentation to ethanol. *Biotechnology and Bioengineering*, 113: 531–539.

McLaughlin, K.J., Strain-Damerell, C.M., Xie, K., Brekasis, D., Soares, A.S., Paget, M.S. and Kielkopf, C.L. (2010). Structural Basis for NADH/NAD+ Redox Sensing by a Rex Family Repressor. *Molecular Cell*, *38*: 563–575.

Meyer, C.L., Roos, J.W. and Papoutsakis, E.T. (1986). Carbon-monoxide gassing leads to alcohol production and butyrate uptake without acetone formation in continuous cultures of *Clostridium acetobutylicum*. *Applied Microbiology and Biotechnology*, 24: 159-167.

Minton, N. and Morris, J. G. (2009). Isolation and Partial Characterization of Three Cryptic Plasmids from Strains of *Clostridium butyricum*. *Microbiology*, 127: 325–331.

Minton, N.P., Ehsaan, M., Humphreys, C.M., Little, G.T., Baker, J., Henstra, A. M., Liew, F., Kelly, M.L., Sheng, L., Schwarz, K. and Zhang, Y. (2016). A roadmap for gene system development in Clostridium. *Anaerobe*, *41*, 104–112.

Mock, J., Zheng, Y., Mueller, A. P., Ly, S., Tran, L., Segovia, S., Nagaraju, S., Köpke, M., Dürre , P. and Thauer, R.K. (2015). Energy conservation associated with ethanol formation from H_2 and CO_2 in *Clostridium autoethanogenum* involving electron bifurcation. *Journal of Bacteriology*, 197: 2965–2980.

Mohammadi, M., Najafpour, G.D., Younesi, H., Lahijani, P., Uzir, M.H., and Mohamed, A.R. (2011). Bioconversion of synthesis gas to second generation biofuels: A review. *Renewable and Sustainable Energy Reviews*, 15: 4255–4273.

Molitor, B., Richter, H., Martin, M. E., Jensen, R.O., Juminaga, A., Mihalcea, C. and Angenent, L.T. (2016). Carbon recovery by fermentation of CO-rich off gases - Turning steel mills into biorefineries. *Bioresource Technology*, 215: 386–396.

Mueller, A. P., Koepke, M., and Nagaraju, S. (2013). Recombinant Microorganisms and Uses Therefor. US20130330809. Washington, DC: U.S. Patent and Trademark Office.

Munasinghe, P.C. and Khanal, S.K. (2010). Syngas fermentation to biofuel: Evaluation of

carbon monoxide mass transfer coefficient (kLa) in different reactor configurations. *Biotechnology Progress*, 26: 1616–1621.

Münch, R., Hiller, K., Grote, A., Scheer, M., Klein, J., Schobert, M. and Jahn, D. (2005). Virtual Footprint and PRODORIC: An integrative framework for regulon prediction in prokaryotes. *Bioinformatics*, 21: 4187–4189.

Nagaraju, S., Davies, N.K., Walker, D. J. F., Köpke, M. and Simpson, S. D. (2016). Genome editing of *Clostridium autoethanogenum* using CRISPR/Cas9. *Biotechnology for Biofuels*, 9: 219.

Nakamura, A., Sosa, A., Komori, H., Kita, A. and Miki, K. (2007). Crystal structure of TTHA1657 (AT-rich DNA-binding protein; p25) from Thermus thermophilus HB8 at 2.16 A resolution. *Proteins*, 66, 755–759.

Nakashima, N. and Miyazaki, K. (2014). Bacterial cellular engineering by genome editing and gene silencing. *International Journal of Molecular Sciences*, 15: 2773–2793.

Ng, Y.K., Ehsaan, M., Philip, S., Collery, M.M., Janoir, C., Collignon, A., Cartman, S.T. and Minton, N.P. (2013). Expanding the Repertoire of Gene Tools for Precise Manipulation of the *Clostridium difficile* Genome: Allelic Exchange Using pyrE Alleles. *PLoS ONE*, *8*: e56051.

Norman, R.O., Millat, T., Winzer, K., Minton, N.P. and Hodgman, C. (2018). Progress towards platform chemical production using *Clostridium autoethanogenum*. *Biochemical Society Transactions*, 46: 523–535.

Novichkov, P.S., Laikova, O.N., Novichkova, E.S., Gelfand, M.S., Arkin, A.P., Dubchak, I. and Rodionov, D.A. (2009). RegPrecise: A database of curated genomic inferences of transcriptional regulatory interactions in prokaryotes. *Nucleic Acids Research*, 38: 111–118.

Oswald, F., Stoll, I.K., Zwick, M., Herbig, S., Sauer, J., Boukis, N. and Neumann, A. (2018). Formic Acid Formation by *Clostridium ljungdahlii* at Elevated Pressures of Carbon Dioxide and Hydrogen. *Frontiers in Bioengineering and Biotechnology*, 6:6.

Overmann, J. (2006). Principles of Enrichment. Isolation, Cultivation and Preservation of Prokaryotes. The Prokaryotes, 80–136.

Phillips, J.R., Huhnke, R.L. and Atiyeh, H.K. (2017). Syngas Fermentation: A Microbial Conversion Process of Gaseous Substrates to Various Products. *Fermentation*, 3:28.

Piatek, P. (2018). Characterisation of Agr Quorum Sensing in Clostridium autoethanogenum. PhD thesis.

Pierce, E., Xie, G., Barabote, R.D., Saunders, E., Han, C.S., Detter, J.C., Richardson, P., Brettin, T.S., Das, A., Ljungdahl, L.G. and Ragsdale, S.W. (2008). The complete genome sequence of Moorella thermoacetica (f. *Clostridium thermoaceticum*). *Environmental Microbiology*, 10: 2550-2573.

Priefer, C., Jörissen, J. and Frör, O. (2017). Pathways to Shape the Bioeconomy. *Resources*, 6: 10.

Pyne, M.E., Bruder, M., Moo-Young, M., Chung, D. A. and Chou, C.P. (2014). Technical guide for genetic advancement of underdeveloped and intractable Clostridium. *Biotechnology Advances*, 32: 623–641.

Pyne, M.E., Bruder, M.R., Moo-Young, M., Chung, D.A. and Chou, C.P. (2016). Harnessing heterologous and endogenous CRISPR-Cas machineries for efficient markerless genome editing in Clostridium. *Scientific Reports*, 6:25666.

Ragsdale, S.W., Ljungdahl, L.G., and DerVartanian, D.V. (1983). Isolation of carbon monoxide dehydrogenase from Acetobacterium woodii and comparison of its properties with those of the *Clostridium thermoaceticum* enzyme. *Journal of Bacteriology*, 155: 1224–1237.

Ragsdale, S.W. (2009). Nickel-based enzyme systems. *Journal of Biological Chemistry*, 284: 18571–18575.

Rasool, U. and Hemalatha, S. (2016). A review on bioenergy and biofuels: sources and their production. *Brazilian Journal of Biological Sciences*, 3: 3.

Ravcheev, D.A., Li, X., Latif, H., Zengler, K., Leyn, S.A., Korostelev, Y.D., Kazakov, A.E., Novichkov, P.S., Osterman, A.L. and Rodionov, D.A. (2012). Transcriptional regulation of central carbon and energy metabolism in bacteria by redox-responsive repressor Rex. *Journal of Bacteriology*, 194: 1145–1157.

Richter, H., Martin, M.E. and Angenent, L.T. (2013). A two-stage continuous fermentation system for conversion of syngas into ethanol. *Energies*, 6: 3987–4000.

Richter, H., Molitor, B., Wei, H., Chen, W., Aristilde, L. and Angenent, L.T. (2016). Ethanol production in syngas-fermenting: *Clostridium ljungdahlii* is controlled by thermodynamics rather than by enzyme expression. *Energy and Environmental Science*, 9: 2392–2399.

Rieu-Lesme, F., Dauga, C., Fonty, G. and Dore, J. (1998). Isolation from the rumen of a new acetogenic bacterium phylogenetically closely related to *Clostridium difficile*. *Anaerobe*, 4: 89–94.

Rodionova, M.V., Poudyal, R.S., Tiwari, I., Voloshin, R.A., Zharmukhamedov, S.K., Nam, H.G., Zayadan, B.K., Bruce, B.D., Hou, H.J.M., Allakhverdiev, S.I. (2017). Biofuel production: Challenges and opportunities. *International Journal of Hydrogen Energy*, 42: 8450–8461.

Savage, M.D. and Drake, H.L. (1986). Adaptation of the acetogen *Clostridium thermoautotrophicum* to minimal medium. *Journal of Bacteriology*, 165: 315–318.

Saxena, J. and Tanner, R.S. (2012). Optimization of a corn steep medium for production of ethanol from synthesis gas fermentation by *Clostridium ragsdalei*. *World Journal of Microbiology and Biotechnology*, 28: 1553–1561.

Schulz, H. (1999). Short history and present trends of Fischer-Tropsch synthesis. *Applied Catalysis A: General*, 186: 3–12.

Schwarz, K.M., Grosse-Honebrink, A., Derecka, K., Rotta, C., Zhang, Y. and Minton, N.P. (2017). Towards improved butanol production through targeted genetic modification of *Clostridium pasteurianum*. *Metabolic Engineering*, 40: 124–137.

Shima, S. and Ataka, K. (2011). Isocyanides inhibit [Fe]-hydrogenase with very high affinity. *FEBS Letters*, 585*:* 353–356.

Sickmier, E.A., Brekasis, D., Paranawithana, S., Bonanno, J.B., Paget, M.S., Burley, S.K. and Kielkopf, C.L. (2005). X-ray structure of a Rex-family repressor/NADH complex insights into the mechanism of redox sensing. *Structure*, 13: 43–54.

Simpson, S. D., Koepke, M., and Liew F. M. (2011). Recombinant Microorganisms and Methods of Use Thereof. US2011/0256600. Washington, DC: U.S. Patent and Trademark Office.

Sun, Y. and Cheng, J. (2002). Hydrolysis of lignocellulosic materials for ethanol production: a review. *Bioresource Technology*, 83, 1–11.

Tanner, R.S., Miller, L.M. and Yang, D. (1993). Clostridial rRNA Homology Group I. *International Journal of Systematic Bacteriology*, 43: 232–236.

Teixeira, L.V., Moutinho, L.F., and Romão-Dumaresq, A.S. (2018). Gas fermentation of C1 feedstocks: commercialization status and future prospects. *Biofuels, Bioproducts and Biorefining*, 12:1103–1117.

Tian, P., Wang, J., Shen, X., Rey, J.F., Yuan, Q. and Yan, Y. (2017). Fundamental CRISPR-Cas9 tools and current applications in microbial systems. *Synthetic and Systems Biotechnology*, 2: 219–225.

Tracy, B.P., Jones, S.W., Fast, A.G., Indurthi, D.C. and Papoutsakis, E.T. (2012). Clostridia: The importance of their exceptional substrate and metabolite diversity for biofuel and biorefinery applications. *Current Opinion in Biotechnology*, 23*:* 364–381.

Tummala, S.B., Welker, N.E. and Papoutsakis, E.T. (2003). Design of Antisense RNA Constructs for Downregulation of the Acetone Formation Pathway of *Clostridium acetobutylicum*. *Journal of Bacteriology*, 185: 1923–1934.

Ungerman, A.J., and Heindel, T.J. (2007). Carbon monoxide mass transfer for syngas fermentation in a stirred tank reactor with dual impeller configurations. *Biotechnology Progress*, 23: 613–620.

Valgepea, K., de Souza Pinto Lemgruber, R., Meaghan, K., Palfreyman, R.W., Abdalla, T., Heijstra, B.D., Behrendorff, J.B., Tappel, R., Köpke, M., Simpson, S.D., Nielsen, L.K. and Marcellin, E. (2017). Maintenance of ATP Homeostasis Triggers Metabolic Shifts in Gas-Fermenting Acetogens. *Cell Systems*, 4: 505–515.e5.

Valgepea, K., De Souza Pinto Lemgruber, R., Abdalla, T., Binos, S., Takemori, N., Takemori, A., Tanaka, Y., Tappel, R., Köpke, M., Simpson, S.D., Nielsen, L.K. and Marcellin, E. (2018). H_2 drives metabolic rearrangements in gas-fermenting Clostridium autoethanogenum. *Biotechnology for Biofuels*, 11: 1–15.

Vega, J.L., Prieto, S., Elmore, B.B., Clausen, E.C. and Gaddy, J.L (1989). The Biological Production of Ethanol from Synthesis Gas. *Applied Biochemistry and Biotechnology*, 20, 781–797.

Wang, E., Bauer, M. C., Rogstam, A., Linse, S., Logan, D. T. and Von Wachenfeldt, C. (2008). Structure and functional properties of the *Bacillus subtilis* transcriptional repressor Rex. *Molecular Microbiology*, 69: 466–478.

Wang, Y., Li, X., Mao, Y. and Blaschek, H.P. (2012). Genome-wide dynamic transcriptional profiling in clostridium beijerinckii NCIMB 8052 using single-nucleotide resolution RNA-Seq. *BMC Genomics*, 13: 102.

Wang, S., Huang, H., Kahnt, H.H., Mueller, A.P., Köpke, M. and Thauer, R.K. (2013). NADP-Specific electron-bifurcating [FeFe]-hydrogenase in a functional complex with formate dehydrogenase in *Clostridium autoethanogenum* grown on CO. *Journal of Bacteriology*, 195: 4373–4386.

Wang, Y., Zhang, Z.T., Seo, S.O., Choi, K., Lu, T., Jin, Y.S. and Blaschek, H.P. (2015). Markerless chromosomal gene deletion in *Clostridium beijerinckii* using CRISPR/Cas9 system. *Journal of Biotechnology*, 200: 1–5.

Wang, Y., Zhang, Z.T., Seo, S.O., Lynn, P., Lu, T., Jin, Y.S. and Blaschek, H.P. (2016). Bacterial Genome Editing with CRISPR-Cas9: Deletion, Integration, Single Nucleotide Modification, and Desirable "clean" Mutant Selection in *Clostridium beijerinckii* as an Example. *ACS Synthetic Biology*, 5: 721-732.

Wang, S., Dong, S., Wang, P., Tao, Y. and Wang, Y. (2017). Genome Editing in Clostridium saccharoperbutylacetonicum N1-4 with the CRISPR-Cas9 System. *Applied and Environmental Microbiology*, 83:e00233-17.

Wasels, F., Jean-Marie, J., Collas, F., López-Contreras, A. M. and Lopes Ferreira, N. (2017). A two-plasmid inducible CRISPR/Cas9 genome editing tool for *Clostridium acetobutylicum*. *Journal of Microbiological Methods*, 140: 5–11.

Wieland, F., Neff, A., Gloess, A.N., Poisson, L., Atlan, S., Larrain, D., Pretre, D., Blank, I. and Yeretzian, C. (2015). Temperature dependence of Henry's law constants: An automated, high-throughput gas stripping cell design coupled to PTR-ToF-MS. *Intenational Journal of Mass Spectrometry*, 387: 69-77.

Wieringa, K.T. (1940). The formation of acetic acid from carbon dioxide and hydrogen by anaerobic spore- forming bacteria. *Antonie Leeuwenhoek, J. Microbiology,* 6: 251–262

Wietzke, M. and Bahl, H. (2012). The redox-sensing protein Rex, a transcriptional regulator of solventogenesis in *Clostridium acetobutylicum. Applied Microbiology and Biotechnology*, 96: 749–761.

Wilkins, M.R. and Atiyeh, H.K. (2011). Microbial production of ethanol from carbon monoxide. *Current Opinion in Biotechnology*, 22: 326–330.

Williams, D.R., Young, D.I. and Young M. (1990). Conjugative plasmid transfer from Escherichia coli to Clostridium acetobutylicum. *Journal of General Microbiology*, 136: 819-826.

Woods, C.A., PhD; Christopher M Humphreys, PhD; Raquel M Rodrigues; Patrick Ingle, PhD; Anne M Henstra, PhD; Michael Köpke, PhD; Sean Simpson, PhD; Klaus Winzer, PhD; Minton. A Novel Conjugal Donor Strain for Improved DNA transfer into Clostridium spp. Anaerobe (submitted).

Xu, D., Tree, D.R. and Lewis, R.S. (2011). The effects of syngas impurities on syngas fermentation to liquid fuels. *Biomass and Bioenergy*, 35: 2690–2696.

Xu, T., Li, Y., Shi, Z., Hemme, C. L., Li, Y., Zhu, Y., Van Nostrand, J.D., He, Z., and Zhou, J. (2015). Efficient genome editing in *Clostridium cellulolyticum* via CRISPR-Cas9 nickase. *Applied and Environmental Microbiology*, 81: 4423–4431.

Xu, H., Liang, C., Yuan, Z., Xu, J., Hua, Q., and Guo, Y. (2017). A study of CO/syngas bioconversion by *Clostridium autoethanogenum* with a flexible gas-cultivation system. *Enzyme and Microbial Technology*, 101, 24–29.

Zhang, L., Nie, X., Ravcheev, D. A., Rodionov, D. A., Sheng, J., Gu, Y., Yang, S., Jiang, W., Yang, C. (2014). Redox-responsive repressor Rex modulates alcohol production and oxidative stress tolerance in *Clostridium acetobutylicum*. *Journal of Bacteriology*, 196: 3949–3963.

Zhang, Y., Grosse-honebrink, A. and Minton, N.P. (2015a). A Universal Mariner Transposon System for Forward Genetic Studies in the Genus Clostridium. PLoS ONE 2: e0122411.

Zhang, X.H., Tee, L. Y., Wang, X.G., Huang, Q. S. and Yang, S.H. (2015b). Off-target effects in CRISPR/Cas9-mediated genome engineering. *Molecular Therapy - Nucleic Acids*, 4: e264.

Zhao, C., Zhao, Q., Li, Y. and Zhang, Y. (2017). Engineering redox homeostasis to develop efficient alcohol-producing microbial cell factories. *Microbial Cell Factories*, 16: 115.

Zheng, Y., Ko, T.P., Sun, H., Huang, C.H., Pei, J., Qiu, R., Wang, A.H., Wiegel, J., Shao, W. and Guo, R.T. (2014). Distinct structural features of Rex-family repressors to sense redox levels in anaerobes and aerobes. *Journal of Structural Biology*, 188: 195–204.

Zheng, Y., Ko, T.P., Yang, Y., Shao, W. and Guo, R.T. (2015). Binding mode of the oxidized α-anomer of NAD+to RSP, a Rex-family repressor. *Biochemical and Biophysical Research Communications*, 456: 733–736.

Zheng, T., Lanahan, A.A., Lynd, L. R. and Olson, D.G. (2018). The redox-sensing protein Rex modulates ethanol production in *Thermoanaerobacterium saccharolyticum*. *PLoS ONE*, 13: 1–18.

Zhou, L., Froment, G.F., Yang, Y. and Li, Y. (2016). Advanced Fundamental Modeling of the Kinetics of Fischer–Tropsch Synthesis. AIChE journal, 62:1495-1502.

Chapter 11

General conclusions and outlook

11.1 Background

The scientific community has given dire warning about the potential irreversible effects of climate change. Over the last decades, this global concern has triggered an immense interest towards the development of environmentally friendly technologies and hence of bio-based economy. In this context, microbe-based technologies are providing a valuable contribution to mitigate dependence on the depleting fossil fuel sources. Successful implementation of microorganisms in the field of bioenergy has been largely demonstrated. Their applicability offers unique advantages such as flexibility, selectivity, self-regenerable capability and mild conditions required for their growth (Lin and Tao, 2017). Additionally, microbes can live either as planktonic cells or biofilm. Recently, the finding that special kind of biofilms can electrically interact with a conductive surface, releasing current as by-product, is attracting wide attention. This capability is deployed in the bioelectrochemical systems (BESs) categorized as Microbial Fuel Cells (MFCs). The main hindrance of the commercial application of MFCs is that these electrochemical devices are intrinsically associated with low performances, with power outputs orders of magnitude lower than that of conventional fuel cells (Santoro et al. 2017). However, the implementation of MFCs for complementing other technologies or as power supply for low energy-demanding electronics remains still conceivable. Beyond electricity generation, production of biological fuels is currently one of the primary topics in science. Several approaches have been explored resulting in different generations of biofuels. Lately, gas fermentation appears as an attractive route, which allows the conversion of C1 gases in high-value chemicals and fuels through the metabolism of gas-fermenting microorganisms. Moreover, the continuous advances of metabolic engineering and synthetic biology are providing the opportunity to build up robust and customized biocatalysts. The major research objective of this thesis is to explore two different microbe-based technologies, MFCs and gas fermentation, using both pure and mixed microbial community.

11.2 Key findings

The first objective of the current work was to provide experimental evidences of the applicability of a novel MFC-based floating set-up as power supply in real marine environment. In order to investigate the potentiality of the marine community as electro-biocatalyst, a novel enrichment approach for anodic biofilm formation was developed. This method consisted in the *in situ* colonization of the carbon-felt material used as anode electrode (La Spezia bay). The marine anodic biofilm enriched with a procedure developed within this study showed promising

performance. The results achieved by the electrochemical characterization of the so formed anodes did not exhibit significant changes compared to that of the anodes developed following the standard laboratory approach. Hence, the novel enrichment procedure was preferred over the conventional one. This study is the first time that small-scale MFCs were encased in a floating set up, resulting in a novel, compact and cost-effective BES. The novelty of the current study also lies in the deployment of a solid-state electrolyte (SSE) as both carbon and nitrogen source for bacteria. The solid-state anolyte has been already proposed by our research group and described in Tommasi et al. 2016. This experiment provided experimental evidences of the successful applicability of the SSE in a dual-chamber MFC. However, here for the first time SSE was employed in single chamber MFCs operating in real marine environment. Results obtained during the two distinct field measurement campaigns conducted in La Spezia, showed that the constructed floating set-up was capable of continuously providing an average power density of 6 mW/m^2 during both summertime and wintertime, with negligible temperature effects.

Regarding the research carried out in the field of gas fermentation, this project represents the first endeavor reported in literature to explore the role of redox sensing transcriptional repressor Rex in the acetogen *Clostridium autoethanogenum*. *In silico* analysis revealed that the Rex protein sequence of *C. autoethanogenum* shares high similarities with the Rex proteins well-described in other clostridium species. Moreover, it was found that Rex might regulate 76 putative genes in *C. autoethanogenum*. So far, deletion of *rex* gene was achieved with conventional intron–based genetic engineering techniques while in the current project the revolutionary CRISPR-Cas9 genome editing tool was successfully implemented to construct the KO strain. The key finding resulting from the phenotypical characterization conducted in CO-batch bottles, revealed that Rex modulates the synthesis of both lactate and 2,3-butanediol, with *rex* deletion strain displaying an 83% increase in 2,3-BDO and a 17-fold higher final concentration of lactate compared to the WT. When this project was conceived, an increase in ethanol production was expected to be achieved. However, the experimental data obtained during semi-batch fermentation experiments deviated from the expectations, since no appreciable changes in terms of metabolite profile emerged across the strains. Interestingly, under continuous CO-supply cultivation conditions, the biphasic behavior observed suggested that *C. autoethanogenum* cultures reassimilate acetate and converted it into ethanol, perhaps to withstand CO-inhibition effects. Although no enhancement of ethanol production was highlighted in the r*ex* deletion strain, a maximum ethanol concentration of ~20 g/L was obtained. This value is higher than those reported in previously published studies carried out in similar working conditions.

11.3 Future perspectives

The results presented in this thesis generated new knowledge about the two microbial technologies investigated throughout this research study. However, there are still some aspects of this study that could be improved.

Concerning the first part of my study, even though the results obtained proved the promising applicability of the novel MFC-based floating system, issues in terms of electrical connections were periodically encountered. Hence, this limitation should be overcome and better investigated. The 3D printing technology could provide the opportunity to optimize the set-up, by re-designing the electrical interfaces of the floating system. With respect to the microbial consortium's biodiversity, its composition should be investigated using currently advanced molecular techniques. As a function of the population structure, optimization of SSE electrolyte could be performed in order to select for exoelectrogenic species. Moreover, to evaluate the versatility of the system, new experiments in different environments should be performed. An investigation of the biofilm formation by scanning electron microscopy (SEM) could be also advantageous to assess the presence microorganisms onto both anode and cathode electrodes. Particularly, cathode electrode's performance could have been affected by the phenomenon of biofouling, hindering ORR. Hence, a deeper investigation is required with the aim to eventually develop new materials able to overcome this issue. Finally, the concept of MFC-based Livestock, consisting in a wide number of *in situ* pre-colonized FMFCs operating in the seawater, needs to be explored in order to provide back-up MFCs to replace malfunctioning devices.

Within BESs, microbial electrosynthesis (MES) is providing nowadays a great opportunity to combine electromicrobiology and fermentation, allowing the production of valuable chemicals or fuels from CO_2 or other compounds. As shown by the carbon mass balance analysis, in perfect accordance with the stoichiometric estimations (Wilkins and Atiyeh, 2011), 67-68% of carbon was dissipated as CO_2 during the production of ethanol. To limit carbon loss, the synergistic combination of MES and gas fermentation could be an alternative path able to furnish extra reducing power for carbon fixation. Another solution that has already been investigated consists in adjusting the gas mixture composition, by increasing H_2 partial pressure. .

Regarding the role of Rex in *Clostridium autoethanogenum*, as aforementioned, the lack of phenotypic changes in bacterial cultures continuously fed with CO may be related to the working conditions. In an attempt to identify potential phenotypic effects some strategies could be undertaken such as reducing the gas flow rate or the agitation speed. Although continuous mode was deliberately avoided for time constraints, an investigation under steady state conditions should be performed.

Moreover, the reducing potential of the substrate can affect metabolite profile. Hence, although out of the scope of this study, clarifying the role of Rex in heterotrophic conditions may help improving the knowledge on this transcriptional repressor. Additionally, even if bioinformatic analysis revealed putative Rex binding boxes within the genome of *C. autoethanogenum,* in part confirmed by the increases in lactate and 2,3-BDO concentrations, a direct experimental evidence for protein-DNA interactions can be assessed by EMSA analysis as already performed in other previous study (Liu et al. 2017; Zhang et al. 2014; Hu et al. 2016). Finally, qRT-PCR or RNAseq would be useful to examine the expression levels of the target genes putatively regulated by Rex in all the three analyzed strains.

11.4 References

Hu, L., Huang, H., Yuan, H., Tao, F. Xie, H. and Wang, S. (2016). Rex in Clostridium kluyveri is a global redox-sensing transcriptional regulator. *Journal of Biotechnology*, 233: 17-25.

Lin, B. and Tao, Y. (2017). Whole-cell biocatalysts by design. *Microbial Cell Factories*, 16: 1-12.

Liu, X., Cheng, Y., Lyu, M., Wen, Y., Song, Y., Chen, Z. and Li, J. (2017). Redox-sensing regulator Rex regulates aerobic metabolism, morphological differentiation, and avermectin production in Streptomyces avermitilis. *Scientific Reports*, 7: 1-13.

Santoro, C., Arbizzani, C., Erable, B., Ieropoulos, I. (2017). Microbial fuel cells: From fundamentals to applications. A review. *Journal of Power Sources*, 356: 225-244.

Tommasi, T., Salvador, G.P. and Quaglio, M. (2016). New insights in Microbial Fuel Cells: novel solid phase anolyte. Science Reports, 6: 29091.

Wilkins, M.R. and Atiyeh, H.K. (2011). Microbial production of ethanol from carbon monoxide. *Current Opinion in Biotechnology*, 22: 326–330.

Zhang, L., Nie, X, Ravcheev, D.A., Rodionov, D.A., Sheng, J., Gu, Y., Yang, S., Jiang, W. and Yang, C. (2014). Redox-responsive repressor Rex modulates alcohol production and oxidative stress tolerance in Clostridium acetobutylicum. *Journal of Bacteriology*, 196: 3949–3963.

Chapter 12

Appendix

12.1 Oligonucleotide list

Table 12.1 Oligonucleotides used in this study. Abbreviations: F=Forward; R=reverse. Table continues next page**.**

Name	Sequence (5'-3')	Description
*rex*LHA_F1	TATATAGCGATCGCCGTATTGTT TCGTAACTTGAG	
*rex*LHA_R1	TAGTATGGATATAGATTAAAAA CTTAAATGAATTCTTTAAG	SOEing-PCR primers for *rex* homology cassette construction
*rex*RHA_F1	TTTAATCTATATCCATACTACAC CTTCTTCTATATTCTTTGATTTC	
*rex*RHA_R1	TATATAGGCGCGCCCATTCTATA GCGTCTAGATCCAGGTG	
sgRNA flank_ F2.0	ATATATTCTAGATTTATATTTAG TCCCTTGCCTTGC	Screening primer for pMTL-CRISPR-Cas9_*rex* construction
*rex*Scr_F1	CATCAAATTCAGGACCATCTAC	
*rex*Scr_F2	GGGCGTAAATTCGGATGAAATT C	*rex* screening primers for deletion mutants
*rex*Scr_R1	CATAGTTGACTGGGTTATAGCAT C	
*rex*HiFi_F1	ATGGTTTATCTGTTACCCCACTA GTGAAATCAAAGAATATAGAAG AAGG	PCR primers for *rex* amplification and Hi-Fi assembly

181

*rex*HiFi_R1	GTGCATTGATTTTTTCGACGCTA GCTTAATCTATATCATTTAAAAG ACACG	PCR primers for *rex* amplification and Hi-Fi assembly
ACE *pyrE*_FSP	GAGCTTATGCAATTCAAGTAGG TACTGCAAAC	*pyrE* screening primers for for deletion mutants
ACE *pyrE*_RSP	CATCAAAGCTATACTATTTTCCG TATTTACATTTGGG	
CH23_F1	CCAATTTATAGTGCAGTAAAAC	Screening primers for *rex* complementation mutants
CH20_RSP	GTCAATTCTGCATCGTGC	

12.2 Restriction enzyme list

Table 12.2 Restriction enzymes used in this study. Abbreviation: HF=High Fidelity.

Enzyme	Sequence
AscI	GG/CGCGCC
AsiSI	GCGAT/CGC
SalI HF	G/TCGAC
SpeI	A/CTAGT
NheI	G/CTAGC

12.3 Single guide RNA list

Table 12.3 Single guide RNAs sequences used in this study and determined by Benchling's CRISPR gRNA scoring tool.

Single guide RNA	Sequence (5'-3)	PAM (5'-3')	On-target score	Off-target score
Sg1	tttgggactttggacagca	GGG	62.4	50
Sg2	agagattgccaaaataccat	AGG	61.2	50
Sg3	cagggatatgggtataatgt	AGG	57.3	50

12.4 Putative Rex-regulated genes

Operons containing candidate Rex-regulated genes were inferred using gene expression data (Henstra et al. unpublished) and custom Python scripts available on request from Rupert Norman at the University of Nottingham (email:rupert.norman@nottingham.ac.uk).

Table 12.4 Putative Rex-regulated genes in *Clostridium autoethanogenum*.

Locus tag	Function	Rex-binding sequence	Alignment score 1*	Alignment score 2**
CLAU_0998	DNA modification/repair radical SAM protein	TTGTTAAAG AAATAACAA	12	13
CLAU_0997	Pyridine nucleotide-disulfide oxidoreductase	TTGTTAAAG AAATAACAA	12	13
CLAU_1149	Aspartate kinase	TTGTCAAAT TATTAACAA	11	13
CLAU_1148	Sigma-54 specific transcriptional regulator Fis family	TTGTCAAAT TATTAACAA	11	13
CLAU_3541	Aspartate carbamoyltransferase	TTGTGAAAA AATTAACAA	11	13
CLAU_2942	Amino acid permease	TTGTTATAA AAATAACAA	12	12
CLAU_0239	L-lactate transport	ATGTTAACA ATATAACAA	11	12
CLAU_0423	Sulfite reductase subunit A	ATGTTAAAT ATATAACAA	11	12
CLAU_1012	Putative membrane protein	TAGTTAATA AGATAACAA	11	12

CLAU_1579	Carbon-monoxide dehydrogenase (acceptor)	TTGTTAAAT ATATACCAA	11	12
CLAU_1580	UspA domain-containing protein	TTGTTAAAT ATATACCAA	11	12
CLAU_2100	Hypothetical protein	TTGTTATGA TATTATCAA	11	12
CLAU_3515	Transcriptional regulator PucR family	TTGATAAAA AAATAACAA	11	12
CLAU_3514	Alcohol dehydrogenase	TTGATAAAA AAATAACAA	11	12
CLAU_1043	Transcriptional regulator CdaR family	ATGATAATA ATTTAACAA	10	12
CLAU_1042	MFS transporter	ATGATAATA ATTTAACAA	10	12
CLAU_1789	Hypothetical protein	TTGTATAAT TTTTAACAA	10	12
CLAU_2502	Nitrogenase iron protein	ATGATAAGT TATTAACAA	10	12
CLAU_2501	DNA-binding domain protein excisionase family	ATGATAAGT TATTAACAA	10	12
CLAU_3331	Hypothetical protein	TTGATAAAA TGTTAACTA	10	12
CLAU_3861	Alcohol dehydrogenase	TAGATAATA TTTTAACAA	10	12
CLAU_1828	Ubiquinone/menaquinone biosynthesis methyltransferase ubiE	TTGTCATGA AGATAACAA	11	11

CLAU_3422	Major facilitator superfamily MFS_1	ATGTTAGAA ATCTAACAA	11	11
CLAU_3528	Transcriptional regulator MarR family	TAGTTAGAA ATCTAACAA	11	11
CLAU_3529	ABC-type transporter related protein	TAGTTAGAA ATCTAACAA	11	11
CLAU_0347	DEAD/DEAH box RNA helicase	TTGTAATAA ATTTATCAA	10	11
CLAU_0346	DNA topoisomerase type IA	TTGTAATAA ATTTATCAA	10	11
CLAU_0388	Acetolactate synthase biosynthetic type large subunit	ATGTGAAAA AAATAACAA	10	11
CLAU_0403	Aspartate/glutamate/uridylate kinase	TTGATAATA AAATACCAA	10	11
CLAU_0711	Glycerol dehydrogenase	TTGTTAAAA AAATAACTA	10	11
CLAU_0711	Glycerol dehydrogenase	GTGTAAAAA TAATAACAA	10	11
CLAU_0842	Transcriptional regulator LysR family	ATGTTAAAA AAATAACTA	10	11
CLAU_0841	3-dehydroquinate dehydratase	ATGTTAAAA AAATAACTA	10	11
CLAU_1093	Cobalt permease	ATGATATAT TTTTAACAA	10	11

CLAU_1559	FAD-dependent oxidoreductase	ATGATAATT AAATAACAA	10	11
CLAU_2244	Radical SAM domain protein	TTGTCAATA AAATAACAT	10	11
CLAU_2560	DegT/DnrJ/EryC1/StrS aminotransferase family	TTGAAAAGA AAATAACAA	10	11
CLAU_2973	Flagellin domain protein	GTGTAAATT AAATAACAA	10	11
CLAU_2974	Flagellar hook-associated 2 domain-containing protein	GTGTAAATT AAATAACAA	10	11
CLAU_3507	Putative Esterase/lipase	ATGTAATTT TGTTAACAA	10	11
CLAU_3506	Transcriptional regulator HxlR family	ATGTAATTT TGTTAACAA	10	11
CLAU_3619	Alcohol dehydrogenase	TTGTAAAAA TAGTATCAA	10	11
CLAU_3687	Hypothetical protein	CTGTTAGTA AATTACCAA	10	11
CLAU_3688	Phage portal protein	CTGTTAGTA AATTACCAA	10	11
CLAU_3848	Arylsulfotransferase	CTGTTAAAA AAGTAGCAA	10	11
CLAU_0531	PAS modulated sigma54 specific transcriptional regulator Fis family	CTGTGAATA AATTAACAT	9	11
CLAU_0530	Transcriptional regulator PadR-like family	CTGTGAATA AATTAACAT	9	11

CLAU_0966	YheO-like domain-containing protein	CTGTAAAAA AATTACCAA	9	11
CLAU_0965	Putative basic membrane protein	CTGTAAAAA AATTACCAA	9	11
CLAU_1182	Lipoyl synthase	GTGTTAAAA AATTAGCAT	9	11
CLAU_1423	Ferric uptake regulator Fur family	AAGTTAATA AATTAACAT	9	11
CLAU_1422	Alpha-ribazole phosphatase	AAGTTAATA AATTAACAT	9	11
CLAU_1576	Formate-tetrahydrofolate ligase	ATGTTAAAA AATTAGCTA	9	11
CLAU_1715	Transcriptional regulator DeoR family	ATGAAAAAA ATTTAACAA	9	11
CLAU_3621	Transcriptional regulator LysR family	GTGTCAAGA AATTATCAA	9	11
CLAU_3620	Oxidoreductase	GTGTCAAGA AATTATCAA	9	11
CLAU_0043	Glycosyl transferase group 1	CTGTAAGTA TAATAACAA	10	10
CLAU_1562	Hypothetical protein	ATGTTATTA AAATAACAT	10	10
CLAU_1563	RNA-binding protein	ATGTTATTA AAATAACAT	10	10
CLAU_3324	Cell division FtsK/SpoIIIE	TTGATATAA ATATAACAT	10	10
CLAU_1054	Hypothetical protein	ATGAAAAAA AGGTAACAA	9	10

CLAU_1600	Putative membrane protein	ATGAAAATA ATATAACAA	9	10
CLAU_1601	Hypothetical protein	ATGAAAATA ATATAACAA	9	10
CLAU_1874	30S ribosomal protein S11	ACGTAAAAA ATGTAACAA	9	10
CLAU_1875	Ribosomal protein S13	ACGTAAAAA ATGTAACAA	9	10
CLAU_1876	50S ribosomal protein L36	ACGTAAAAA ATGTAACAA	9	10
CLAU_2166	Cellulase	GTGTAATTA AATTATCAA	9	10
CLAU_2452	Glycosyl transferase family 2	ATGAAATAT AATTAACAA	9	10
CLAU_2451	Two component transcriptional regulator winged helix family	ATGAAATAT AATTAACAA	9	10
CLAU_3462	Hypothetical protein	CTGTAATAA AATTAACTA	9	10
CLAU_3463	Putative phage derived protein	CTGTAATAA AATTAACTA	9	10
CLAU_3464	Transcriptional regulator XRE family	CTGTAATAA AATTAACTA	9	10
CLAU_3544	Putative nucleoside transporter family protein	AAGTGATTT ATTTAACAA	9	10
CLAU_2210	Polysaccharide deacetylase	ATGATATAA AAATAACAT	9	9

| CLAU_2209 | Hypothetical protein | ATGATATAA AAATAACAT | 9 | 9 |
| CLAU_3486 | Histidine kinase-like ATPase | AAGTAATAA ATGTAACAA | 9 | 9 |

*number of matches (out of 12) to TTGTTANNNNNNAACCA
** number of matches (out of 14) to TTGTTAANNNNTTAACAA

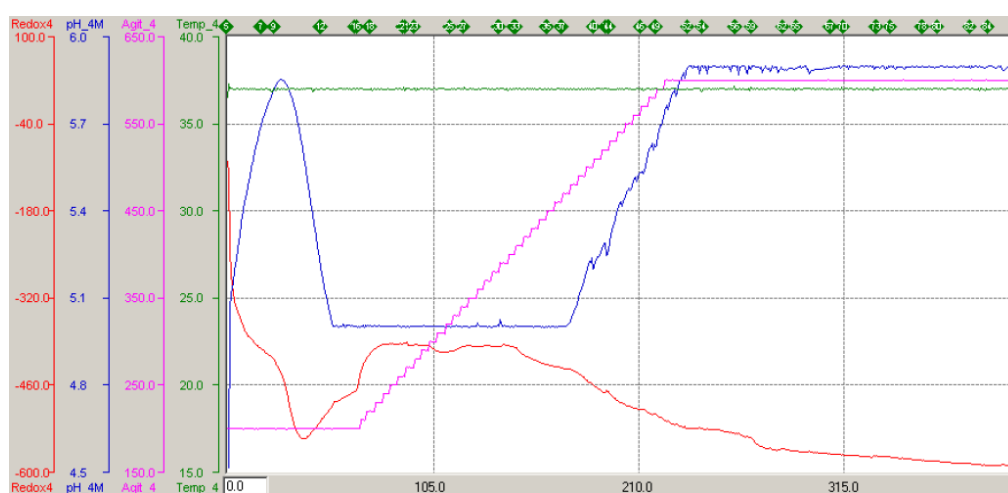## 12.5 Profile of fermentation parameters

Figure 12 Real-time monitoring of fermentation process parameters (pH, redox, agitation and temperature) using Biocommand software.

12.6 Publications

Margaria V., Tommasi T., **Pentassuglia S.**, Agostino V., Sacco A., Armato C., Chiodoni A., Schilirò T., Quaglio M. (2017). Effect of pH variations on anodic marine consortia in a dual chamber microbial fuel cell. *International Journal of Hydrogen Energy*, 43:1820-1829.

Pentassuglia, S., Agostino, V. and Tommasi, T. (2017). EAB—Electroactive Biofilm: A Biotechnological Resource. In: *Reference Module in Encyclopedia of Interfacial Chemistry: Surface Science and Electrochemistry, Elsevier* (Chapter 131461).

Massaglia, G., Margaria, V., Sacco, A., Tommasi, T., **Pentassuglia, S.**, Ahmed, D., Mo, R., Pirri, C.F., Quaglio M. (2018). In situ continuous current production from marine floating microbial fuel cells. *Applied Energy*, 230:78-85.

Pentassuglia, S., Humphreys, C.M., Rowe, P., Robbazza, A., Millard, J., Henstra, A., Saracco, G., Minton, N. Investigation of redox-sensing transcriptional represssor Rex in gas fermenting *Clostridium autoethanogenum*. Under preparation.

Piatek, P, Humphreys, C.M., **Pentassuglia, S.**, Raut, M., Wright, P., Minton, N., Winzer, K. Characterization of agr quorum sensing in *Clostridium autoethanogenum*. Under preparation.